The Role of Stratification in the Spring Ice Edge Bloom in the Bering Sea: A Numerical Model

George W Happhut

Thomas C. Royer

Vm Alexander

Henry Joseph Wisdom

Chairman, Advisory Committee

John J Goering

Department Head

Vm Alexander

Director, Institute of Marine Science

APPROVED:

W. S. Reeburgh

Director of Graduate Programs

22 July 84

Date

The Role of Stratification in the Spring Ice Edge Bloom in the Bering Sea: A Numerical Model

A
Thesis

Presented to the Faculty of the University of Alaska
in Partial Fulfillment of the Requirements
for the Degree of

Master of Science

by
Martin Freed, B. S.

Fairbanks, Alaska
September 1984

Abstract

Marginal ice edge zones are unique frontal systems with air-ice-sea interfaces. Phytoplankton blooms which occur along the edge of some melting ice packs in the spring, appear to be related to melt water driven density stratification. In this thesis a numerical model of a marginal ice edge zone is constructed. The wind driven circulation and spring phytoplankton bloom at the Bering Sea ice edge are simulated as functions of air-ice-sea-biology interaction. It was found that as long as the ice was allowed to melt, blooms occur regardless of wind direction. However, because of the compactness dependent melt scheme invoked, the faster the ice advects out from the pack, the faster the water column stratifies. The speed and the area of the bloom depend on the rate and extent of stratification. The model data compare favorably with field data.

Table of Contents

List of Figures

List of Tables

table page

Dedication

This thesis is dedicated to Drs. George Mercer and Richard Dame my undergraduate advisors, for pointing in the direction

Acknowledgements

I would like to thank my committee members Tom Royer, Vera Alexander and George Kipphut for their valuable comments and their tolerance of a pestering graduate student. I would also like to acknowledge Frank Muller-Karger, Sathy Naidu, Zigmut Kowalik, T. Nisniyama, Ted Cooney and Walt Jonnson for their assistance. The data management team at IMS was most helpful and Morgan Parker's advice on programing with the Honeywell system was invaluable.

Of course my committee chairman Joe Niebauer deserves more praise than I can write down here. We literally spent hundreds of hours together working on this and other projects.

Introduction

"The marine habitat is a geophysical fluid, and any attempt to understand biological processes therein must be firmly based in a matrix of relevant physical oceanography" (Walsh, 1975). Since the developement of computers physical oceanographers have used numerical models as tools in understanding the processes that control both large and small scale circulation, but biological oceanographers have been slower in adapting these methods. One of the reasons might be that the number of state variables in biological simulations is much larger than that traditionally used by physicists and that variability presents real obstacles in most systems. However with the advent of faster computers, numerical models have recently taken their place along side other methods used by biologists studying the sea.

The benefits derived from computer simulations are many. Perhaps an investigator wishes to determine the effect on the trophic level dynamics of a region by a

particular parameter. This may in theory be accomplished by simply holding all the other factors constant and running the program. To illustrate, if we wish to determine the effect of sinking rate on a phytoplankton population we can hold all the other arguments (light, nutrients, etc.) at constant values and observe the calculated plant concentrations at various sinking rates. Needless to say this would be quite impractical in the real world but is as easy as rearranging a few lines in the computer program that defines the simulation. In addition physical oceanographers can utilize biological simulations based on physics to verify their circulation models by using plankton as tracers. Even though plankton are not conservative much of their dynamics is understood, therefore modelling is possible. If the biological simulation does not describe the real world either the physical parameters or the model are faulty (Walsh, 1975).

In this study a model of the spring ice edge phytoplankton bloom, to be referred to as the bloom in the following sections of this thesis, is constructed. Though this simulation may be adapted to many high latitude oceanic regions, we restrict ourselves to the

Bering sea shelf (figure 1) because of the availability of data which may be used as a confirmation for the model. This shallow region is unique because of its size (12 X 10^6 km^2; Hood, 1981) and high primary production. This energy source is transformed into higher trophic level biomass. Fishing fleets from numerous nations converge on the area to take advantage of its substantial pelagic and benthic stocks. Many species of sea mammals and birds use the region as breeding and/or feeding grounds. In turn the indigenous peoples are dependent on these organisms for their subsistence. Mineral development is planned, lease sales have already taken place. Insight into the food chain dynamics may aid in the management of the region. With this model otherwise impossible experiments may be performed.

Background

Seasonal sea ice cover in the Bering Sea varies from approximately 50% of surface area in winter to 0% in summer (Overland and Pease, 1982). The advance of the ice starts in November in the northern reaches and pushes south in a "conveyor belt" manner reaching its

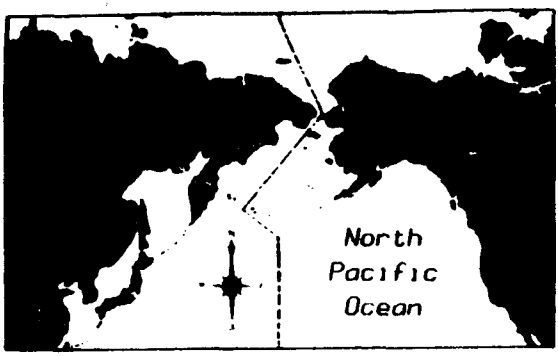

Figure 1:
Approximate ice edge positions relative to the Bering Sea shelf break and 'Alpha Helix' cruise areas □
(lower part of drawing shows North Pacific Ocean floor and Aleutian trench).

AFTER MULLER-KARGER (1984)

———————— 4 May, 1982
— — — — — — — — 26 April, 1983

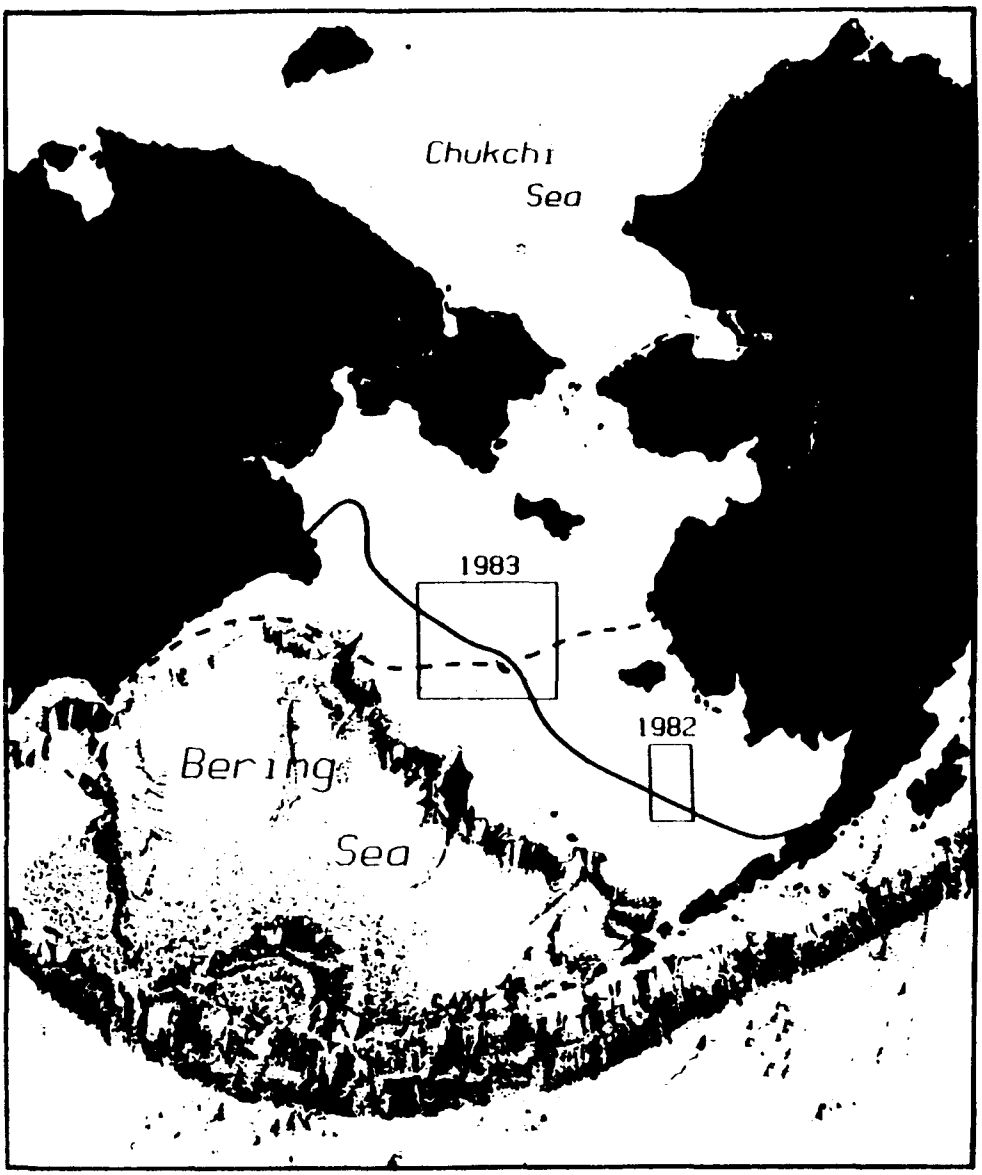
Chukchi
Sea
1983
1982
Bering
Sea

maximum extent in March-April (Overland and Pease, 1982). Figure 1 shows that maximum ice extent varies from year to year. Niebauer (1980a) has found that these large yearly fluctuations in the ice extent are highly correlated with the northerly wind component and sea surface temperature.

Oceanic frontal structure and upwelling have been observed at marginal ice edges (Buckley, et al.,1979; Alexander and Niebauer, 1981; Johannessen et al., 1983). It is hypothesized that these phenomena are due to a combination of, 1) upwelling: wind driven Ekman transport associated with change in surface stress in regions with ice and without ice and 2) frontal structure: the surfacing isopleths seaward of the ice edge are mainly due to melting ice (Alexander and Niebauer, 1981). Associated with these phenomena, high primary productivity was first reported by Marshall (1957). Since that time this type of bloom has been observed at ice edges at high latitudes around the world (Ivanov, 1964; El Sayed and Taguchi, 1981; Alexander and Cooney, 1979; Niebauer et al., 1981).

Early sea ice models were developed to study the possibility of ice edge upwelling. Gammelsrod et al. (1975) used a simulation invoking a stationary ice

cover to determine if upwelling was possible in the marginal ice zone (MIZ). Clarke (1978) extended this work by considering the effects of stratification while Niebauer (1982) induced stratification by including melting at the ice edge. All three of the above models found that stationary ice sheets were analogous to coasts in that a large curl of the wind stress is produced at the point of transition between water and ice. Buckley et al. (1979) investigated water velocities near the ice edge north of Svalbard, Spitsbergen and were probably the first to actually observe ice edge upwelling.

All three of the above models lacked a basic feature of the MIZ: the ice is not stationary. Velocities of ice of over 30 cm/sec are common (Johannassen et al., 1983). Roed and O'Brien (1983) developed a two layered ocean model with ice moving in response to wind. Now the sign of the curl of the wind stress on the ocean at the point of transition between ocean and ice cover is reversed from that of the previous three models because the coupling of atmosphere through ice to water is more efficient than that from atmosphere directly to water. Therefore assuming the same wind forcing as Niebauer (1982) and

Gammelsrod et al. (1975), Roed and O'Brien (1983) obtained the opposite results, a weak downwelling. Independently, Markham (1983) included melting at the ice edges with a moving ice cover and obtained results similar to Roed and O'Brien (1983).

Both Markham (1983) and Roed and O'Brien (1983) models assumed depths of greater than 500m. A large portion of the area of the Bering Sea has a depth of less than 100m and most of the ice covered regions are shallower than this. The model presented here will take this shallow region into account. In addition the previous models which included melting assumed a constant buoyancy flux in the areas that were wholly or partially covered by ice. However the melt rate of sea ice is a function of thermal input and percent ice cover (Langleben, 1972). In this model thermal input is considered a constant but ice is melted as a function of percent ice cover.

Among the earliest plankton simulations was Walsh (1975b) who used a two dimensional model in an attempt to predict biological production in the Peru upwelling system. The simulation included those physical and biological terms thought to be significant within the region. They are the physical advection and diffusion

and the nutrient requirements of the phytoplankton biology. Walsh (1975b) employed the simulation to resolve the differences obtained by two other investigators (Ryther, 1969; Cushing, 1969) as to the spatial extent of the productive region and food chain efficiency. The results of the model suggest that these differences do occur if there is a one step food chain and smaller upwelling region in the fall and a two step food chain and larger upwelling region in the winter.

In a later plankton model Winter et al. (1975) developed a simulation for Puget sound. Here the authors assessed the effects of vertical advection and turbulence, light intensity, self shading, sinking and horizontal advection due to wind stress. They concluded after numerous experiments that phytoplankton growth is limited by a combination of the factors. Similarly a time dependent two dimensional model was used by Wroblewski (1977) to relate wind events to upwelling and primary productivity off the Oregon coast. Daily production intensifications were calculated after an increase in the southward wind component. The highest concentration of chlorophyll occurs after the winds have relaxed because if the winds are brisk and

of long duration the plant cells experience only short euphotic zone residence time due to offshore advection and downwelling.

The questions

Niebauer and Alexander (1984) have reported several stratification related blooms at the Bering sea ice edge. This density difference at the surface is caused by the input of less saline melt water from sea ice. The questions that we attempt to answer by the following set of experiments are:

1- the effect of ice melt and wind direction and magnitude on:
   a) ice movement and dispersion
   b) water velocity
   c) primary production

2- the role of the ice algae in the development of the bloom

Table 1 is a list of the initial conditions for the experiments performed. For these cases the following

Table 1: Initial conditions for the model experiments, wind magnitudes in dynes/cm^2, melt rate in percent per day, algae concentrations in mg Chl/m^3, nutrient concentrations are 280 mg N/m^3.

Case	INITIAL CONDITIONS					
	Wind		Ice		Algae Conc	
	mag	direction	melt rate	location	ice	water
Ia	1	neg. y	0	100% ice cover from 50-70 km	NA	NA
Ib	1	neg. x	0	same as Ia	NA	NA
IIa	0	NA	eq. 11	50% cover from 40-50 km and 100% from 50-80 km	NA	NA
IIb1	0	NA	NA	NA	NA	5
IIb2	same as IIb1 but w/o nitrogen regeneration					
IIc1	0	NA	eq. 11	90% cover from 40-80 km	35	5
IIc2	0	NA	eq. 11	same as IIc1	0	5

IIIa1	1	pos. y	eq. 11	100% cover from 40-80 km	35	5
IIIa2	1	neg. y	eq. 11	same as IIIa1	35	5
IIIb	1	neg. x	eq. 11	same IIIa1	35	5
IIIc	1	pos. y	no melt	same as IIIa1	NA	5
IV	0.5	pos. y	eq. 11	same as IIIa1	35	5

descriptions of wind, water and ice velocity directions are defined (figure 2):

1-an along-ice wind with the ice to the right (pos. y).

2- an along-ice wind with the ice to the left (neg. y).

3- on-ice wind: an across-ice wind blowing from open water toward the ice (pos. x).

4-off-ice wind: an across-ice wind blowing from ice toward open water (neg. x).

Throughout the text of this thesis we will refer to Alpha-Helix cruise HX25 (1982) and HX43 (1983) as the Bering Sea ice edge cruises. The purpose of this project was to investigate the dynamics of the spring ice edge bloom in the Bering Sea and was supported by NSF. The chief scientists were Dr. H. J. Neibauer and Dr. Vera Alexander both of the Institute of Marine Science, University of Alaska, Fairbanks.

Methods

A time dependent finite differencing numerical scheme is used to generate a set of two dimensional across-ice (x) vs. depth (z) (figure 2) cross-sections of parameters (e.g. temperature, salinity, etc.) at each time step. This figure also describes where each of the parameters, that will be discussed in the following sections, are calculated. The along-ice (y) distance is viewed as infinitely long and d(phi)/dy=0, where phi is any parameter except pressure. This means that phi(a,y,b,c)=const, where a,b is a particular spatial x-z coordinate at time c. The channel is 80 km in the across-ice (x) direction and a constant 70 m deep.

Ocean

Table 2: Variables and Constants for Ocean Model

Symbol		Variable Units and value if const
g	gravity	980 cm/sec^2
f	Coriolis parameter	0.00126 1/sec
K_x	horizontal eddy diffusivity	10^4 cm^2/sec
K_z	vertical eddy diffusivity	cm^2/sec
N_x	horizontal eddy viscosity	$5*10^6$ cm^2/sec
N_z	vertical eddy viscosity	cm^2/sec
p	pressure	$dyne/cm^2$
ϕ	generalized scalar (e.g., S, T)	NA
R_i	Richardson number	dimensionless
ρ_w	water density	g/cm^3
S	salinity	ppt
T	temperature	degrees celcius
t	time	seconds
$\bar{\tau}$	wind stress	$dynes/cm^2$
$\bar{\tau}_z$	stress vector	$dyne/cm^2$
u	water velocity component in x direction	cm/sec
v	water velocity component in y direction	cm/sec

$\mathbf{V}$	velocity vector	cm/sec
$\mathbf{V}_h$	horizontal velocity vector	cm/sec
w	vertical velocity component	cm/sec
x	position in across-ice direction	cm
Δx	model x increment	200,000cm
y	position in along-ice direction	cm
z	position in vertical direction	cm
Δz	model z increment	500cm

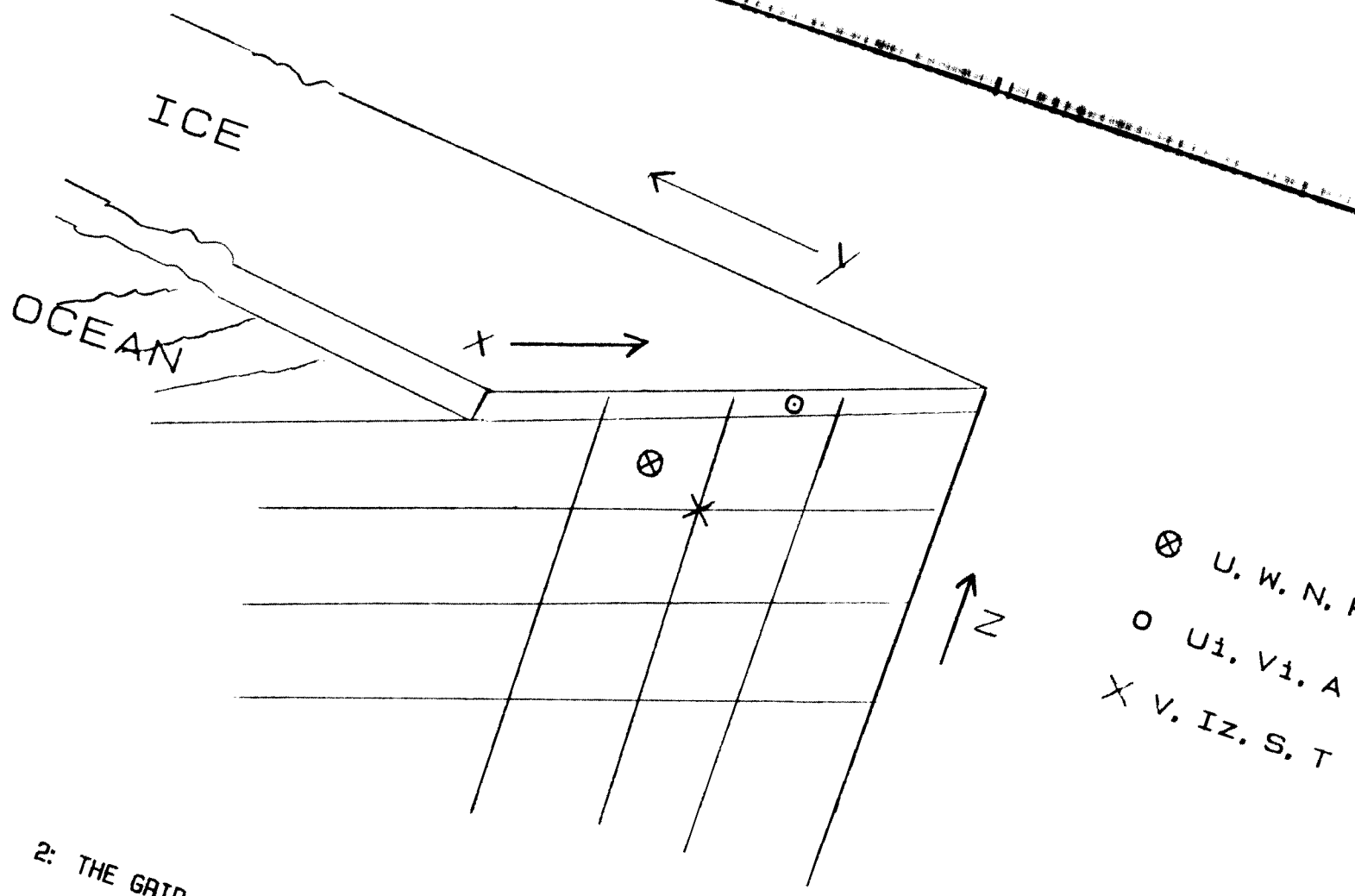

FIGURE 2: THE GRID AND THE POSITIONS FOR THE CALCULATIONS OF THE PARAMETERS

The ocean model is a modification of a Lake Ontario computer simulation by Bennett (1973). It was used by Niebauer (1982) in his ice edge simulation as well as his coastal upwelling model (1980b).

The momentum equation is,

$$\frac{D\bar{V}}{Dt} + fk\bar{X}\bar{V} = \frac{-1}{\rho_w}\nabla p + \frac{1}{\rho_w}\frac{\partial \bar{\tau}_z}{\partial z} + N_x \frac{\partial^2 \bar{V}_h}{\partial x^2} \qquad (1)$$

where, $\bar{V}$ is the water velocity vector, ρ_w is the water density, x is the across-ice direction, z is the vertical direction, V_h is the horizontal water velocity vector, p is pressure, N_x is the horizontal eddy viscosity , $\bar{\tau}_z$ is the stress, f is the Coriolis parameter and t is time.

The first term on the left is the total derivative of the velocity vector and the second expresses the Coriolis acceleration. The horizontal pressure gradient is given by the first term on the right, followed by the vertical and horizontal stress or friction. The variables and constants are listed in table II.

The rate of change of the scalars (eg. salinity, temperature, etc.) is given by,

$$\frac{\partial p}{\partial t} + u \frac{\partial p}{\partial x} + w \frac{\partial p}{\partial z} = K_z \frac{\partial^2 p}{\partial x^2} + K_x \frac{\partial^2 p}{\partial x^2} \qquad (2)$$

where, p is any scalar, K_z and K_x are the vertical and horizontal eddy diffusivities, u is the across-ice (x) water velocity component and w is the vertical (z) water velocity component.

Continuity is given by,

$$\nabla \cdot \bar{V} = 0 \qquad (3)$$

and the hydrostatic equation as derived from equation 1 is,

$$\frac{\partial p}{\partial z} = \rho_w g \qquad (4)$$

where g is the acceleration of gravity.

The equation of state used is that as given by Cox, McCartney and Culkin (1970), where density is a function of temperature and salinity. The pressure effect was considered insignificant because of the 70 m depth. The water temperature is held constant which is a reasonable assumption for early spring on the Bering Sea shelf (ice edge cruise data reports, 1982 and 1983). Now ρ_w is function of just salinity which can

be further justified because of the low water temperatures (-1.7 to 1°C) at that time of year. This is because density and salinty curves in the world's oceans at low temperatures are almost congruent.

The no slip condition is applied to the bottom requiring that the velocities go to zero right at the boundary. Both ends in the across-ice (x) direction are open which means that flows are allowed through the vertical boundaries. The Boussinesq approximation is applied where variations in density are assumed negligible except where multiplied by gravity as in the pressure term and the Richardson number calculation.

Below the mixed layer N_z (the vertical eddy viscosity) and K_z (the vertical eddy diffusivity) are functions of the Richardson (R_i) number as described by Hamilton and Rattray (1978),

$$K_z=50(1+3.33R_i)^{-1.5} \qquad (5a)$$

$$N_z=5+50(1+10R_i)^{-.5} \qquad (5b)$$

with R_i calculated as follows,

$$R_i = \frac{-g}{\rho_w} \frac{\partial \rho_w}{\partial z} / \left[\left(\frac{\partial u}{\partial z} \right)^2 + \left(\frac{\partial v}{\partial z} \right)^2 \right] \quad (6)$$

where, v is the along-ice (y) velocity component of the water.

The mixed layer is defined to be that region from the surface to a depth where the change in sigma-t over 5 m in the vertical direction is greater than 0.05 units. In the mixed layer N_z and K_z are functions of wind stress,

$$K_z = 50 \left| \vec{\tau} \right| \quad (7a)$$

$$N_z = 55 \left| \vec{\tau} \right| \quad (7b)$$

where, $\vec{\tau}$ is the wind stress vector.

Ice

The sea ice velocity calculations are from Roed and O'Brien (1983). This model incorporates stresses at the ice/atmosphere and ice/ocean interfaces. Stress imparted from the ice to the water is proportional to the fraction of the surface area covered by ice. This is important because in the MIZ ice compactness varies

Table 3: Variables and Constants for the Ice Model

Symbol	Variable	Units and value if const
A	percent ice cover	dimensionless
C_{wi}	ice/water drag coefficient	$8.6*10^{-2}$ cm/sec
h	thickness of ice	50 cm
P_m	percent ice melt per day	dimensionless
ρ_i	density of ice	0.92 g/cm^3
$\bar{\tau}_{ai}$	air/ice stress	dyne/cm^2
$\bar{\tau}_{wi}$	water/ice stress	dyne/cm^2
V_i	the ice velocity vector	cm/sec

from near 0% to 100%. In addition, Hibler (1979) claims that the ice acceleration term due to oceanic tilt is only important in long time scales (i.e., a year or longer) therefore it is left out of the momentum equations because the time scales of these experiments are of the order of the phytoplankton blooming period (5-14 days). A final simplification is that internal ice stress is only important in regions of fast ice, ice that is not free to move, for example, that which is frozen in place around barriers like coasts (Roed and O'Brien, 1983). Since the ice in this model is allowed to float free that term is eliminated.

With these simplifications ice acceleration is now a balance between the interfacial drags at the air/ice and ice/ocean interfaces and Coriolis acceleration. The momentum equation is,

$$\frac{D\bar{V}_i}{Dt} + fk\bar{X}\bar{V}_i = [\ \bar{\tau}_{ai} + C_{wi}\ (\bar{V} - \bar{V}_i)\ ]\ /\ \rho_i h \qquad (8)$$

where, $\bar{V}_i$ is the ice velocity, $\bar{\tau}_{ai}$ is the stress applied to the ice by the wind, C_{wi} is the drag coefficient, ρ_i is the density of the ice, h is ice thickness (see table III).

The two terms on the left are the total time derivative of the ice velocity, and Coriolis acceleration. On the right the first term in parenthesis is the air/ice drag. This vector ($\bar{\tau}_{ai}$) is taken as twice that of the air/ocean drag coefficient ($\bar{\tau}_{aw}$) (Feldman et al., 1981). The water/ice coupling term is $C_{wi}(\bar{V}_w-\bar{V}_i)$, where, C_{wi} is the water/ice drag coefficient as calculated by Mcphee (1979). The sign of the term indicates whether the ice is driving the water or the water is driving the ice.

The right hand side of the continuity equation for sea ice consists of an advective term and a melting term,

$$\frac{DA}{Dt} = \frac{\partial(Au_i)}{\partial x} - P_m A \qquad (9)$$

where, A is ice compactness and P_m is the melt rate.

This equation simply states that the change in the percent ice coverage over time is equal to the amount entering less the amount exiting (term 1 on the right) less the amount that melts (term 2 on the right).

At times ice compactness of over 100% is cal-

culated. This occurs because for computational simplicity in the calculation of compactness we assume that ice thickness (h) is a constant (50 cm). Therefore, a percent ice coverage of over 100 is interpreted as an increase in h or a "piling up" of the ice.

Melting is a complicated function of heat input from ocean and atmosphere ice age. salinity and compactness (Langleben. 1972). The thermodynamics of ice melt is beyond the scope of this study. therefore we assumed that heat input is constant and that melt rate is a linear function of ice compactness.

$P_m=1.01-0.01A$ $0.01<=A<=0\ 95$ (10)

$P_m=0.01$ $A>0\ 5$ (11a)

$P_m=1.0$ $A<0\ 01$ (11b)

For simplicity it is assumed that at concentrations over 95% the melt rate is 1% per day. At concentrations under 1% the melt rate is a constant 100% per day. Using this melting scheme the maximum input of fresh water into the system occurs at approximately 50% ice coverage (figure 3). The change in salinity of the

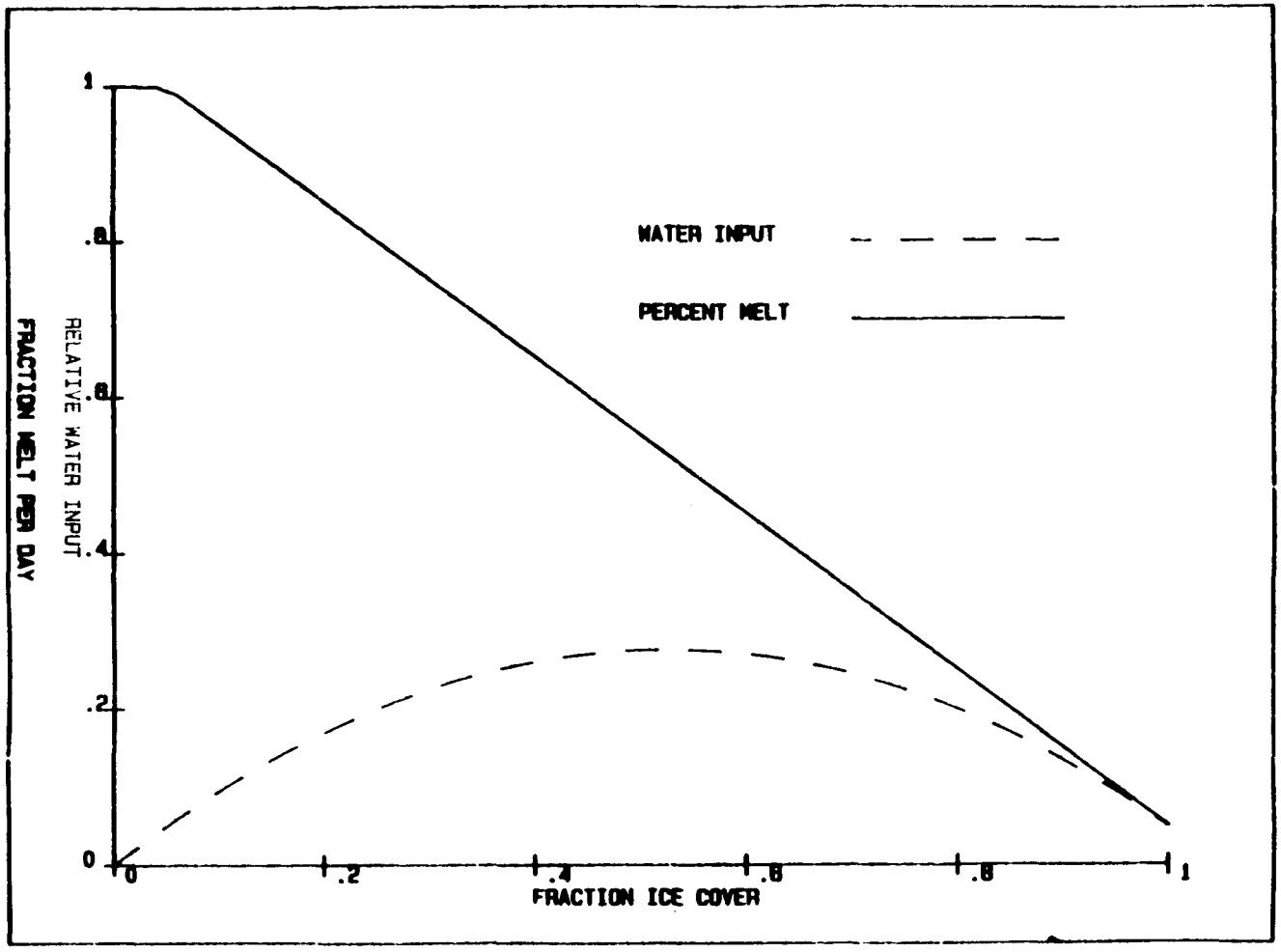

FIGURE 3: PERCENT MELT AS A FUNCTION OF COMPACTNESS AND THE RESULTANT RELATIVE WATER INPUT

water due to this melting is modelled as a salt flux,

$$\frac{\partial S}{\partial t} = \frac{-S\Delta z}{\Delta z + P_{ms} A h \Delta t} \left(\frac{1}{\Delta t} \right) \qquad (12)$$

where, S is salinity and Δz is the water depth increment, Δt is the time step and P_{ms} is the fraction melted per second ($P_m/84600$).

The salinity of the ice is a constant 10 ppt for all the experiments (Reeberg and Springer-Young, 1983).

Biological dynamics

The general equation for nutrient and biological dynamics is:

sources and sinks=

$$\frac{\partial p}{\partial t} - \nabla \cdot \bar{V} p - \nabla_L \cdot K_x \nabla_L p + K_z \frac{\partial^2 p}{\partial z^2} \qquad (13)$$

here phi represents scalars such as phytoplankton particulate nitrogen, NO_3, NH_4, etc. and ∇_L

Table 4: Variables and Constants for the Biological Dynamics

Symbol		Variable Units and Value if Const
Chl	chlorophyll concentration	mg/m^3
G	grazing rate	1/sec
G_r	growth	mg/sec
I	light intensity	$einsteins/m^2/sec$
I_{max}	maximum irradiation for the day	$einsteins/m^2/sec$
I_o	light intensity on deck	$einsteins/m^2/sec$
I_s	the irradiation for which photosynthesis is max.	1 $einsteins/m^2/hr$
I_t	total irradiation per day	$einsteins/m^2/day$
I_z	ligth intensity at depth z	$einsteins/m^2/sec$
K_n	the concentration of nutrient nitrogen that produces $0.5V_{max}$	24.78 mg/m^3
N	nitrogen concentration in water	mg/m^3
N_i	nutrient concentration in ice	0 mg/m^3
P	phytoplankton concentration in water in terms of	mg N/m^3

	nitrogen	
P_i	phytoplankton concentration in ice in terms of nitrogen	mg N/m^3
P_h	photosynthesis in terms of nitrogen uptake	mg N/sec
ψ	proportionality constant relating uptake NH_4:NO_3	dimensionless
P_{max}	maximum photosynthetic rate in terms of nitrogen	mg N/sec
r	time of sunrise	sec
R_e	regeneration rate (other organisms)	1/sec
R_p	extracellular release rate constant or phytoplankton.	1/sec
R_z	excretion rate constant of zooplankton	1/sec
s	time of sunset	sec
S_k	sinking velocity of plants	m/sec
V_m	maximum uptake rate constant for inorganic N NH_4 + NO_3	0.05 1/hr
V_n	uptake rate of inorganic N	1/sec
Z	zooplankton in terms of N	mg N/m^3

is the horizontal operator ($\hat{i}\frac{\partial}{\partial x} + \hat{j}\frac{\partial}{\partial y}$).

The first term on the right is the local time derivative, the second is the advective term and the last is the change caused by the x-z turbulent mixing. To simplify the equation two assumptions are used:

1- mass is conserved therefore the velocity field is non-divergent and,

2- from the ocean section, all derivatives in the along-ice (y) direction are zero.

Now equation 13 reduces to,

sources and sinks=

$$\frac{\partial p}{\partial t} + u\frac{\partial p}{\partial x} + w\frac{\partial p}{\partial z} - K_x\frac{\partial^2 p}{\partial x^2} - K_z\frac{\partial^2 p}{\partial z^2} \qquad (14)$$

Much of the data from the Bering Sea ice edge in the spring indicates that the magnitude and duration of the bloom is ultimately limited by the amount of inorganic nutrient nitrogen available (Alexander and Niebauer, 1981; Niebauer and Alexander, 1984). The biological dynamics of this model can be expressed by

the relationship between:

1- the concentration of dissolved inorganic nitrogen in the water (mg N/m^3) and,

2- the concentration of chlorophyll in the water (mg Chl/m^3).

To calculate the chlorophyll, we first calculate phytoplankton in terms of the concentration of particulate nitrogen in the water (i.e., the total mass of nitrogen that is incorporated into the phytoplankton biomass divided by the water volume, mg phytoplankton N/m^3). We assume that very little detritus is present at this time of year in the region. This ratio is then multiplied by the chlorophyll/(particulate nitrogen) ratio (1/15.75) as calculated by Caperon et al. (unpublished data).

The sources of particulate nitrogen are nutrient uptake (insitu growth) and the input of ice algae from melting. The sinks for particulate nitrogen are grazing by zooplankton, the extracellular release , sinking and decomposition resulting in the regeneration of particulate nitrogen to inorganic nutrient nitrogen. The sources of nitrogen are the extracellular release

by phytoplankton, zooplankton excretion, the regeneration of phytoplankton to nitrogen and the input from the melting ice. The sink for inorganic nutrient nitrogen is the uptake by phytoplankton. In equation form,

$$\text{sources and sinks}_{(P)} = UP - G_r P - R_p P - \frac{S_k P}{\Delta z} + AP_i P_m \frac{\rho_i h}{\rho_w \Delta z} - R_e P \qquad (15)$$

$$\text{sources and sinks}_{(N)} = -UP + R_e P + R_z Z + R_p P + AN_i P_m \frac{\rho_i h}{\rho_w \Delta z} \qquad (16)$$

where, P is phytoplankton particulate nitrogen concentration in the water column, U is the uptake rate of that nutrient by phytoplankton, G_r is the grazing rate of zooplankton on phytoplankton, S_k is the sinking velocity, P_i is the concentration of ice algae in the ice in terms of particulate nitrogen, P_m is the rate of ice melt, N is the inorganic nutrient nitrogen concentration in the water column, N_i is the inorganic nutrient

ice, Z is the

terms of particulate

of the ice ρ_i is

ρ_w the density of

e of the zooplank-

ase rate of nitrogen

st of the regenera-

rger animals, etc.; a

(1984) n of less than 50 mg

Bering Sea ice in the

ant 50 cm thickness

verything within this

refore the nitrogen

ller-Karger (1984) is

over our 50 cm thick-

tration we assume the

is negligible and

the right of equation

cellular release of

refore the third term

fourth (equation 16)

and Coyle (1982) imply

that there is only a small biomass of zooplankton present in the early spring on the Bering Sea shelf, term 2 on the right (equation 15) and term 3 (equation 16) are considered negligible. Regeneration and recycling of nitrogen are handled in terms 6 (equation 15) and 2 (equation 16). Now equation 15 and equation 16 reduce to,

$$\text{sources and sinks}_{(P)} = UP + AP_i P_m \frac{\rho_i h}{\rho_w \Delta z} - R_e P - \frac{S_k P}{\Delta z} \tag{17}$$

$$\text{sources and sinks}_{(N)} = -UP + R_e P \tag{18}$$

Of primary interest in this study is total particulate nitrogen. It appears that in short time scales the form that most of the regenerated nitrogen takes is ammonium (Goering and Iverson, 1981). This is usually the preferred form of the nutrient because its incorporation into macromolecules is more energy efficient. This leads to almost steady state conditions between ammonium and particulate nitrogen in the non-light limited mixed layer (Goering and Iverson,

1981). Therefore within the mixed layer term 3 on the right (equation 17) and term 2 on the right (equation 18) are eliminated. However at depths greater than this it is assumed that 1/3 of the phytoplankton nitrogen is decomposed to nutrient nitrogen per day (Sambrotto, 1983). For simplicity, we do not attempt to separate the various types of nutrient nitrogen (e.g., nitrate, nitrite and ammonium). One value is calculated for the total inorganic nutrient nitrogen available.

Uptake

Uptake of nitrogen by phytoplankton is a multivariate function;

$$U=U(N, T, I_z, t) \qquad (19)$$

where, I_z is the ambient light intensity,

Wroblewski (1977) gives the following equation for the uptake of ammonium and nitrate as a function of the

concentration of each, assuming the other factors (T, I_z) are constant and not limiting. This formula takes into account the suppression of nitrate uptake by increasing concentrations of ammonium because the latter is preferred.

$$V_n = V_m \left[\frac{NO_3 \exp(-\Psi NH_3)}{K_n + NO_3} + \frac{NH_3}{K_n + NH_3} \right] \quad (20)$$

where, V_n is the "velocity" (biologist jargon for non-specific rate, units 1/time) of the uptake, K_n is the concentration that produces $.5V_m$, V_m is the maximum rate of uptake, NO_3 and NH_3 are expressed in units of concentration and Ψ is a constant that is calculated from measurements for each species within a location.

Since we lumped all the nitrogen into one term, equation 20 is simplified to the standard Michaelis-Menten (Parsons, Takahashi and Hargrave, 1979) relationship;

$$V_n(N) = \frac{V_m N}{K_n + N} \quad (21)$$

Light

In addition to nutrient concentration, uptake is dependent on temperature, diel and annual periodicity and light intensity. Photosynthesis in some high latitude marine algae does appear to have some temperature dependence below 0°C (Neori and Holm-Hansen, 1982). In this model we hold the temperature at a constant 1°C and therefore neglect that relationship. In his Peru upwelling model Walsh (1975b) included a diel as well as seasonal signal in V_n. In our model periodicity is controlled by light input and the seasonal signal is unimportant because of the short time scales, 7-10 days. Uptake as function of light and nitrogen concentration is now,

$$U = P_h (I) \frac{V_m N}{K_n + N} \qquad (22)$$

where, $P_h(I)$ is photosynthesis as a function of light intensity.

We assume that light intensity and inorganic nitrogen concentration each independently regulate photosynthetic rate. Covering a broad range of condi-

tions Steele (1962) gives the following expression for the rate of photosynthesis measured by carbon uptake as a function of light intensity.

$$P_h = P_{max} \frac{I_z}{I_s} \exp \left(1 - \frac{I_z}{I_s} \right) \qquad (23)$$

where, I_s is the light intensity for which P_h is a maximum, P_{max} is the maximum photosynthetic rate and I_z is the ambient light intensity at a specific depth.

This formula describes the effects of photoinhibition. Primary productivity measurements conducted by Muller-Karger (1984) during the ice-edge cruises of 1982 and 1983 indicate photoinhibition was present at times within the upper 10m. Normalizing this equation by dividing by P_{max} and assuming that nitrogen uptake is linearly related to carbon uptake, the equation is,

$$U = \frac{I_z}{I_s} \exp \left(1 - \frac{I_z}{I_s} \right) V_m \frac{P}{K_n + N} \qquad (24)$$

V_m and K_n are assumed constant (see table 4 for values).

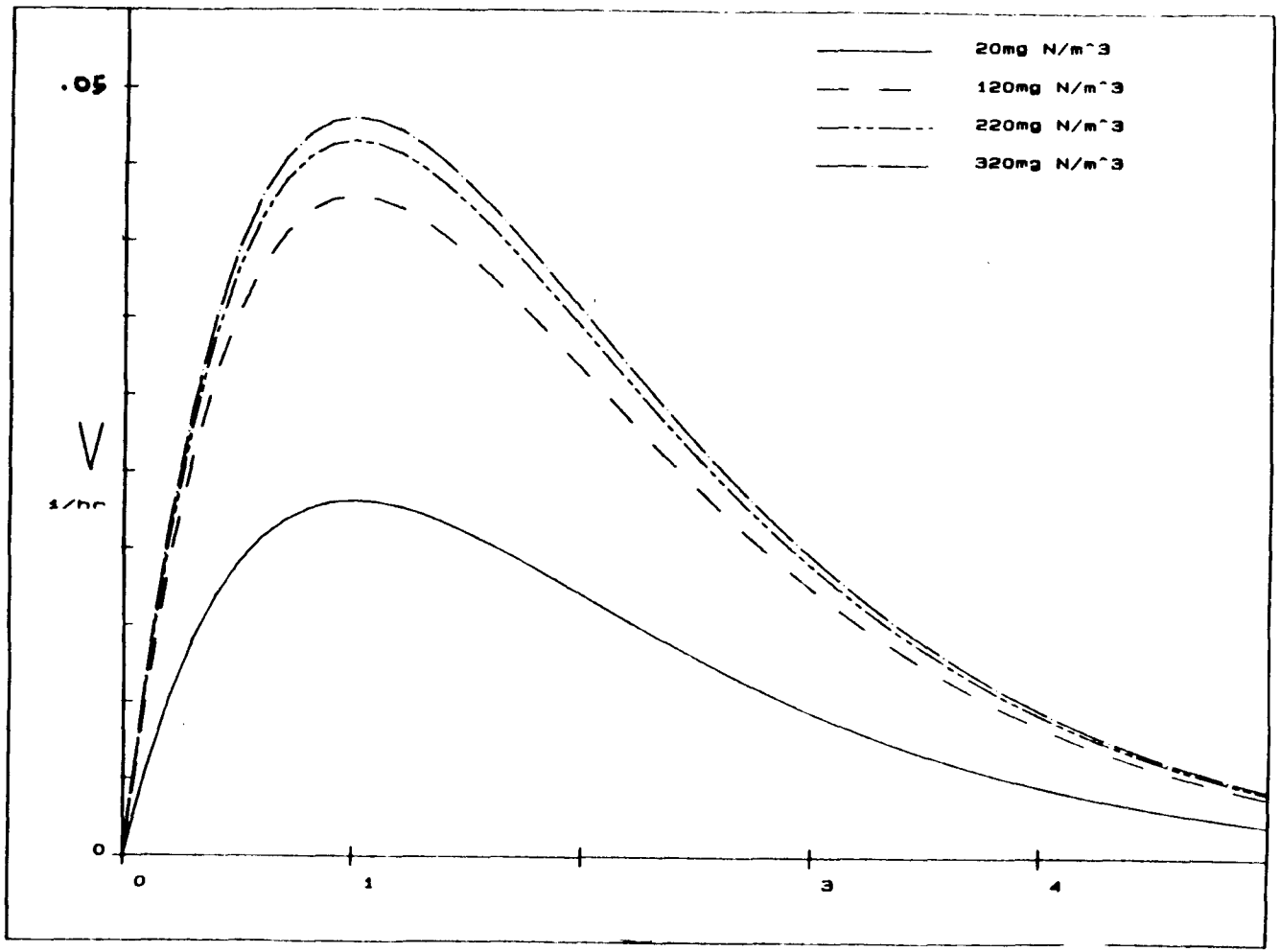

FIGURE 4: PHYTOPLANKTON UPTAKE OF NITROGEN AS A FUNCTION LIGHT INTENSITY AND NITROGEN CONCENTRATION

Values of U under varying conditions of light and nitrogen concentrations are shown in figure 4. As light increases, at first photosynthesis increases, then after reaching approximately 1 einstein $m^{-2}hr^{-1}$ it begins to decrease, quickly at first then slower. The point of photoinhibition is within the range of that measured at the Bering Sea ice edge (Muller-Karger, 1984). The lowermost curve is for 20 mg N/m^3 which we chose arbitrarily. Successive curves are 100 mg N/m^3 apart. The difference in nutrient concentration between the four curves of figure 4 are equal (100 mg N/m^3). It may be noted that as the concentrations increase the the change in the uptake rate decreases (i.e. increasing concentration does not increase uptake linearly, but hyperbolically).

To calculate the variations in light with time it is assumed that day one of all the experiments is May 1. The integral of incoming solar radiation, approximately 30 einsteins m^{-2} day^{-1}, for that day was determined by a mean value using the PROBES data reports (82-009). The mean increase in light was about 0.75 einsteins m^{-2} day^{-1}.

Hourly variations in incoming solar radiation above the sea surface are given by,

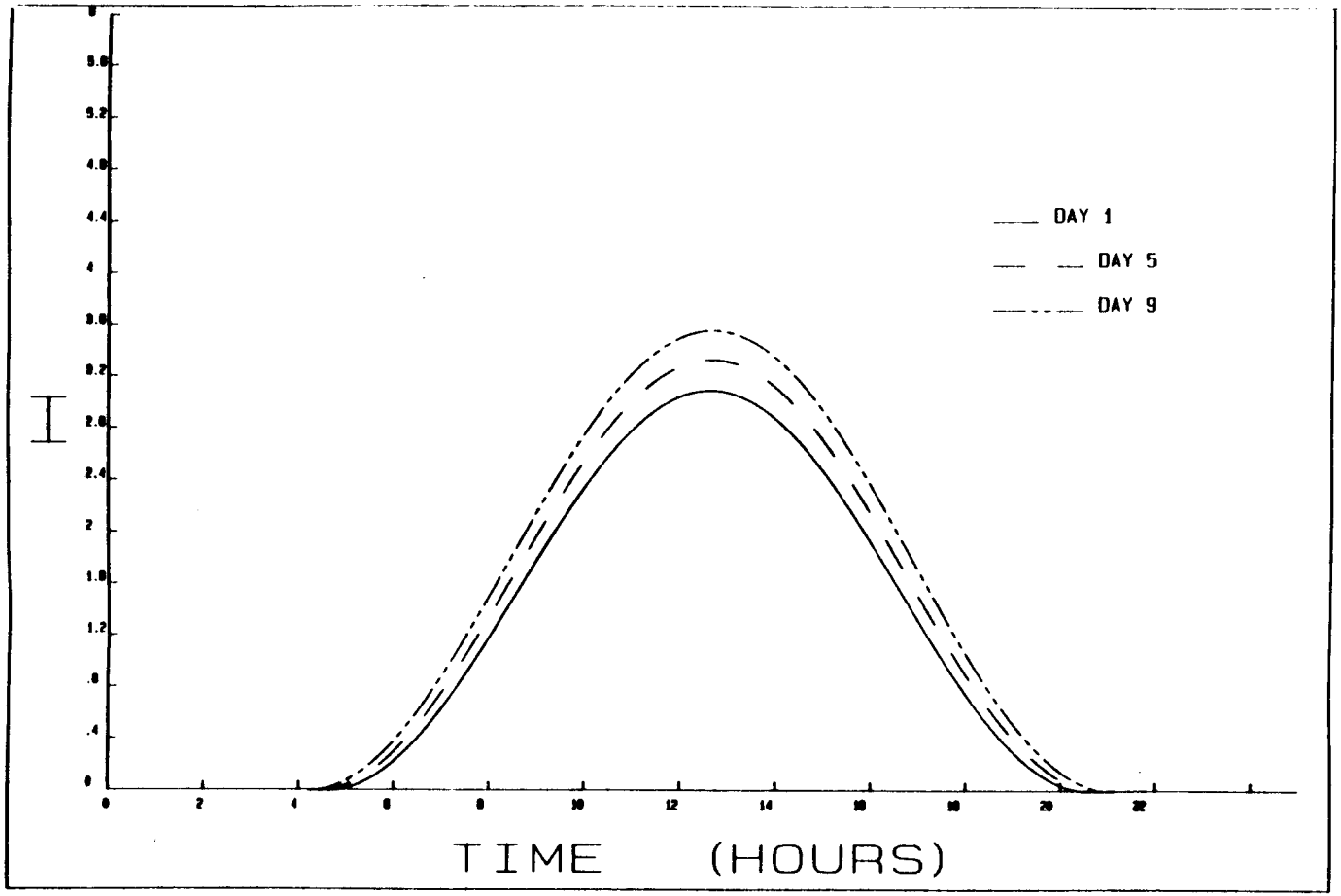

FIGURE 5: LIGHT INTENSITY AT OCEAN SURFACE AS A FUNCTION OF MODEL DAY NUMBER AND TIME OF DAY

$$I = I(t) - 0.5I_{max} \left(-\text{Cos} \left(2\pi \frac{t}{s - r}\right) + 1 \right) \qquad (25)$$

where, s is the time of sunset, r is the time of sunrise and I_{max} is the the maximum radiation (at midday when t=0.5* (s-r))

The change in the time of sunrise and sunset in early May is approximately,

$$dr/dt=-0.05 \text{ hr/day} \qquad (26a)$$

$$ds/dt=0.05 \text{ hr/day} \qquad (26b)$$

I_{max} is calculated from equation 25,

$$I_T = \int_r^s 0.5 \, I_{max} \left[\left(-\text{COS} \frac{2\pi t}{s - r} \right) + 1 \right] dt$$

where, I_t is the total input of light energy each day.

This implies that,

$$I_{max} = \frac{2I_t}{\int_r^s \left[-\text{COS} \left(\frac{2\pi t}{s - r} \right) + 1 \right] dt}$$

Examples of daily light curves are shown in figure 5. As the season progresses light intensity at any particular time of the day as well as day length increase.

From the ice edge cruises of 1982 and 1983 the ratio of light directly below surface to that on deck varied from .2 to .65 with a mean of ~0.4. Therefore, directly below the surface we use 0.4*I as the light intensity. Subsequently, light falls off with depth as:

$$I_z = I_o \exp(-kz) \qquad (27)$$

where, I_o is the light intensity in the water at the surface and k is the extinction coeffient given by Riley (1956) and adjusted to Bering Sea water.

The coefficients of each of the terms for k were adjusted such that they generated the best correlation coefficient to the data collected by on the Bering Sea ice edge cruises of 1982 and 1983,

$$k=.06+.007Chl+.04Chl^{3/4} \qquad (28)$$

where Chl is chlorophyll concentration.

This equation assumes that chlorophyll is homogeneous in the water column which is not always the case. Therefore a new k is calculated for each depth and $I_{z-\Delta z}$ is substituted for I_o. The equation of light with depth is now,

$$I_z = I_{z-\Delta z} \exp(-k\Delta z) \qquad (29)$$

where Δz is the depth increment of the grid.

A comparison of model generated light curves with real data is shown in figure 6. It appears as though the curves fit better where chlorophyll values are low (figure 6a) and the model slightly underestimates light levels where chlorophyll is high (figure 6b).

Sinking

For the purposes of this model sinking rate is

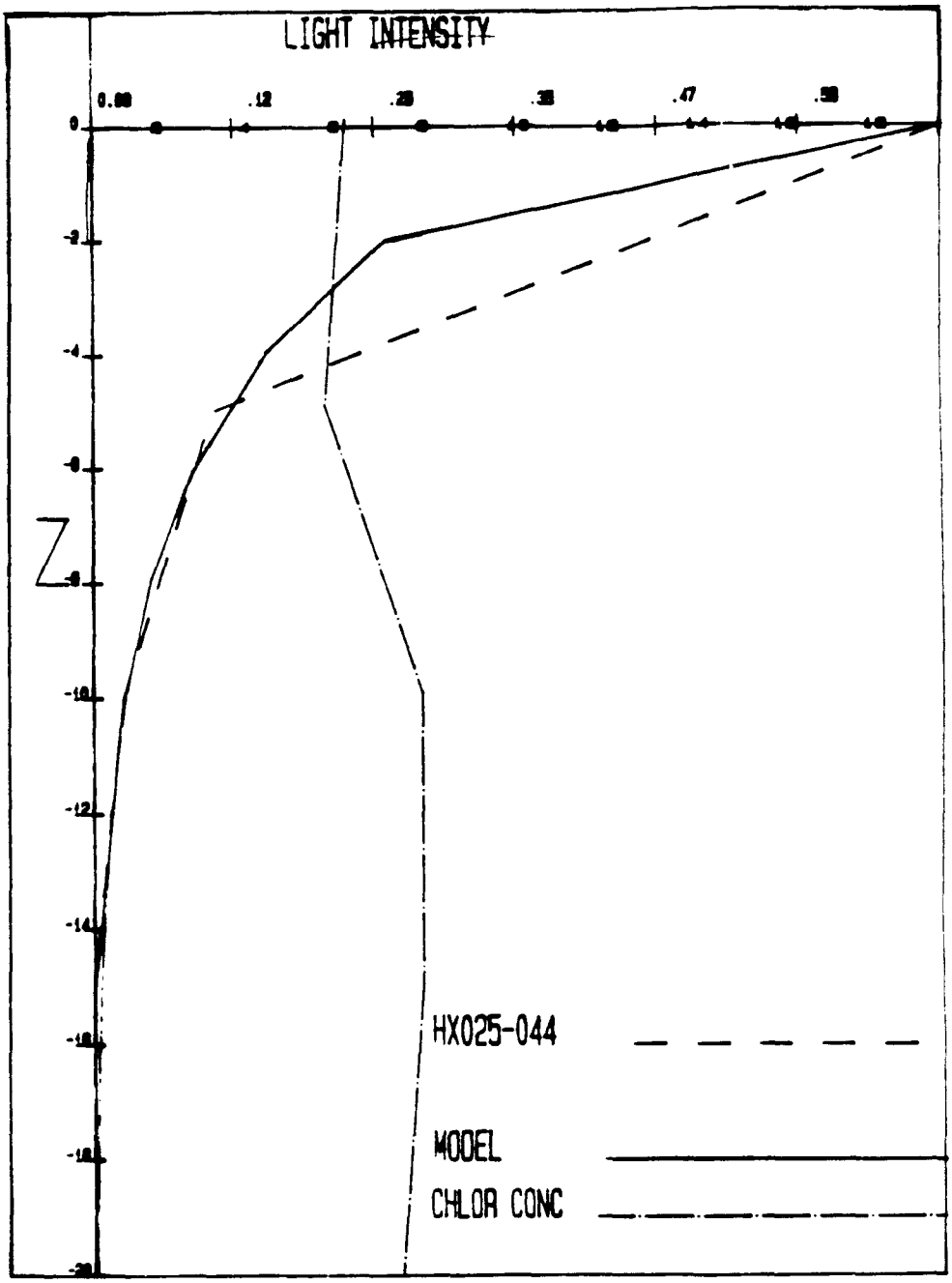

FIGURE 6A: LIGHT WITH DEPTH, MODEL VS. REAL DATA
1982 ICE EDGE CRUISE STA. 19, LOW CHLOR. VALUES

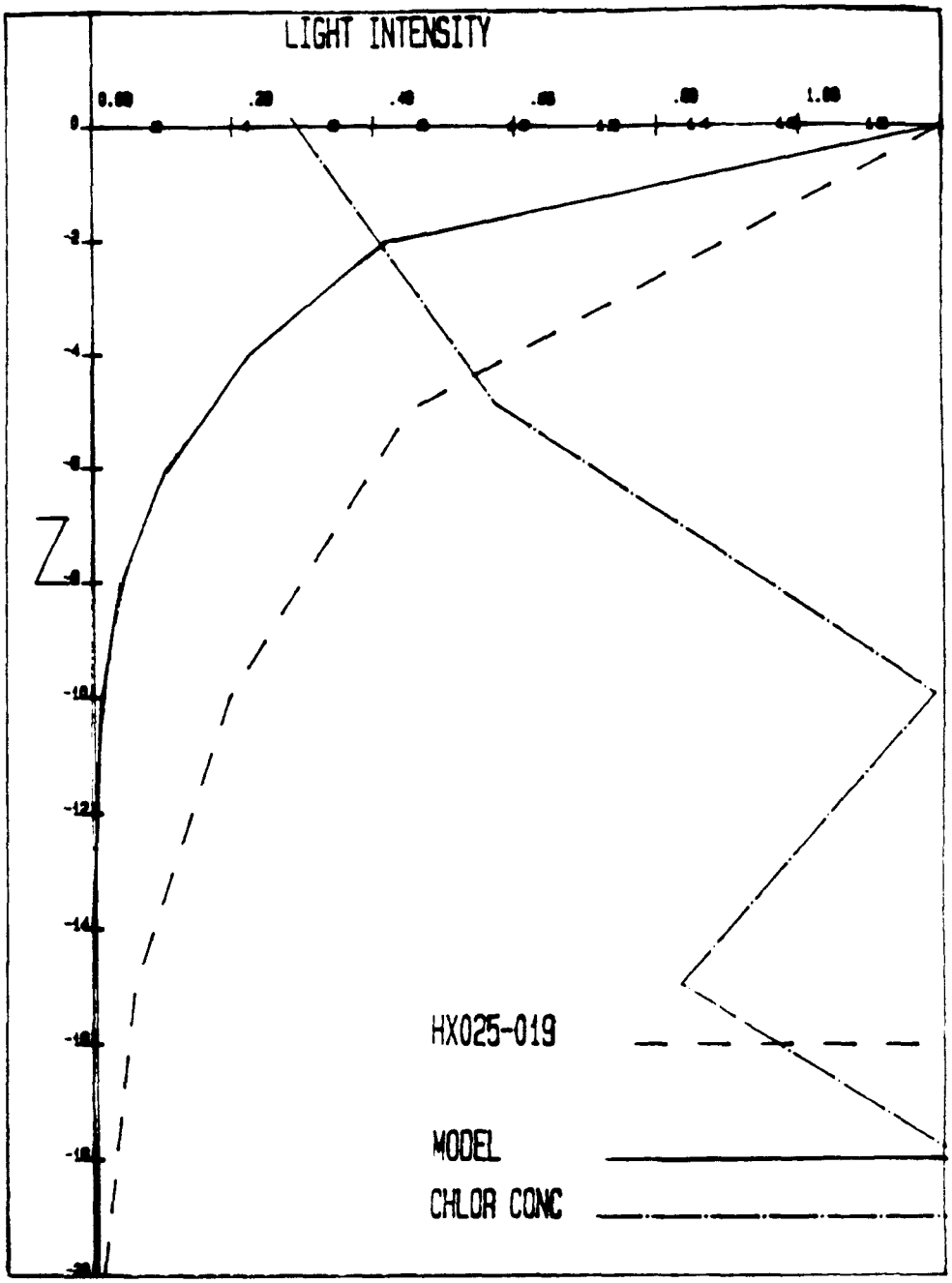

FIGURE 68: LIGHT WITH DEPTH, MODEL VS. REAL DATA
1982 ICE EDGE CRUISE STA. 19, HIGH CHLOR. VALUES

defined as settling velocity. There are two ways in which the ratio of vertical displacement of phytoplankton with time can vary:

1- settling velocity, and

2- vertical turbulence.

In a stratified water column the ratio of vertical displacement of phytoplankton to time is smaller than in one which is unstratified. The causative factors are:

1- In the unstratified case the vertical turbulence is greater, and

2- If the the mixed layer is shallower than the euphotic zone and if nutrients are available then the algae are assumed "healthier". This usually implies that the mass to surface area ratio is smaller thereby decreasing their settling velocity (Eppley et al., 1967).

The first of the above is accounted for in the model physics. The second is handled as suggested by Eppley et al. (1967) with 0.5 to 2 m per day as a mean sinking velocity. This is the base rate used in the model.

When light and nutrients are adequate they sink at 0.5 meters per day, when either is deficient the rate is 2 meters per day. At night, if light and nutrients were adequate during the day the sinking rate is calculated at the slower velocity.

Results

Four general case studies are presented each with several experiments (table 1). In case I, the physical oceanographic and ice cover response to varying directions of a constant one dyne/cm^2 (approximately 8 m/sec or 16 knots) wind is presented. In case II melting of ice is considered with its effects on water and ice movement. The hypothesis that the ice algae seed the bloom, by their release into the water column by melting, is also considered. In case III we consider the effects of both wind forcing and melting on ice edge phytoplankton blooms with algae in both ice and water. Case IV addresses the hypothesis that wind driven ice edge upwelling prolongs the bloom.

The output of each model run consists of fields of horizontal and vertical water velocities, stratifica-

tion, ice velocities, percent ice cover and chlorophyll and nitrogen concentrations. The contour intervals unless otherwise noted are, 0.2 sigma-t units, 50 mg N/m^3, 5 mg chl/m^3 and 50 % ice cover. Wind directions are noted in the upper left hand corner of the appropriate figures. In addition, time series of ice and water velocities, chlorophyll and nitrogen concentrations are presented.

Case I: the response of the model to wind forcing

The first case illustrates the differences in the response of the ocean and ice to wind stress along-ice (y), case Ia and across-ice (x), case Ib. The initial hydrography and ice cover for each of the experiments are shown in figure 7. The water column is slightly stratified below 30 m to aid in model stability. This may be justified by data taken on the ice edge cruise of 1983. There is a 20 km region of 100% ice cover at the surface away from either vertical boundary. This enables us to look at the water column and ice dynamics at both the following and leading ice edges. A wind stress of 1 $dyne/cm^2$ (8 m/sec, 16 knots) is applied for

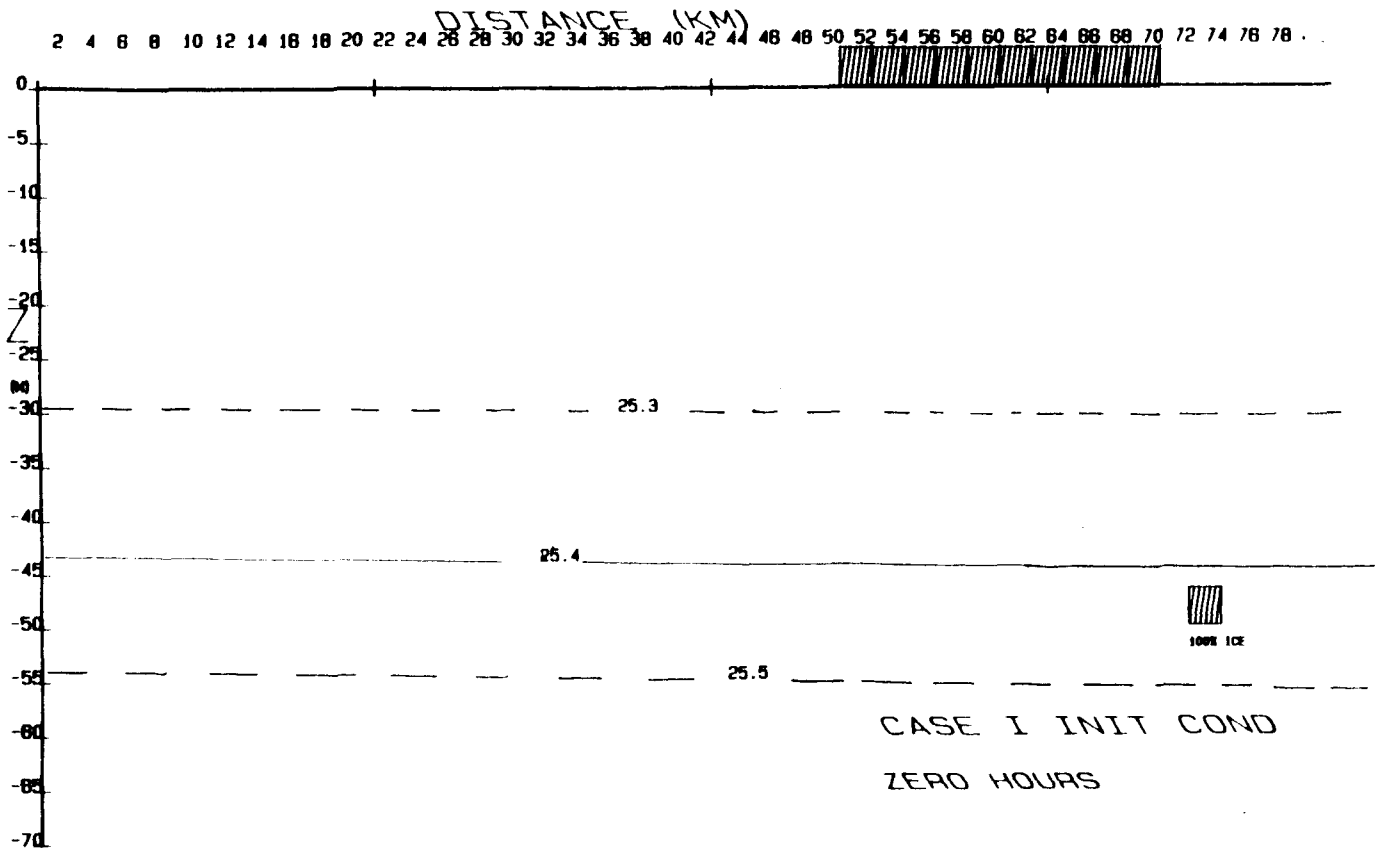

FIGURE 7: INITIAL CONDITIONS CASE I

the first 18 hours and then turned off for the duration of the experiments, 96 hours total for each case.

Case Ia: along-ice (y) wind

ice velocities and position

With the wind blowing along-ice with ice to the left (neg. y) (figure 8) there is Ekman transport of ice as indicated by the ice vectors. The leading ice edge is located at the 50km position at zero hours and has moved 4 km in eight hours (approximately 14 cm/sec) to the 46 km position (figure 8). Likewise the following edge has moved 4 km from the 70 km to the 66 km location. The ice has thinned out at the edges with the leading edge containing approximately 50% and the following 30% cover. The ice in the main pack is moving faster than the ice at the leading edge which results in a "pile up" of ice in the vicinity (50 km) of the original leading edge where ice cover fractions are in excess of one (figure 8). The reason the ice velocities are at a maximum in regions of high ice cover is that the water under these areas is moving faster because ice/water coupling is a function of compactness. This water velocity carries the ice along

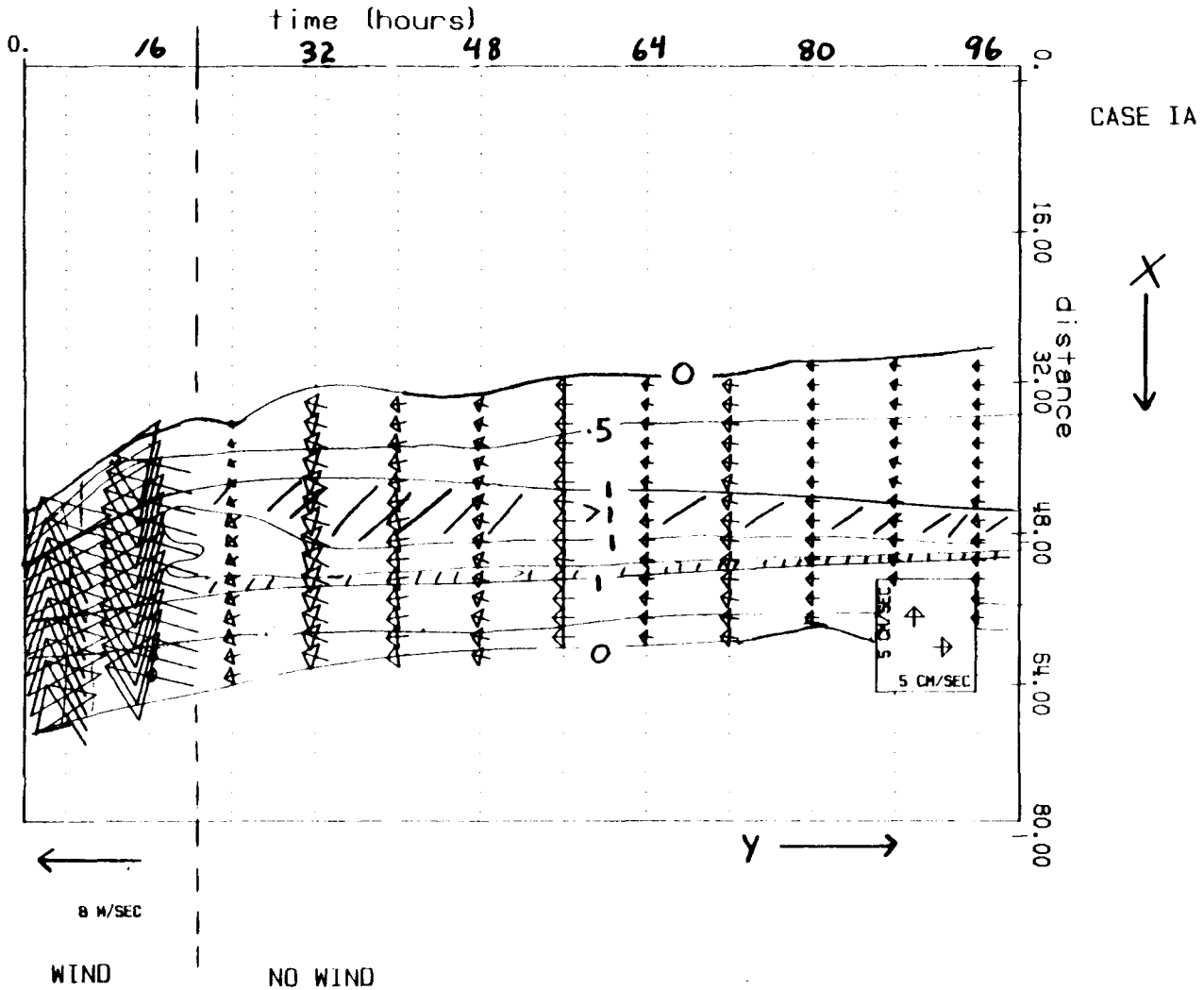

FIGURE 8: CASE IA, TIME SERIES OF ICE VELOCITIES AND COMPACTNESS
CONTOUR INTERVAL=0.5

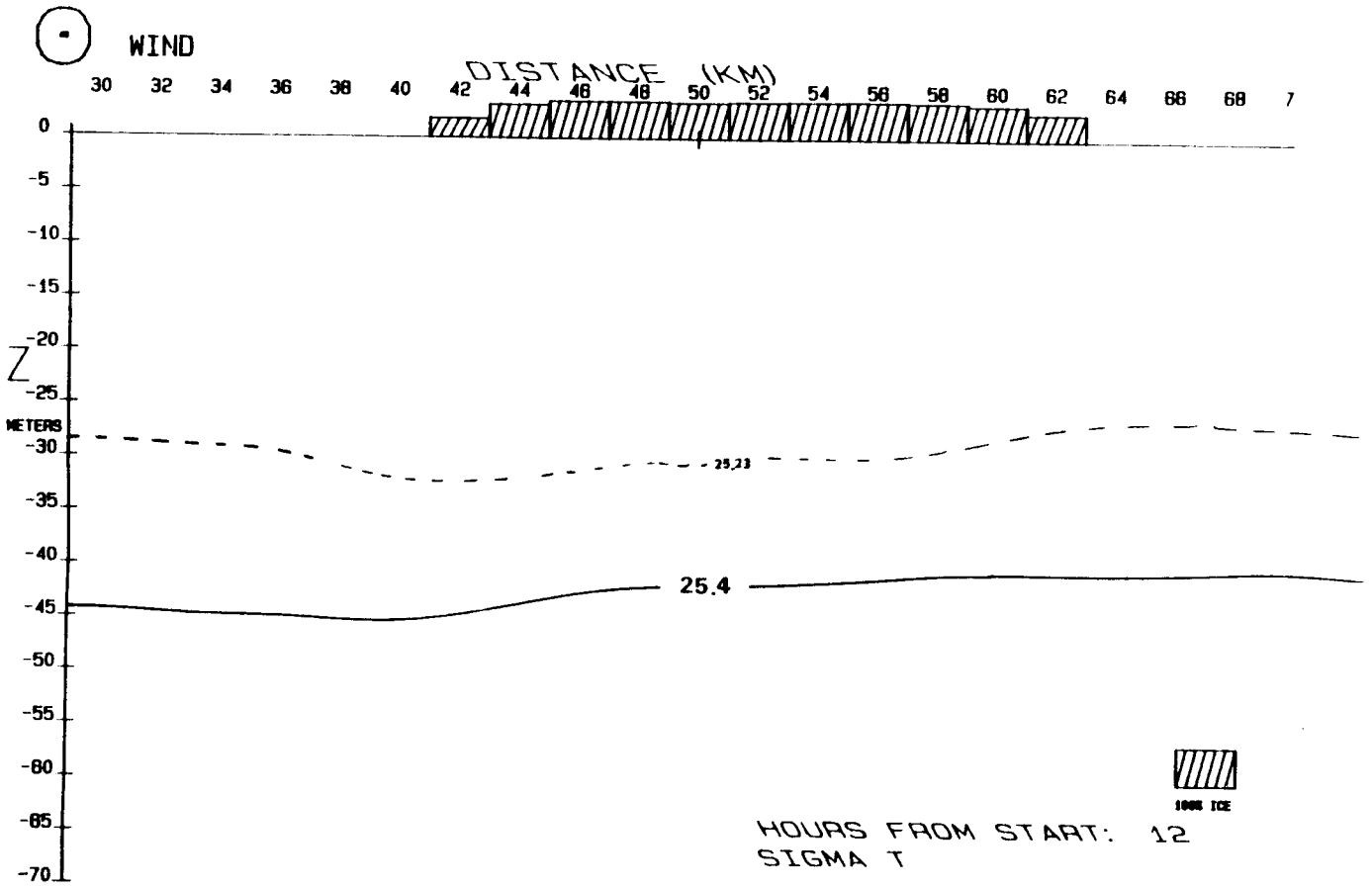

FIGURE 9A: CASE IA, AT 12 HOURS

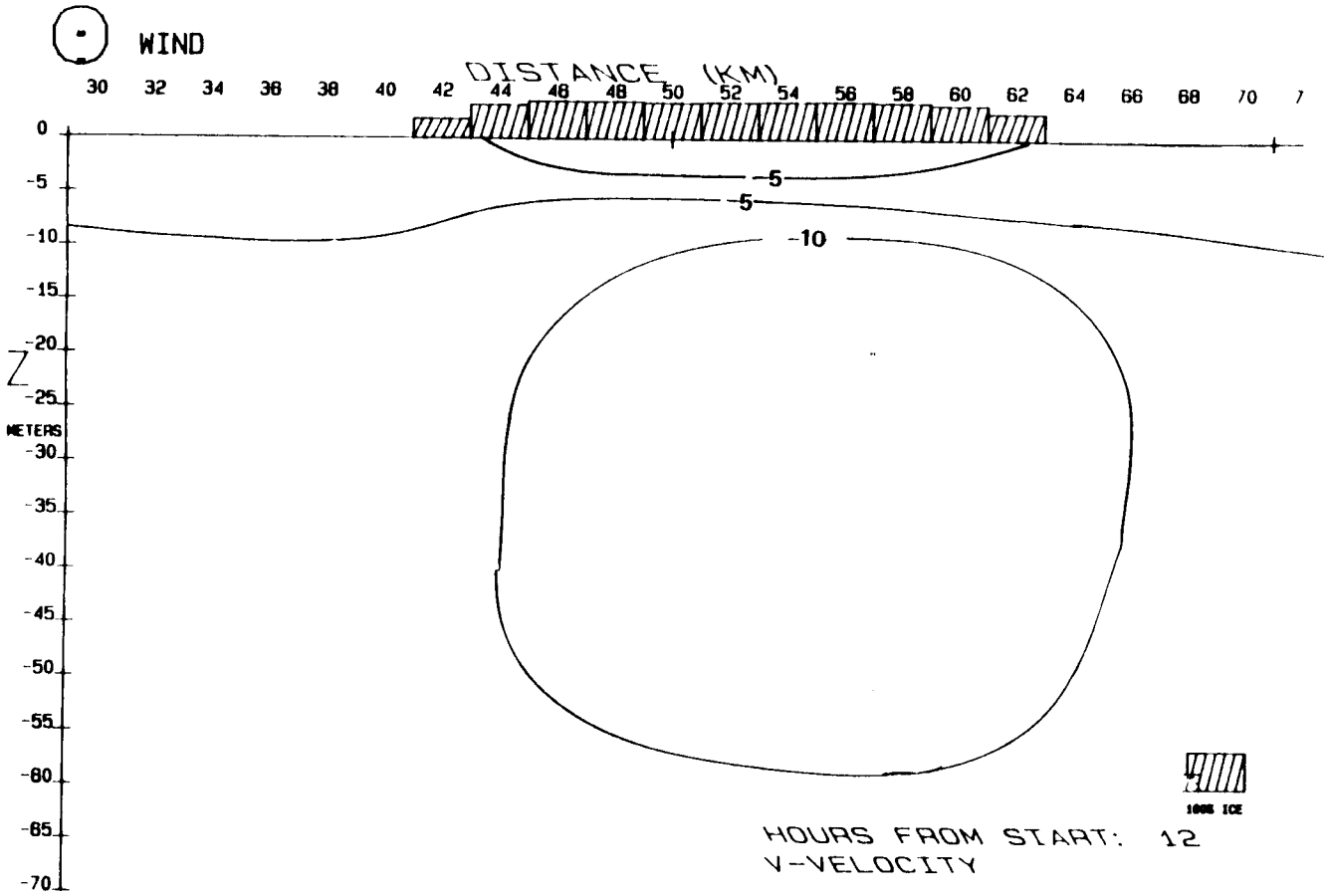

FIGURE 9B: CASE IA, AT 12 HOURS, ALONG-ICE VELOCIY

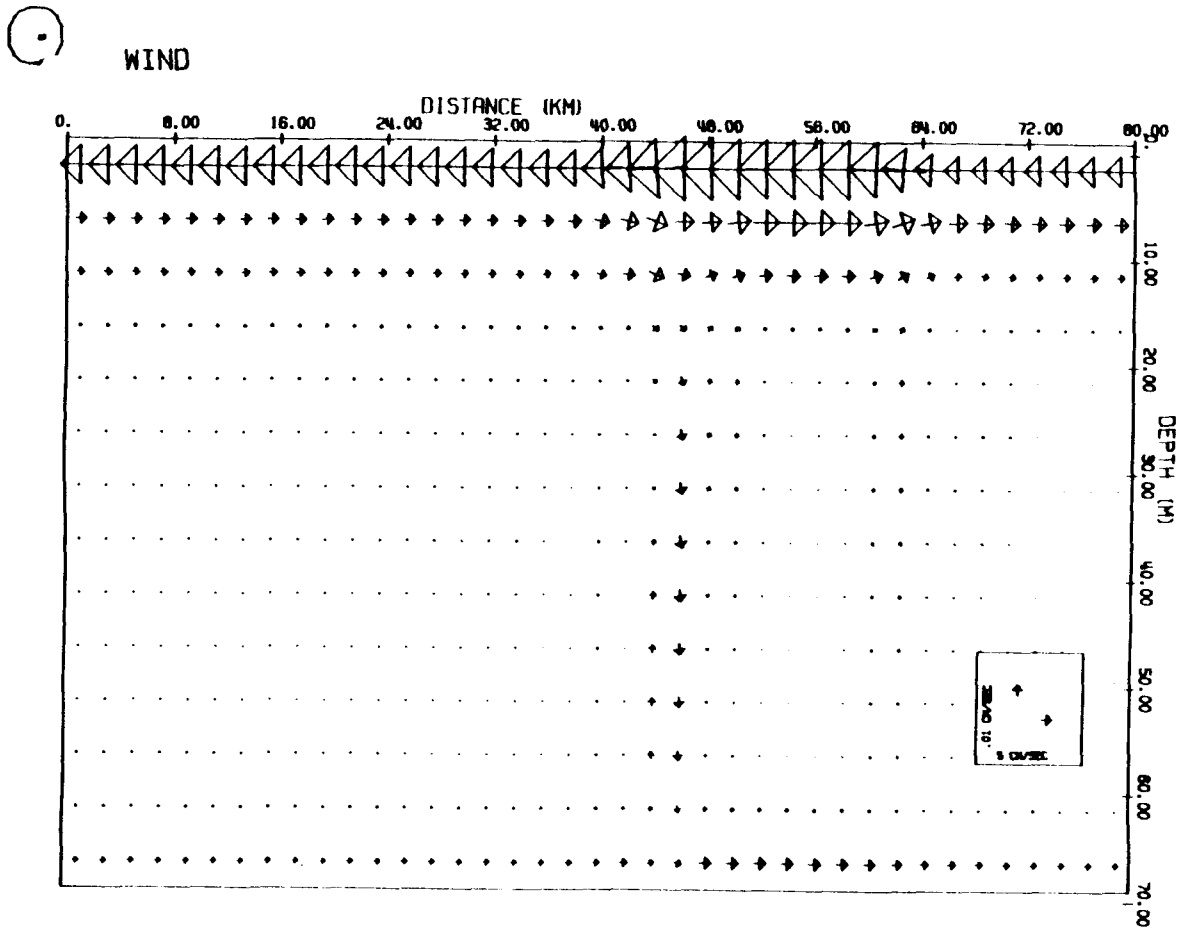

FIGURE 9C: CASE IA, AT 12 HOURS, ACROSS-ICE/VERTICAL VELOCITY ARROW PLOT

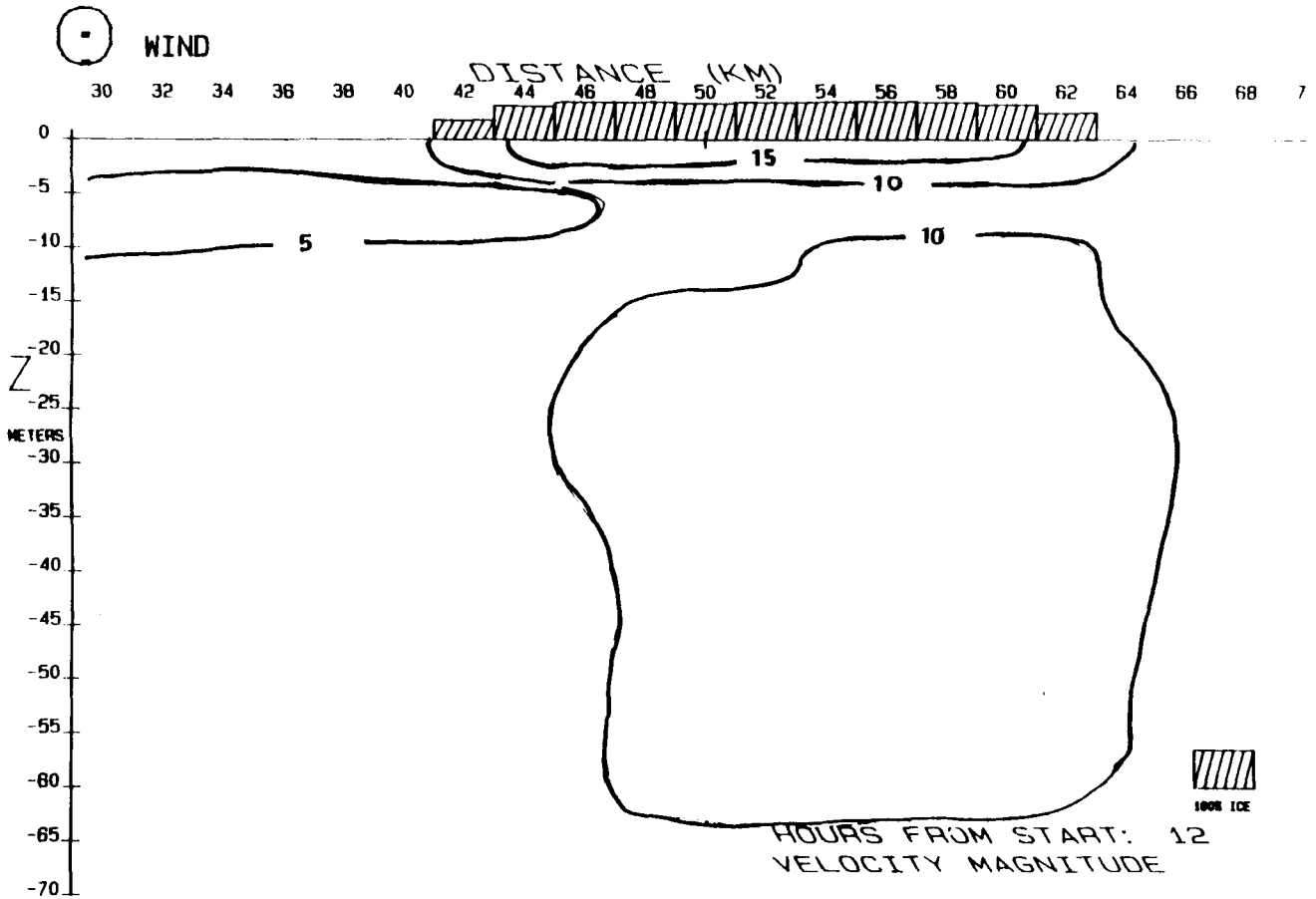

FIGURE 9D: CASE IA, AT 12 HOURS, VELOCITY MAGNITUDE

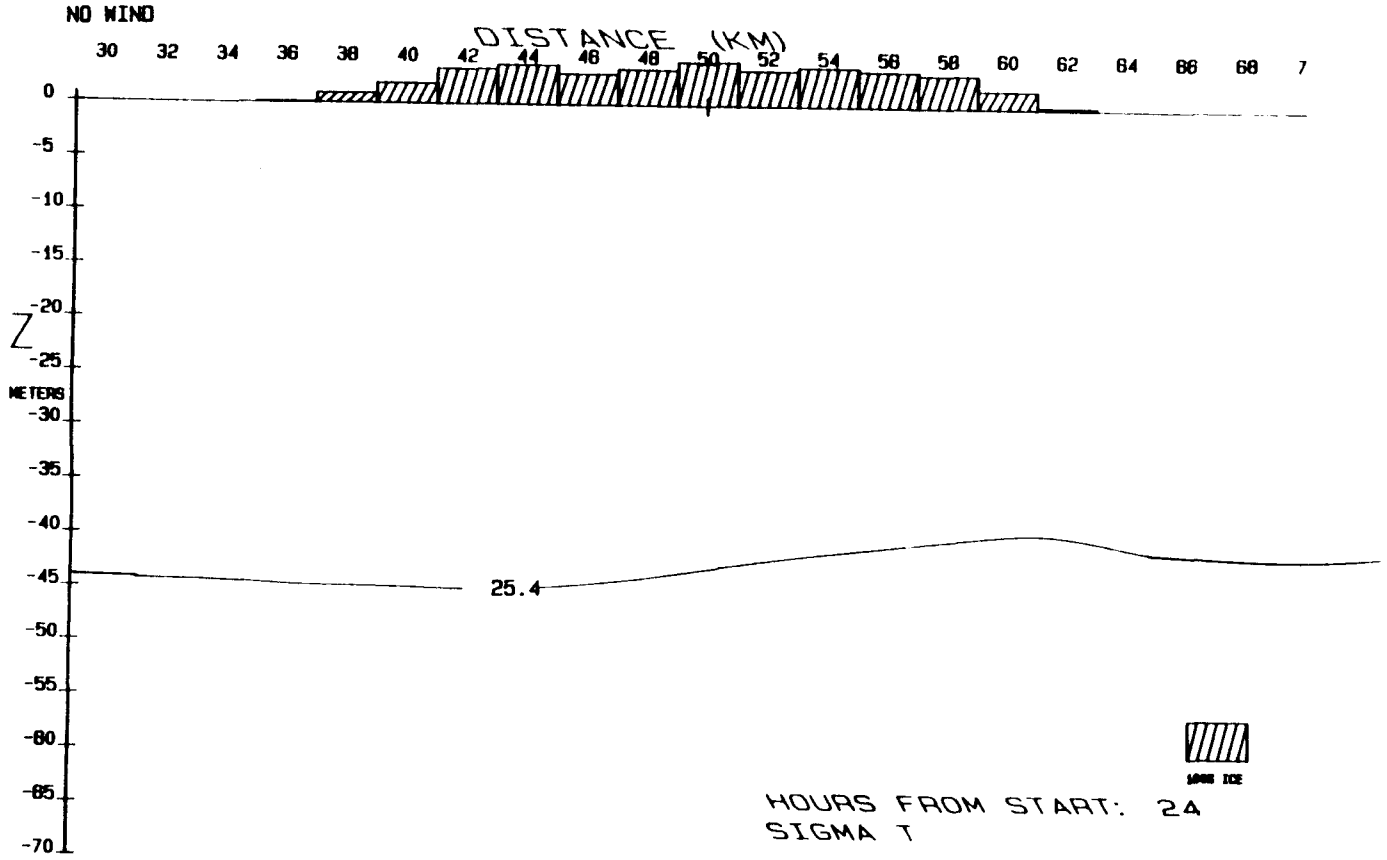

FIGURE 10A: CASE IA, AT 24 HOURS, SIGMA-T

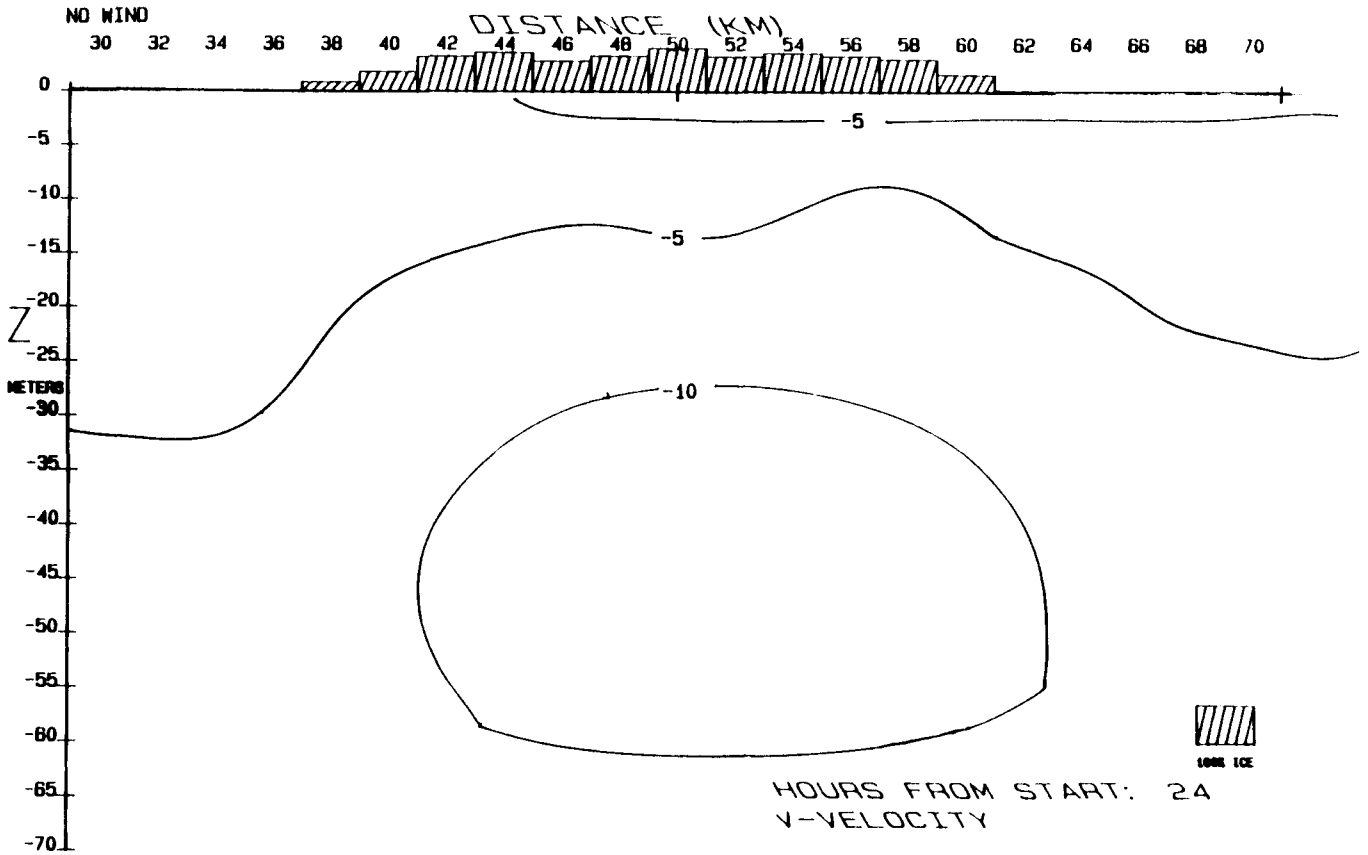

FIGURE 10B: CASE IA, AT 24 HOURS.

NO WIND

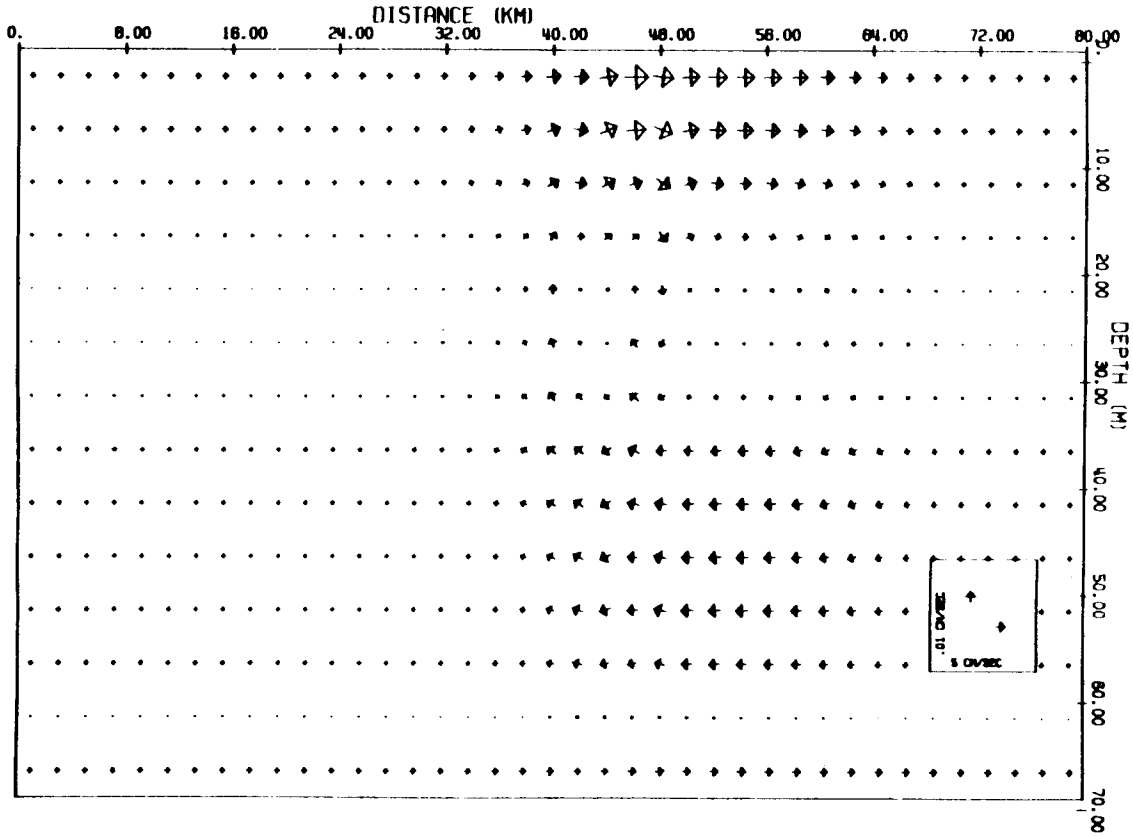

FIGURE 10C: CASE IA, AT 24 HOURS, ACROSS-ICE/VERTICAL VELOCITY ARROW PLOT

with it and will be explained in more detail in later sections.

The across-ice ice velocities (neg. x) are 13-18 cm/sec while the along-ice (neg. y) ice velocities are 26-29 cm/sec. These are within the range of the ice velocities measured by Johannessen et al. (1983). In both cases the highest values are in the areas with the most ice cover. These variations in ice velocities result in ice convergence and divergence as illustrated by the varying ice compactness (44-48 km positions, figure 8). At 16 hours the ice velocity magnitudes are similar to what they were at 8 hours but turned more toward the along-ice (neg. y) direction. The leading edge has advanced approximately 14 km to the 36 km position, 14 km from the starting point which is approximately 24 cm/sec.

The wind is shut off at 18 hours and by 24 hours the velocities have diminished considerably. The across-ice velocities have reversed by 24 hours because of inertial oscillations causing the ice to retreat somewhat toward its original position (e.g., the 0% ice contour at 24 hours). At subsequent times the leading as well as the following edges oscillate over a 4 km distance from the 30-34 km position for the leading

edge and the 56-60 km position for the following edge. The along-ice (neg. y) velocities remain approximately constant (5 to 7 cm/sec). The across-ice (x) component varies from 1 cm/sec to -1 cm/sec over an inertial period.

water velocities

After 12 hours, while the wind stress is still being applied, the along-ice (neg. y) water velocities (second panel figure 9) are greatest at depth (15-55 m) under the ice while the across-ice (neg. x) water velocities are greatest at the surface directly under the ice (third panel figure 9). The resultant magnitude of the across-ice (x) and along-ice (y) components are also greatest at the location of the maximum stress directly under ice at the surface (fourth panel figure 9).

A circulation cell has developed beneath the region of ice with weak upwelling at the following edge and stronger downwelling at the leading edge (third panel figure 9). This is because in our model the stress imparted to the water by wind is greater in regions of ice than over open ocean (regions without ice cover). This curl of the stress on the water, due to the tran-

sition from open ocean to ice covered ocean results in Ekman pumping. The ice edge upwelling phenomenon is the opposite result of that obtained by Niebauer (1982) for stationary ice cover. The earlier model assumed the stress went to zero when ice was present. The downwelling may be noted in the snap shot of the hydrography at 12 hours (figure 9a) with downward displacement of the isopycnals at 40 km.

Six hours after the wind has stopped, 24 hours from the start of the experiment, the along-ice (neg. y) water velocity cross-section (second panel figure 10) appears similar to the one at 12 hours except the maximum is slightly greater 16 cm/sec as opposed to 14 cm/sec at 12 hours. This is due in part because wind was applied for an additional 6 hours after the snap shot at 12 hours which caused additional tilt in the density surfaces (figure 10a). The surface across-ice (pos. x) velocities (third panel figure 10) have changed direction as a result of inertial oscillations. Because of the change in direction of the surface water (figure 10c) and ice, upwelling is now occuring in the region where downwelling occured previously but is weaker due to the reduced differences in velocities between open ocean and ice covered ocean (u at 12

hours ~10 cm/sec, u at 24 hours ~5 cm/sec). For the remainder of the experiment the the direction of the along-ice (neg. y) water velocities remains nearly constant but the magnitudes decrease slowly to less than 1 cm/sec. The across-ice (x), water velocities oscillate between on-ice (pos. x), and off-ice (neg. x), as does the ice itself and diminishes in magnitude with time.

The effect of ice on water velocity

To assess the effect of ice drag on water velocity a time series of ice velocities and surface water velocity vector diagrams (figures 11 a-c) are presented. While the wind stress is being applied, the ice moves at about 45 degrees to the right of the wind direction (figure 11a) and the surface water at about 30 degrees to the right of the ice. The angle of the ice velocity to the wind is within the ranges of that observed by Nansen (1902). After the wind stops, the ice and the surface water appear to move approximately in the same direction. The coupling term, C_{wi} $(\bar{V}_w - \bar{V}_i)$ (equation 8) cause the two vectors to converge. Water under the ice is turned more to the right of the wind than the water at the surface away from the ice until about 11 hours (figure 11b). The water under the ice

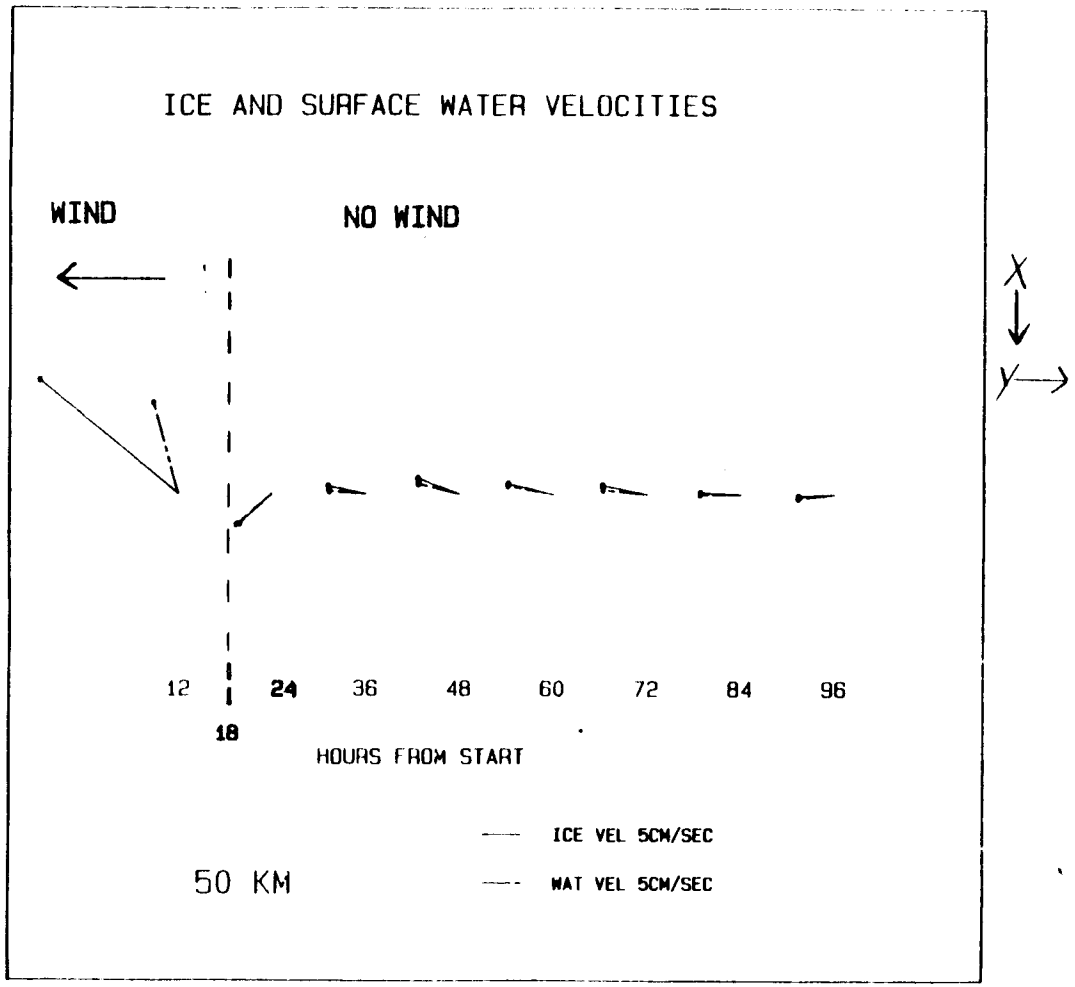

FIGURE 11A: CASE IA, TIME SERIES OF ICE AND SURFACE WATER VELOCITIES

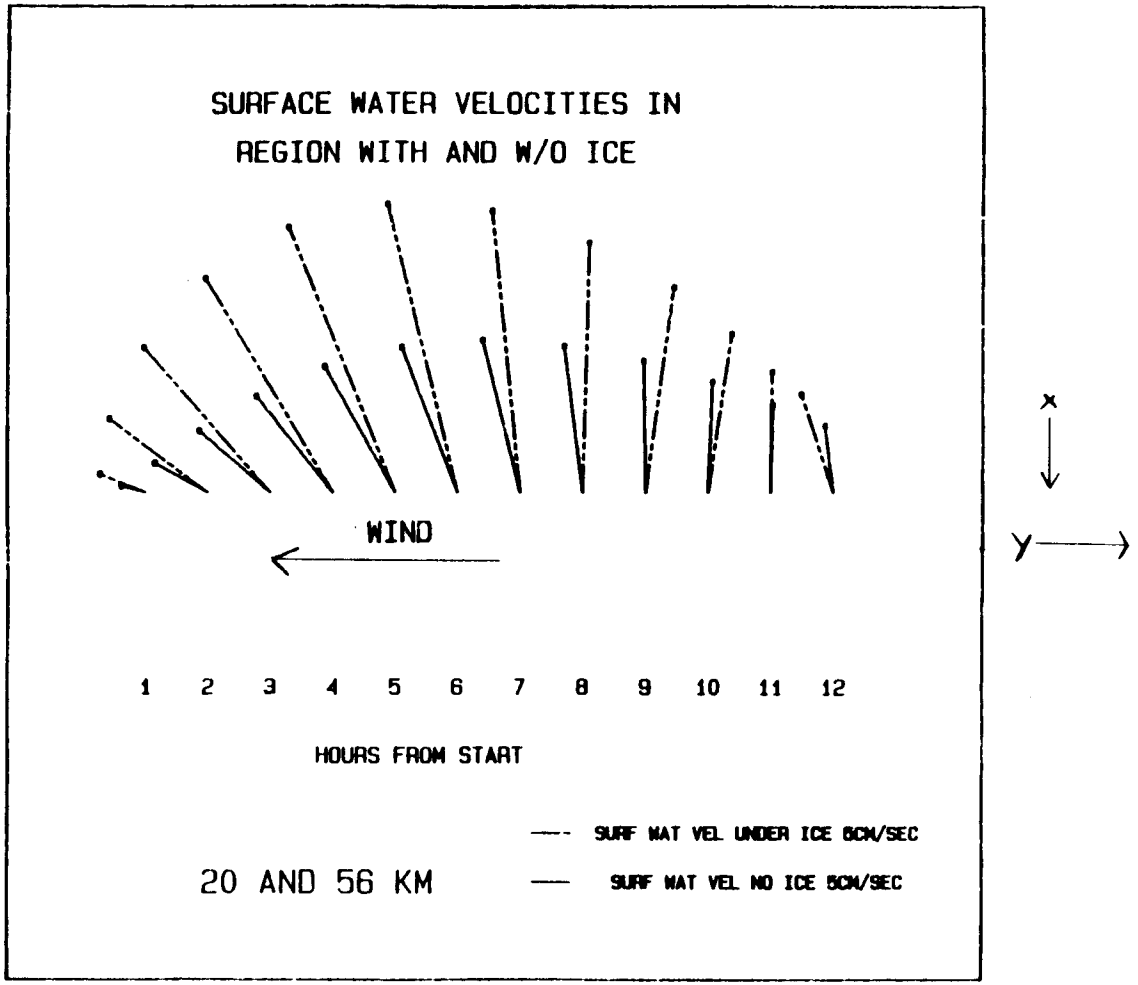

FIGURE 11B: CASE IA, TIME SERIES OF SURFACE WATER VELOCITY IN REGIONS WITH AND WITHOUT ICE

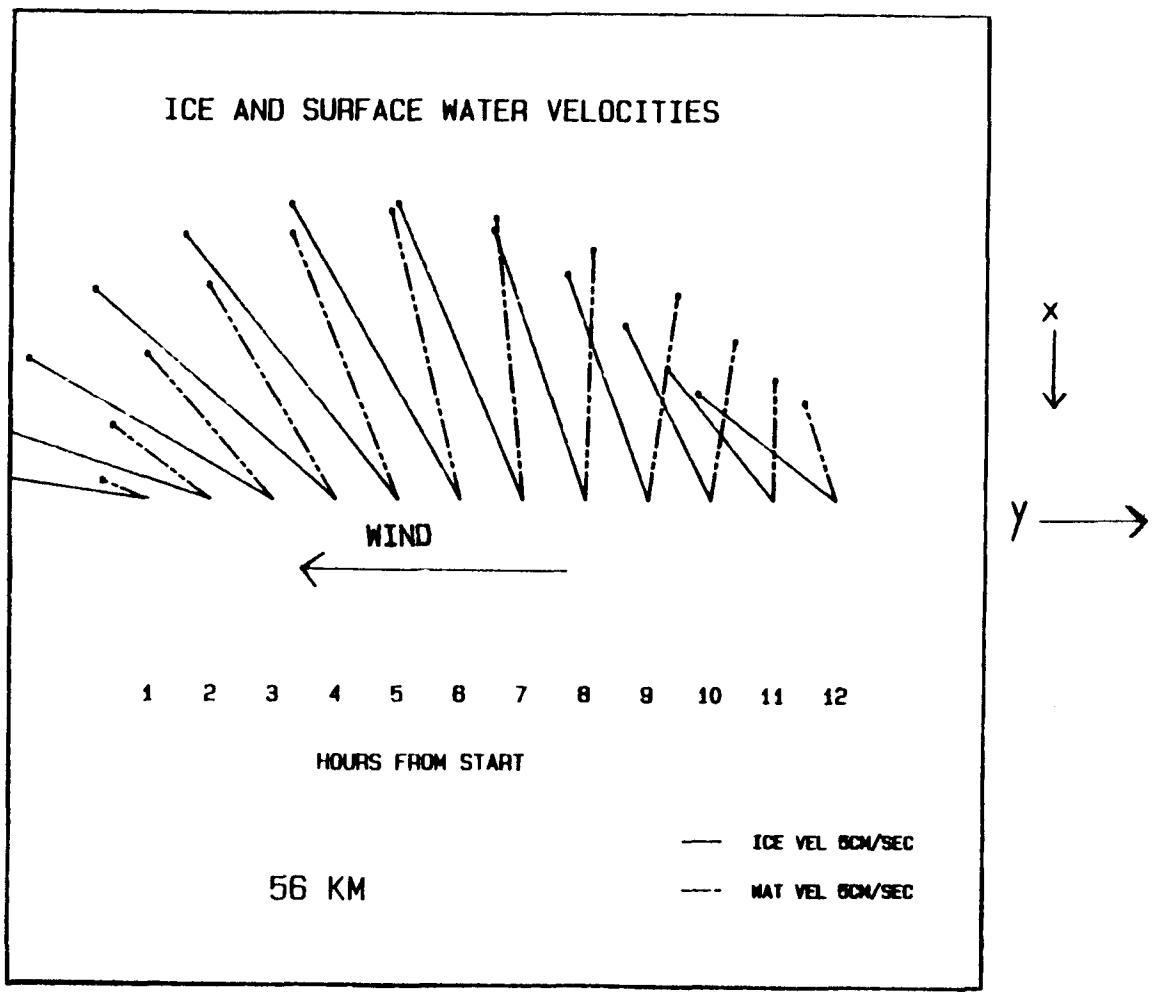

FIGURE 11C: CASE IA, TIME SERIES OF ICE AND SURFACE WATER VELOCITY FOR FIRST 12 HOURS

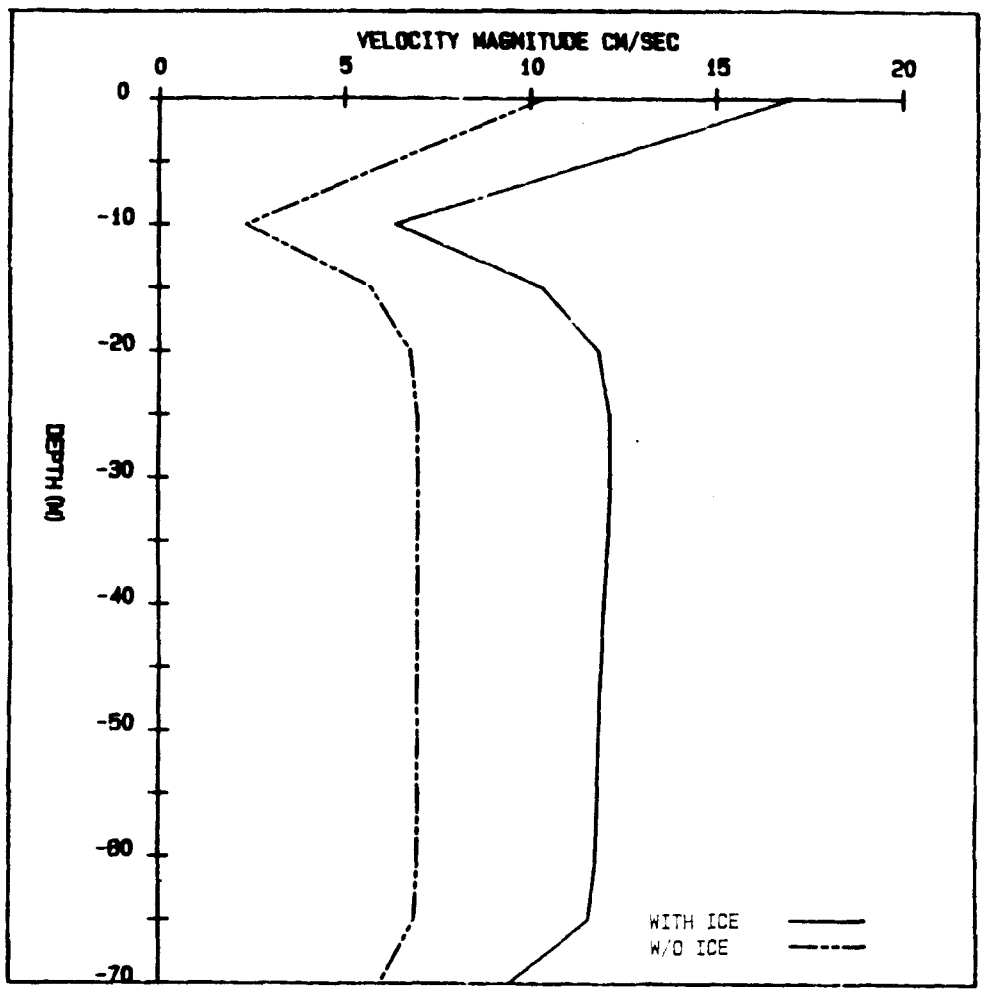

FIGURE 12A: CASE IA, VELOCITY PROFILE AT 12 HOURS

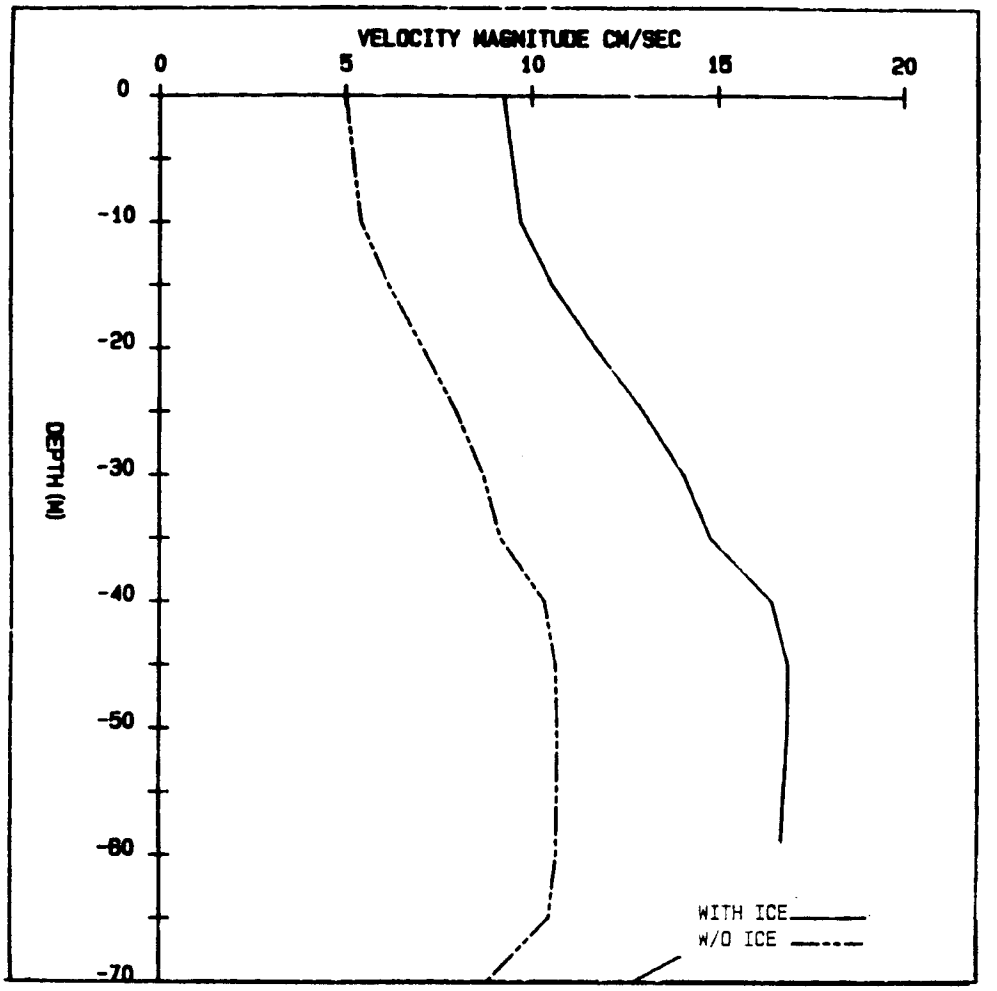

FIGURE 12B: CASE IA, VELOCITY PROFILE AT 24 HOURS

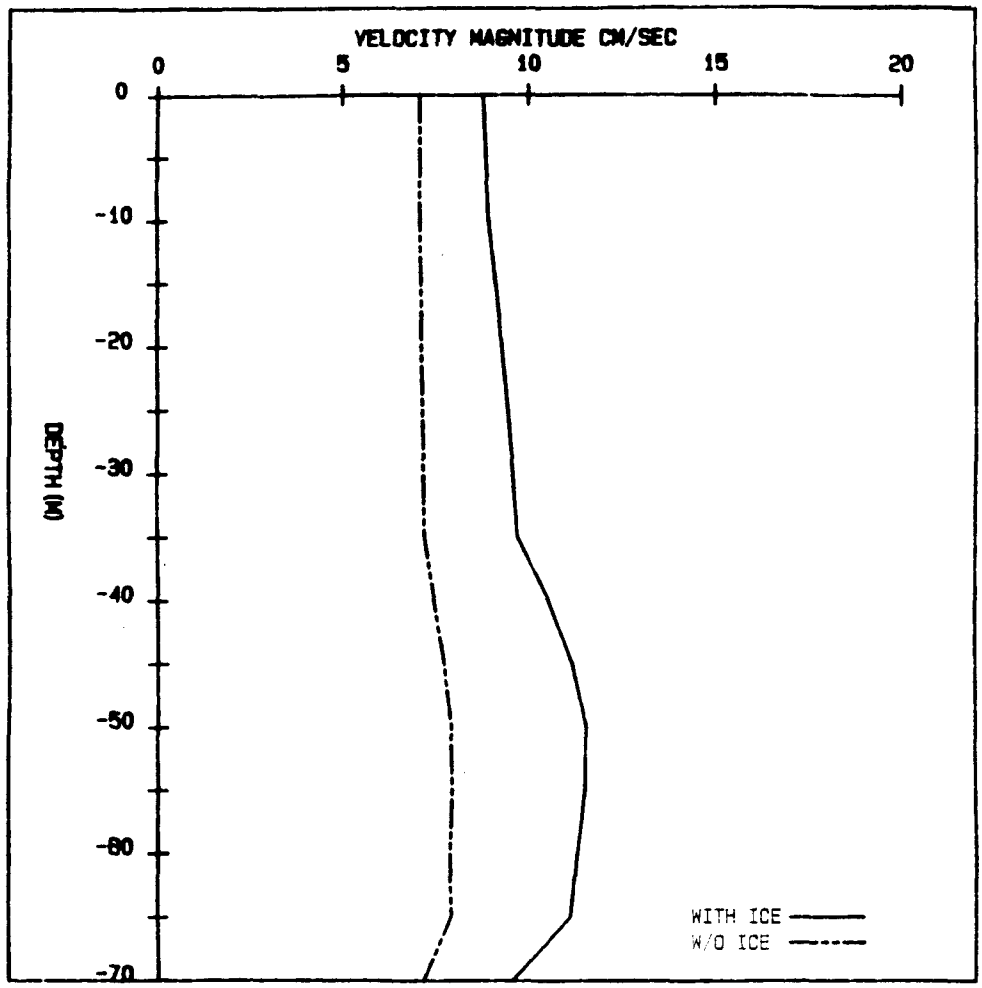

FIGURE 12C: CASE IA, VELOCITY PROFILE AT 48 HOURS

begins to turn to the left at this point because an inertial oscillation in the ice velocity pulls the water along with it because of the coupling (figure 11c). This is a common phenomenon in models due to impluse starting of the wind. This leads to exaggerated inertial oscillations until the systems comes into steady state.

Generally in regions of ice, the water magnitudes are greater than in regions without ice (figures 12a to 12c). It is interesting to note that the velocity profiles for the two cases have about the same shape but are offset by a scalar multiplier. This means that change in velocity magnitude with depth is consistent at different surface stresses.

Case Ib: the across-ice (x) wind

Ice velocities and percent cover

The initial conditions for this experiment are the same as those for case Ia (figure 7) except that now we have an across-ice (x) wind blowing perpendicular to

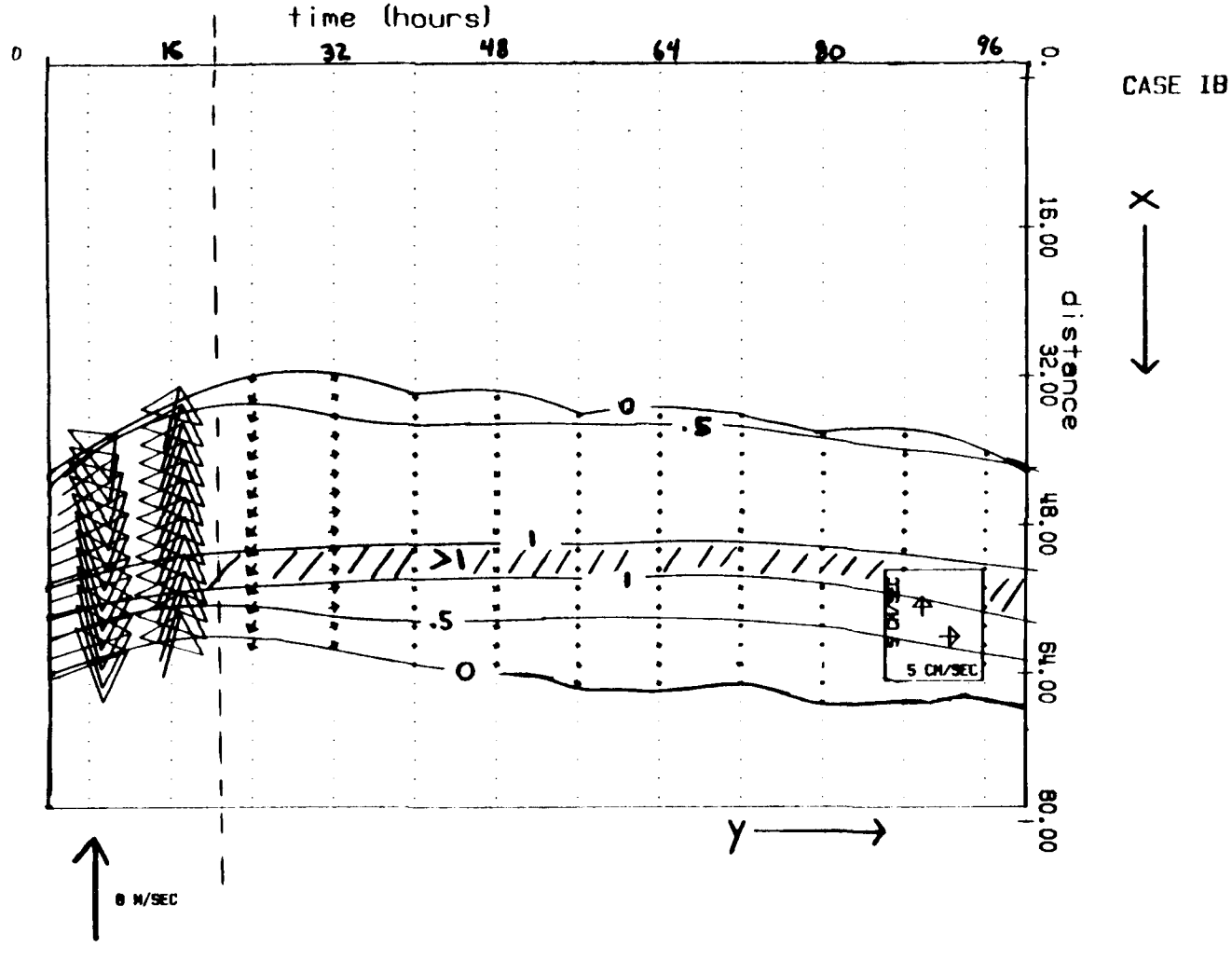

FIGURE 13: CASE IB, TIME SERIES OF ICE VELOCITIES AND COMPACTNESS

and off the ice (neg. x).

After the wind stress has been applied for 8 hours the leading ice edge has moved 8 km (figure 13) from the initial 50 km position to the 42 km (figure 13) position where there is approximately only 7% ice cover. Ice speeds of approximately 28 cm/sec in the across-ice (neg. x) direction are twice those of the previous experiment (case Ia, figure 8, 14 cm/sec). The along-ice (pos. y) ice velocities are approximately 12 cm/sec as opposed to approximately 28 cm/sec in case Ia and in the opposite direction due to Ekman transport. The following edge is now 6 km (at 64 km) from its initial starting point (70 km) and there appears to be some "piling up" of ice in the 56-60 km region. At 16 hours the wind stress is still being applied and the leading edge has moved an additional 4 km while the following edge has only advected an additional 2 km in the direction of the wind. The percentages of ice cover remain relatively constant.

The wind ceases at 18 hours and by 24 hours it appears as though the ice "falls back" due to inertial oscillations. It is now moving at approximately 180 degrees to what it was at the 16 hour point, due to an inertial oscillation, and the magnitudes have decreased

substantially (to about 6 cm/sec). By comparison, at 16 hours in the along-ice (y) wind case (experiment Ia, figure 8), the vectors had turned only about 30 degrees to what they were at 16 hours.

By 32 hours the ice vector has rotated approximately 300 degrees from what it was at 24 hours and the magnitudes have again substantially decreased. These inertial oscillations and magnitude reduction continue throughout the balance of the time period of this simulation.

The rotational angle of the ice velocities is greater in this case than in the along-ice case (y) but because the Coriolis parameter is the same, the period is the same. However the velocity magnitudes here decrease faster. In addition, the across-ice (x) velocities are greater for the first 32 hours of the experiment. This results in a greater advection of ice near the leading edge. The greater advection then results in lower ice compactness and will be referred to later when we look at the phytoplankton bloom cycle under various wind conditions.

Water velocity

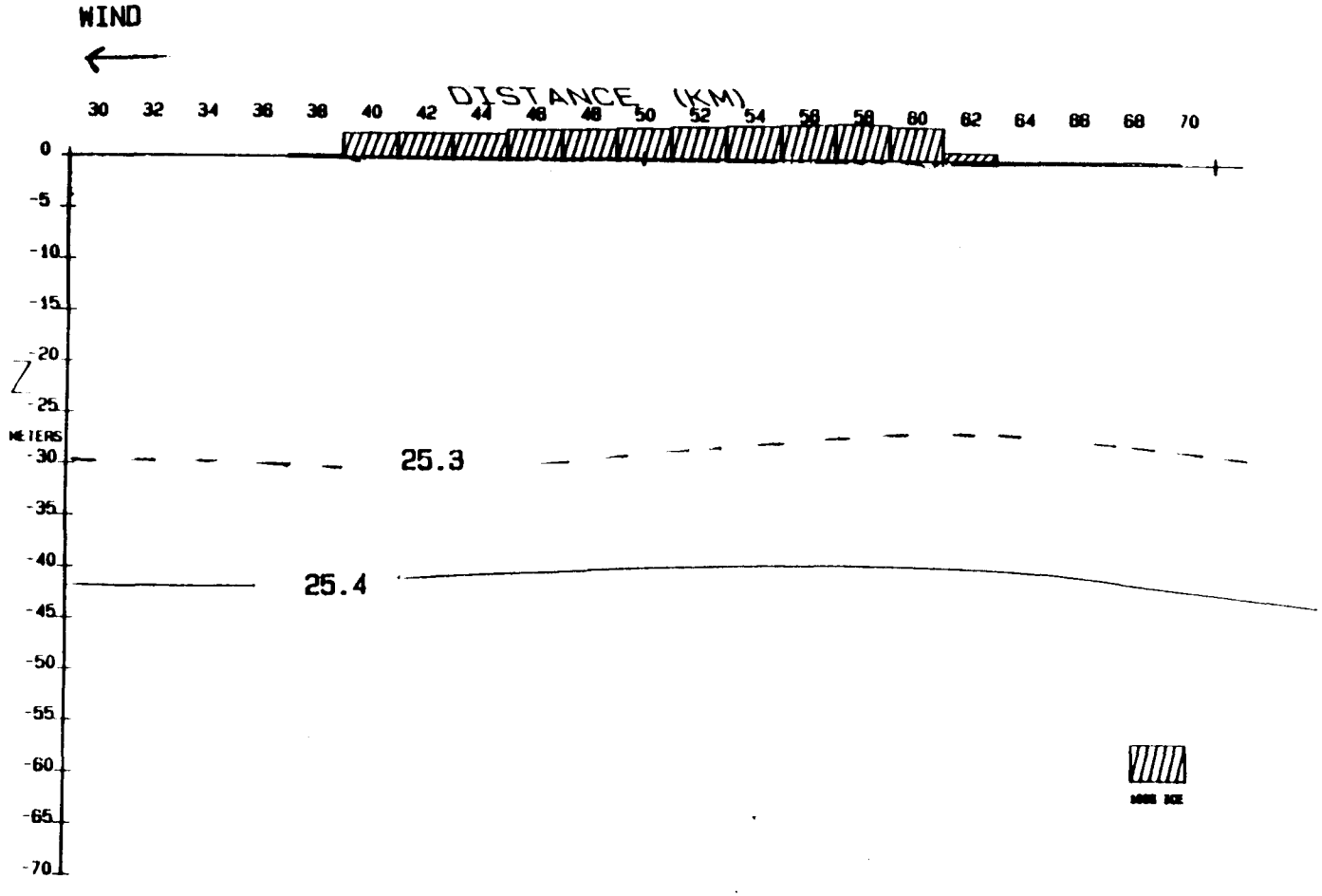

FIGURE 14A: CASE IB AT 12 HOURS, SIGMA-T

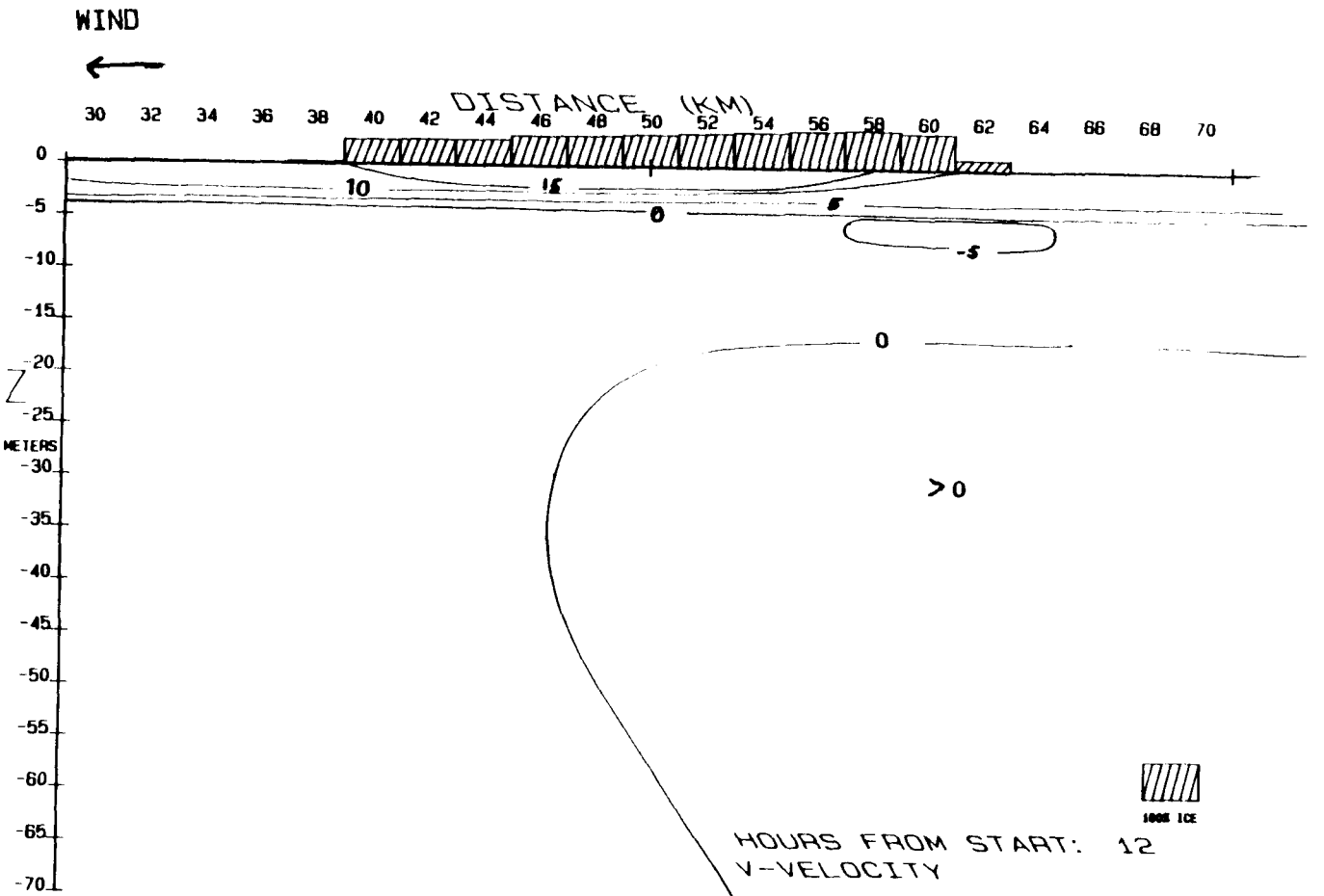

FIGURE 14B: CASE IB AT 12 HOURS, ALONG-ICE VELOCITY

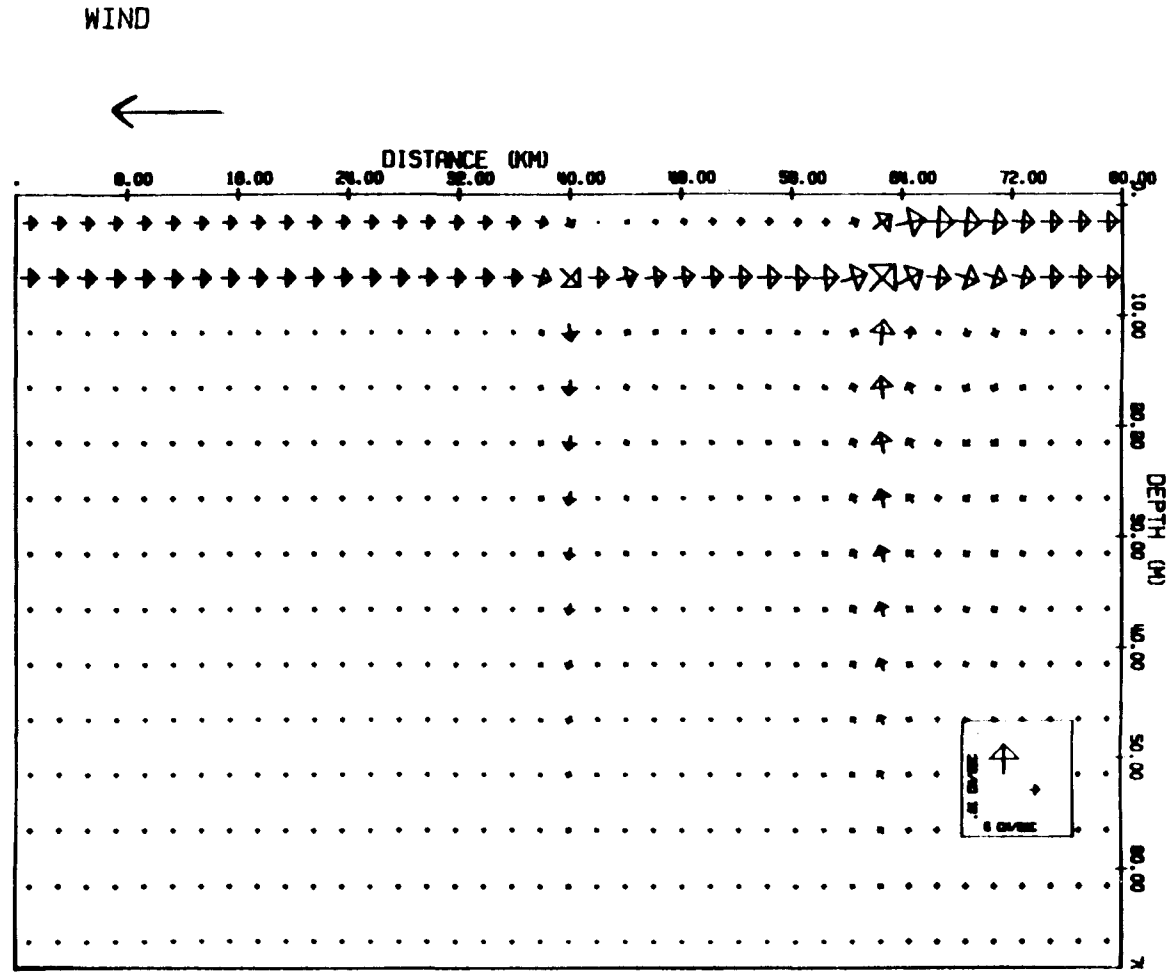

FIGURE 14C: CASE IB AT 12 HOURS, ACROSS-ICE/VERTICAL ARROW PLOT

As Niebauer (1982) notes the picture of the water velocities induced by this wind are not as straight forward as those induced in the along-ice (y) experiment. The greatest magnitudes in the along-ice (pos. y) water velocities at 12 hours (second panel figure 14) are at the surface under the regions of heaviest ice cover. This is due to the greater coupling of wind through ice to water than wind directly to water. With depth, the along-ice (y) water velocities change direction at about 5 m and then again at about 20 m in areas that ice cover has just passed over. Note that in the 50-70 km region (second panel figure 14) at depths greater than 20 m the ice coverage was greater for most of the time prior to this snap shot.

The across-ice (x) (third panel figure 14) water velocities in the uppermost layers are opposite to the wind. This again is due to the increased magnitude of the inertial oscillations due to the impluse starting ot the wind. By this time most of the velocity is in the along-ice (pos. y) direction (second panel figure 14). In the vertical there is substantial upwelling at the following edge of the ice (62 km, third panel figure 14) and some upward motion of the isopynals at this location is noted (figure 14a). Downwelling is

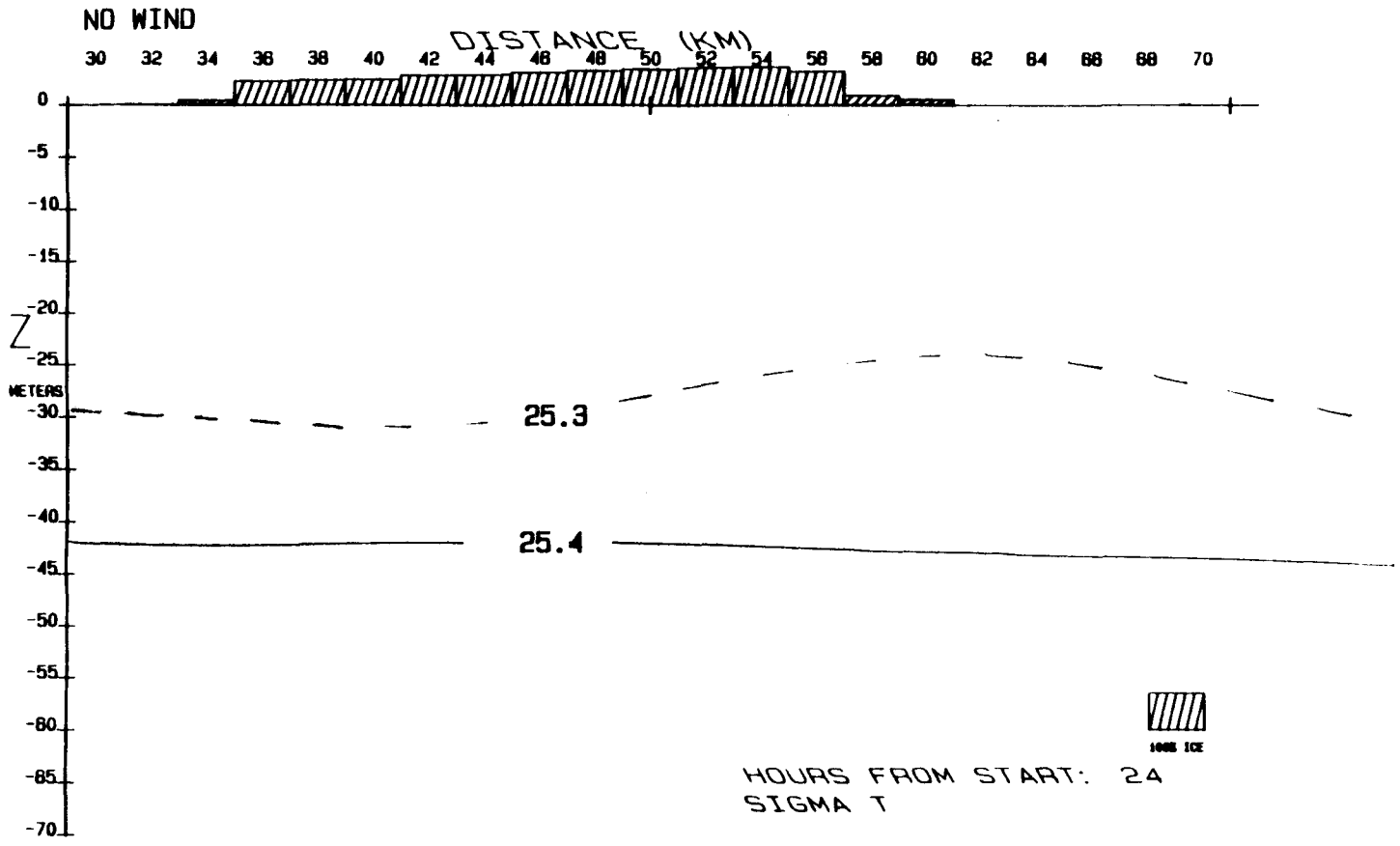

FIGURE 15A: CASE IB AT 24 HOURS, SIGMA-T

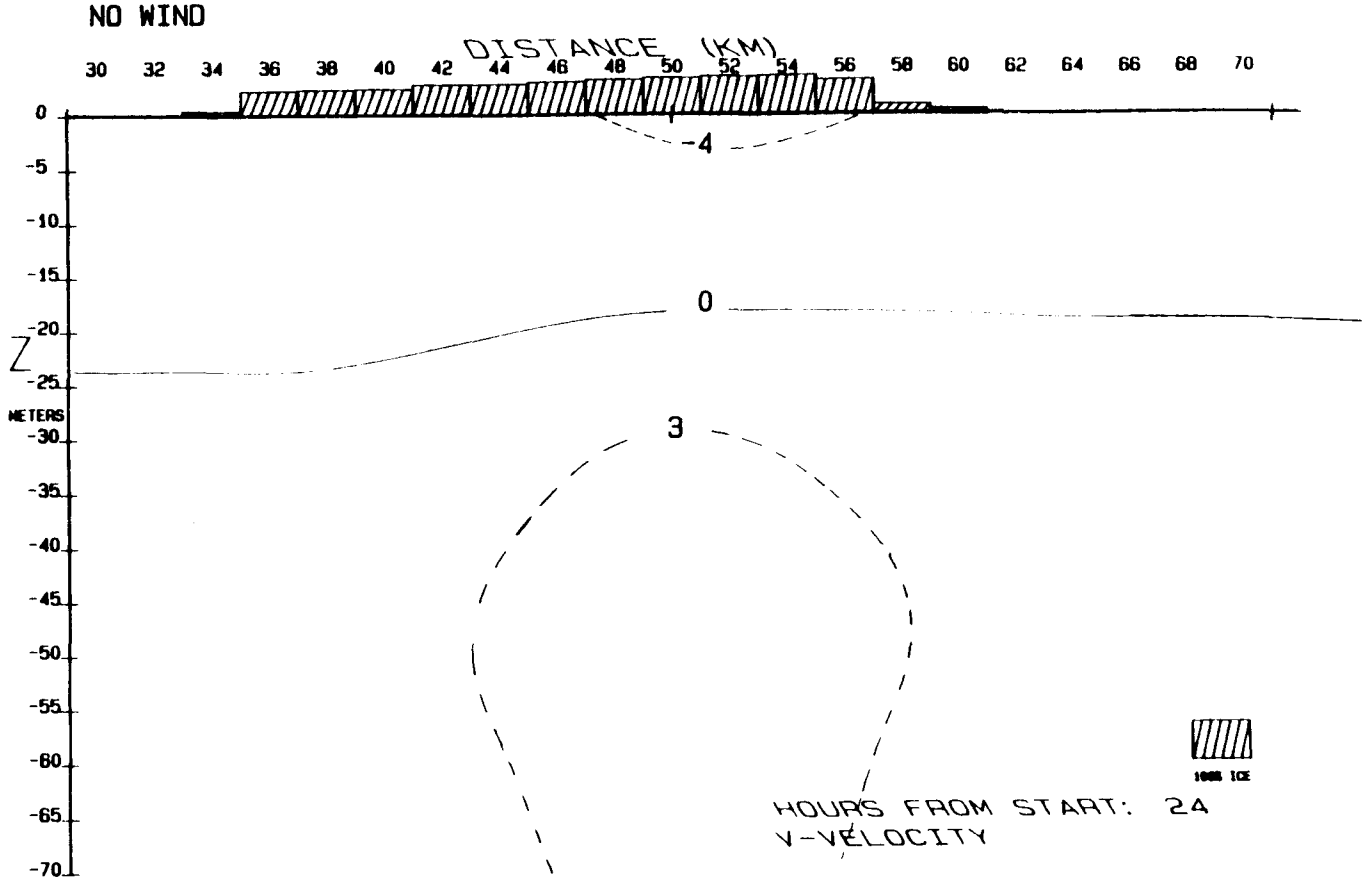

FIGURE 15B: CASE IB AT 24 HOURS, ALONG-ICE VELOCITY

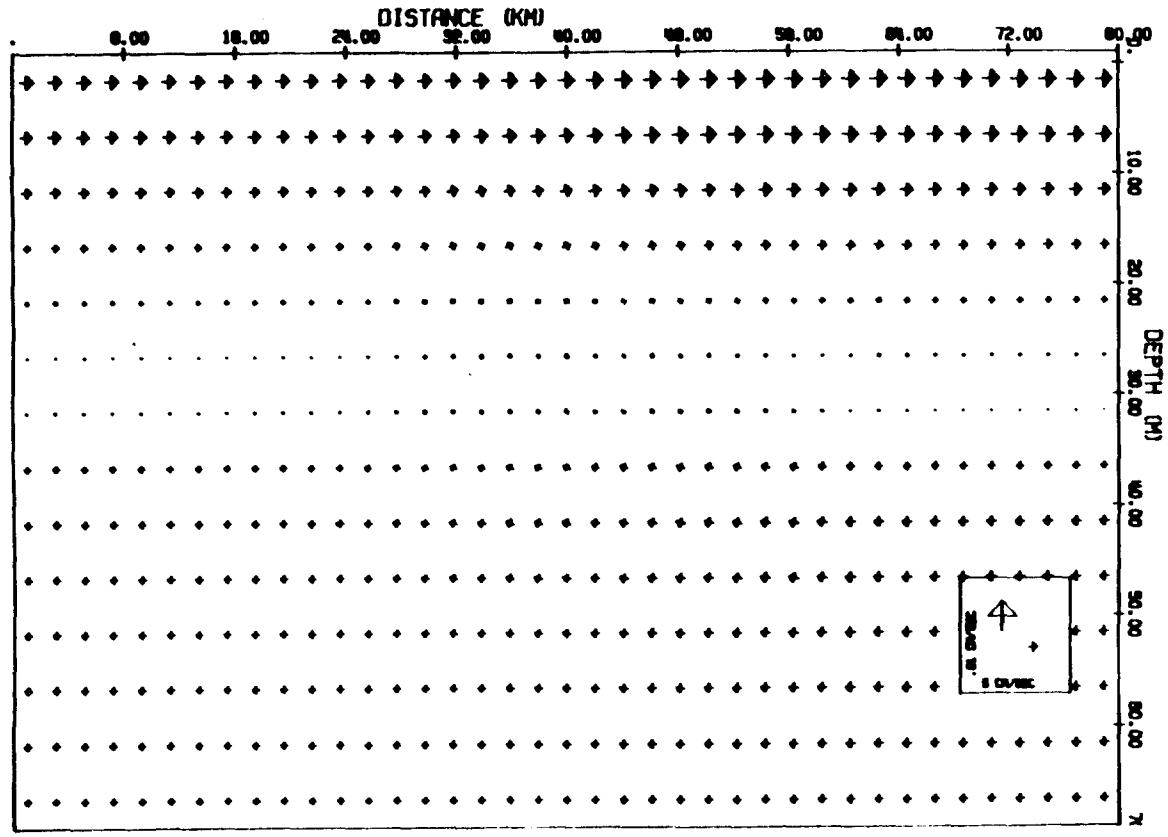

FIGURE 15C: CASE IB AT 24 HOURS, ACROSS-ICE/VERTICAL VELOCITY ARROW PLOT

evident at the leading edge (40 km).

After 24 hours, 6 hours after the wind has stopped water velocity magnitudes have decreased substantially to approximately 10 cm/sec (second and third panel figure 15). This may be explained by the water/ice coupling term of the water velocity equation,

$$C_{wi}(\bar{V} - \bar{V}_i)$$

If $\bar{V}_i$ is very different from $\bar{V}_w$ then the resultant stress on both the ice and water is large, whereas if they are similar the stress is small and the velocities would change little with time. This relationship is illustrated in figure 16a. $\bar{V}_i$ and $\bar{V}_w$ are very different at 12 hours and by 24 hours the two velocities almost overlap ($u \sim 5$ cm/sec and $v \sim 15$ cm/sec, $u_i \sim 14$ cm/sec and $v_i \sim -17$ cm/sec at 12 hours; $u \sim 4$ cm/sec and $v \sim -2$ cm/sec, $u_i \sim 4$ cm/sec and $v_i \sim -2$ cm/sec at 24 hours). In the vertical almost no motion is evident (third panel figure 15) and only a slight upward vertical displacement of the isopycnals is noted at about 50 km (figure 15a).

At 48 hours (cross-sections not shown) and beyond

the velocities have decreased to almost zero throughout the water column. Inertial oscillations are present in the water as well as the ice and may be noted in figure 16a. Upward displacement of the isopycnals is also noted in approximately the same location as they were at 24 hours.

The effect of ice on water

At 12 hours (figure 16a) the ice is moving at about 40 degrees to the right of wind and the the water is moving at about 60 degrees to the right of the ice. After the wind is stopped the main driving force is Coriolis acceleration which causes the water and ice to go into inertial oscillations. After 24 hours it appears as though the vectors are turning counter to Coriolis acceleration (to left). This is because of data aliasing. The velocities turn 360 degrees every inertial period (approximately 14 hours). We observe them every 12 hours (12/14 of an inertial period) when they had rotated only approximately 300 degrees from the last time increment. This gives the appearance that the velocities rotated 60 degrees to the left. A

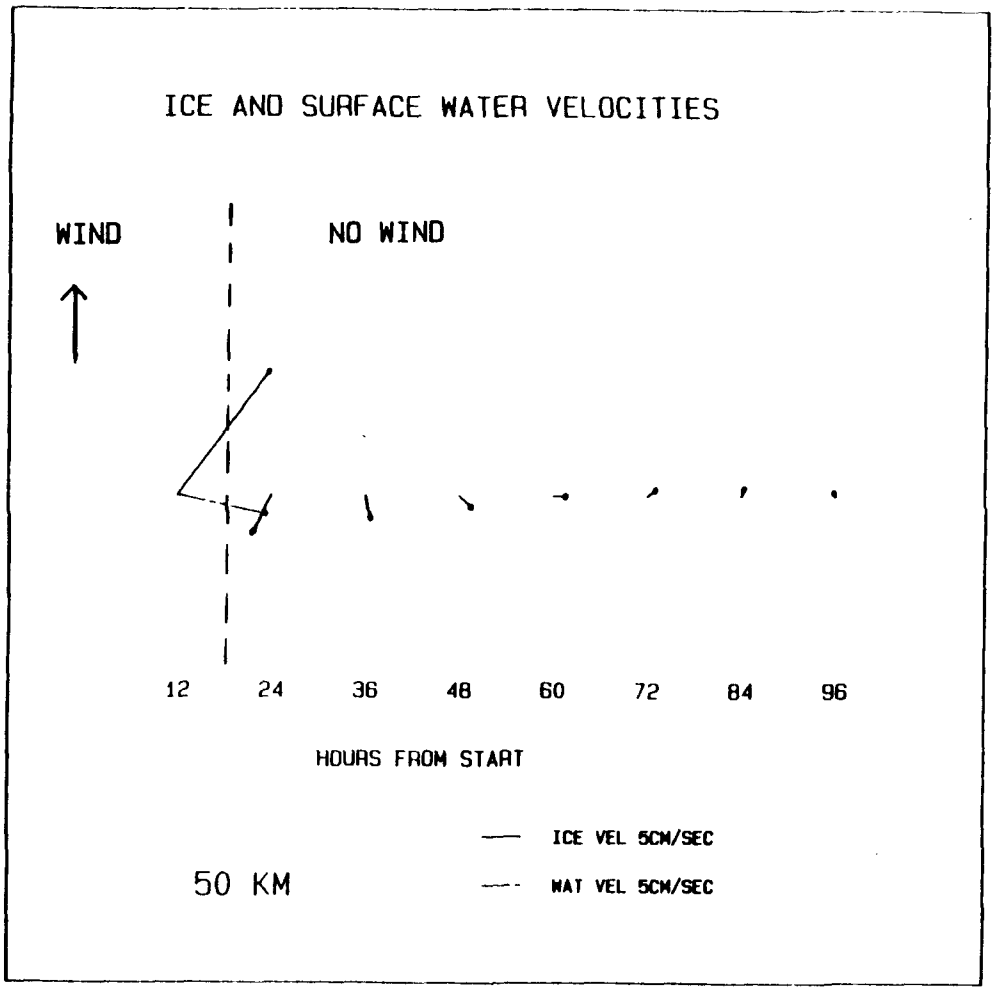

FIGURE 16A: CASE IB, TIME SERIES OF ICE AND SURFACE WATER VELOCITY

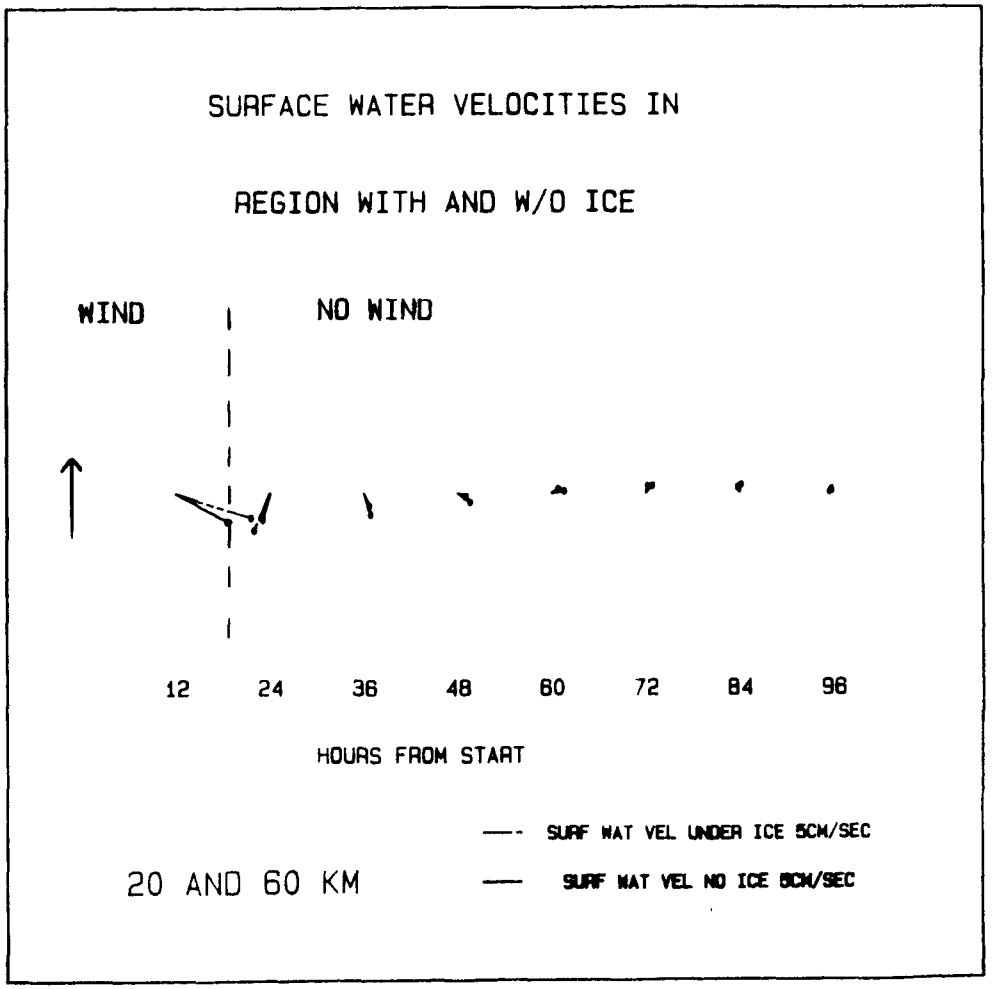

FIGURE 16B: CASE IB, TIME SERIES OF SURFACE WATER VELOCITY IN REGION WITH AND W/O ICE

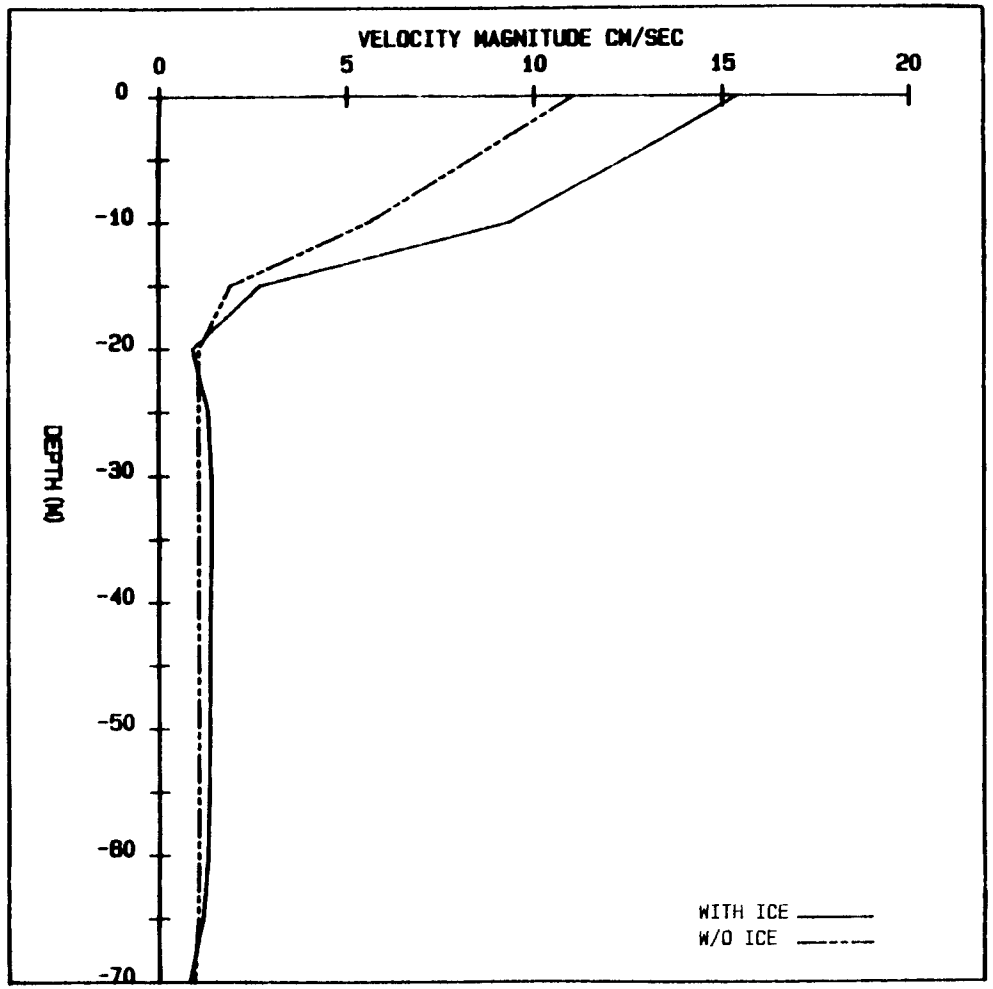

FIGURE 17A: CASE IB, VELOCITY PROFILE AT 12 HOURS

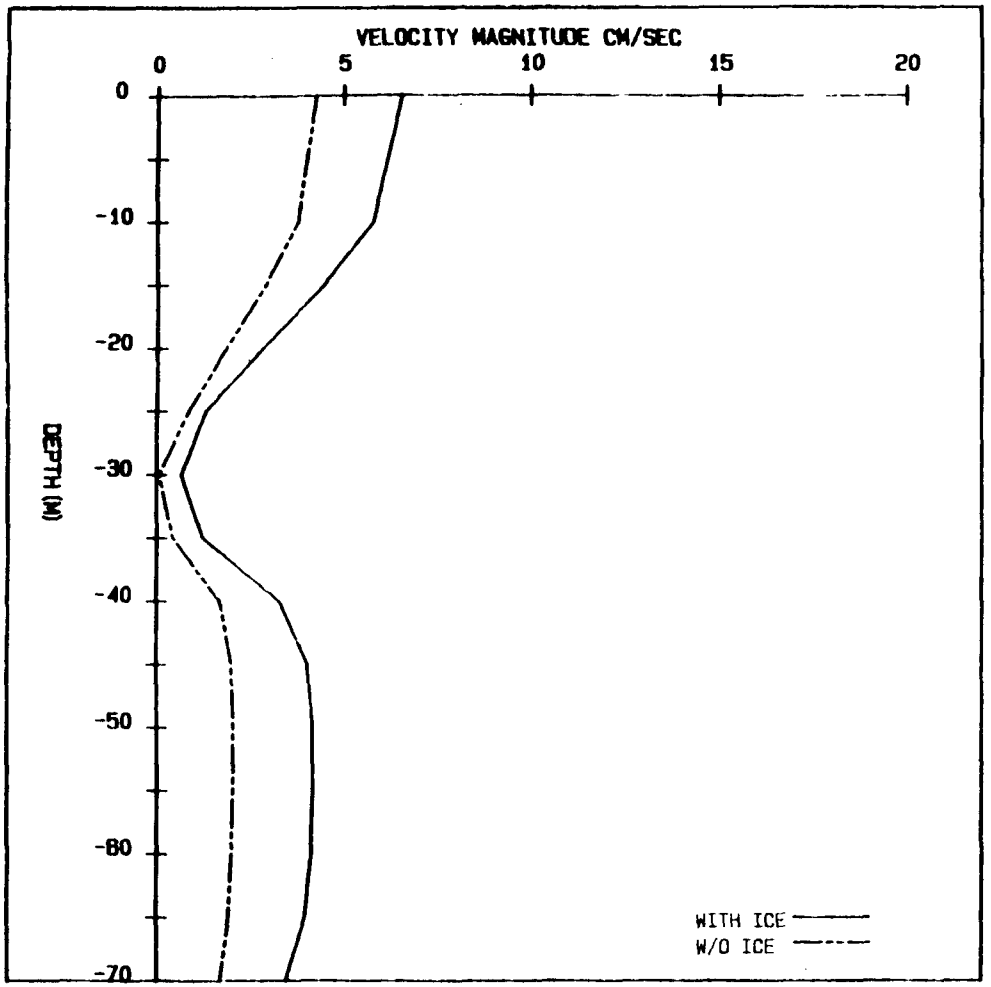

FIGURE 17B: CASE IB. VELOCITY PROFILE AT 24 HOURS

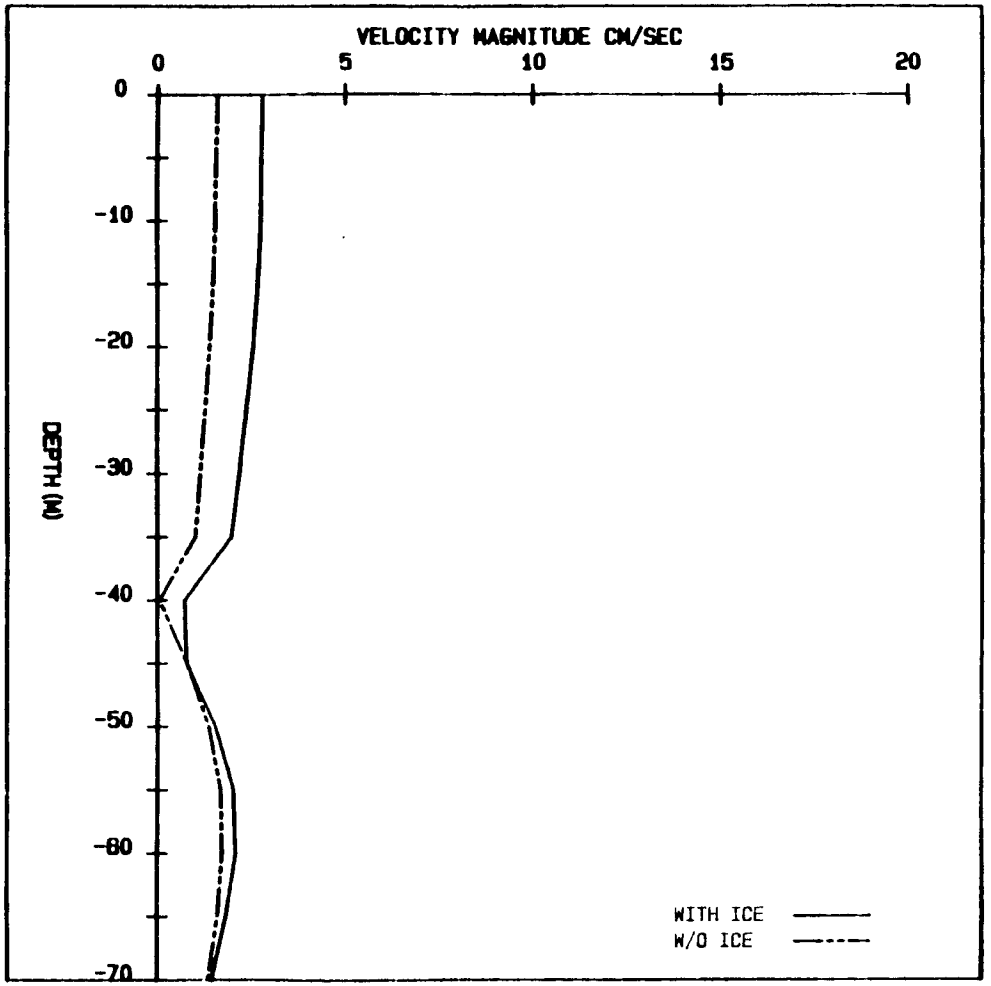

FIGURE 17C: CASE IB, VELOCITY PROFILE AT 48 HOURS

time series of surface water velocities in regions with and without ice cover is shown in figure 16b. Here it may be seen that the velocities are similar but the one associated with ice is a bit larger in magnitude.

Snap shots of the resultant velocity magnitude profiles at 12, 24 and 48 hours in regions with and without ice cover are shown in figures 17a, 17b and 17c. The shapes of the profiles appear similar but the magnitudes of the velocities are greater in the region of ice cover. The velocity minima at approximately 35 m in the 24 and 48 hour profiles (figures 17b and 17c) coincide with the Ekman depth given by Pond and Pickard, 1978; $D_e=pi(2N_z/f)**0.5$, for an $N_z=55$ cm^2/sec and $f=0.000126$, $D_e \sim 30$ m. Above this point wind stress is important while below it the velocities are baroclinic geostrophic in nature due to the upward displacement of the isopycnals (figure 15a).

Case II: the effects of melting and regeneration of nitrogen

The following experiments are described to illustrate the reponse of the model to ice melt. The

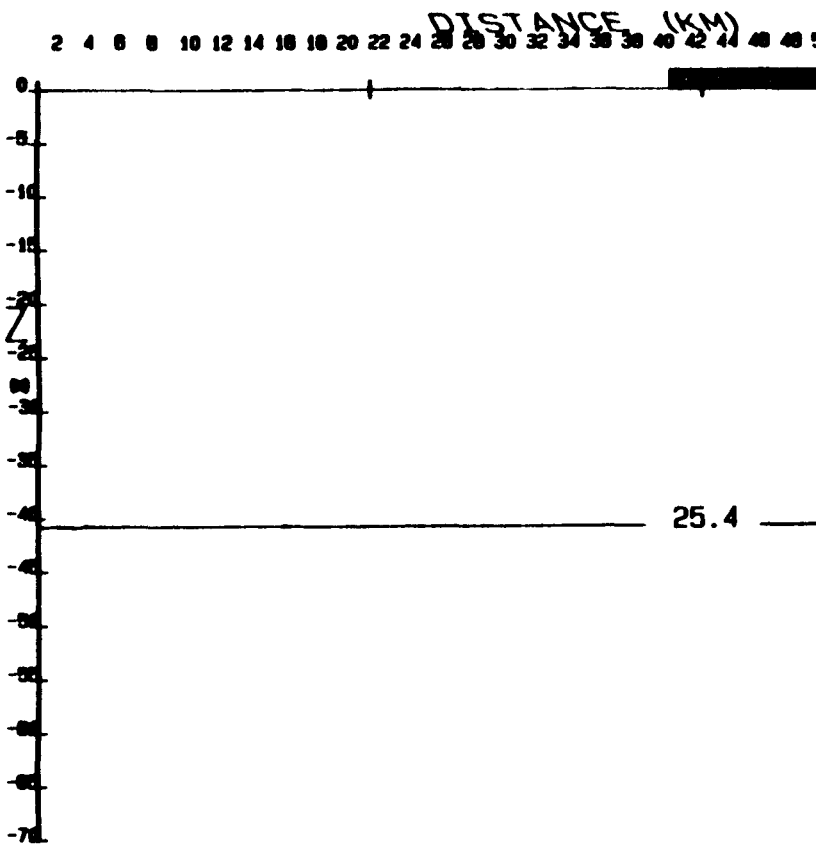

FIGURE 18: INITIAL CONDITIONS CASE IIA

[redacted]

[redacted]

ZERO HOURS

nitrogen regeneration scheme as presented in the methods section is also tested in this case. The ice is melted as a function of percent ice cover (equation 11) and no wind forcing is applied. The physical response of the model is tested in case IIa. The biological response to the regeneration scheme is discussed in case IIb. The phytoplankton growth cycle with and without algae input from the ice is followed in case IIc.

Case IIa: the physical effect of melting

ice velocities and percent cover

In this experiment we wish to determine how water and ice velocities are affected by differential input of low saline water from melting ice. The initial conditions (figure 18) are a 10 km region of 50% ice cover starting at 40 km then 100% cover from 50 km to the boundary at 80 km. The water is stratified at depths greater than 30 m (figure 18) and no wind stress is applied.

The region of 100% cover initially has a much smaller input of fresh water. In that area the melting

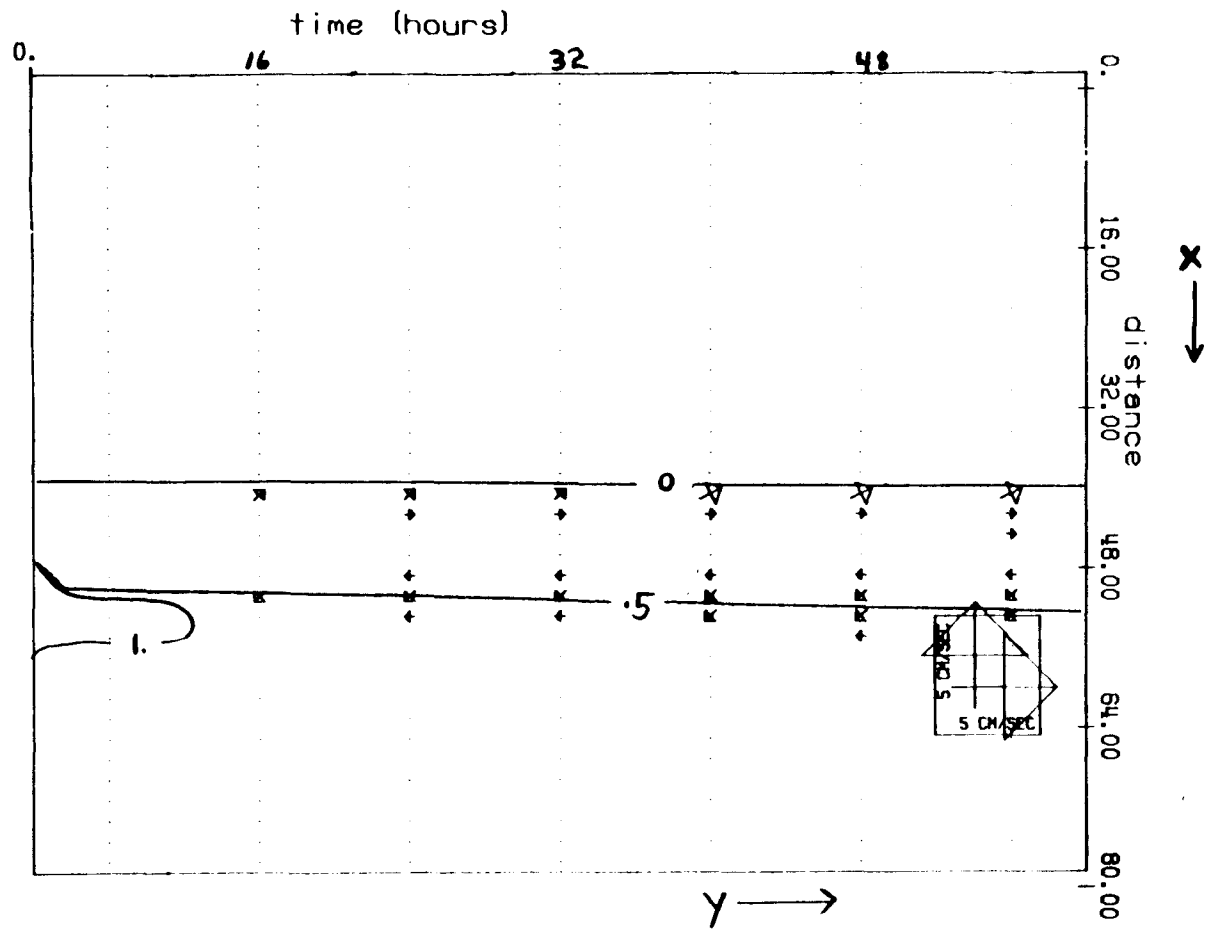

FIGURE 19: CASE IIA TIME SERIES OF ICE VELOCITY AND COMPACTNESS

rate is 1% per day as opposed to a region with 50% cover where the melt rate is approximately 50% per day (equation 11, figure 3). Though no wind stress is applied, ice velocities (figure 19) by 16 hours are approximately 1.5 cm/sec. They are generated by the baroclinic water velocities to be examined in the next section. These ice velocities occur at the ice/open water boundary (40 km) and the heavy ice/light ice boundary (50 km). Their directions are at 180 degrees to each other. This may be explained by the hydrography (figure 20a) which shows the stratification of the water column generated by the larger input of fresh water from the lightly iced area (39 to 48 km). The ice is accelerated by the water and turned to the right by Coriolis acceleration. The ice velocities propagate outward in a wavelike manner from the center of the ice pack over time (figure 19). By the end of the experiment ice velocities are noted from 40 to 56 km.

water velocities

The resultant vector of the across-ice (x) and ver-

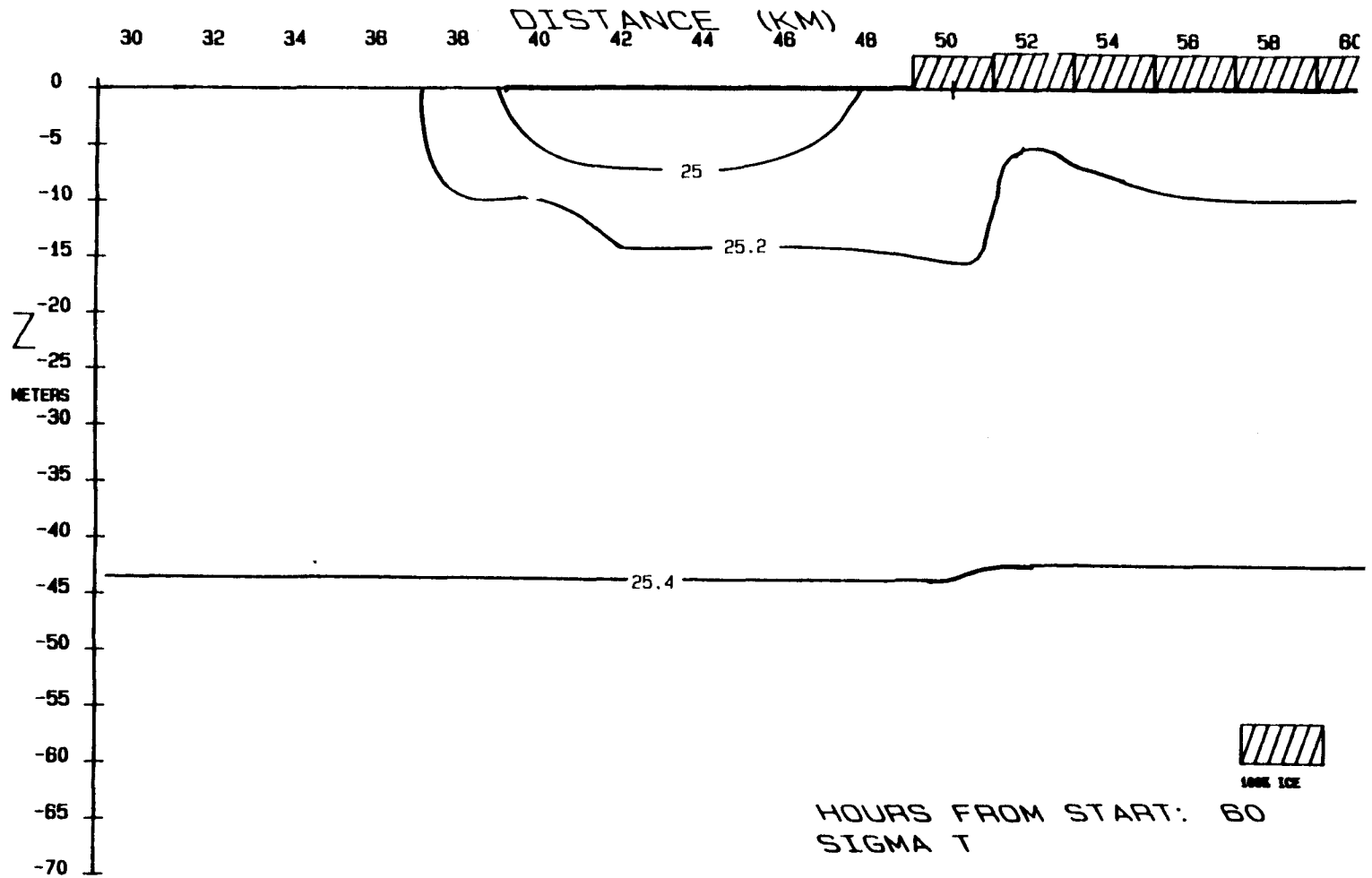

FIGURE 20A: CASEIIA AT 60 HOURS, SIGMA-T

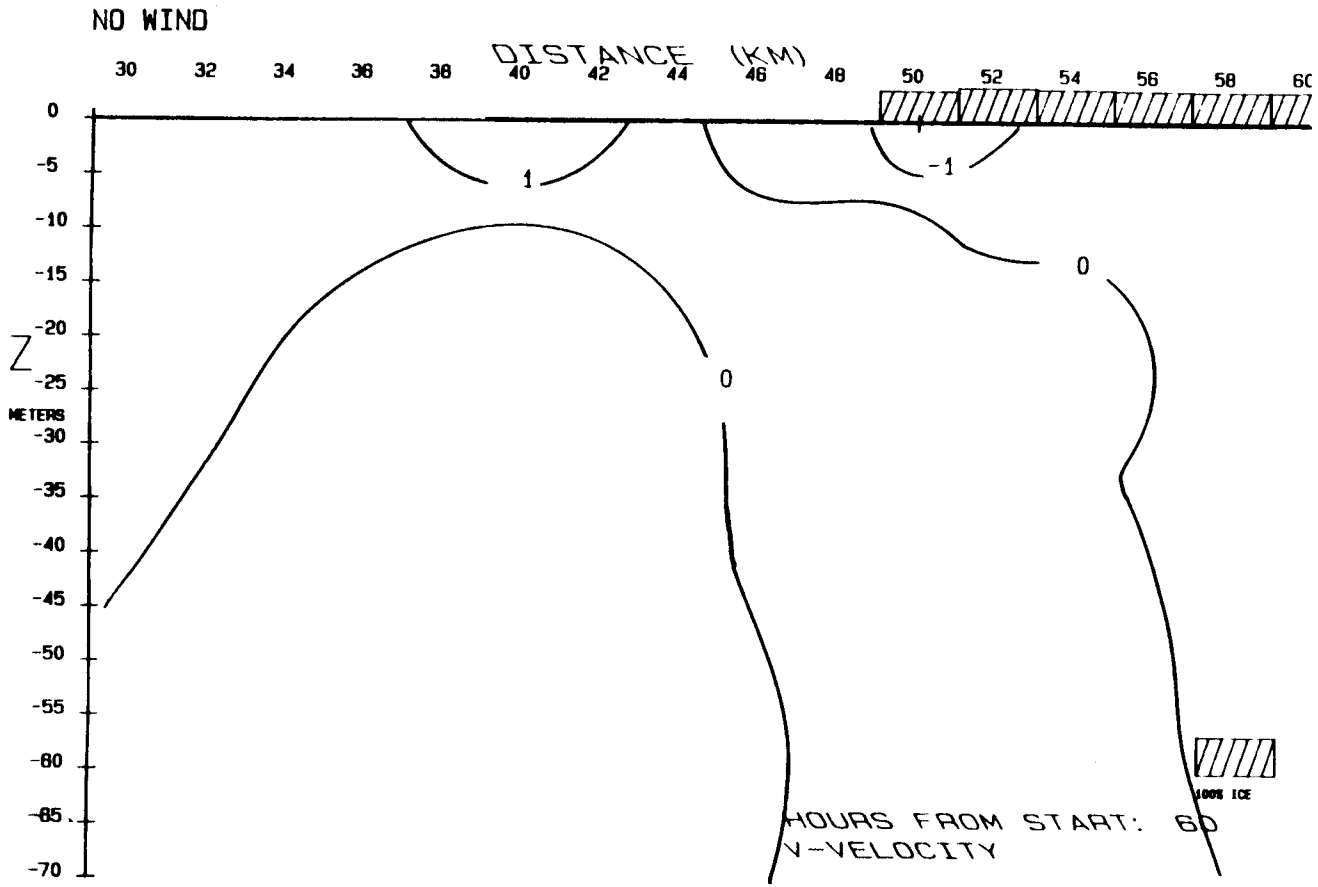

FIGURE 20B: CASE IIA AT 60 HOURS, ALONG-ICE VELOCITY, CONTOUR INTERVAL 1 CM/SEC

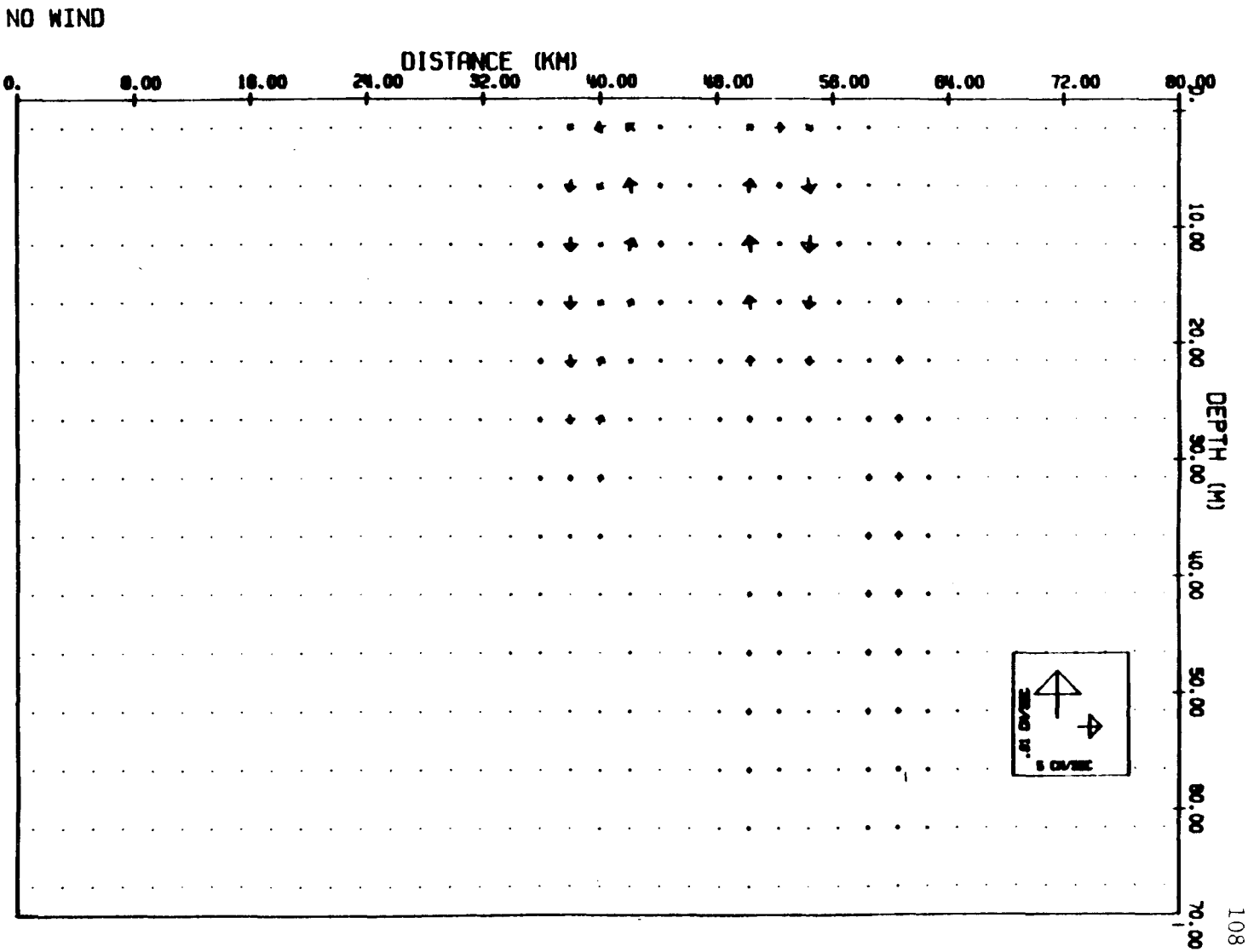

FIGURE 20C: CASE IIA, ACROSS-ICE AND VERTICAL ARROW PLOT AT 60 HOURS

tical water velocities at 60 hours (third panel figure 20) exhibits two regions of divergence at the boundary between the heavy and light ice cover (52 km) and the boundary of open ocean and light ice cover (40 km). These are similar to those that Niebauer (1982) found. This coincides somewhat with the upward displacement of the 25.2 isopycnal in the snap shot of the hydrography (figure 20a). The along-ice (y) velocity maximums are in the region of the boundaries (40 and 50 km, figure 20b). This is because this component of the water velocity is caused by Coriolis acceleration from the across-ice (x) velocities which are at a maximum here (figure 20c). Some baroclinic geostrophic along-ice (y) velocity is noted at depth (figure 20b). This is due to the upward displacement of the isopycnals caused by the downwelling-upwelling.

The surface water velocities are always slightly larger in magnitude and approximately in the same direction as the ice velocities at the same location (figure 19). This implies that the ice movement is totally dependent on the water movement, unlike the previous experiments where wind-driven ice dragged the water along.

Case IIb: The model response to phytoplankton growth and the regeneration of Nitrogen

The following two experiments were conducted to examine the model response to phytoplankton growth through the uptake of inorganic nutrient nitrogen. The effect of the regeneration of particulate nitrogen to inorganic nutrient nitrogen is also tested here. In case IIb1 the regeneration scheme is invoked while in case IIb2 the phytoplankton are grown without regeneration. The initial conditions for the two experiments (figure 21) are no wind stress applied, no ice cover, 5 mg Chl/m^3 and 280 mg N/m^3 mixed homogenously though the water column. These numbers are within the range found at the ice edge in 1982 and 1983. Light is applied in the daily cycles as described in the methods assuming conditions for May 1. The experiment duration is 108 hours.

Comparing the time series of chlorophyll and inorganic nitrogen for the two experiments with and without regeneration (figures 22a, 22b and 23a, 23b) very little difference is noted between the amounts of chlorophyll (figures 22a and 23a) and the amounts of inorganic nitrogen (figures 22b and 23b) in the mixed

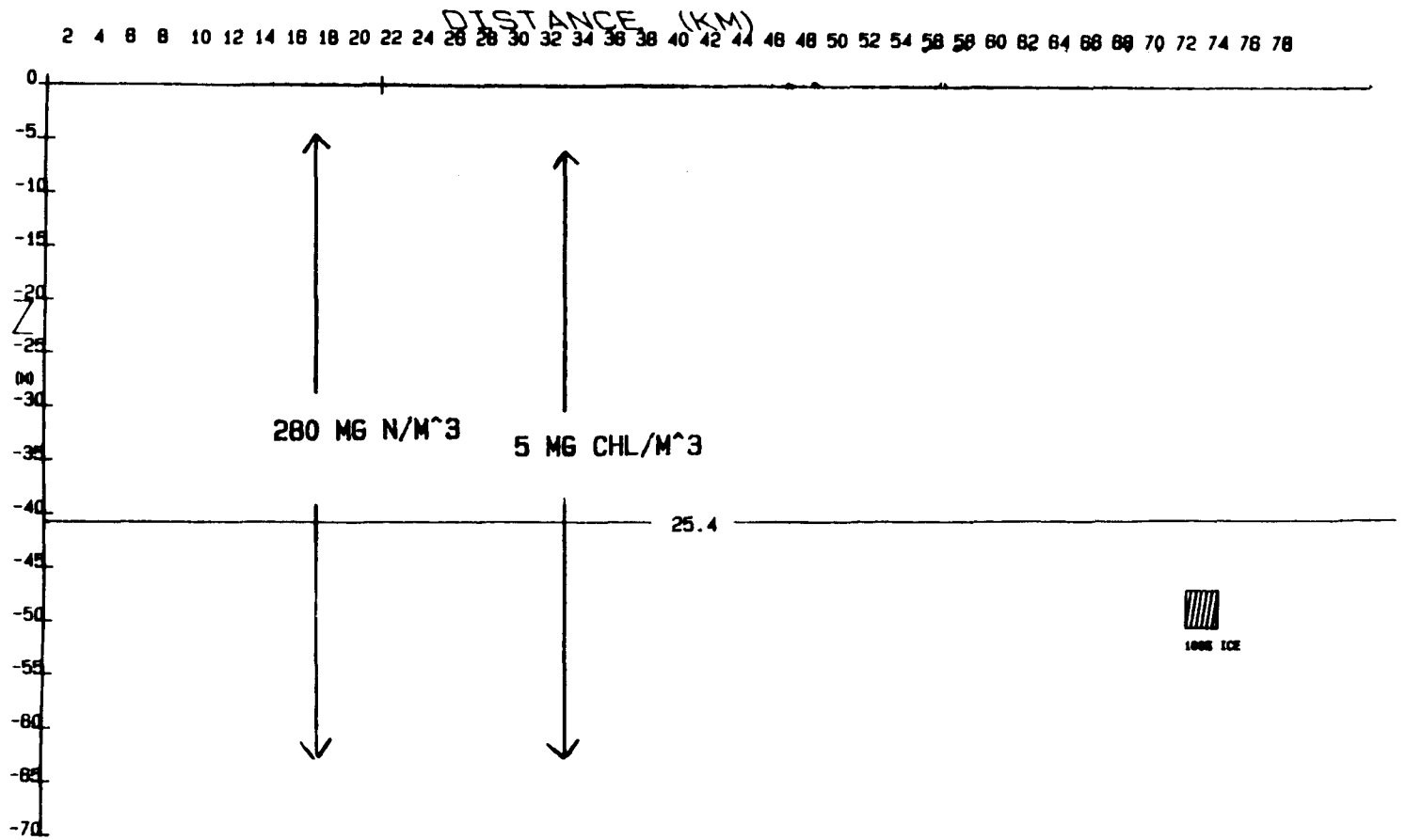

FIGURE 21: CASE IIB, INITIAL CONDITIONS

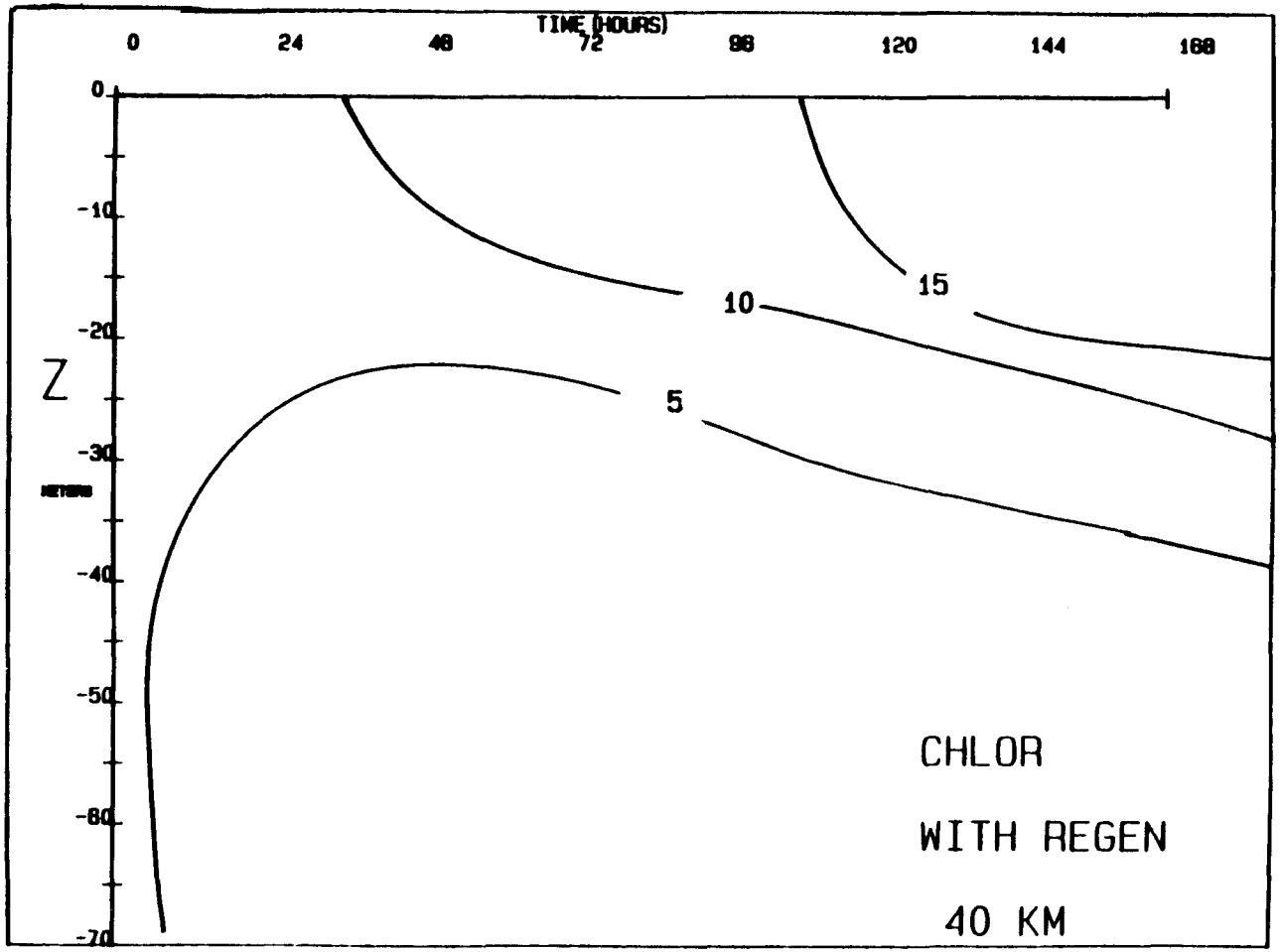

FIGURE 22A: CASE IIB1, TIME SERIES OF CHLOROPHYLL CONCENTRATIONS

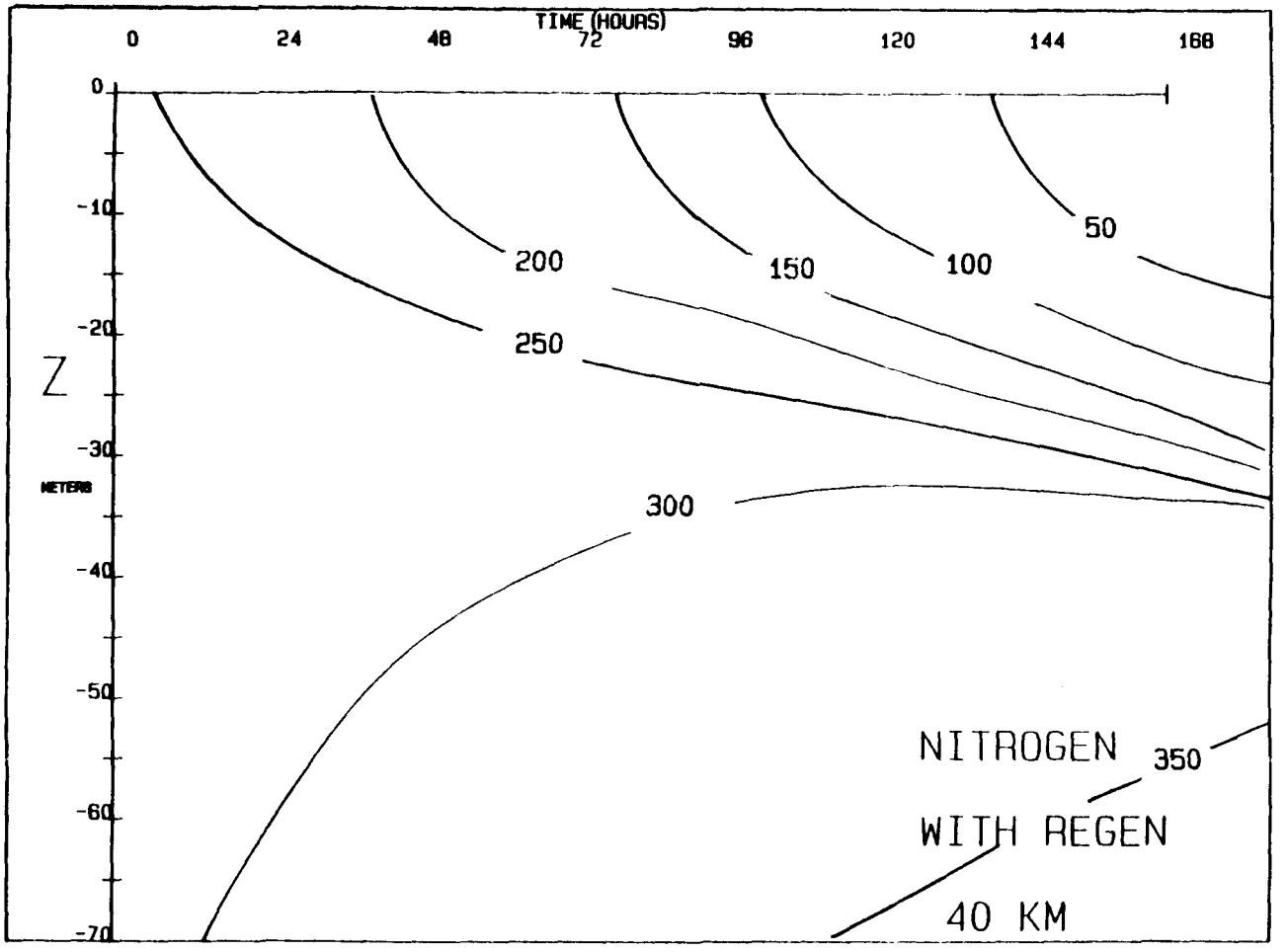

FIGURE 22B: CASE IIB1, TIME SERIES OF NITROGEN CONCENTRATION

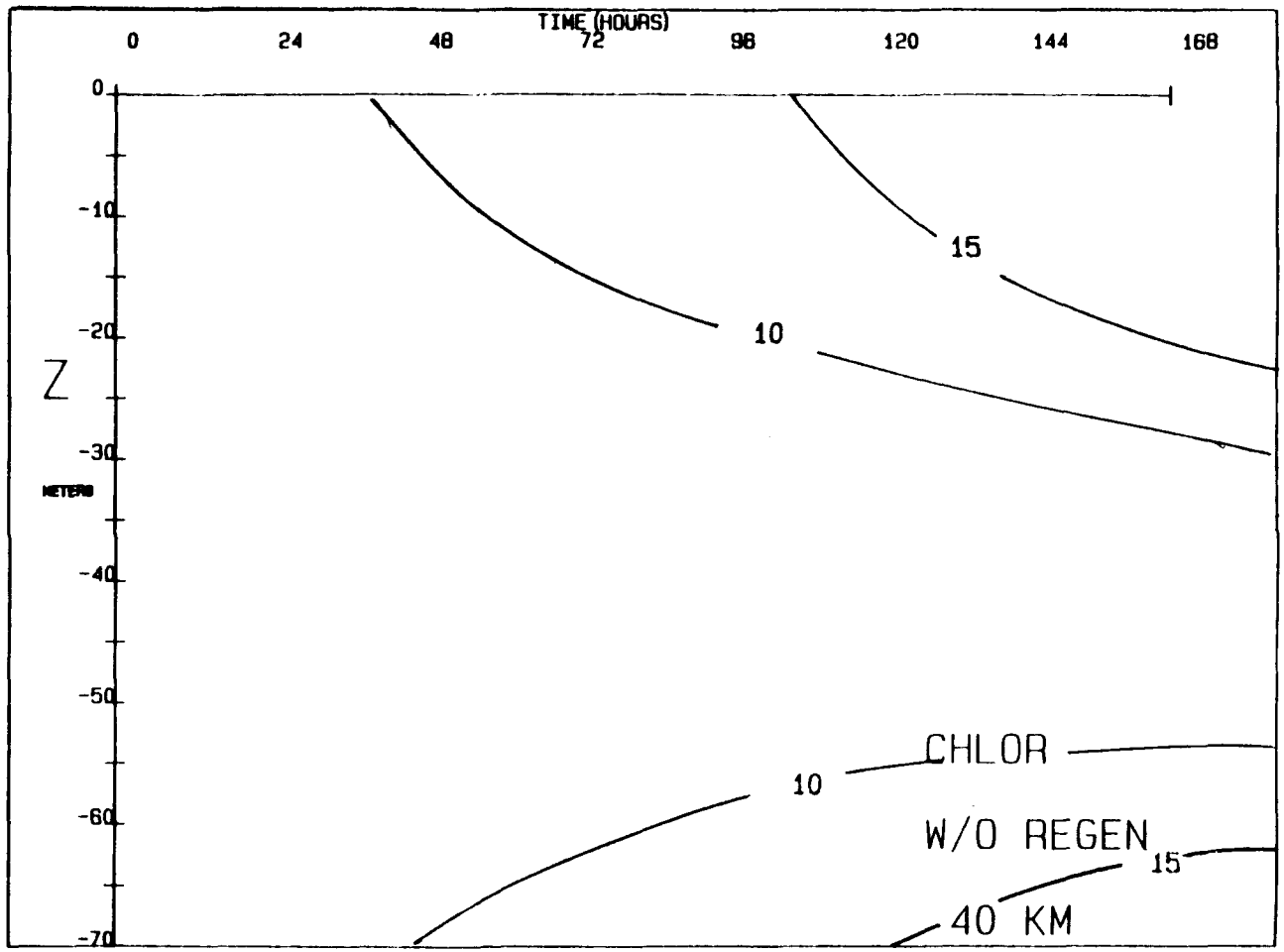

FIGURE 23A CASE IIB2, TIME SERIES OF CHLOROPHYLL CONCENTRATIONS

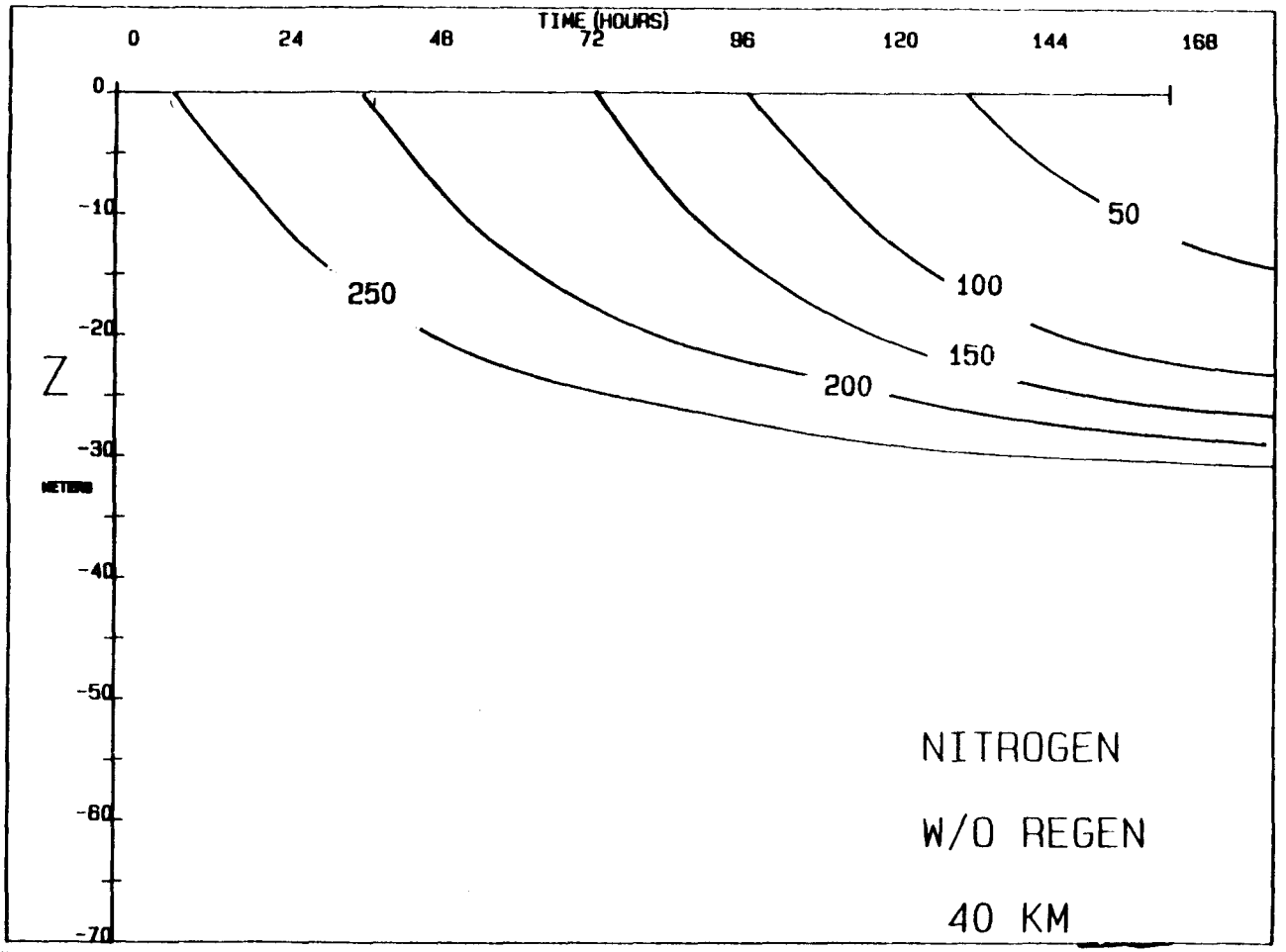

FIGURE 23B: CASE IIB2, TIME SERIES OF NITROGEN CONCENTRATION

layer (above 30 m). This is because it is assumed that in the surface layer the phytoplankton remove the regenerated nitrogen as fast as it is produced, resulting in no net change in plant biomass or nutrient concentration due to uptake of regenerated nitrogen. However, deeper, with regeneration (case IIb1 figure 22a). less chlorophyll and more nitrogen (figure 22b), are present. This is particularly noticable at the bottom where in the case with no regeneration (case IIb2) the chlorophyll accumulation is greater (figure 23a). With regeneration some chlorophyll accumulates but much of it is decomposed to inorganic nitrogen (figure 22b), with high values at 60-70 m after 96 hours. In the real world chlorophyll is not decomposed readily. But in the model it is calculated from particulate nitrogen, when this decomposes the chlorophyll values decrease. This means that a bloom at the surface may be accompanied by increases in inorganic nitrogen at depth.

Case IIc: The role of the ice algae

In this case the hypothesis that the ice algae seed

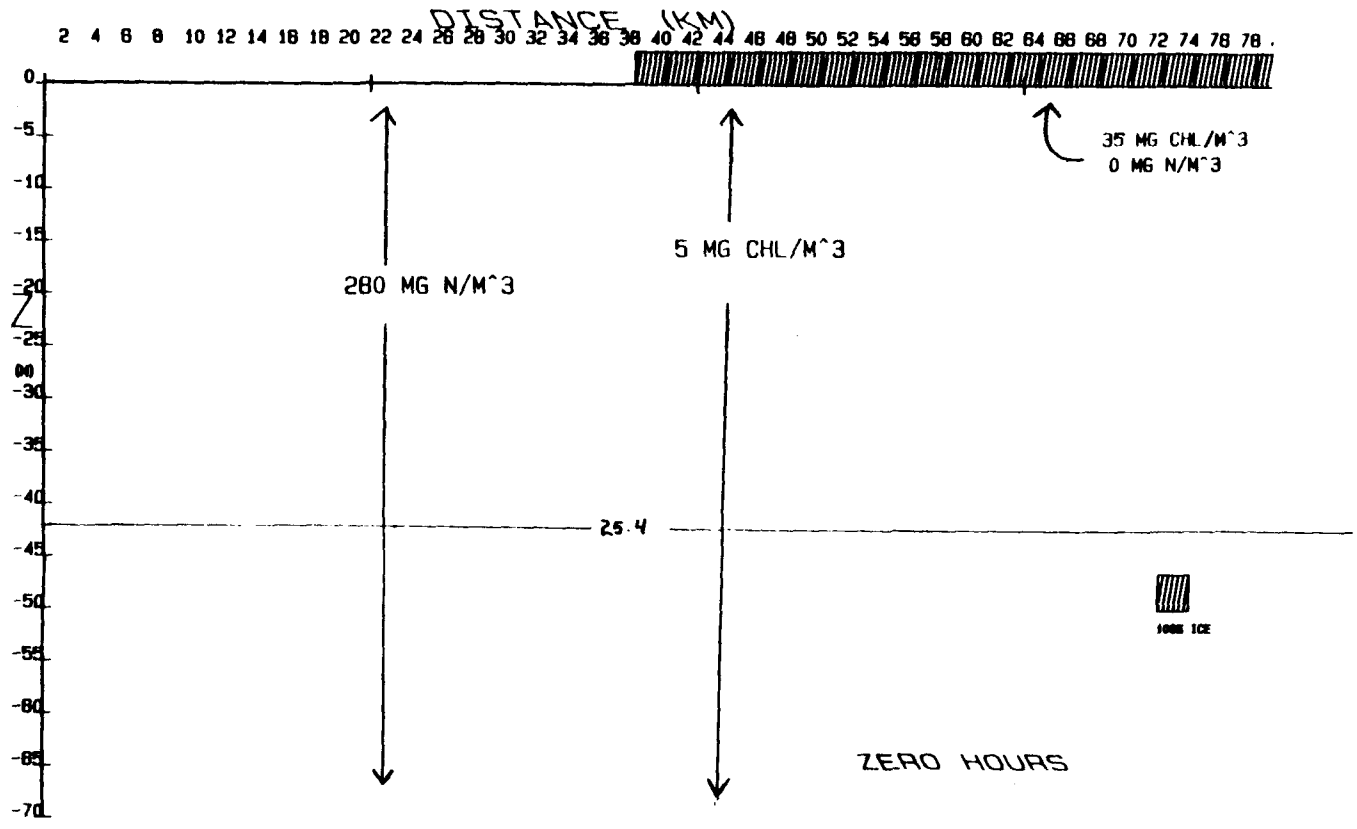

FIGURE 24: CASE IIC, INITIAL CONDITIONS

the bloom is tested. Two experiments are presented. In case IIc1 the ice is melted with an ice algae concentration of 35 mg/m^3 in the ice. This concentration, because it is considered homogeneous through our 50 cm thickness of ice, is on the high side of the values measured on the ice edge cruises of 1982 and 1983 (10-38 mg/m^3) and those reported by Alexander and Chapman (1981). However we desired to check the assumption that the ice algae could possibly make a difference so a high concentration was used. In case IIc2 it is assumed that no algae are present in the ice. Initially 5 mg Chl/m^3 and 280 mg N/m^3 are present in the water for both parts of IIc. These are within the ranges found on the ice edge cruises in 1982 and 1983. Muller-Karger (1984) measured a mean of about 50 mg N/m^3 in the bottom 10 cm of ice. Because we consider this concentration to be mixed homogeneously in our 50 cm thickness of ice, the resultant concentration is approximately 10 mg N/m^3. Therefore for simplicity it is assumed that no inorganic nitrogen is added to the system by melting ice. No wind stress is applied in either experiment and the initial hydrography is the same as for the previous experiments (figure 7). The initial ice conditions are a region of 90% ice cover

from 40 to 80 km (figure 24). We use 90% instead of 100% cover to speed up the melting process. It would take approximately 7 days for the 100% ice cover to melt down to 90% cover according to our melting scheme (equation 11), but less than one day to decrease from 90 to 80%.

Case IIc1: With ice algae

The cross-section of sigma-t at 48 hours (figure 25a) shows that as the ice melts, the water column becomes stratified under the ice. Small along-ice (y) velocities develop (figure 25b), with the maximum magnitudes in the region of the ice edge. These velocities are baroclinic geostrophic because of the establishment of a stratification gradient due to the input of fresh water from melting ice. In the vertical (z) and across-ice (x) directions (figure 25c) a circulation cell has developed in the region of the ice edge. The upwelling results in the bending upward of the isopycnal at 38 km (figure 25a).

Chlorophyll values at the surface under the ice (figure 25d) have about doubled to 10 mg/m^3. In the

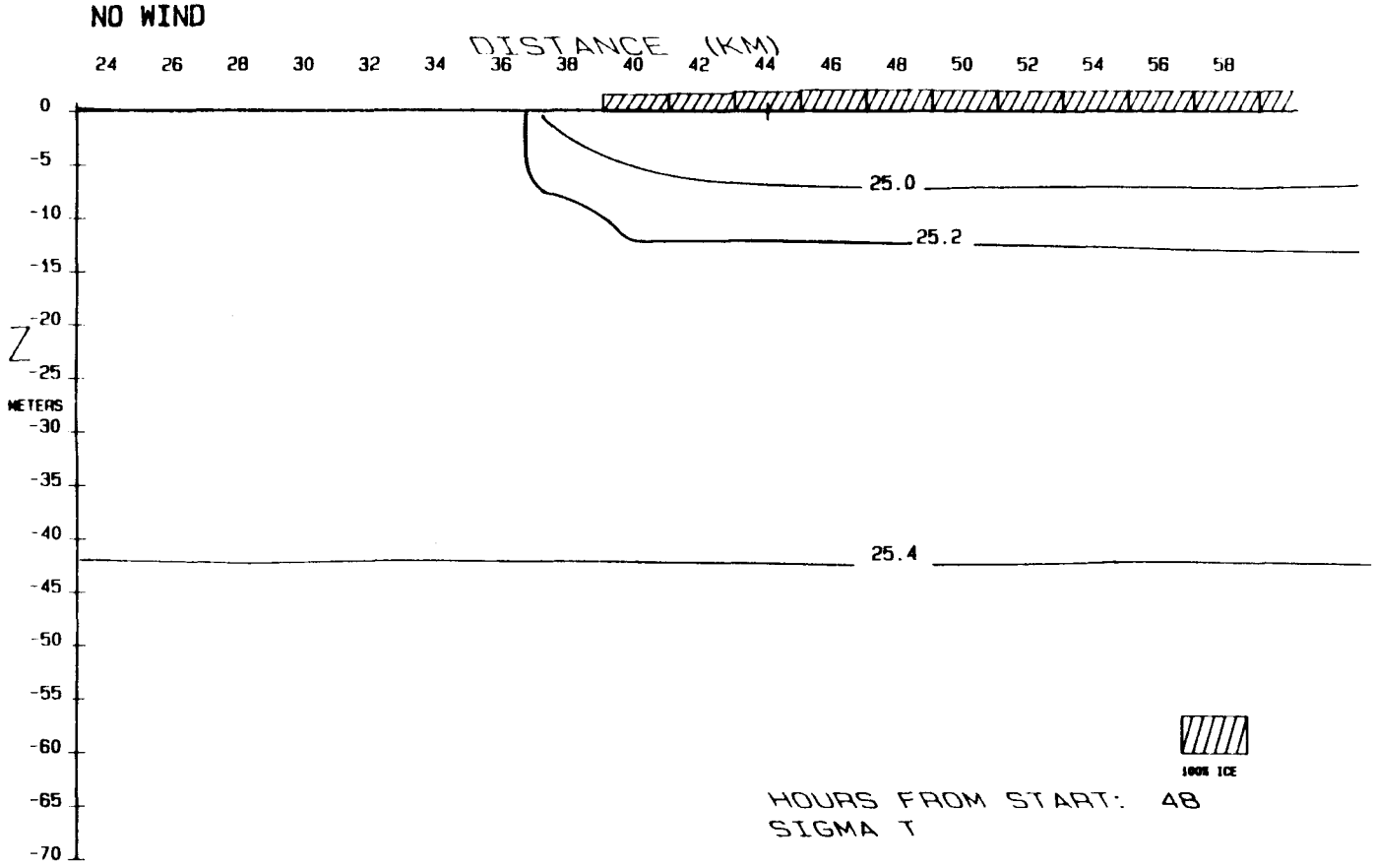

FIGURE 25A: CASE IIC1 AT 48 HOURS, SIGMA-T

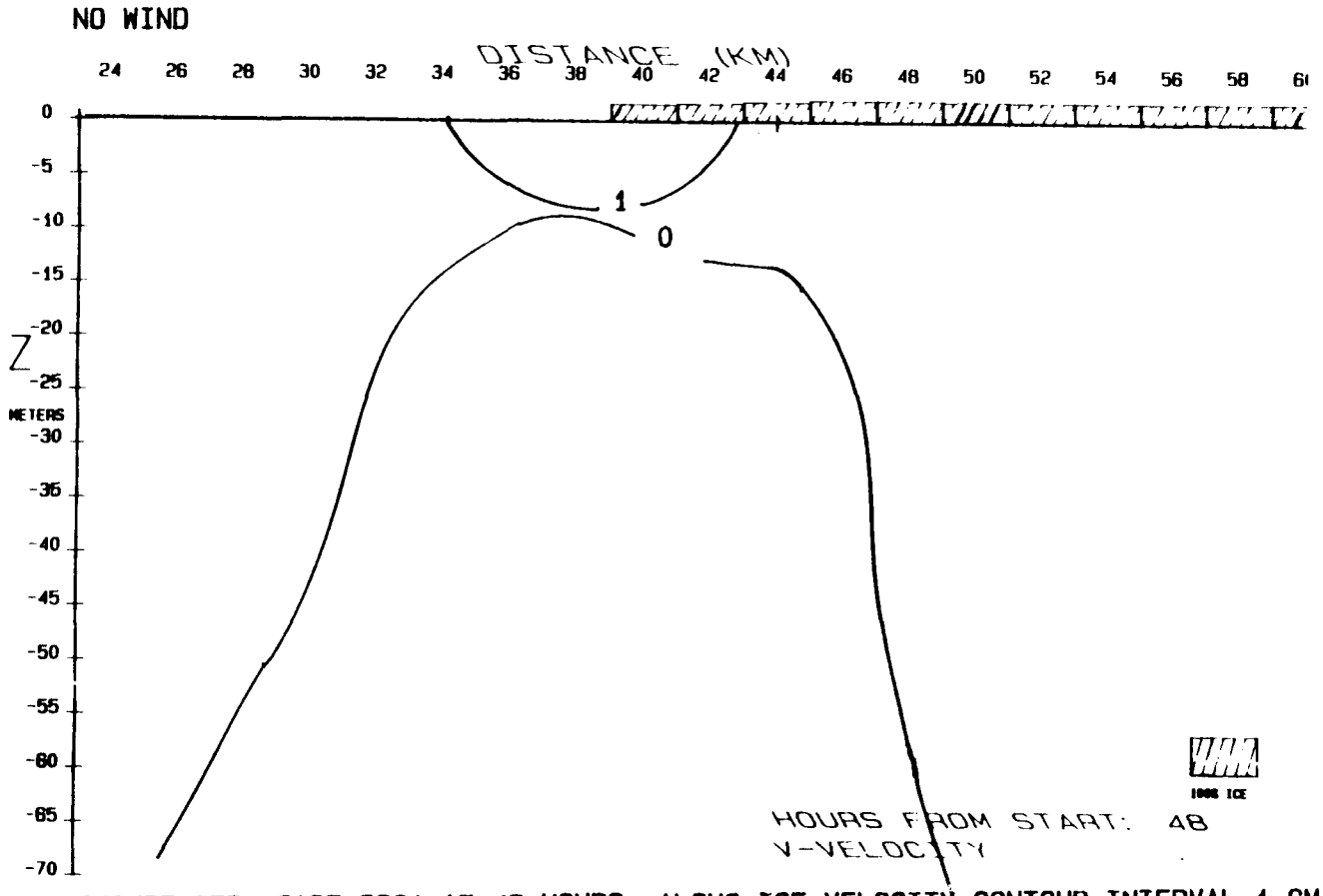

FIGURE 25B: CASE IIC1 AT 48 HOURS, ALONG-ICE VELOCITY, CONTOUR INTERVAL 1 CM/SEC

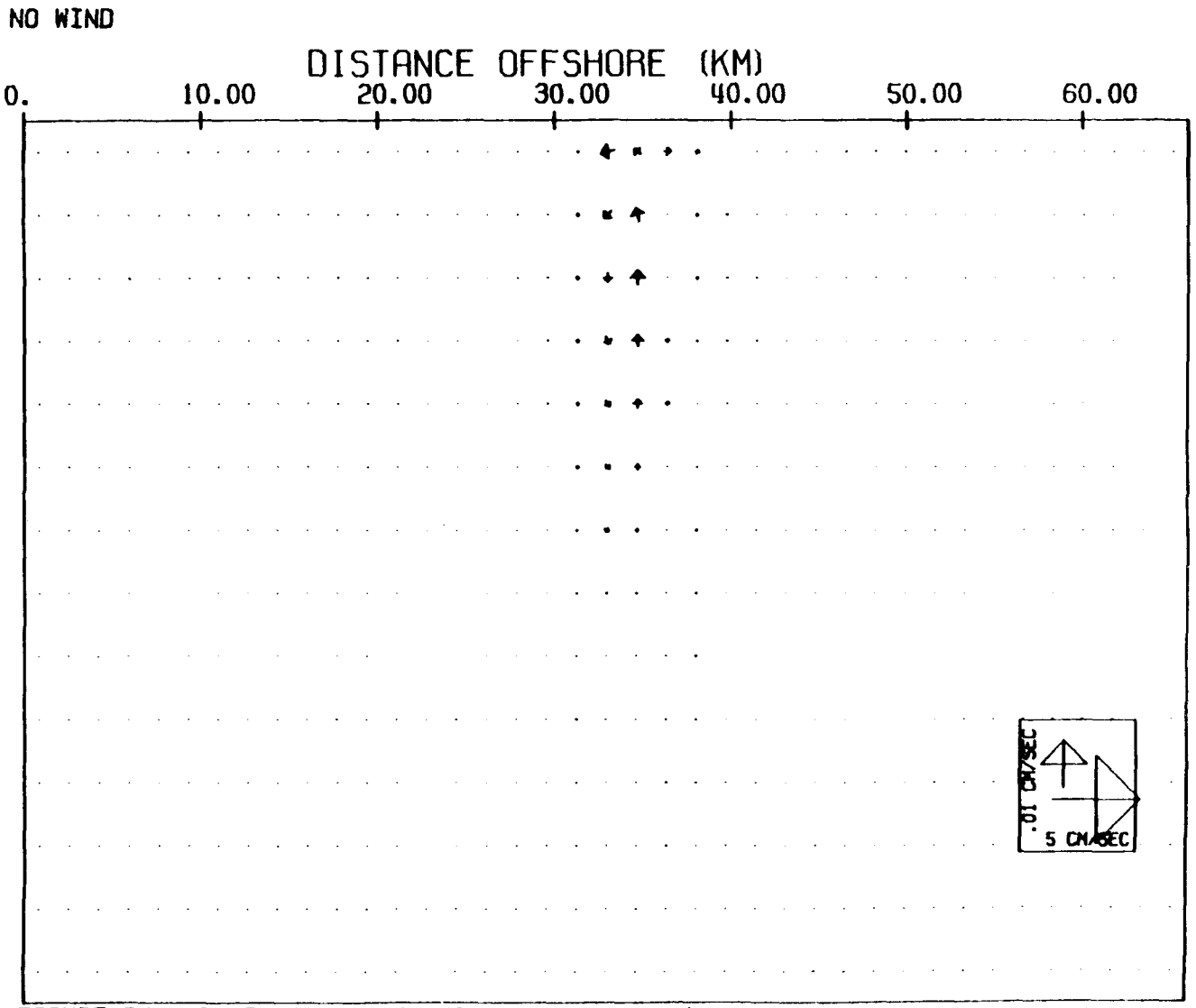

FIGURE 25C: CASE IIC1 AT 48 HOURS, ACROSS-ICE/VERTICAL VELOCITY ARROW PLOT

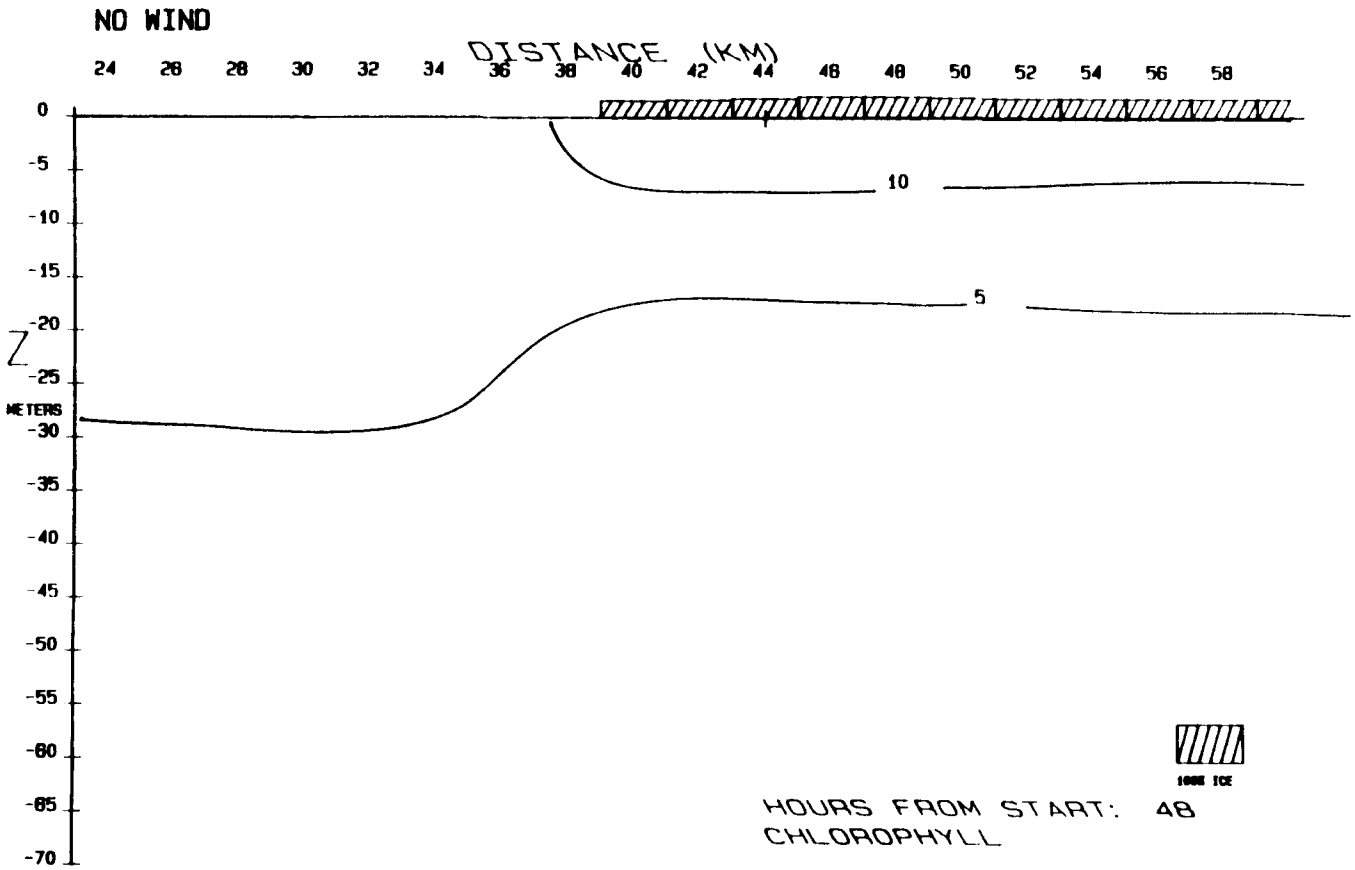

FIGURE 25D: CASE IIC1 AT 48 HOURS, CHLOROPHYLL CONCENTRATION

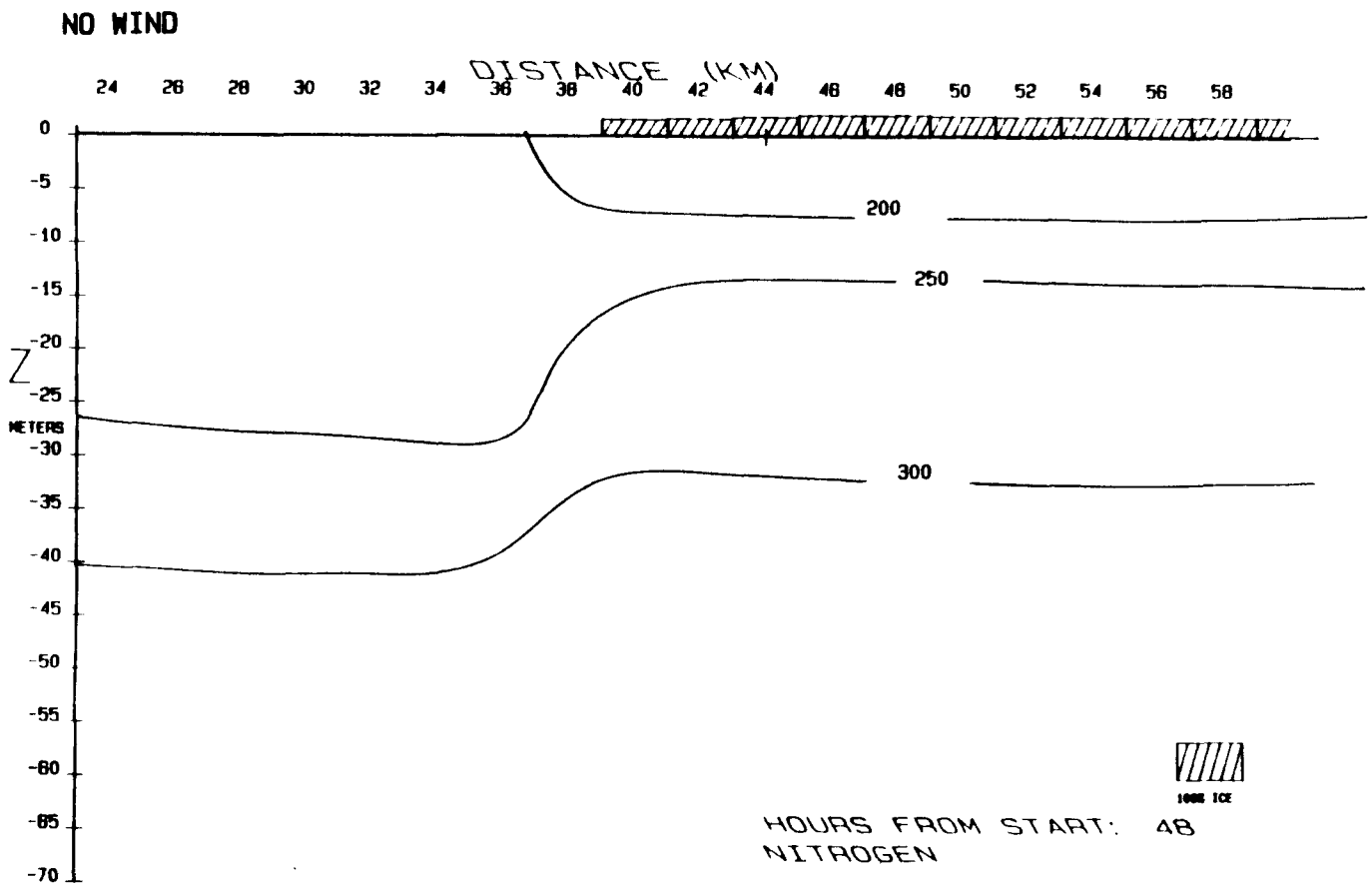

FIGURE 25E: CASE IIC1 AT 48 HOURS, NITROGEN CONCENTRATION

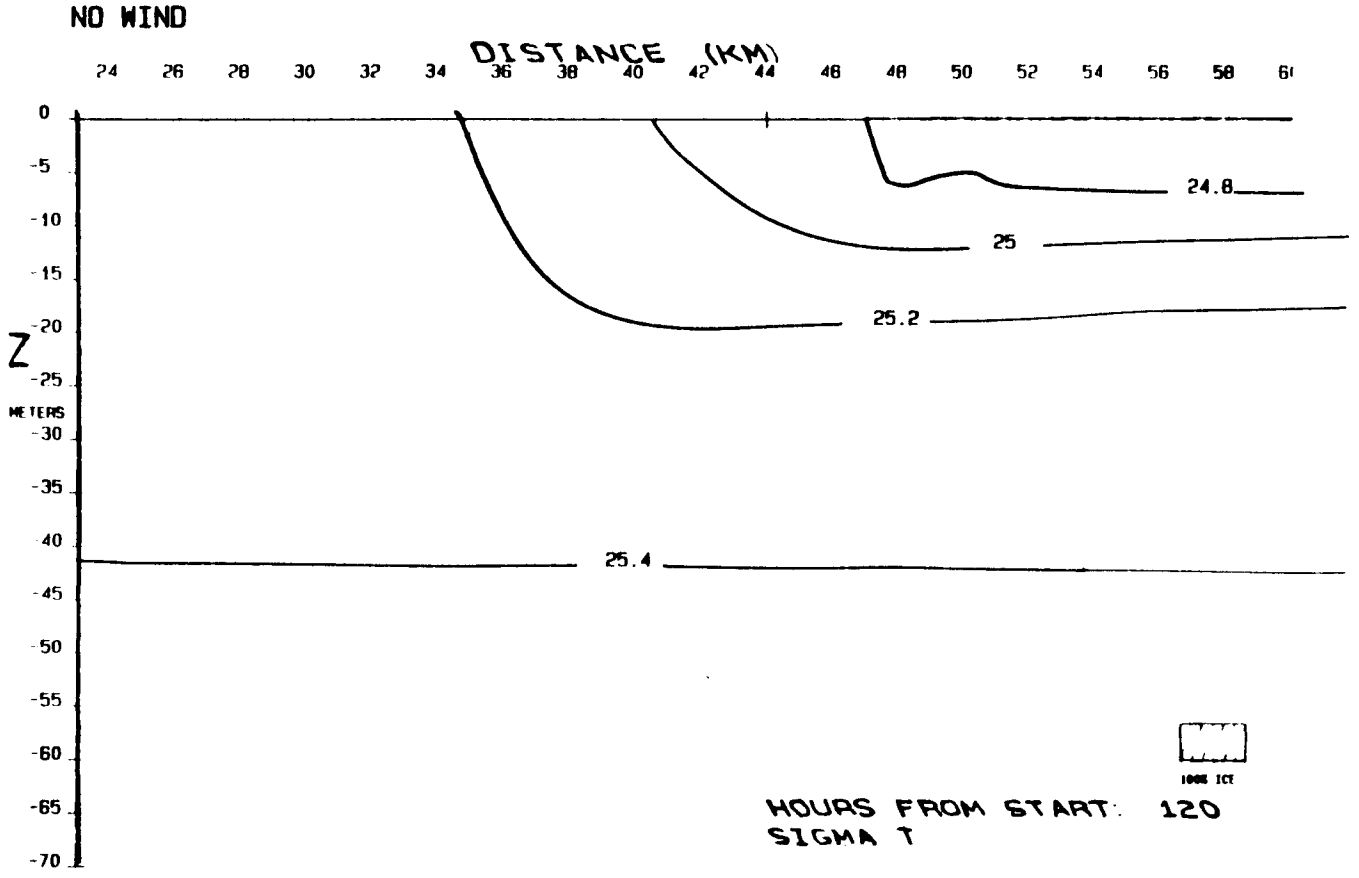

FIGURE 28A: CASE IIC1 AT 120 HOURS, SIGMA-T

NO WIND

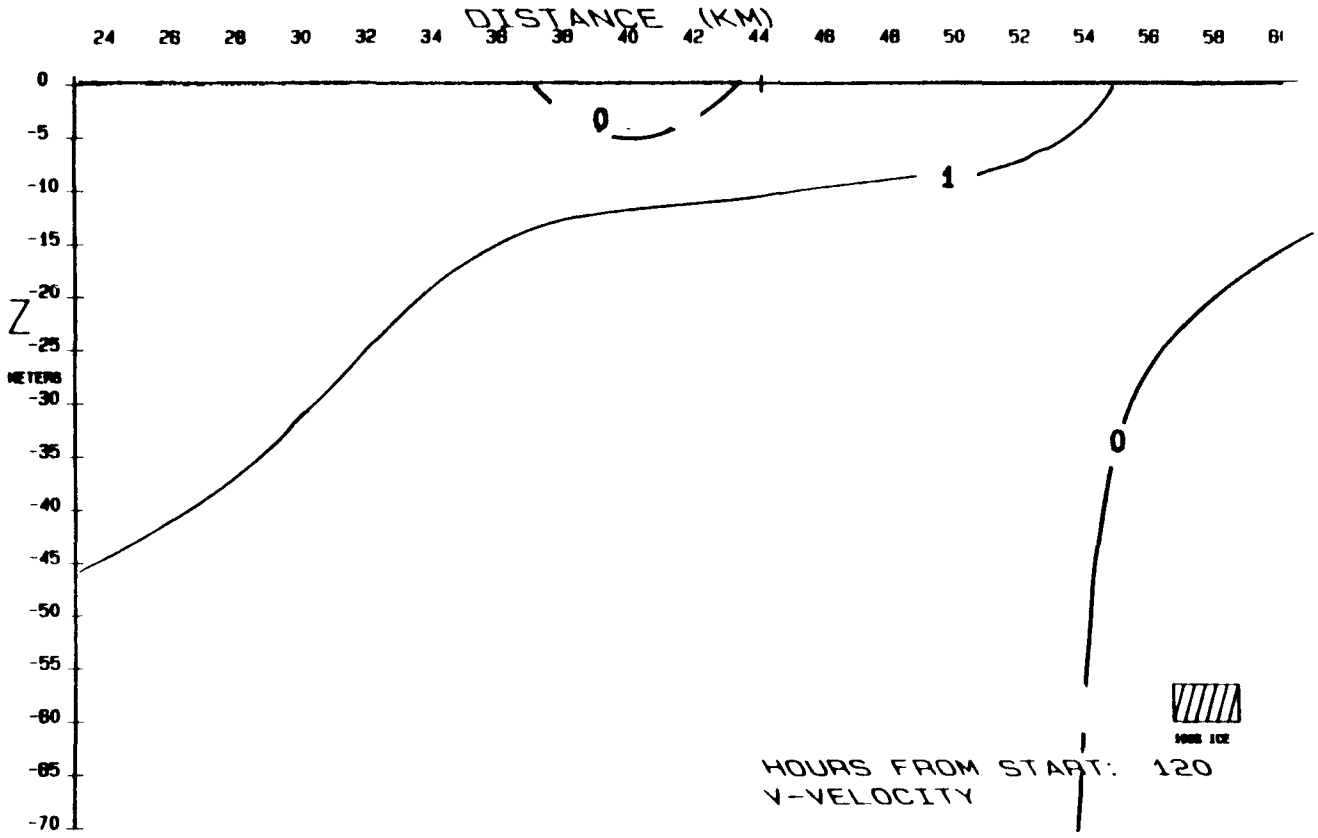

FIGURE 28B: CASE IIC1 AT 120 HOURS, ALONG-ICE VELOCITY, CONTOUR INTERVAL 1 CM/SEC

NO WIND

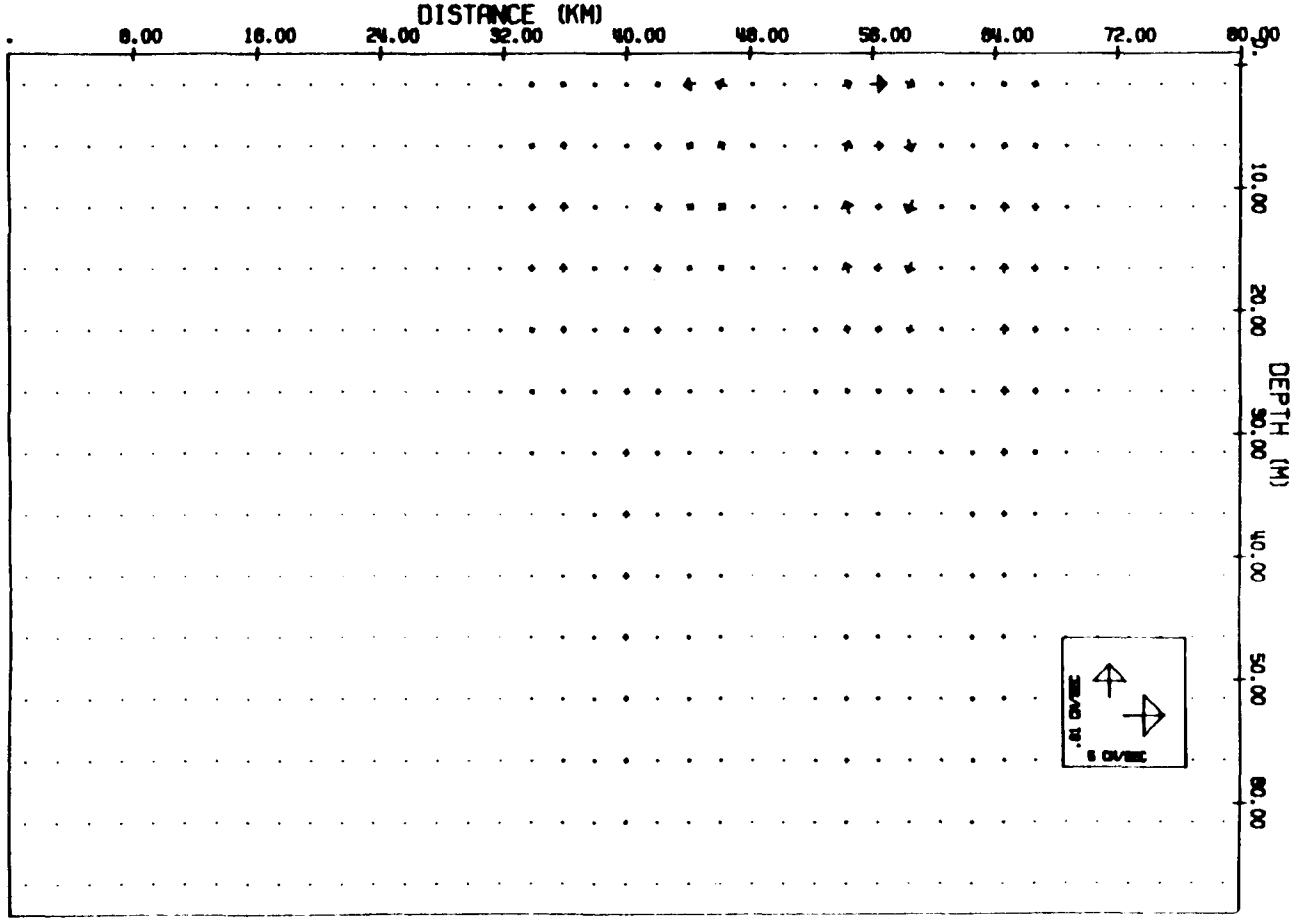

FIGURE 26C: CASE IIC1 AT 120 HOURS, ACROSS-ICE/VERTICAL VELOCITY ARROW PLOT

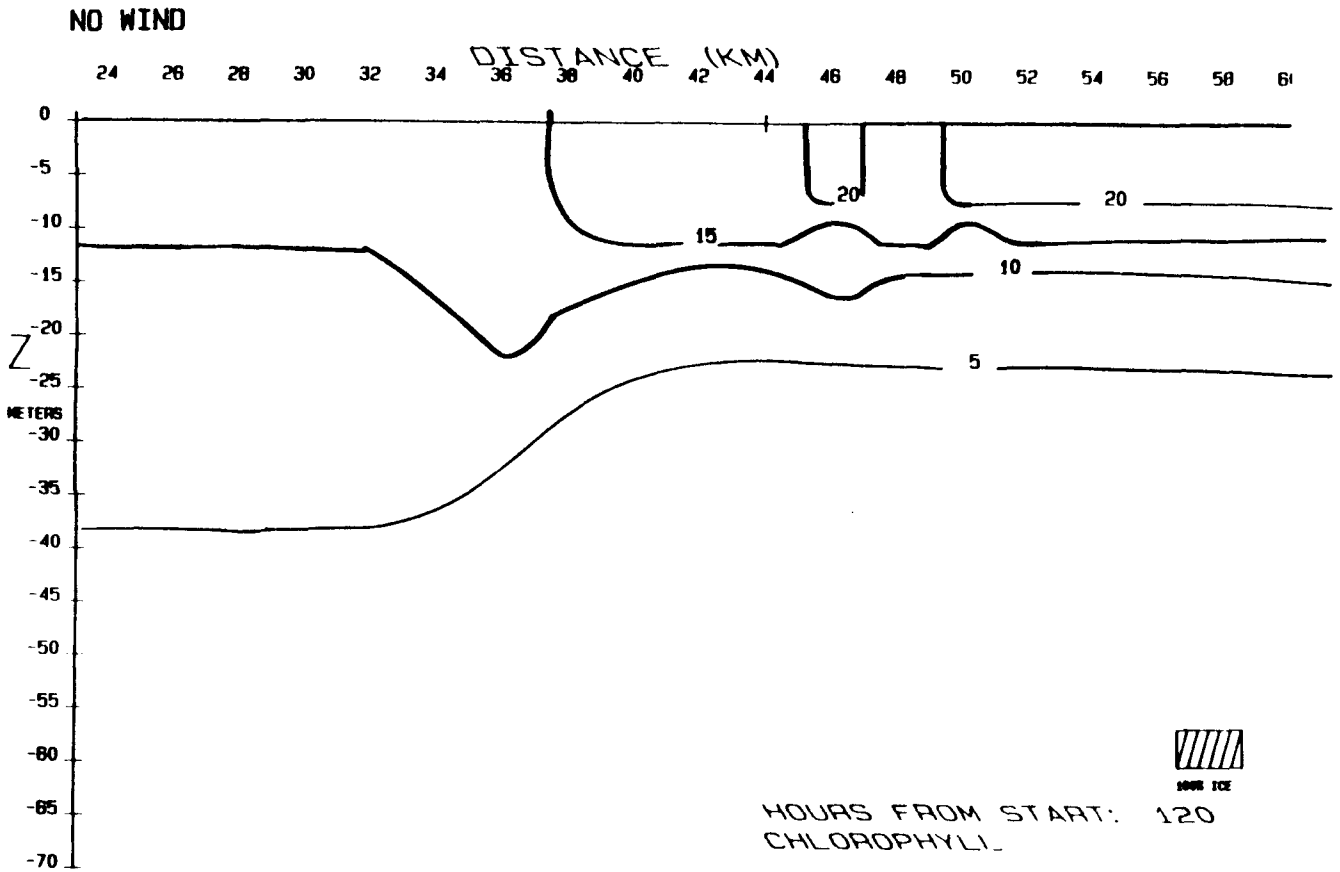

FIGURE 26D: CASE IIC1 AT 120 HOURS, CHLOROPHYLL CONCENTRATION

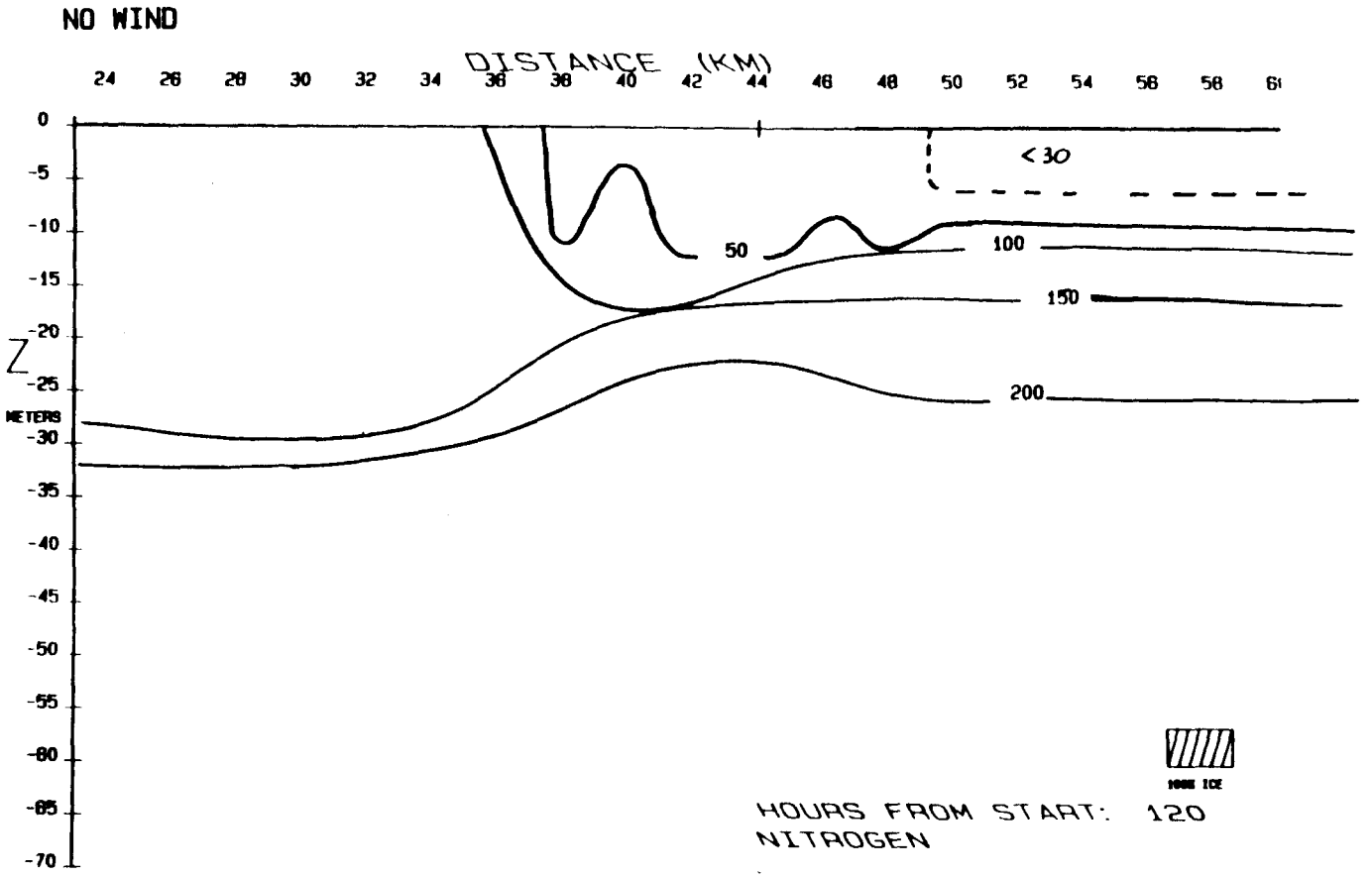

FIGURE 26E: CASE IIC1 AT 120 HOURS, NITROGEN CONCENTRATION

surface well removed from the ice the values are approximately 7 mg Chl/m^3. Photosynthesis is occurring here, but chlorophyll is being mixed downward further and faster in this unstratified region than in regions with stratification. This is because in regions without stratification, the vertical eddy diffusivity (K_z~55 cm^2/sec) is greater than where the water column is stratified (K_z~1 cm^2/sec). This phenomenon is evidenced by the slope in the isopleth of 5 mg/m^3 chlorophyll at about 38 km. At depth chlorophyll values are higher away from the ice than nearby it within the stratified layers.

The distribution of inorganic nitrogen (figure 25e) has a similar structure to chlorophyll and sigma-t (figures 25a and 25d). The lowest nitrogen concentrations are in the surface water under the ice where most of the chlorophyll is located. With depth the isopleth of 250 mg N/m^3 is in the same approximate position as the 5 mg Chl/m^3 isopleth. Below about 35-40 m the nutrient concentrations have increased to over 300 mg N/m^3 from 280 mg N/m^3, at time zero. This is due to regeneration and to the light limiting conditions which result in a depression in phytoplankton uptake rate. The increase in nitrogen is not seen in the surface

because it is assumed that regenerated nitrogen in the mixed layer is instantaneously available for photosynthesis providing light is not limiting.

After 120 hours most of the ice is melted and the stratification has intensified (figure 26a) with sigma-t values of less than 24.8 under the ice at the surface. Velocities in the horizontal directions as well as the vertical have intensified somewhat but the maxima remain in association with the ice edge (figure 26b and 26c). Chlorophyll (figure 26d) maxima of 20 mg/m^3 are under the ice (50-80 km) and in a small pocket adjacent to the ice edge at 48 km. The 5 mg Chl/m^3 isopleth has sunk somewhat, from 20 to 25 m under the ice and 28 to 38 m away from the ice. The reason it sunk less under the ice is because of the greater primary production here. This results in a greater input of algae from the surface to depth. Nutrient concentration (figure 26e) again reflects the chlorophyll cross-section (figure 26d) and the sigma-t cross-section (figure 26a). The regions of maximum vertical velocities may also be noted by the displacement upward and downward of the isopleths of nitrogen, particularly at 38-40 km and 48-50 km. High nutrient concentrations, >350 mg N/m^3, at the bottom are the

result of chlorophyll that either sank or was mixed downward and subsequently turned into regenerated nitrogen.

Case IIc2: Without ice algae

The cross-sections (not shown) of this experiment look approximately the same as those for case IIc1. The only difference is that the surface chlorophyll values are slightly lower while the surface inorganic nitrogen values are minutely smaller. Here the chlorophyll values are about 1 mg/m^3 less than those in the previous experiment at 120 hours. Input of ice algae appear to make very little difference. However this is probably due to our initial condition of water column chlorophyll (5 mg/m^3) which is a high value to start with. If we invoked an initial condition of 1 mg chl/m^3 in the water, the end results of case IIc2 might have looked very different. This is addressed further in the discussion section.

Case III: Physical and Biological response to Wind and Melting

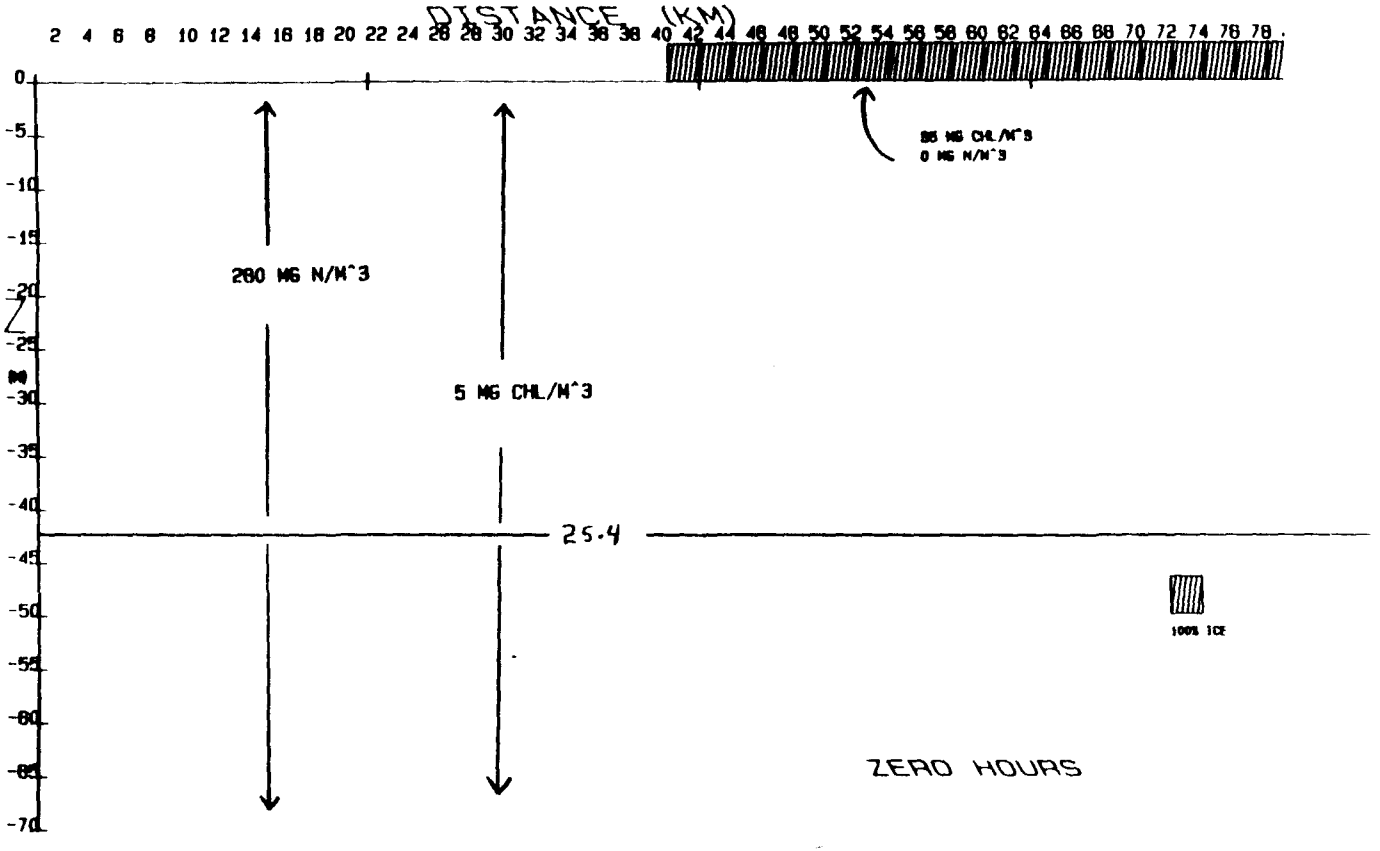

FIGURE 27: CASE III INITIAL CONDITIONS

The physical and biological response of the model to two different winds are explored. The initial conditions (figure 27) for the experiments are the same hydrography as the previous cases, 100% ice cover from 40 to 80 km, 35 mg Chl/m^3 in the ice, 5 mg chl/m^3 in the water, 280 mg inorganic N/m^3 in the water and no inorganic nitrogen in the ice (see case IIc for the rationale of these values). The ice is allowed to melt (equation 11) and the regeneration scheme is invoked. In case IIIa1 an along-ice wind with the ice to the right (pos. y) is applied while in case IIIa2 we invoke an along-ice wind with the ice to the left (neg. y). In case IIIb we investigate the across-ice (x) situation with an off-ice (neg. x) wind. In addition to the two above experiments, in case IIIc we investigate the effects of melting in relation to the wind and biology. Here the experiment is run with all the same conditions as case IIIa but the ice is not allowed to melt. In all three cases the wind stress of 1 dyne/cm^2 is applied for 18 hours and the experiment durations are 120 hours.

Case IIIa1: along-ice (pos. y) wind with ice to right

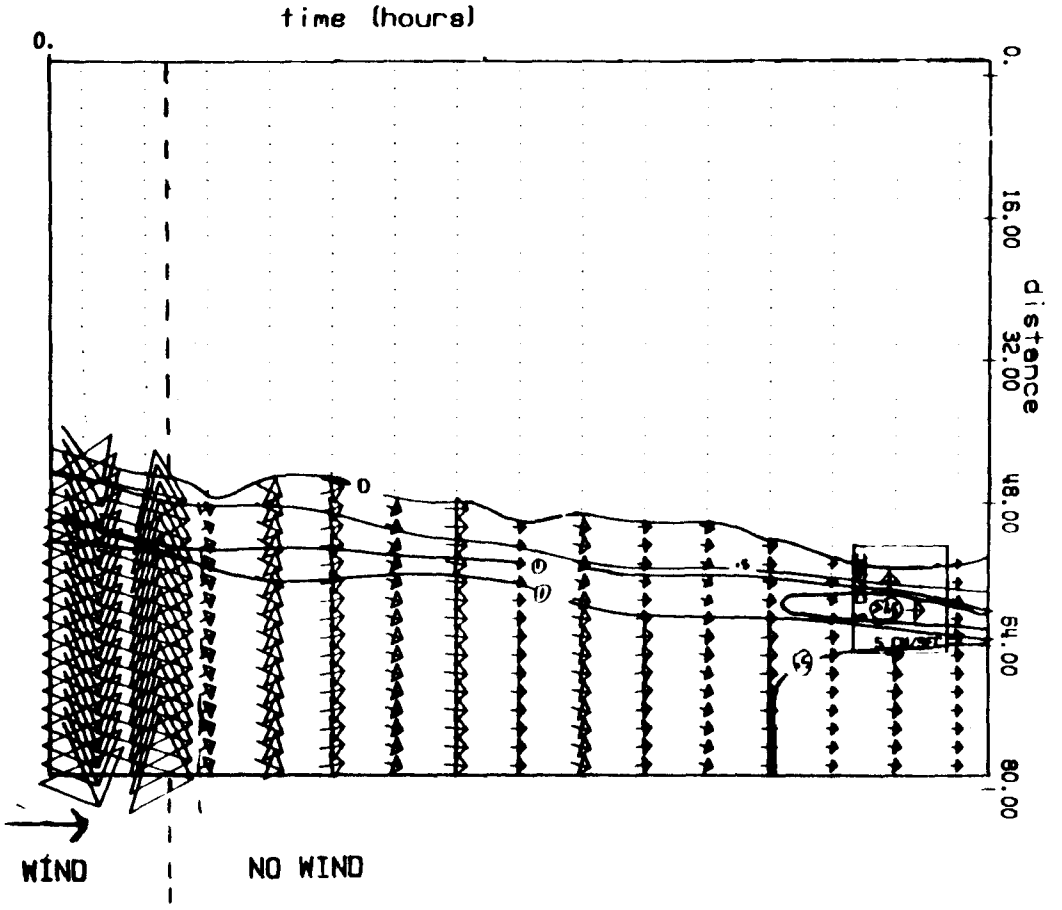

FIGURE 28: CASE IIIA1 TIME SERIES OF ICE VELOCITIES AND COMPACTNESS

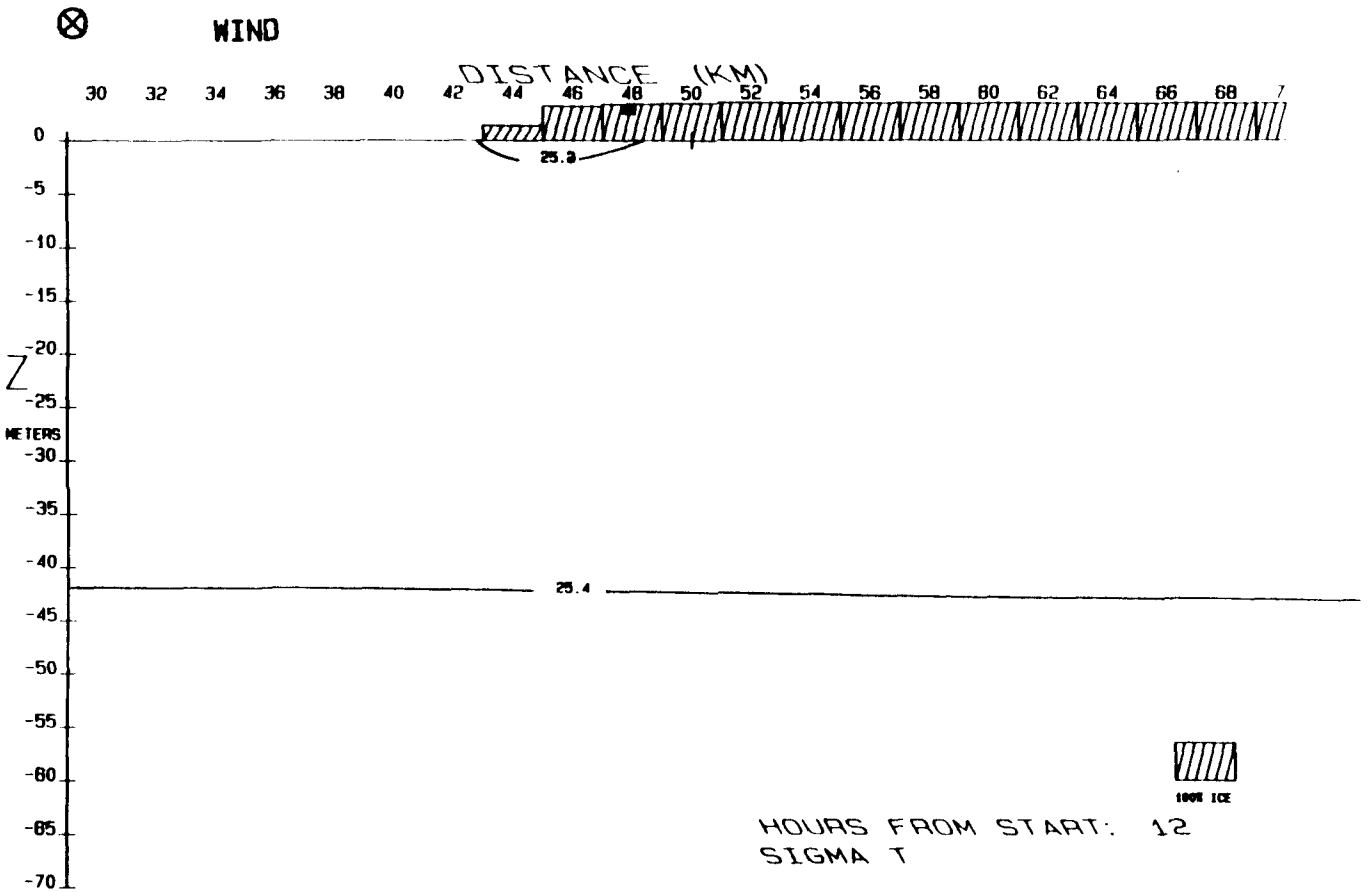

FIGURE 29A: CASE IIIA1 AT 12 HOURS, SIGMA-T

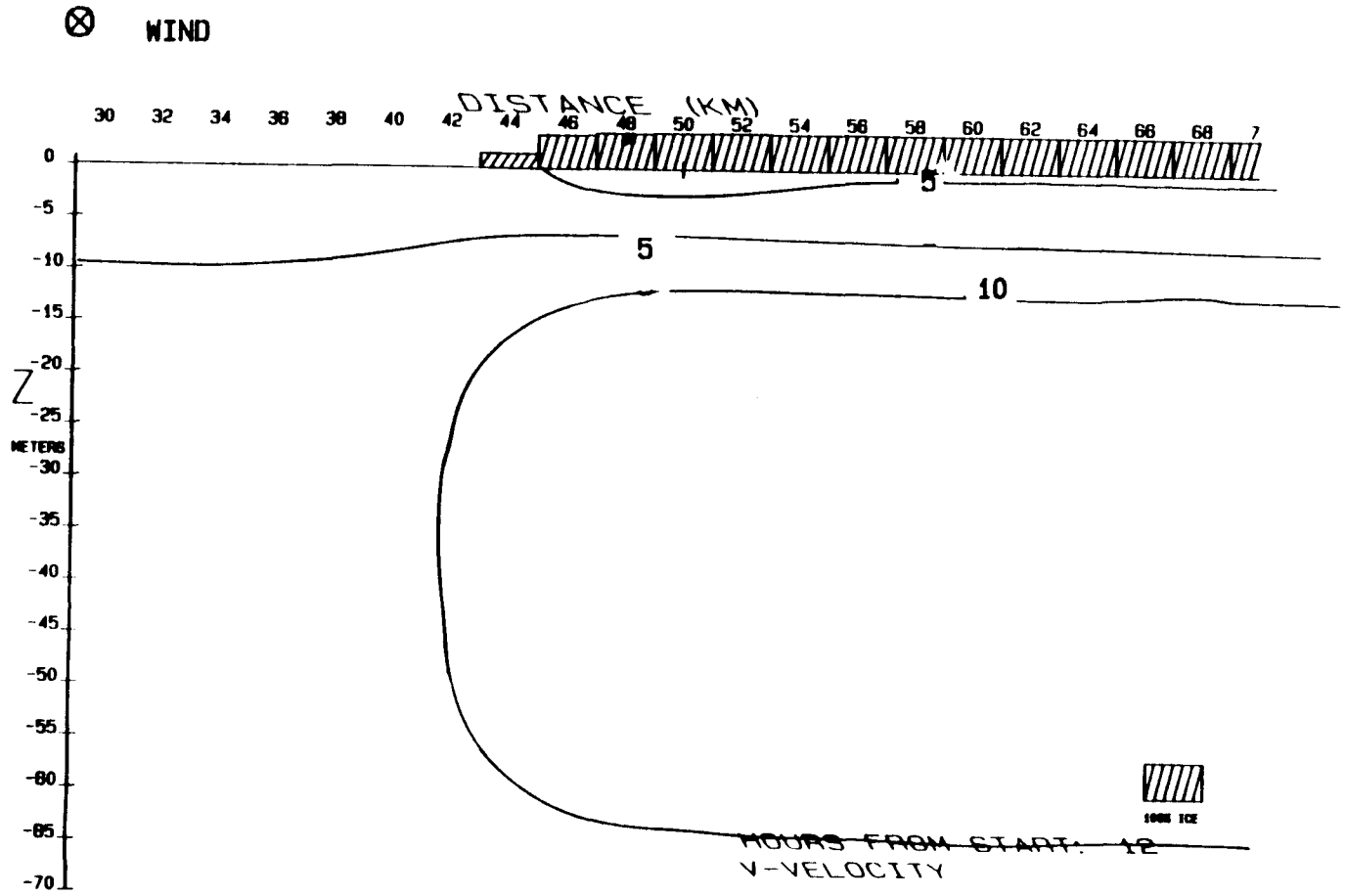

FIGURE 29B: CASE IIIA1 AT 12 HOURS, ALONG-ICE VELOCITY

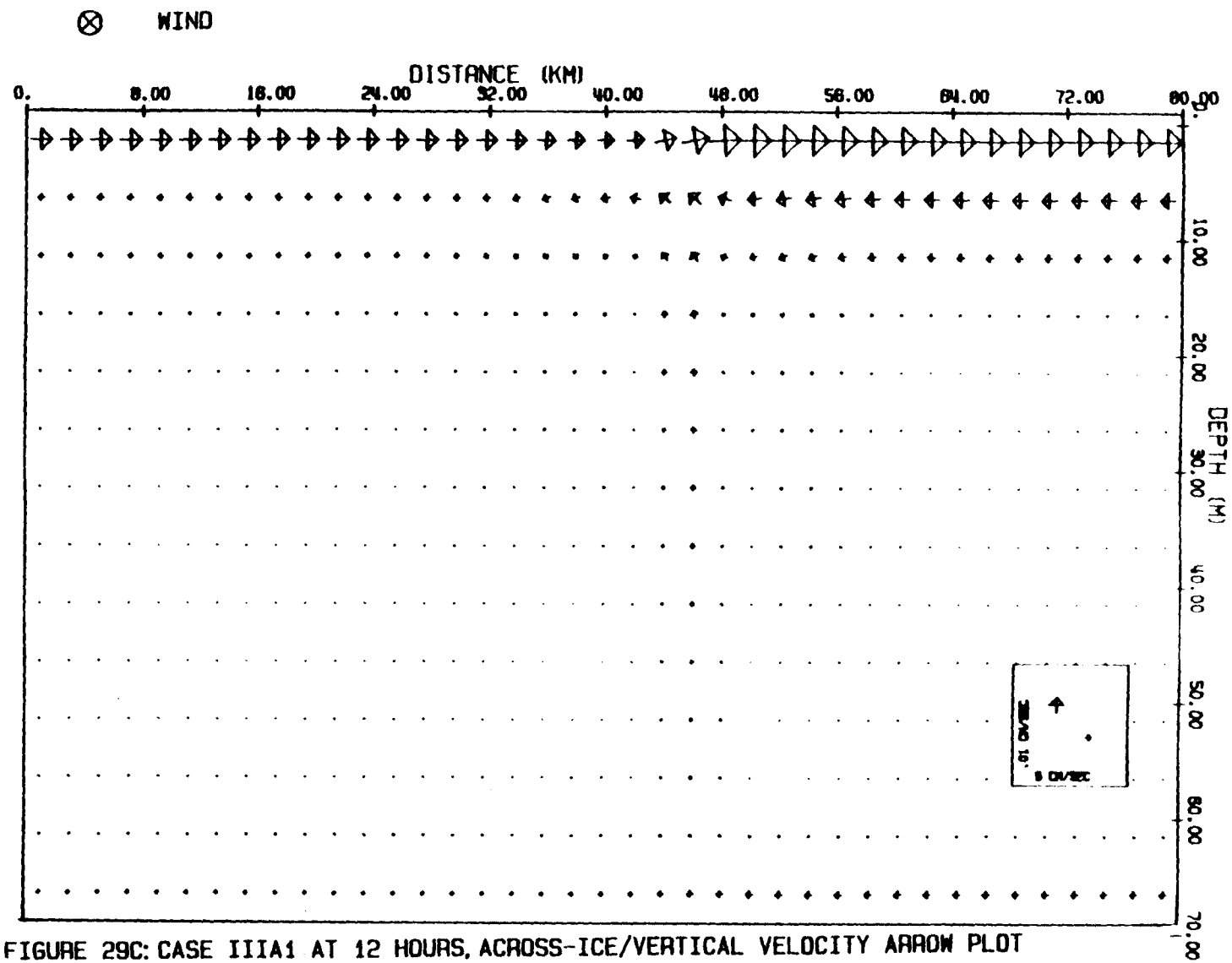

FIGURE 29C: CASE IIIA1 AT 12 HOURS, ACROSS-ICE/VERTICAL VELOCITY ARROW PLOT

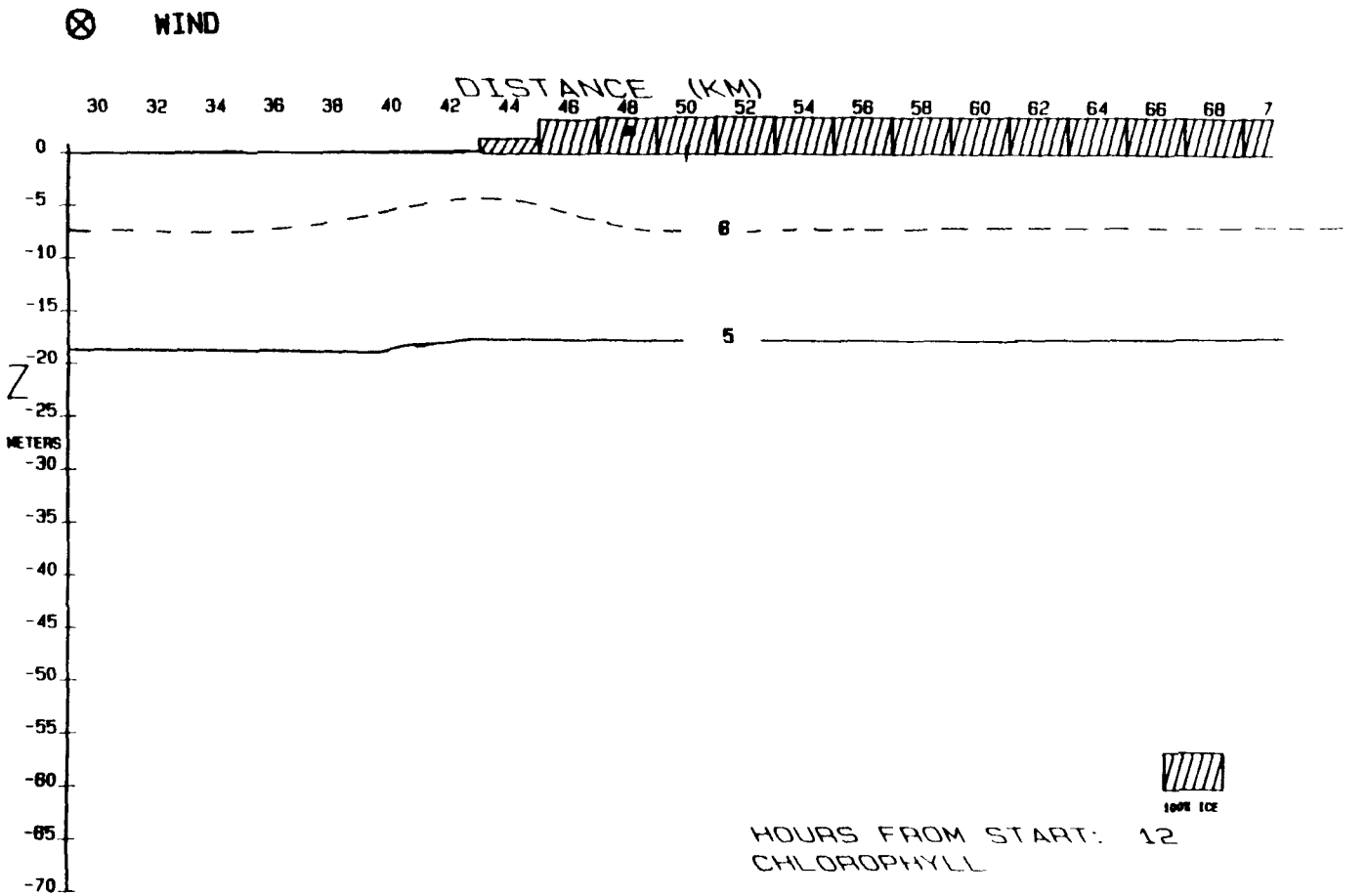

FIGURE 29D: CASE IIIA1 AT 12 HOURS, CHLOROPHYLL CONCENTRATION

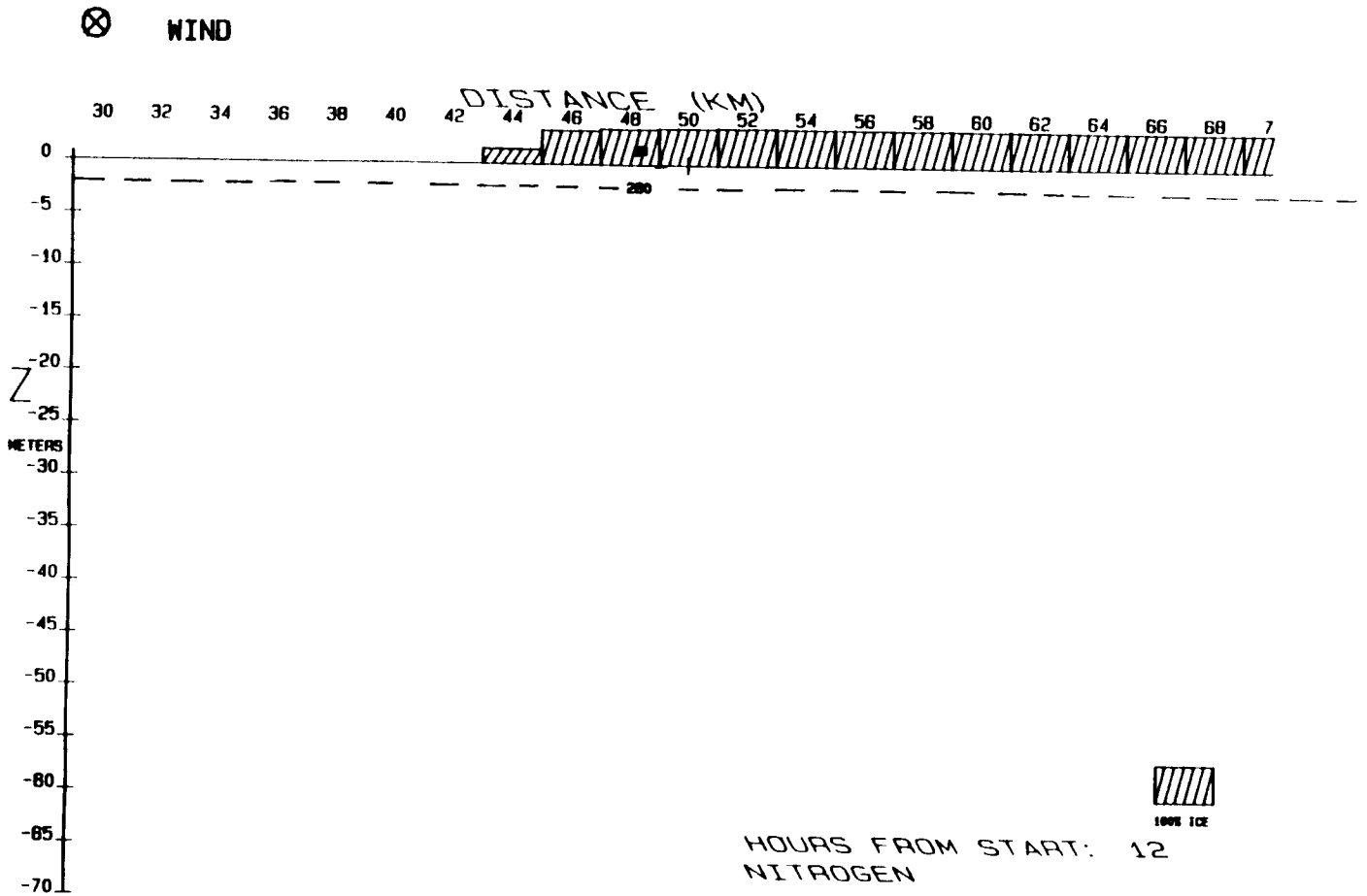

FIGURE 29E: CASE IIIA1 AT 12 HOURS, NITROGEN CONCENTRATION

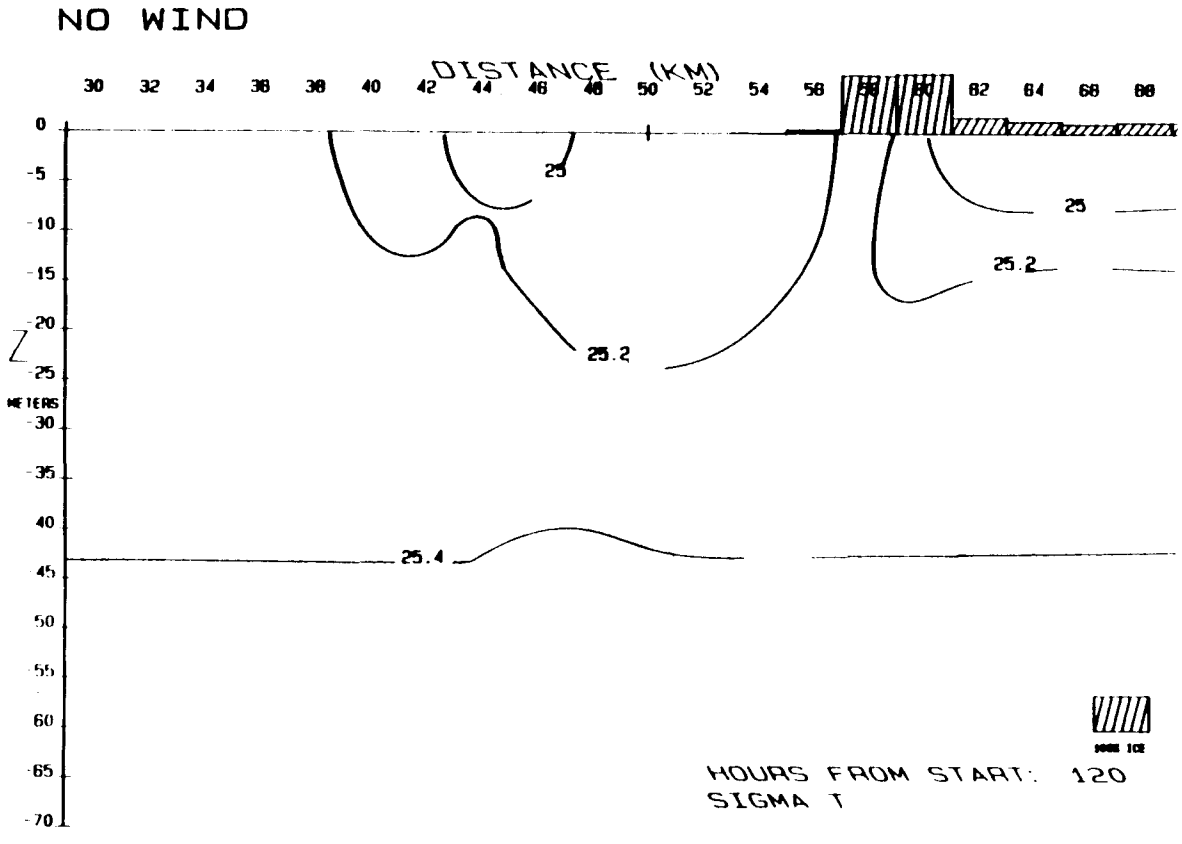

FIGURE 30A: CASE IIIA1 AT 120 HOURS, SIGMA-T

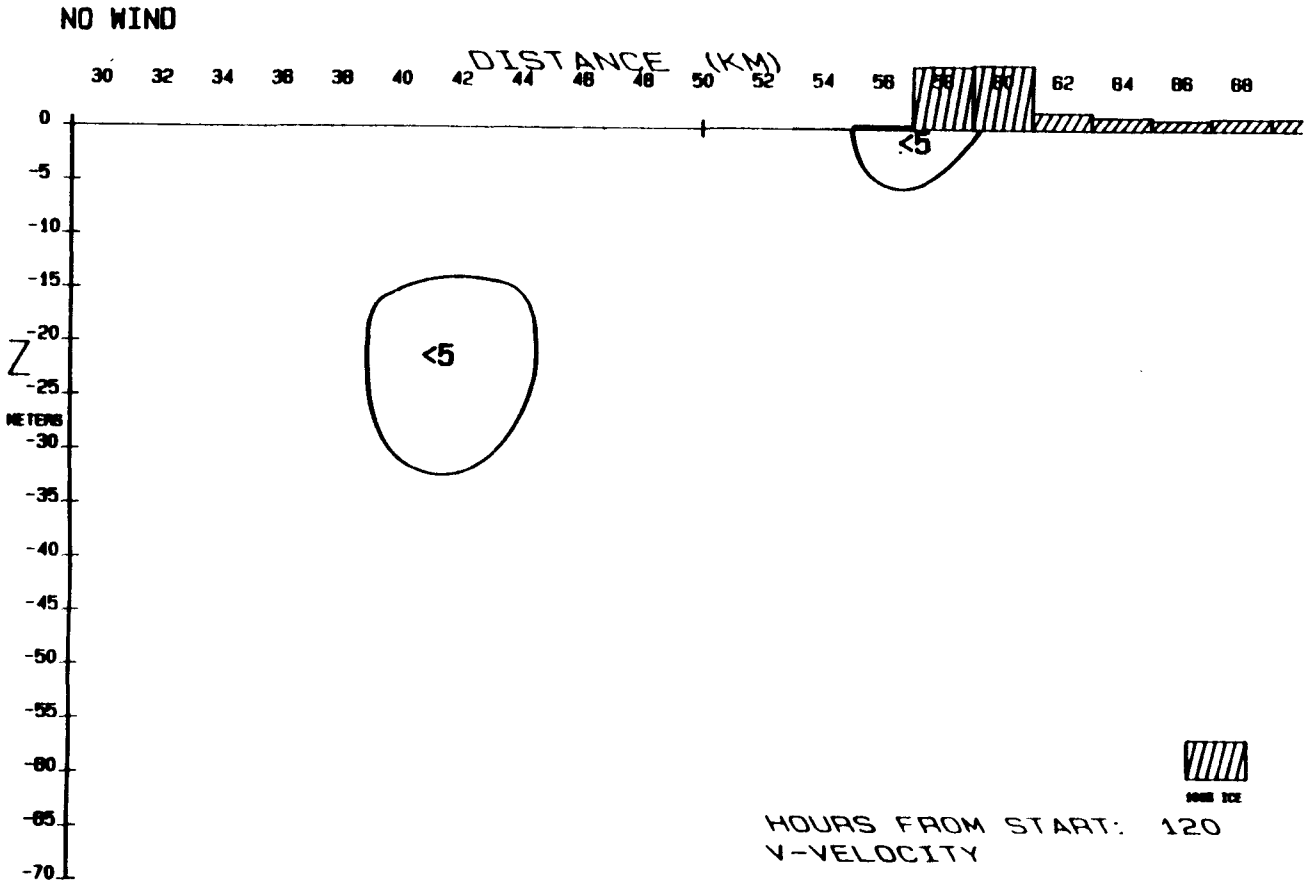

FIGURE 30B: CASE IIIA1 AT 120 HOURS, ALONG-ICE VELOCITY

NO WIND

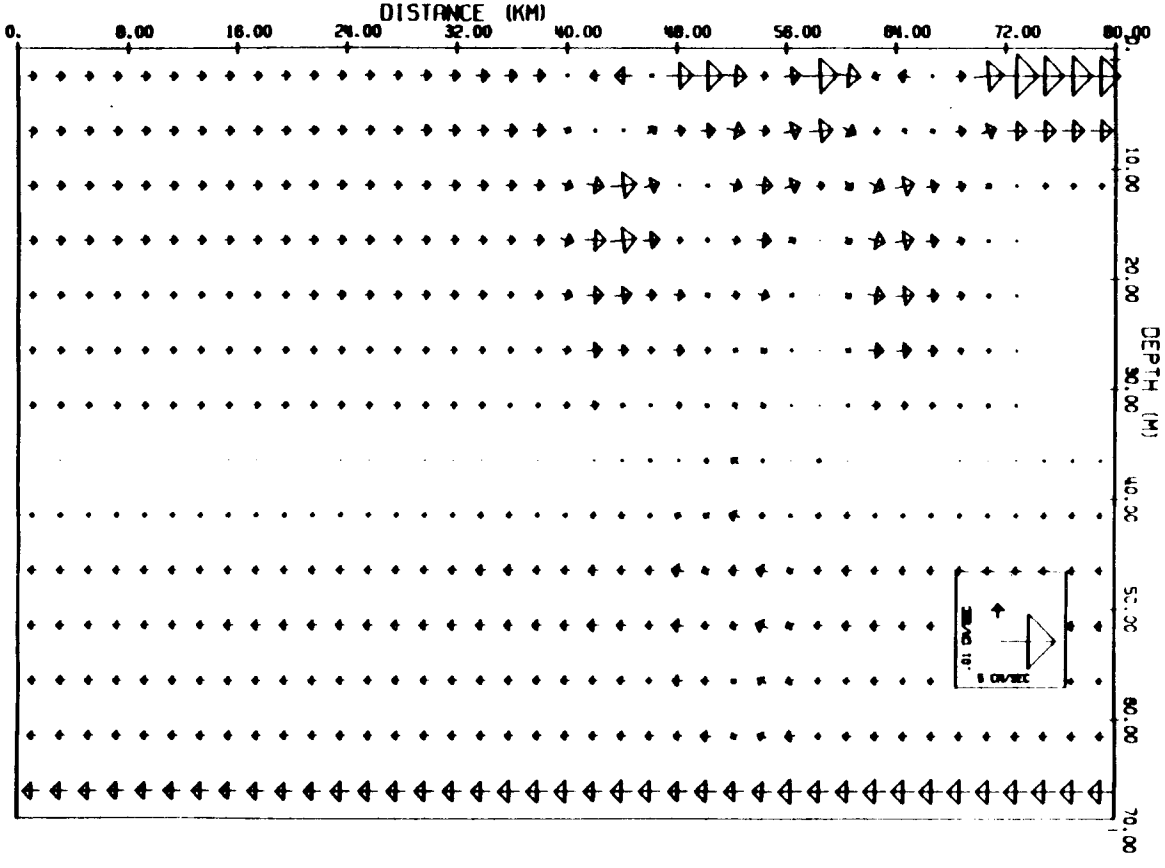

FIGURE 30C: CASE IIIA1 AT 120 HOURS, ACROSS-ICE/VERTICAL VELOCITY ARROW PLOT

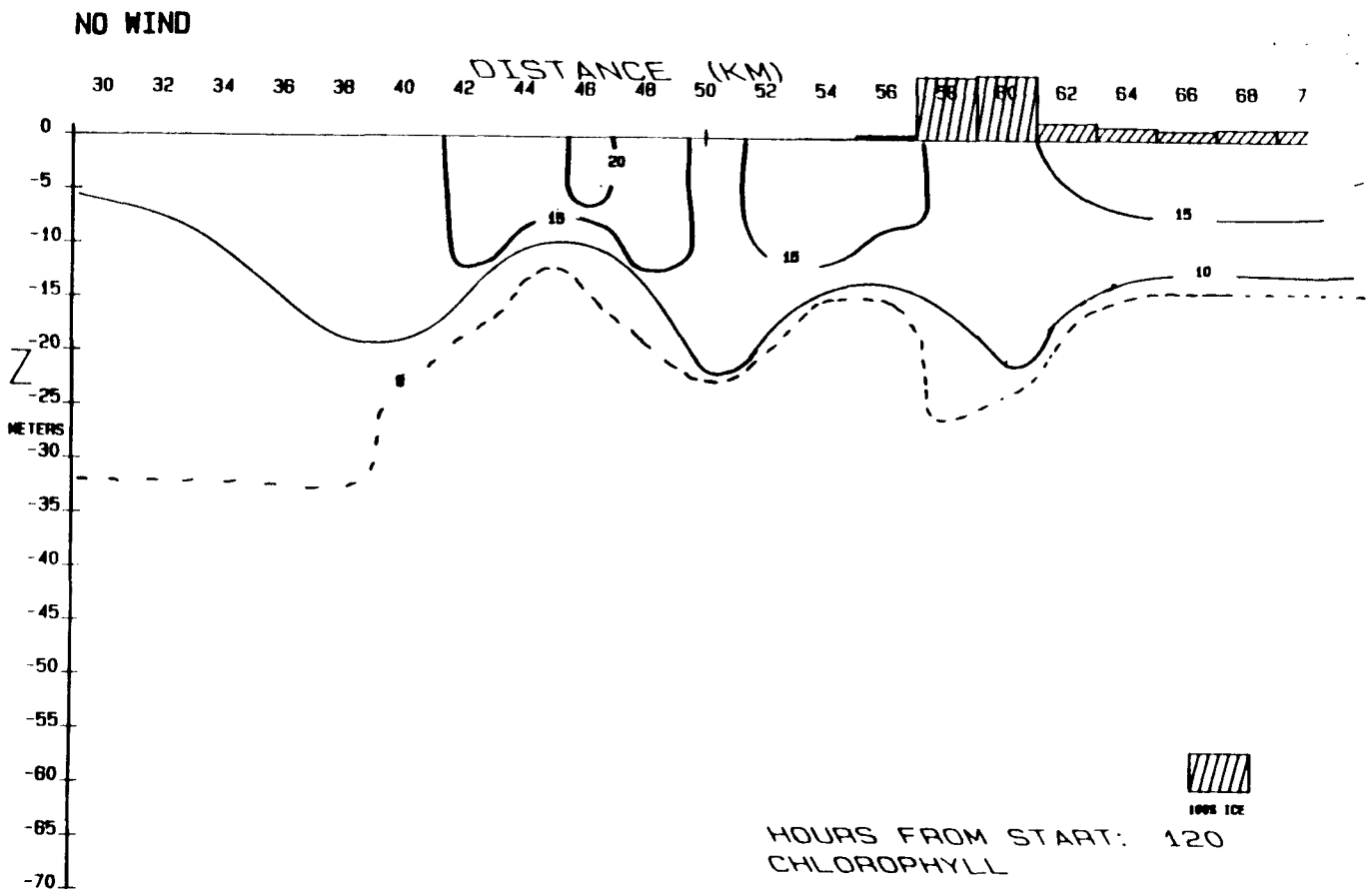

FIGURE 30D: CASE IIIA1 AT 120 HOURS, CHLOROPHYLL CONCENTRATION

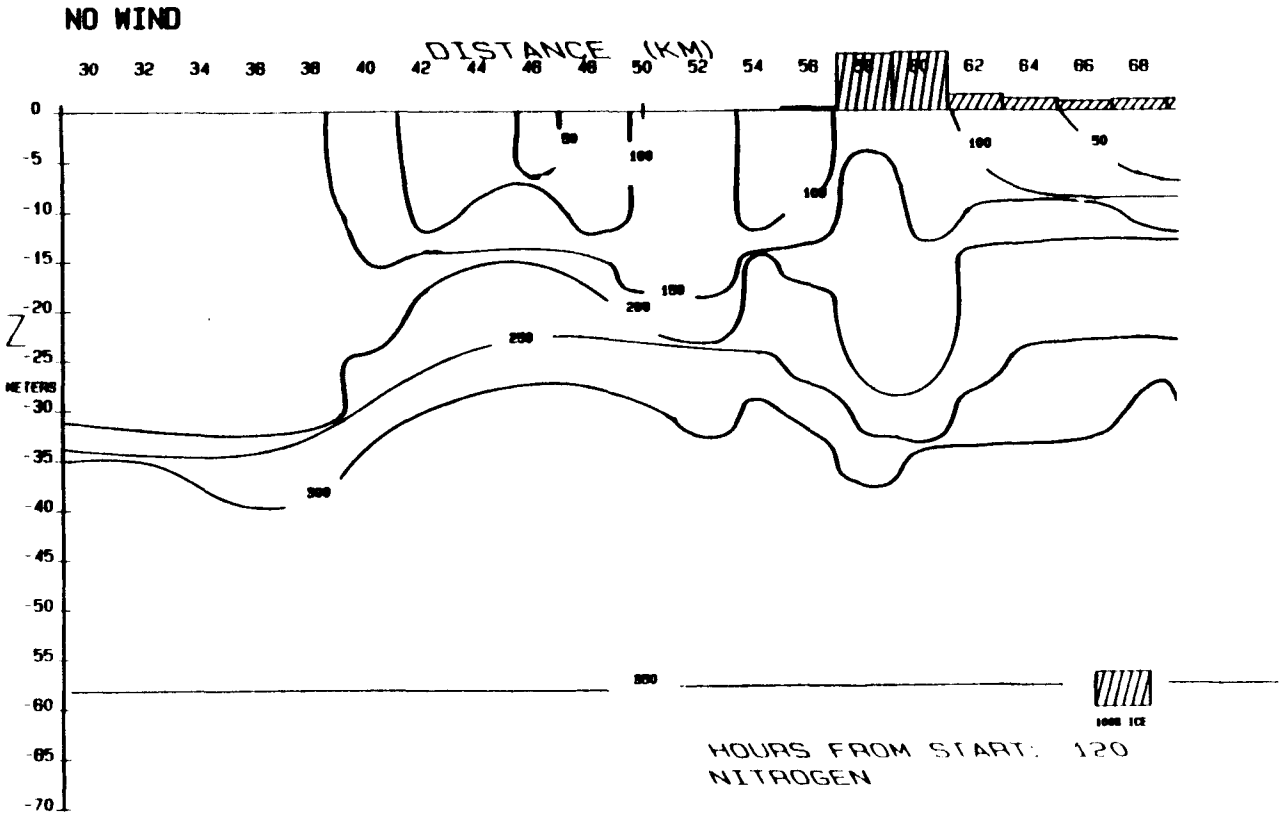

FIGURE 30E: CASE IIIA1 AT 120 HOURS, NITROGEN CONCENTRATION

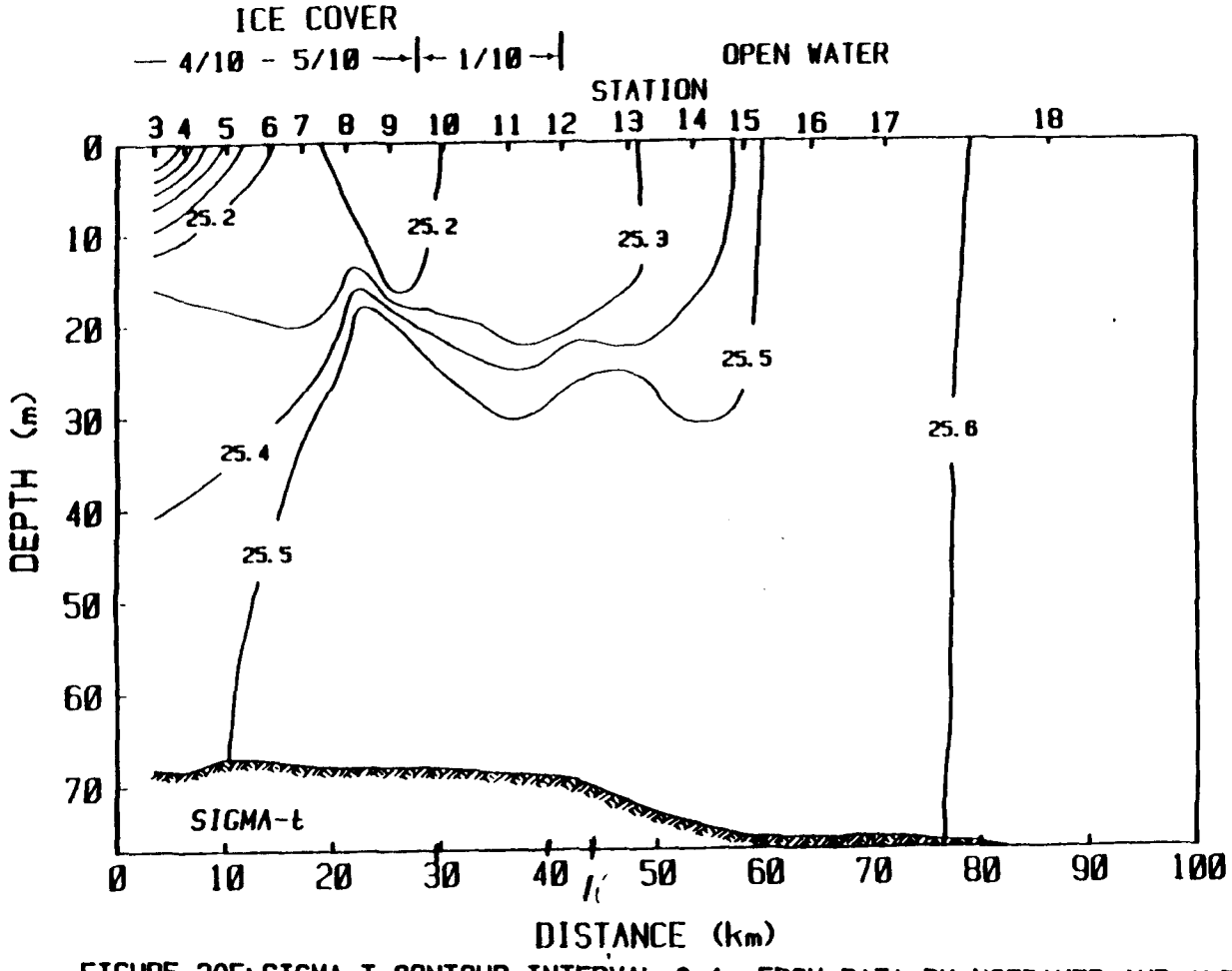

FIGURE 30F: SIGMA-T, CONTOUR INTERVAL 0.1, FROM DATA BY NIEBAUER AND ALEXANDER (1984)

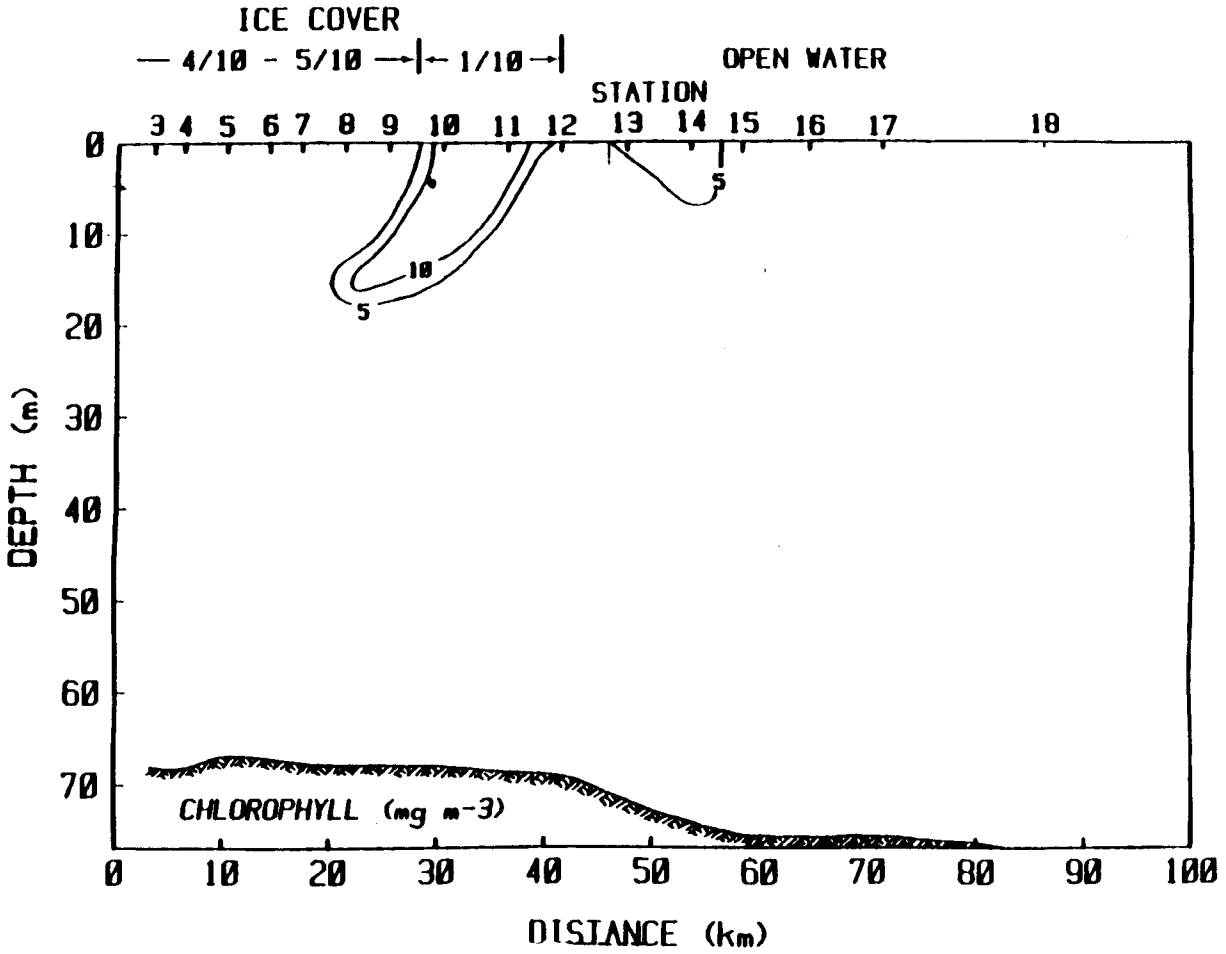

FIGURE 30G: CHLOROPHYLL CONCENTRATION, FROM DATA BY NIEBAUER AND ALEXANDER (1984)

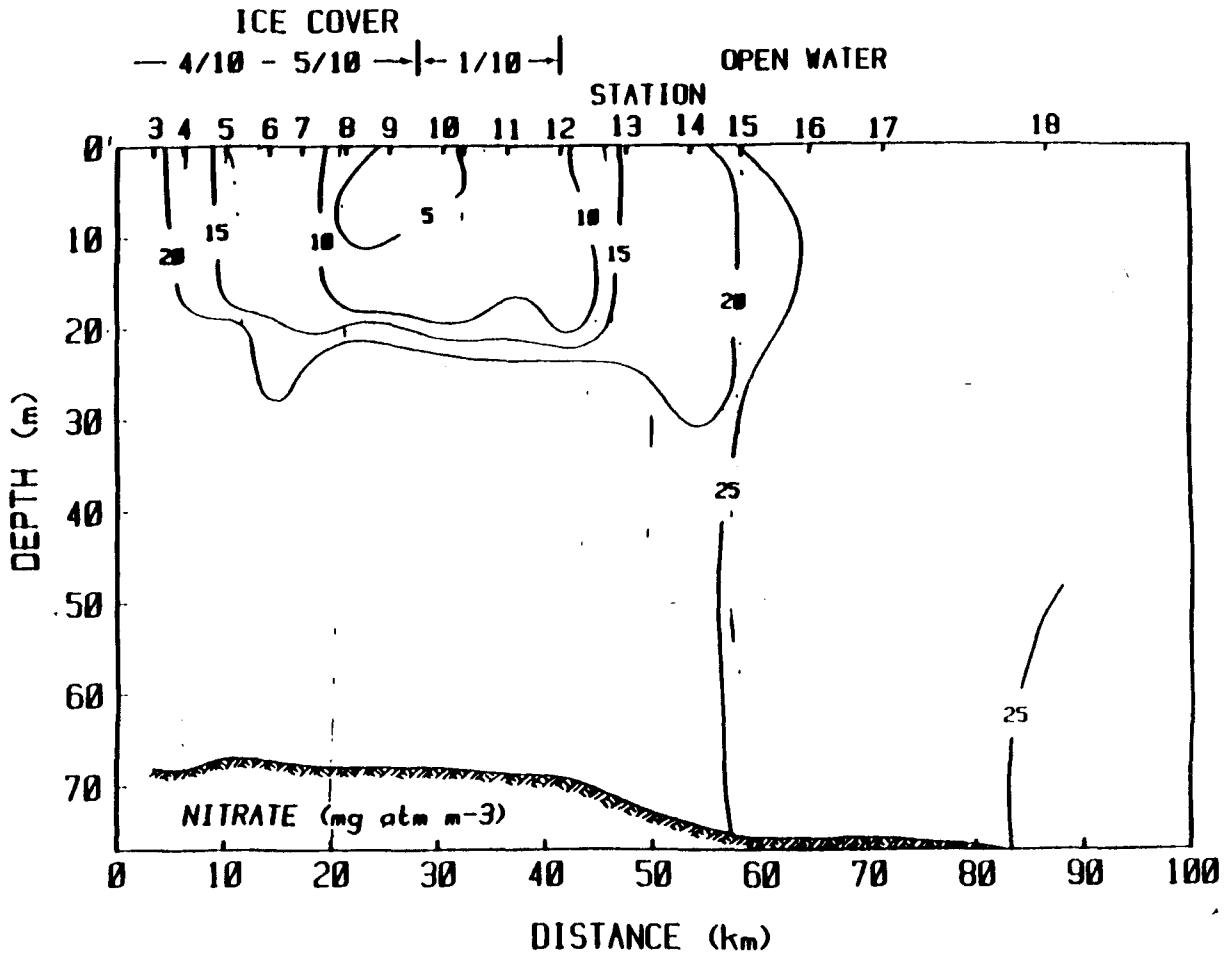

FIGURE 30H: NITRATE (MG AT/M^3), FROM DATA BY NIEBAUER AND ALEXANDER (1984)

An along-ice wind with ice to right (pos. y) is invoked here. Starting at the 40 km position at zero hour, after 8 hours the following edge has moved 4 km to the 44 km position (figure 28). The ice velocities are approximately 14 cm/sec in the across-ice (pos. x) direction and 27 cm/sec in the along-ice (pos. y) direction. Near the following edge the ice concentrations are about 60%. In the on-ice (pos. x) direction these concentrations increase to slightly over 100% at the 48 km point and then decrease to 98-99% coverage and remain relatively constant with distance to the boundary at 80 km.

After 12 hours some stratification is noted at the ice edge (44-48 km, figure 29a). The water speeds are greatest at the surface under the ice (figures 29b and 29c, ~16 cm/sec). The surface across-ice (pos. x) water velocities under the ice are approximately 14 cm/sec which are larger than the along-ice (pos. y) of approximately 6 cm/sec. Away from the ice, the along-ice (pos. y) velocities are only approximately 2 cm/sec at the surface while the across-ice (pos. x) are approximately 6 cm/sec. With depth the across-ice (neg. x) velocities change direction at aproximately 5 m while the along-ice (pos. y) velocities (figure 29b)

at first decrease then increase at depths greater than 10 m. The maximum along-ice (pos. y) velocities occur at depth under the ice (15-65 m) but the maximum resultant velocity magnitudes are at the surface. Upwelling is noted at the the 44-46 km positions (figure 29c).

Chlorophyll values (figure 29d) have increased slightly from 5 originally to 6.1 mg/m^3 under the ice in the water. This increase is due to a combination of algae input from melting ice and growth, 0.15 mg Chl/m^3 comes from melting ice, equation 17. The upwelling can be seen in the chlorophyll cross-section by the upward displacement of the isopleth of 6.1 mg Chl/m^3 at 44 km (figure 29d). Nutrient concentrations have decreased only slightly at the surface from 280 to 260 mg N/m^3 (figure 29e).

At 16 hours the ice speeds (figure 28) have remained about constant but turned more toward the along-ice (y) direction. The following edge has moved an additional 4 km to the 48 km position. Ice concentrations have remained about constant with following edge having about 50% cover. At 24 hours, six hours after the wind is terminated, an inertial oscillation is evident in the ice as evidenced by the 0% contour of figure 28 at 24 hours. The direction of the ice vector

has rotated about 60 degrees from what it was at 16 hours. Ice speeds have also decreased markedly. From 32 hours to the end of the experiment the ice velocities oscillate slightly about the along-ice (pos. y) axis and generally decrease in magnitude. Along-ice (pos. y) velocities are ~5 cm/sec while across-ice (x) velocities are ~1 cm/sec.

At the end of the experiment the ice edge has been displaced by melting and advection to about the 54 km position where there is only 7% ice cover. At the 58 km position the compactness is over 160% while the surrounding regions only contain a small amount of ice (10-20%, figure 30a). The regions of convergence and divergence of surface water are obvious (figure 30c). The area from 56-60 km has surface convergence and 54-50 and 64-70 are regions of divergence. The wind has been turned off for 102 hours and the prime driving force is the density gradient established from differential melting as described in case IIa. The ice moves along with the water causing increased compactness over time in areas of convergence. As the compactness increases the melt rate decreases (equation 11). In regions of divergence the opposite is found. As ice is advected out of an area the melt rate in-

creases due to the small percent cover present. These two phenomena may lead to ice banding. When wind is applied the horizontal density gradient velocities are overwhelmed. However the piling up of ice with such small velocities appear unrealistic. For these blocks of ice to slide onto one another, very rough sea conditions would be necessary. This may be a flaw in the model and will be discussed in following sections.

The along-ice (pos. y) water velocities have also decreased in magnitude by 120 hours (figure 30b) with the surface maximum (6 cm/sec) near high ice cover. The water column is now strongly stratified (figure 30a) with sigma-t values less than 25 near 46 km and within the ice pack at 62-80 km. The fresh water lens centered at 44 km was caused by ice that recently melted. The isopycnals which break the surface at 58-62 km are the result of diminished input of melt water in this region because of the higher compactness.

The chlorophyll cross-section (figure 30d) looks approximately like the sigma-t cross-section (figure 30a) with the highest values in the regions of those lowest sigma-t values. This is an interesting and perhaps important feature and will be considered in detail in the discussion section and in case IIIc where this

exact experiment is run without melting. Chlorophyll values greater than 20 mg/m^3 are found in the lens at 46 km. Again, the nitrogen cross-section (figure 30e) is similar to the chlorophyll and the sigma-t cross-sections (figures 30a and 30d). Minimum nitrogen values accompany maximum chlorophyll. These figures look remarkebly like those published by Niebauer and Alexander (1984) for the Bering sea ice edge in the spring of 1982 (figures 30f, 30g and 30h). These will be discussed in detail later.

Case IIIa2: Along-ice with ice to left (neg. y).

This experiment was run as a comparison to case IIIa1 (pos. y). Therefore we only look at the last snap shots generated. After 120 hours strong vertical stratification is noted from about 27 km to the boundary at 80 km (figure 31a), compared to the previous case where the area from 38-80 km is stratified (figure 30a). Chlorophyll maxima in case IIIa2 (figure 31b) are only slightly above 15 mg/m^3 while in case IIIa1 they are greater than 20 mg/m^3 (figure 30d). Inorganic nitrogen concentrations are less than 50 mg/m^3 over a

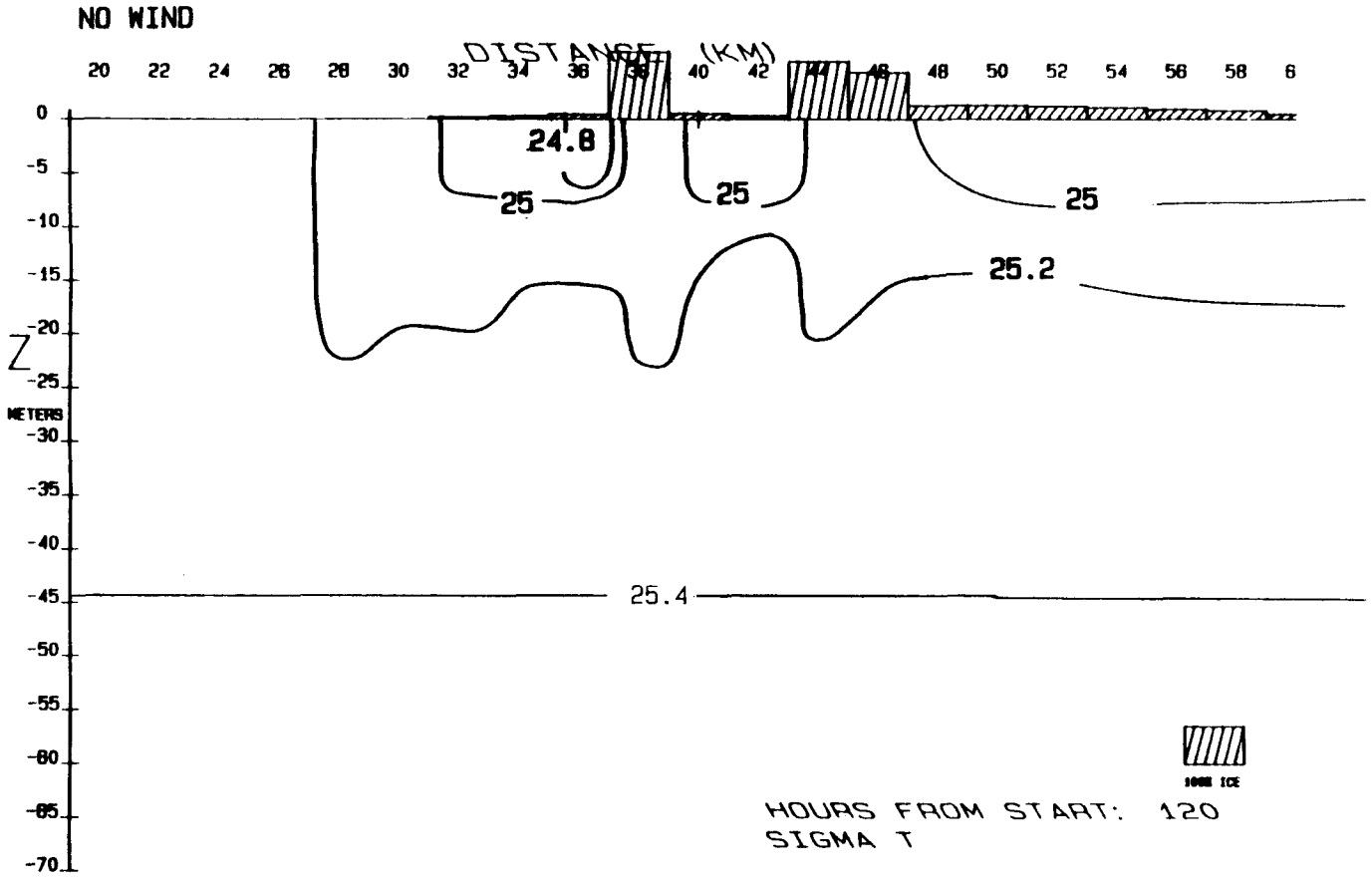

FIGURE 31A: CASE IIIA2 AT 120, SIGMA-T

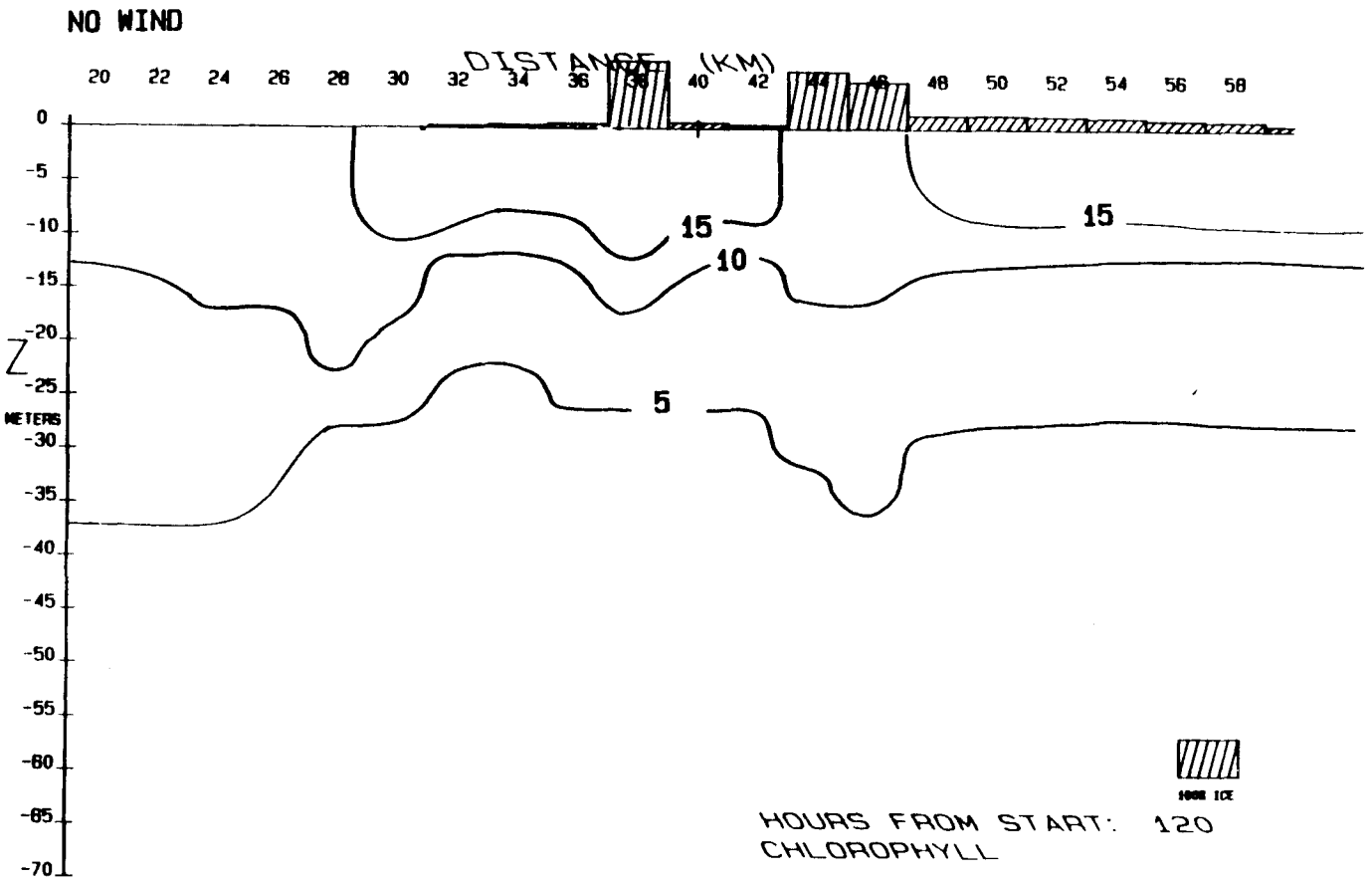

FIGURE 31B: CASE IIIA2 AT 120 HOURS, CHLOROPHYLL CONCENTRATION

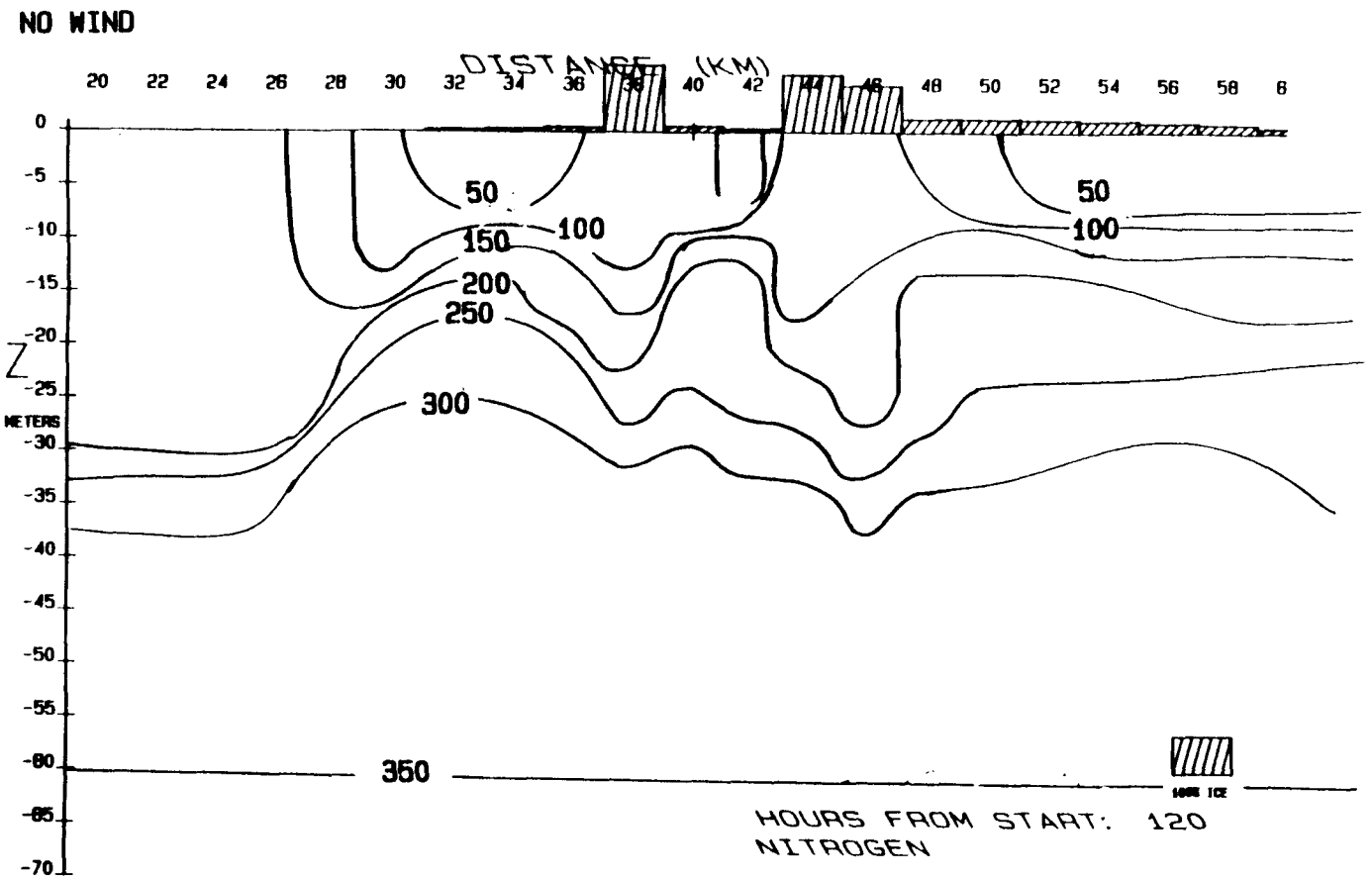

FIGURE 31C: CASE IIIA2 AT 120 HOURS, NITROGEN CONCENTRATION

wider region in case IIIa2 (figure 31c) than in case IIIa1 (figure 30e). Comparing the two blooms, it appears that the bloom in case IIIa2 covers a larger area but is not as intensive, in the sense that chlorophyll maxima are lower.

Case IIIb: across-ice (x) wind with melt

In this case an off-ice (neg. x) wind is applied for 18 hours and then turned off. The initial ice conditions and hydrography are the same as for case IIIa (figure 27) and the ice is allowed to melt for the entire experiment duration (120 hours). After 8 hours the leading edge has moved 10 km to the 30 km position (figure 32). The ice velocities are approximately 35 cm/sec in the across-ice (neg. x) direction and 12 cm/sec in the along-ice (neg. y) direction. Near the leading edge the ice concentrations are about 4%. However these concentrations increase rapidly with distance into the pack. At 32 km the compactness is 64% and at 42 km it is over 90%. Throughout the remainder of the ice pack the percent coverage remains about 99%.

After 12 hours some stratification due to melting

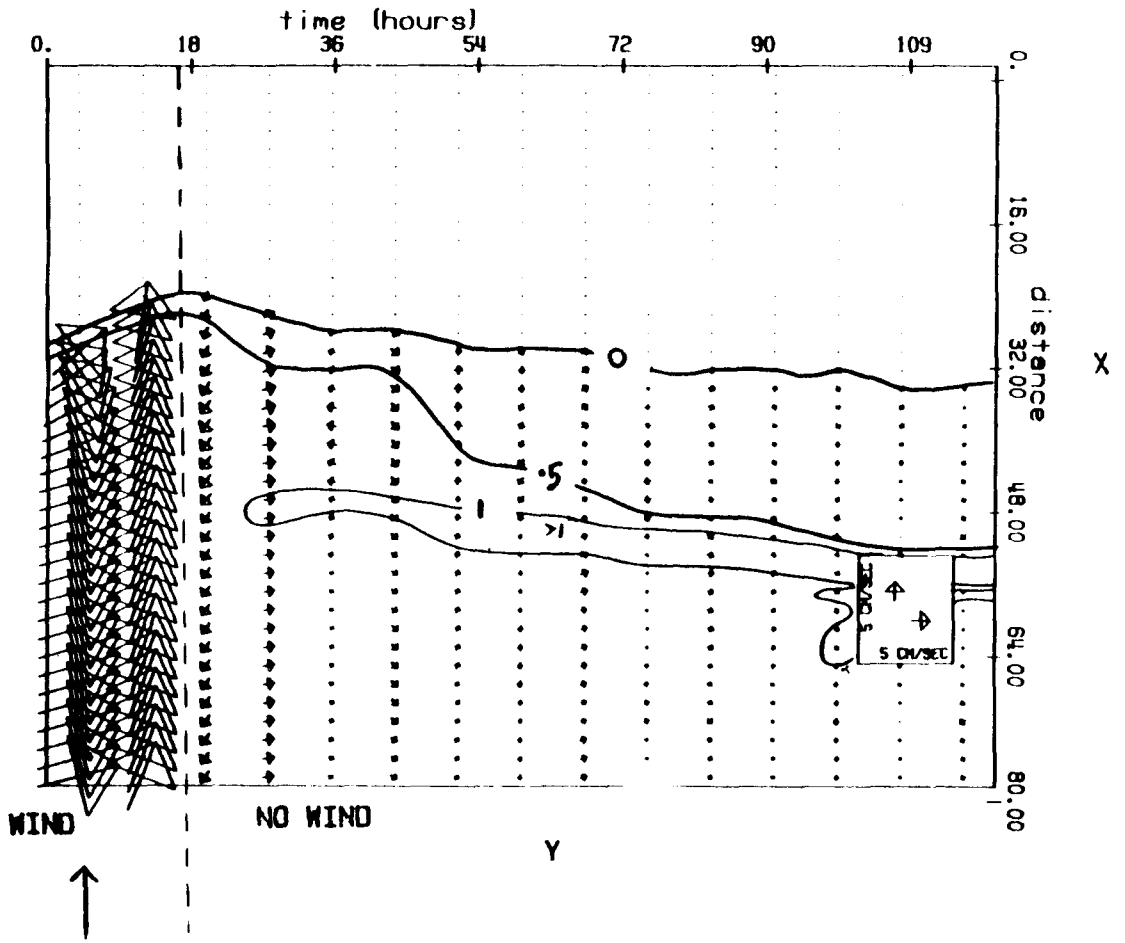

FIGURE 32: CASE IIIB, TIME SERIES OF ICE VELOCITIES AND COMPACTNESS

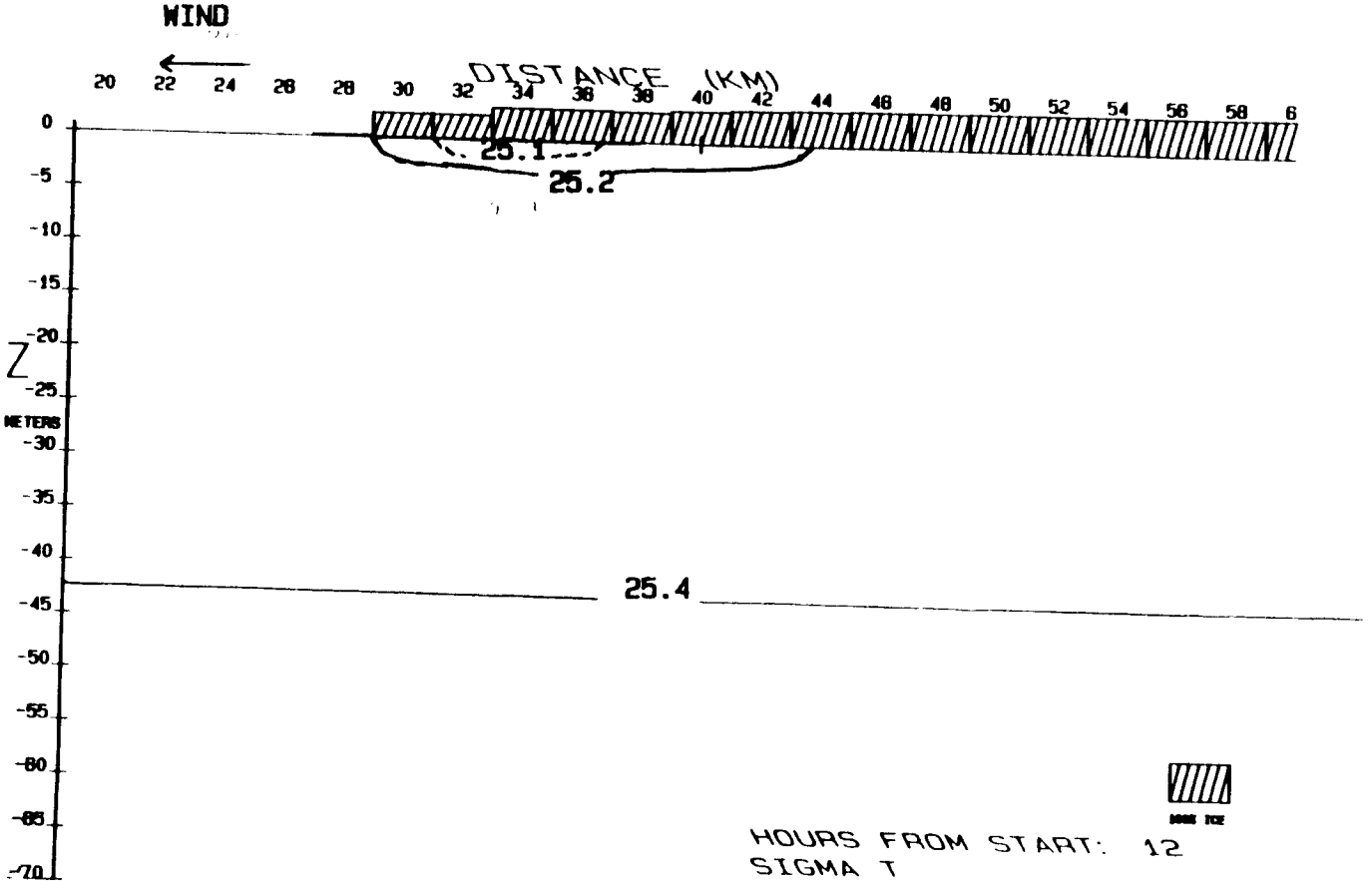

FIGURE 33A: CASE IIIB AT 12 HOURS, SIGMA-T

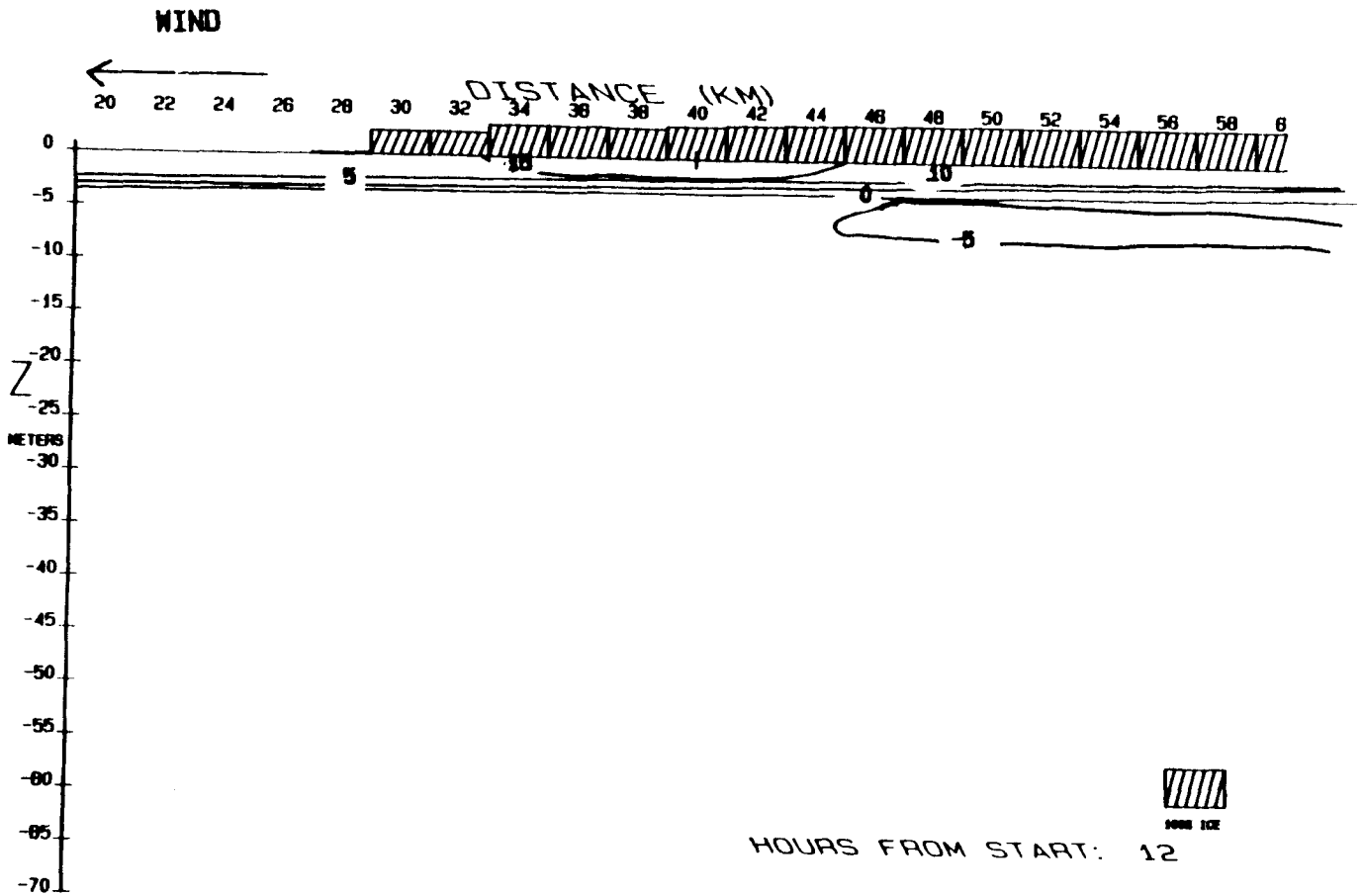

FIGURE 33B: CASE IIIB AT 12 HOURS, ALONG-ICE VELOCITY

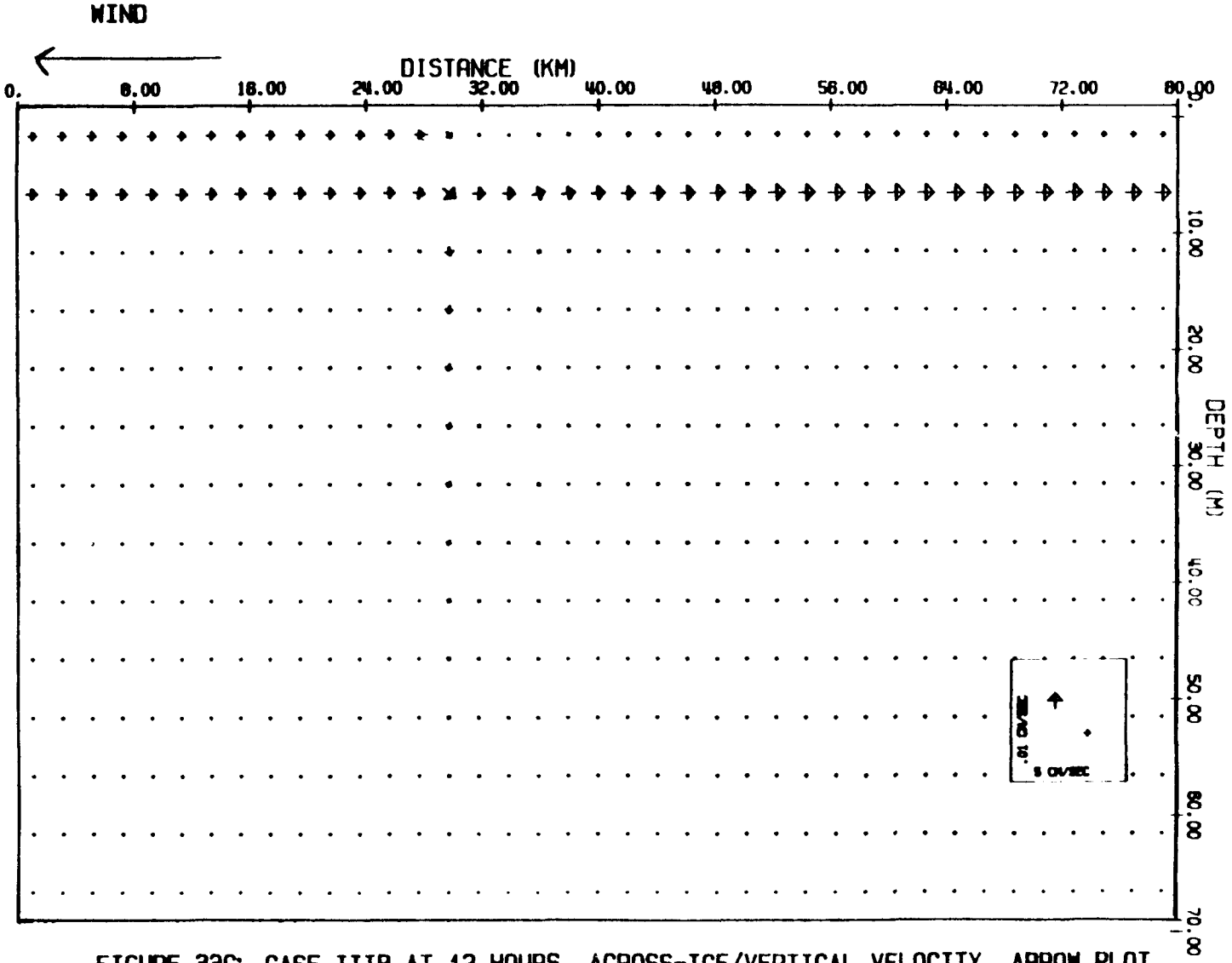

FIGURE 33C: CASE IIIB AT 12 HOURS, ACROSS-ICE/VERTICAL VELOCITY, ARROW PLOT

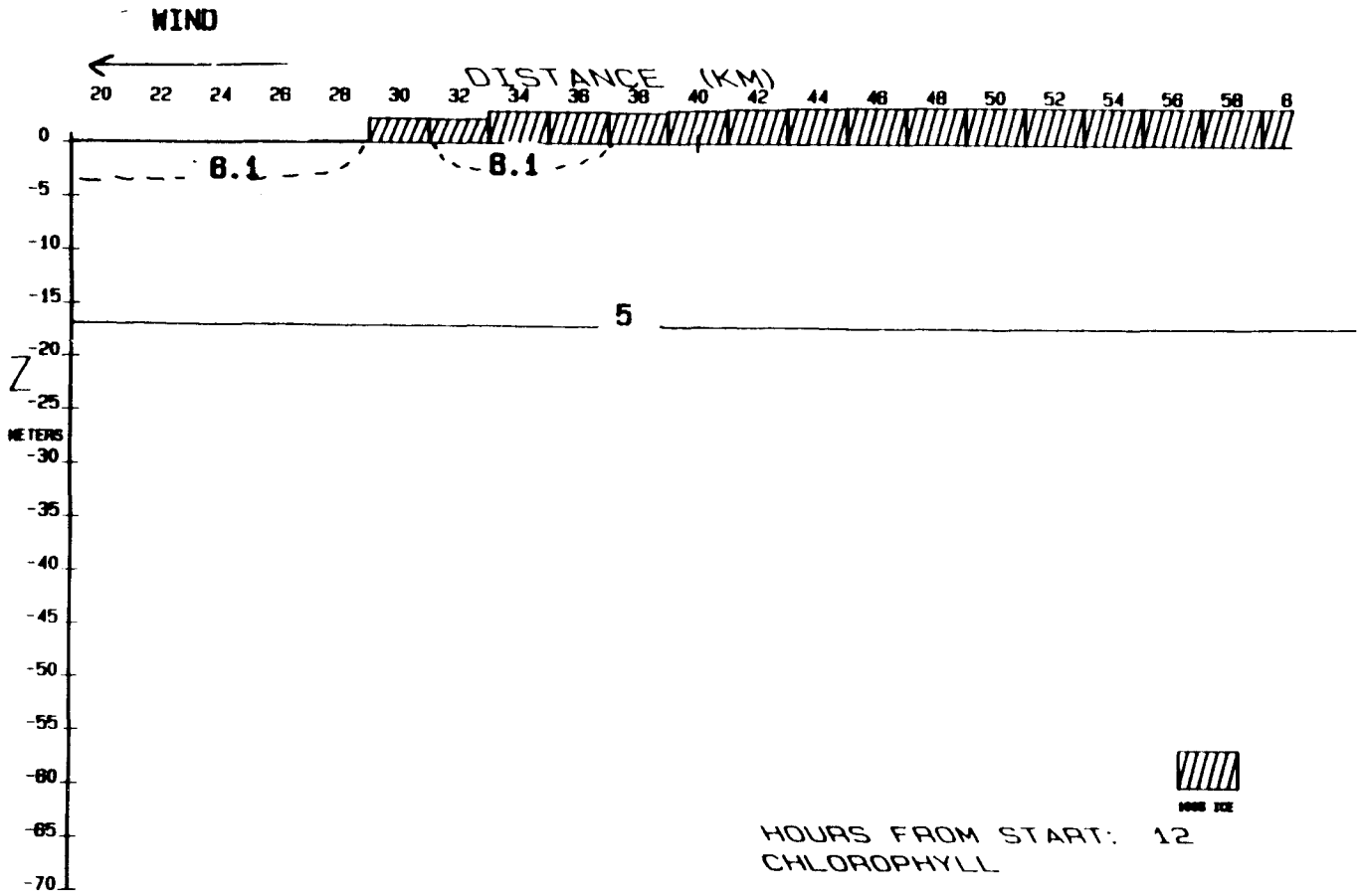

FIGURE 33D: CASE IIIB AT 12 HOURS, CHLOROPHYLL CONCENTRATION

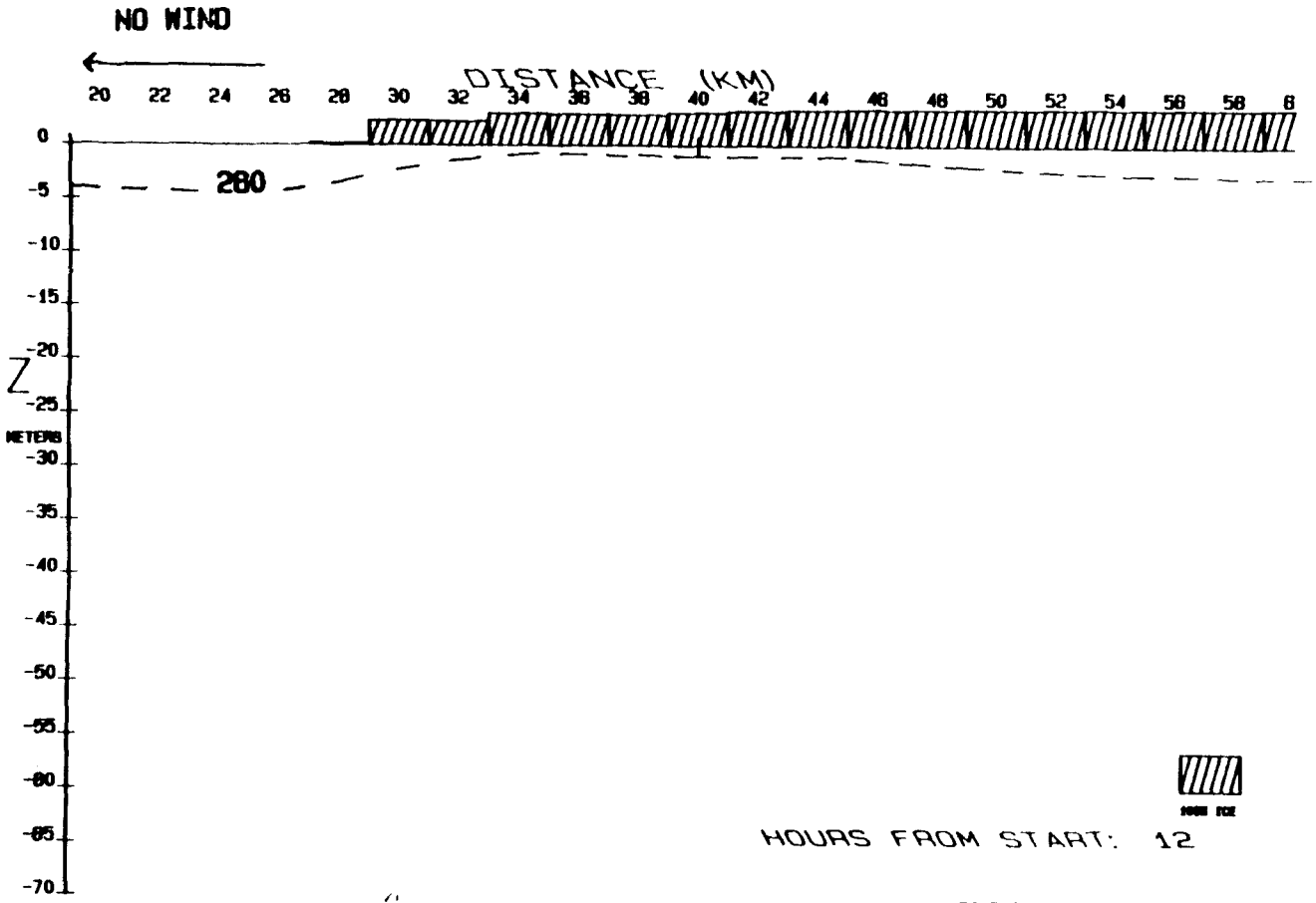

FIGURE 33E: CASE IIIB AT 12 HOURS, NITROGEN CONCENTRATION

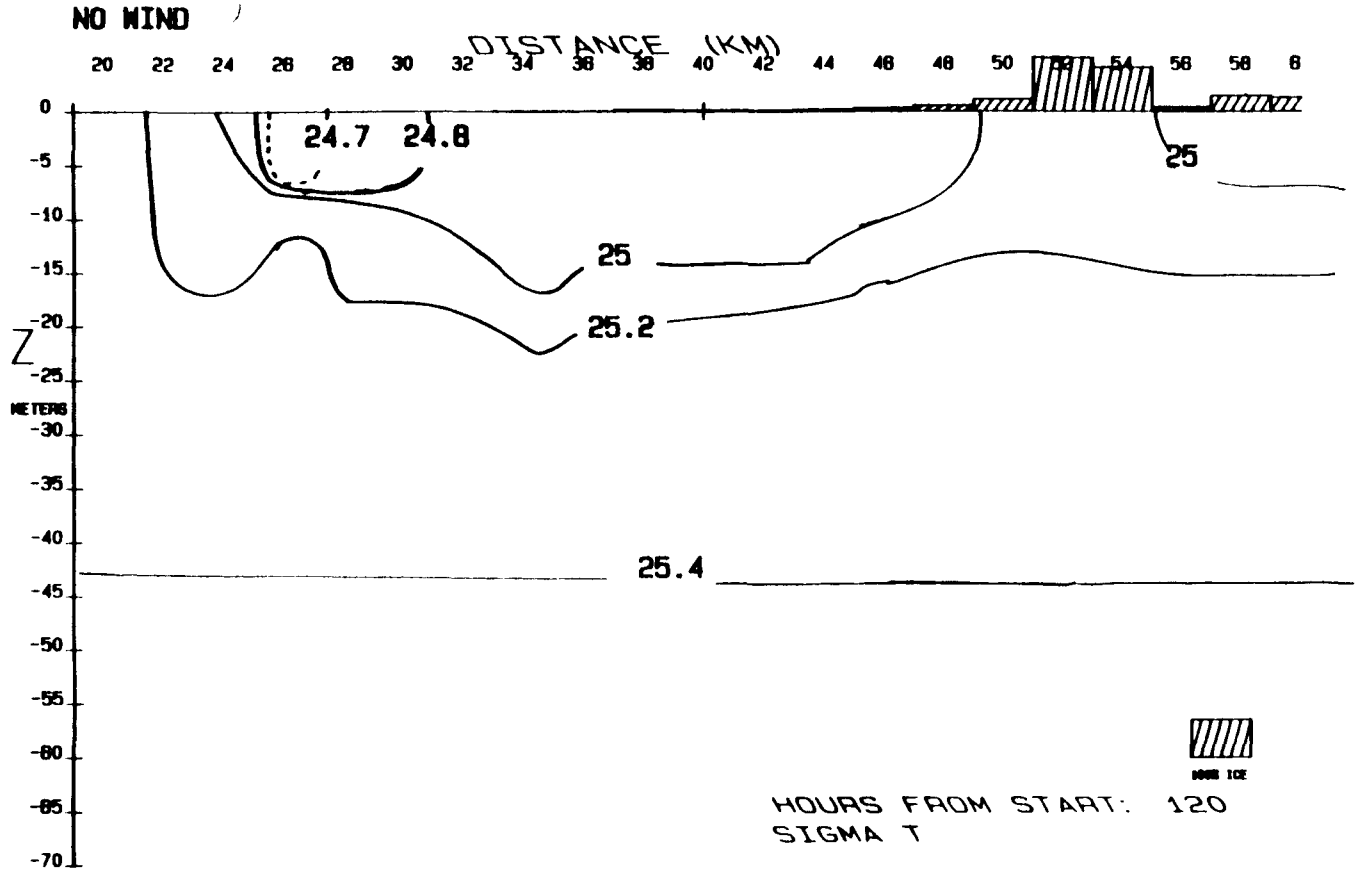

FIGURE 34A: CASE IIIB AT 120 HOURS, SIGMA-T

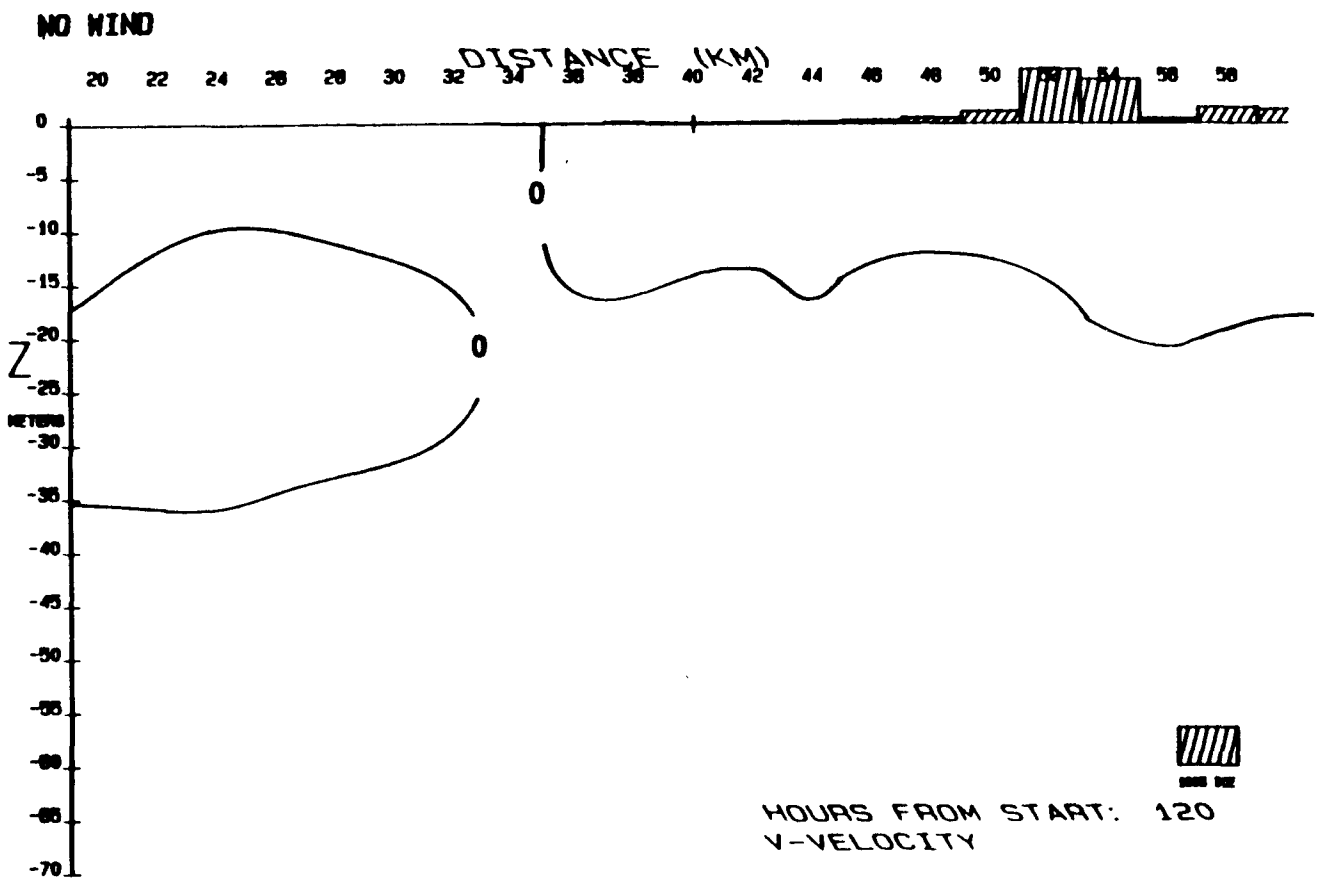

FIGURE 34B: CASE IIIB AT 120 HOURS, ALONG-ICE VELOCITY, CONTOUR INTERVAL 5 CM/SEC

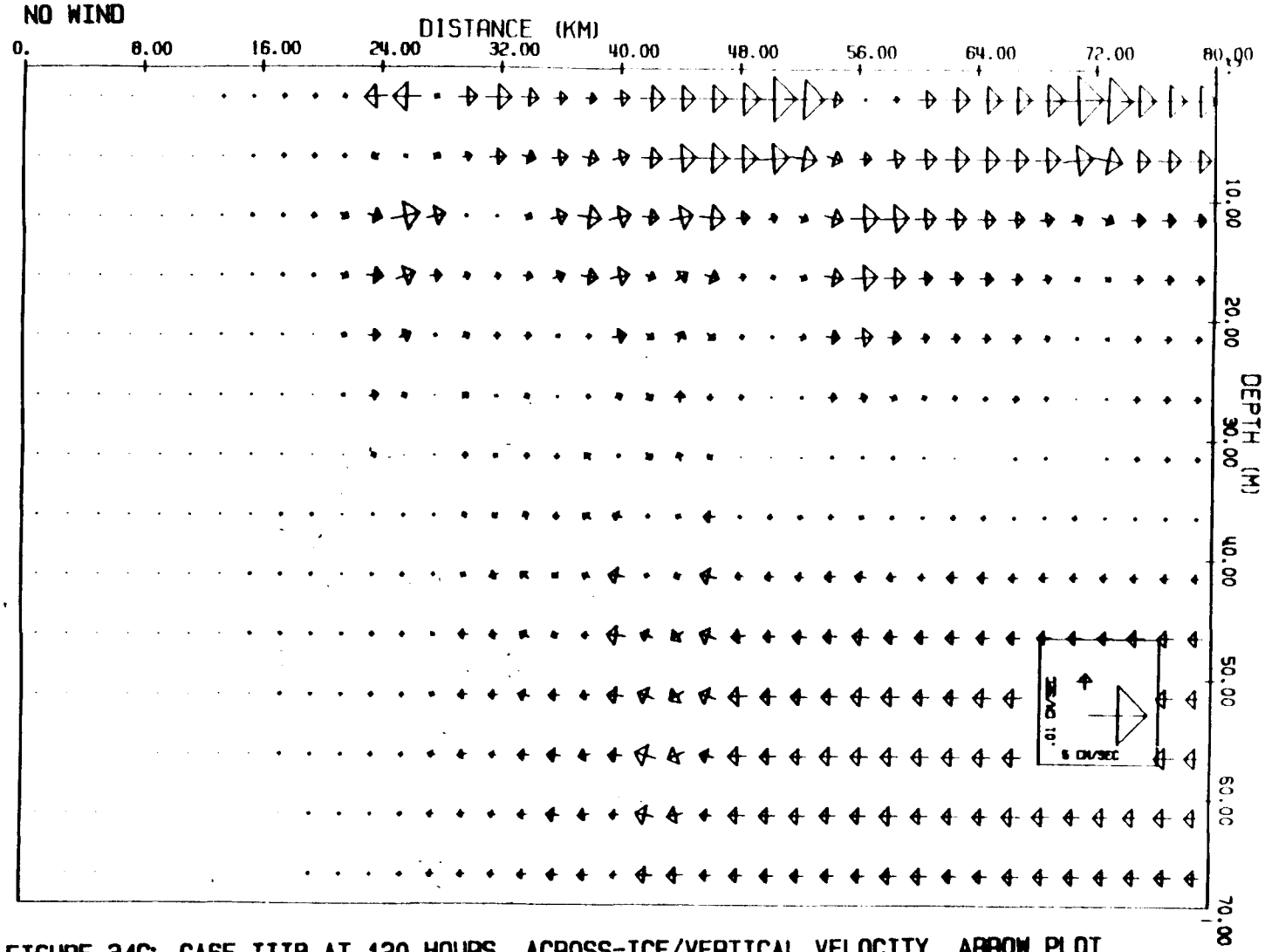

FIGURE 34C: CASE IIIB AT 120 HOURS, ACROSS-ICE/VERTICAL VELOCITY, ARROW PLOT

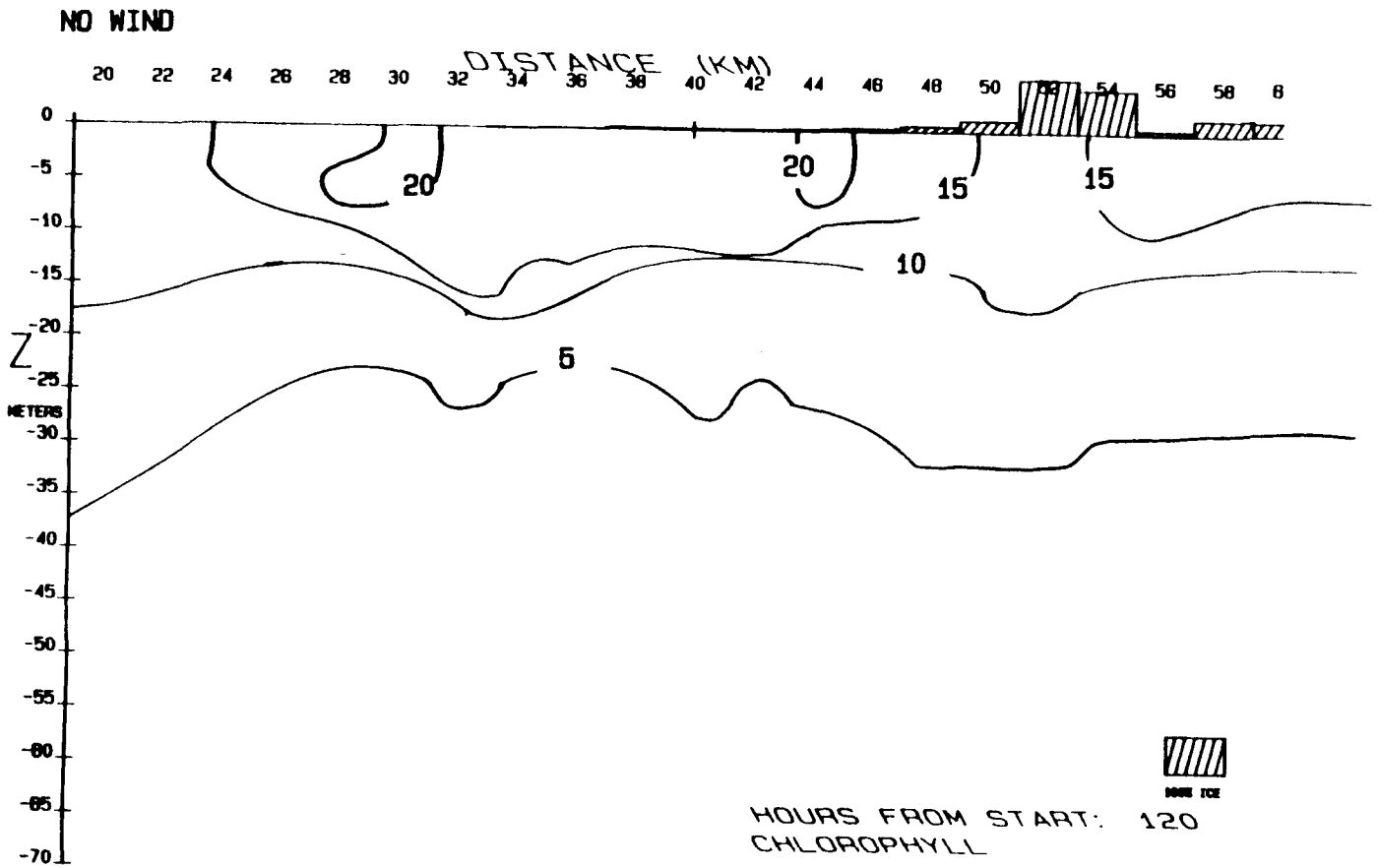

FIGURE 34D: CASE IIIB AT 120 HOURS, CHLOROPHYLL CONCENTRATION

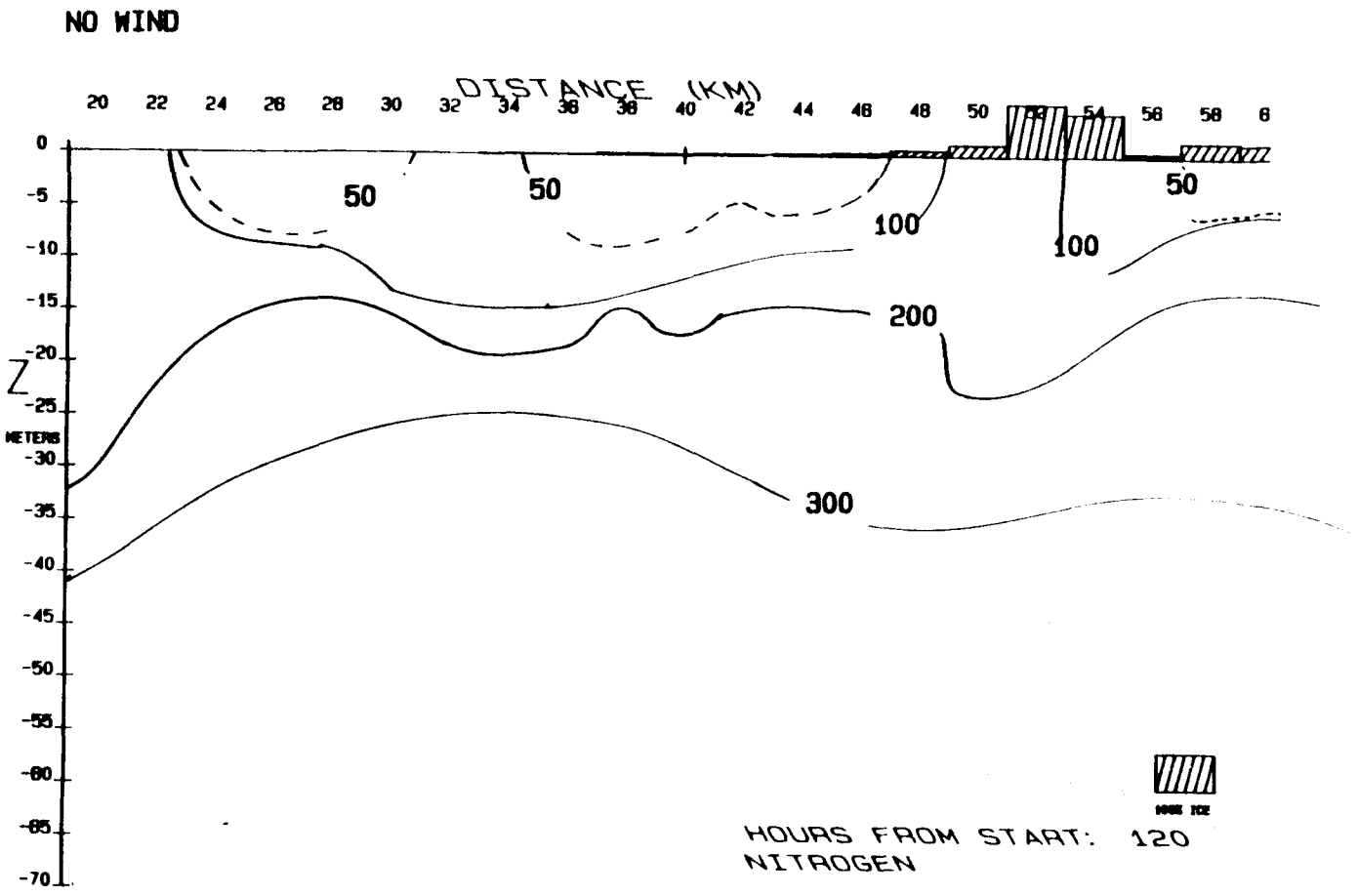

FIGURE 34E: CASE IIIB AT 120 HOURS, NITROGEN CONCENTRATION

is noted near the ice edge (33-42 km, figure 33a). The resultant horizontal water speeds are greatest at the surface under the ice (figures 33b and 33c, 20 cm/sec at 40 km). The across-ice (pos. x) water velocities at the surface are smaller and in the opposite direction to the wind (figure 33c). The across-ice (x) velocities change direction at 5 m (figure 33c) and diminish greatly. The along-ice (y) water velocities decrease rapidly with depth (figure 33b), from 15 cm/sec to -5 cm/sec at 5 m depth under the ice, and from 10 cm/sec to about 0 cm/sec away from the ice at 5 m depth. Downwelling is noted at the leading edge (30 km, figure 33c).

By 12 hours chlorophyll values (figure 33d) have increased slightly from 5 to 6.2 mg/m^3 in the water near the ice edge. This increase is due to a combination of algae input from melting ice and growth. Case IIc deals with what portion of this increase in chlorophyll is due to growth and what is due to input from the ice. This chlorophyll concentration is slightly greater than that in case IIIa because more rapid melting occurs due to the more rapid spreading out of the ice (ie. the leading edge here has only 4% cover whereas the following edge in case IIIa has 50%,

figure 28). Away from the ice, chlorophyll values are less than 6.1.

Nutrient concentrations have decreased only slightly at the surface from 280 to 260 mg N/m^3 (figure 33e). The vertical displacement of the nitrogen isopleths at 32 km is due to the greater amount of stratification here which inhibits mixing. The minimum sigma-t value (25.13, figure 33a) is at 34 km. Though melting is faster at 28-32 km the ice has been in the 34 km region longer, therefore more fresh water was added.

At 16 hours the resultant ice speeds have remained about constant but the vectors turned more toward the across-ice (x) direction (figure 32). The leading edge moved an additional 4 km to the 26 km position. Ice concentrations remained about constant with the leading edge having about 2% cover. At 24 hours, six hours after the wind is terminated, an inertial oscillation is evident in the ice motion (figure 32). The directions of the ice vectors have rotated about 180° from their directions at 16 hours. The ice speeds have also decreased markedly to, ~1 cm/sec in the along-ice (neg. y) direction and ~3 cm/sec in the across- ice direction (pos. x) (figure 32). From the 32 hour point to the

end of the experiment the ice velocities oscillate inertially and generally decrease in magnitude. "Piling up" of ice is noted at 46 km at 24 hours (figure 32). This phenomenon is due to surface water convergence as described in case IIIa. However, in this experiment the areas of heavy (>100%) ice appear to "migrate" toward the boundary at 80 km (figure 32), from 46 km at 32 hours to 54 km at 120 hours. The reason for this is that the compactness on the leading side of the ice pack is consistently lower than that on the following side. This results in a higher input of melt water (equation 11) to the leading side which further results in a baroclinic velocity toward the 80 km boundary (figure 33c). This surface water carries the ice with it.

At the end of the experiment, due to a combination of melting and advection the edge has moved back to about the 34 km position where there is only 1% ice cover (figure 32). The along-ice (y) velocities (water and ice) have decreased in magnitude, to under 1 cm/sec, with the greatest being at the surface near the high ice cover (second panels figures 34 and 32). As in the along-ice (pos. y) wind experiment (case IIIa1. figure 30c) regions of convergence and divergence are

noted at the surface (fourth panel figure 34). The water column is now highly stratified (figure 34a) with sigma-t values of less than 25 in the 24-48 km region and further back in the ice pack at 56-72 km. The lens at 26-30 km was caused by ice that has recently melted. The isopycnals which break the surface at 50-56 km are due to reduced input of melt water in this region because of the higher compactness.

The chlorophyll cross-section (fourth panel figure 34) looks approximately like the sigma-t cross-section (figure 34a) with the highest values in the regions of the minimum sigma-t values. Chlorophyll concentrations of nearly 25 mg/m^3 are found in the lens at 29 km and at 44 km. Again the nitrogen cross-section (fifth panel figure 34) follow the chlorophyll and the sigma-t cross-sections (figures 34a and fourth panel 34). Minimum inorganic nitrogen values are found with maximum chlorophyll.

In this case high chlorophyll values are more wide spread than in case IIIa1 or case IIIa2. The comparison between case IIIa1 and case IIIb is that for an off-ice (neg. x) vs. an on-ice (pos. x). But even in the case of an along-ice wind with ice to the left (case IIIa2, neg. y), off-ice velocities (neg. x) are

not nearly as strong as with an off-ice (neg. x) wind (14 cm/sec as opposed to 35 cm/sec). This slows the spreading of the ice restricting the range of melt water input, thereby stratifying a slightly smaller region resulting in a smaller bloom area. So actually the more the ice spreads out, the greater the magnitude of the bloom.

Case IIIc: along-ice (pos. y) wind without melt

The case with the wind along-ice with ice to right (pos. y) without melt is shown to gain insight into the role of melt water driven stratification in the bloom process at the ice edge in the spring. The initial conditions are the same as those for case IIIa (figure 27). The wind is blown for 18 hours along-ice with the ice to the right (pos. y) and the experiment duration is 120 hours. The ice is not allowed to melt.

There is little difference between the initial hydrography and the hydrography at 120 hours (figure 35a). A slight upward displacement of the 25.4 sigma-t isopleth near the original edge is a result of ice edge upwelling.

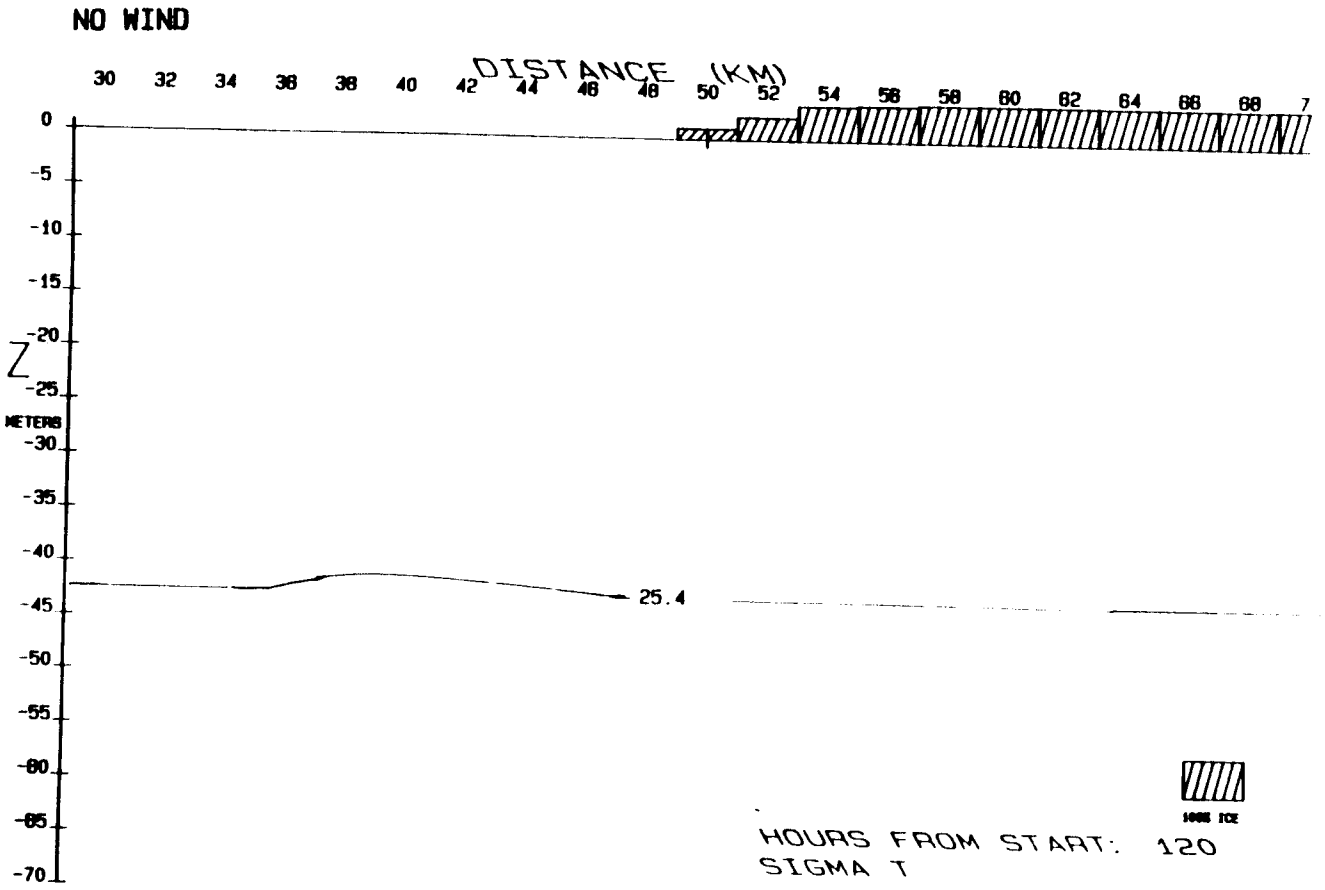

FIGURE 35A: CASE IIIC AT 120 HOURS, SIGMA-T

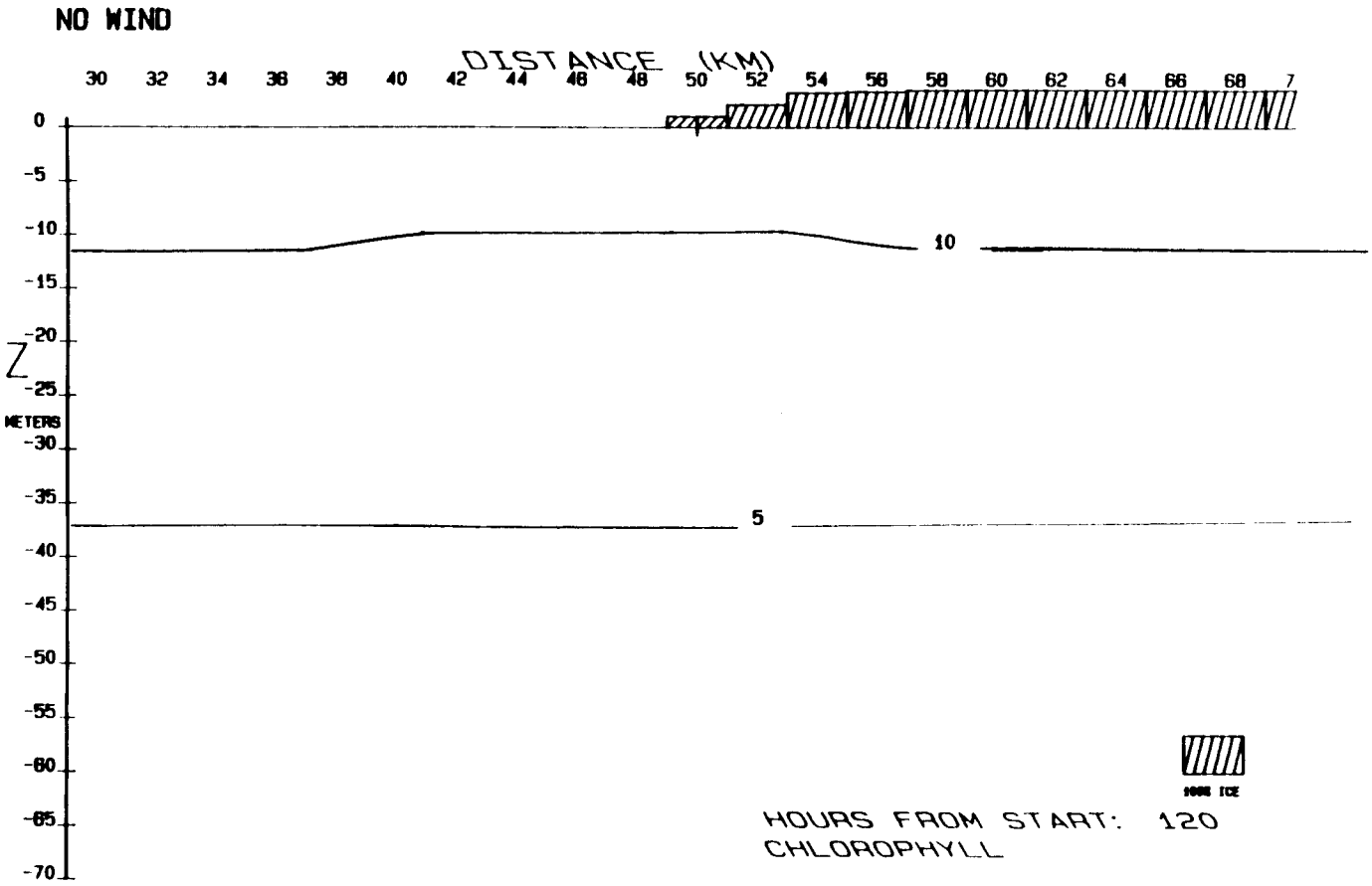

FIGURE 35B: CASE IIIC AT 120 HOURS, CHLOROPHYLL CONCENTRATION

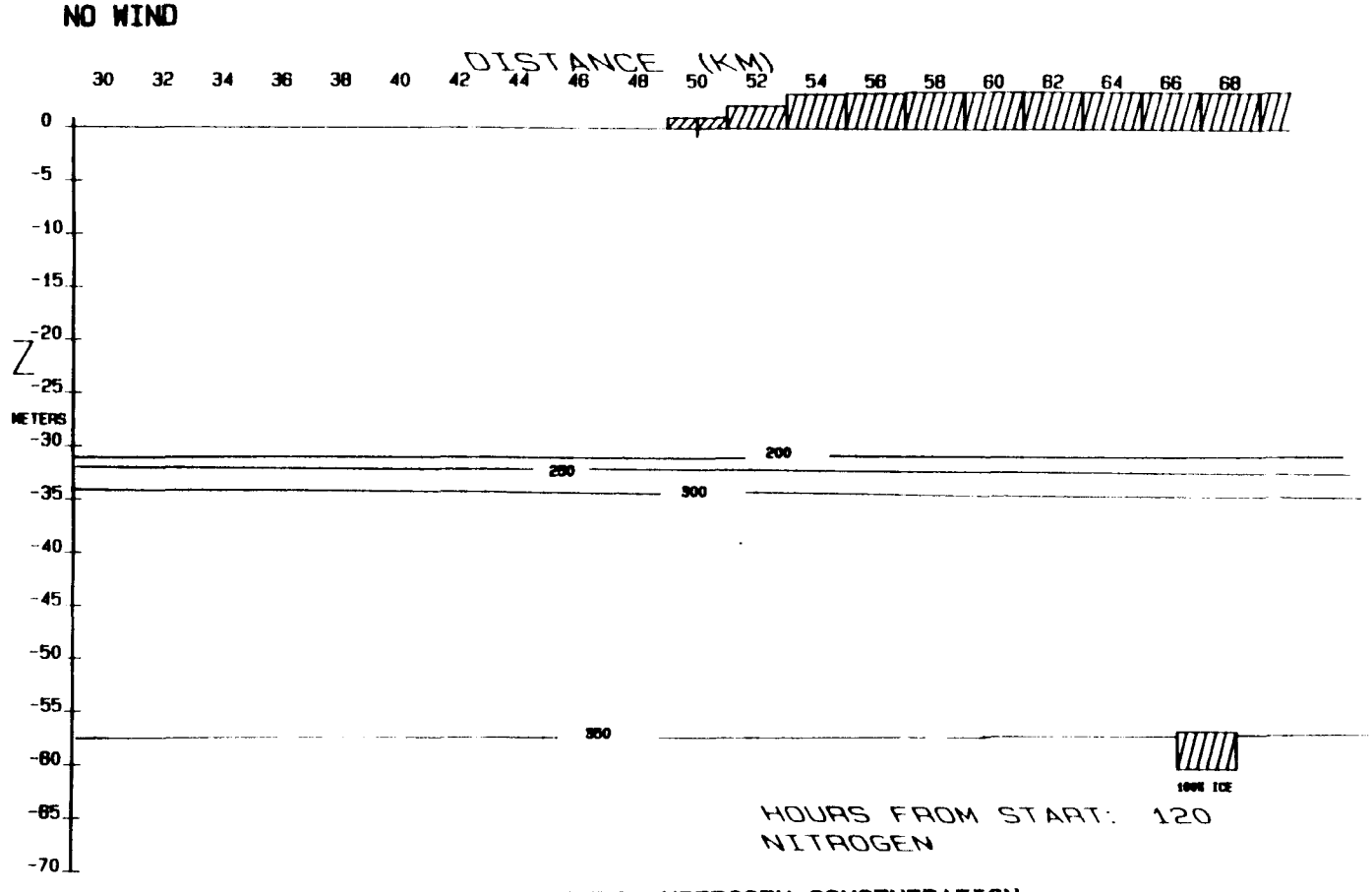

FIGURE 35C: CASE IIIC AT 120 HOURS, NITROGEN CONCENTRATION

Similar to the sigma-t cross-section, chlorophyll (figure 35b) shows little horizontal structure. Concentrations of more than 10 mg/m^3 are found in the upper 10 m of the water column but there is little difference between areas of ice cover and areas without ice cover. A small vertical displacement upward of the isopleth of 10 mg Chl/m^3 is seen at around 40 km. This again is due to to the upwelling. The nitrogen cross-section (figure 35c) also looks approximately the same as the others. Some of the nutrient concentrations are reduced above 30 m in the water column but they are still high (>180 mg N/m^3).

Comparing case IIIc with case IIIa1 the role of the ice melt becomes apparent. In IIIa1 the water column is highly stratified in the surface (figure 30a). Vertical mixing is greatly restricted because the eddy diffusivity is low, K_z= 1 cm^2/sec, in the surface layers. Correspondingly the phytoplankton are not mixed out of the euphotic region and continue to grow as long as nutrients are adquate. However inorganic nitrogen quickly becomes limiting from the lack of mixing in the stratified regions (e.g. figure 30a). In case IIIc the phytoplankton are growing but they get mixed downward because of the high vertical eddy dif-

fusivity, 55 cm^2/sec in the surface to 30 m. Nutrient concentrations (figure 35c) remain high as a result of this mixing.

Case IV: the effects of ice edge upwelling

In this experiment the hypothesis that ice edge upwelling enhances the bloom is tested. The initial conditions are 20 mg Chl/m^3 and 0 mg N/m^3 above 35 m in the water column. Below 35 m there is no chlorophyll and the inorganic nitrogen concentration is 280 mg N/m^3. The initial hydrography is the same as for all the other experiments. The wind is blown for the entire experiment duration (120 hours) along-ice with the ice to the right (pos. y) at a constant stress of 0.5 dynes/cm^2. The reason for this is to maintain the upwelling for the entire experiment.

Time series of chlorophyll and nitrogen concentrations are presented for a region with (figures 36 and 37) upwelling and for one without upwelling. It is evident that high chlorophyll concentrations remain near the surface water longer in the region of up-

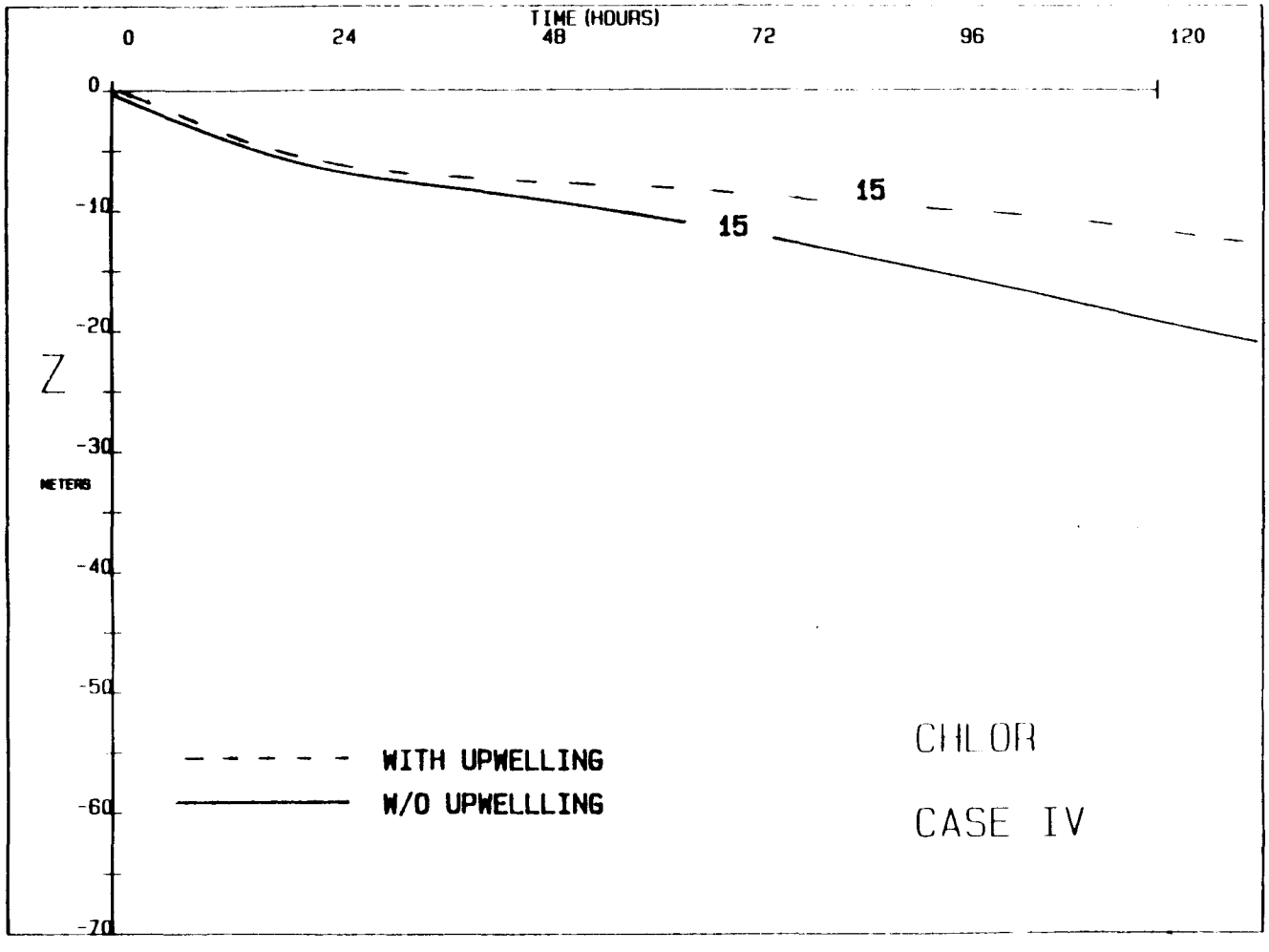

FIGURE 38: CASE IV, TIME SERIES OF 15 MG CHL/M^3 ISOPLETH, WITH AND W/O UPWELLING

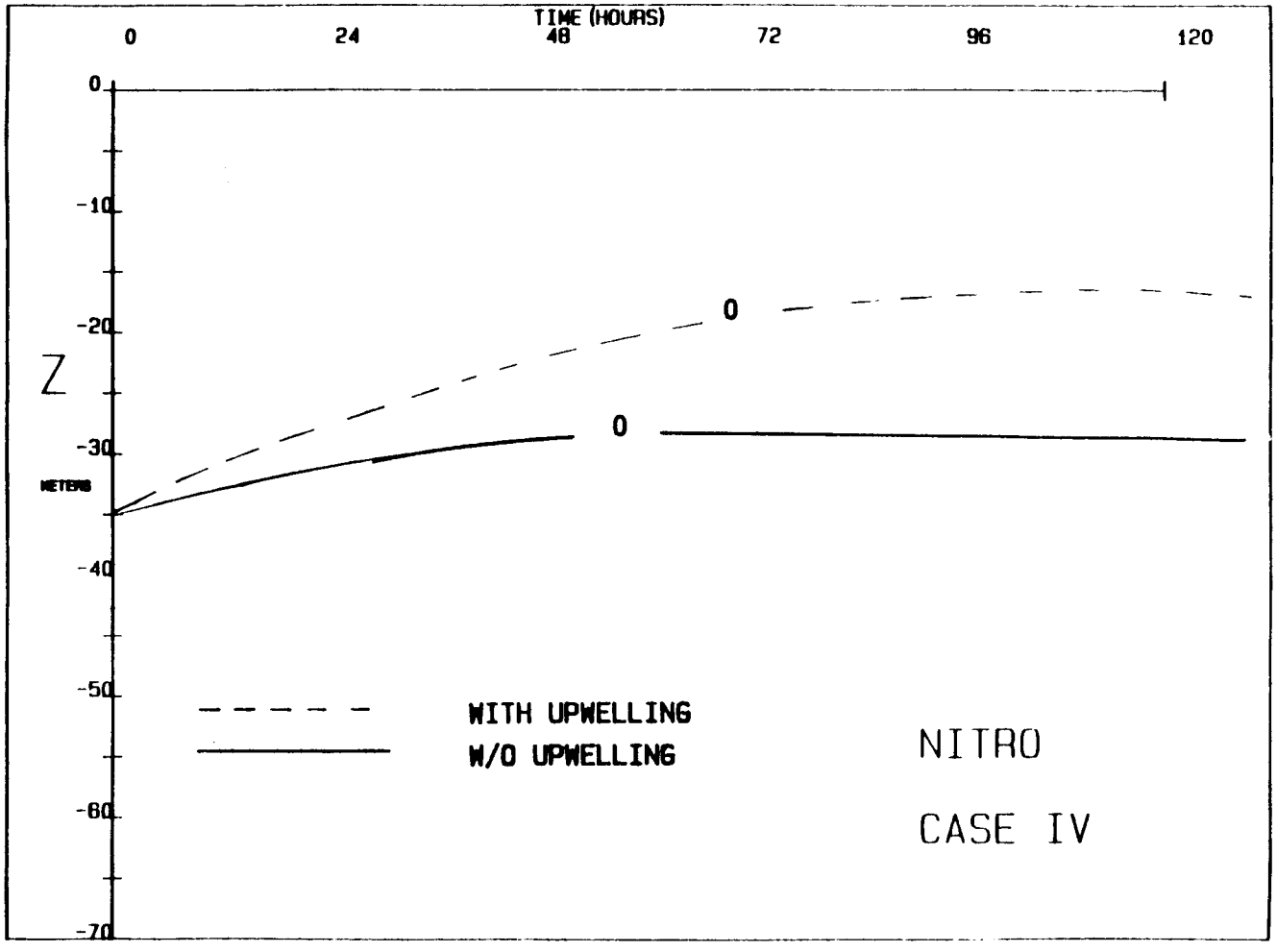

FIGURE 37: CASE IV, TIME SERIES OF 0 MG N/M^3 ISOPLETH, WITH AND W/O UPWELLING

welling (figure 36). This is because nutrients are being pumped into the surface layers (figure 37) in the region with upwelling. The zero nitrogen isopleth at 96 hours is at less than 20 m. In regions without upwelling the 15 mg Chl/m^3 isopleth is deeper (at 15 m at 96 hours) and the zero nutrient isopleth is at about 30 m.

Discussion

In the following sections the importance of the physical, biological and chemical factors which influence the spring ice edge blooms are discussed. First, the physical findings of this model are compared with other models and data. Then the primary production blooming process is related to the data gathered on the ice edge cruises of 1982 and 1983. Finally, some of the problems, limitations and possible improvements to the model are discussed.

Water and ice movement due to wind

This model frictionally couples wind-ice-water system at twice the efficiency of wind coupled directly to water, resulting in increased water velocities beneath the ice (e.g., figures 9b and 9c, case Ia). The results presented in this thesis are similar to Roed and O'Brien (1983) though there is not as much velocity structure detail in their simulation because

they simulatled the ocean as a two layer system as opposed to our multilayered approach with 5 m increments. Markham (1983) also uses a multilayered approach with a 500 m bottom depth and he also obtains similar results. Niebauer (1982) obtained opposite results for a stationary ice cover lower velocities under the ice, because in his model the wind stress could not act on the water under the ice.

Data gathered by Johannessen et al. (1983) in the MIZ near Svalbard tends to verify our model's response of the ice and the water to wind stress. The ice in their study is generally moving at some angle to the right of the wind. For example in figure 38 the angles range from ~20° to ~200°. On September 23, 1979 after a calm period of about 12 hours, a wind of about 2.5 m/sec almost along ice with ice to left was observed. The ice begins to move at about 90° to the right of this wind velocity which results in ice divergence. Water movement at 6 m is at about 270° to the right of the ice. Unfortunately the authors do not present data for the surface water. In our case Ia we invoke a similar but stronger (8 m/sec) wind. We found after 8 hours (figure 8) that the ice is moving at about 90° to the right of the wind while the water at 5 m (figures

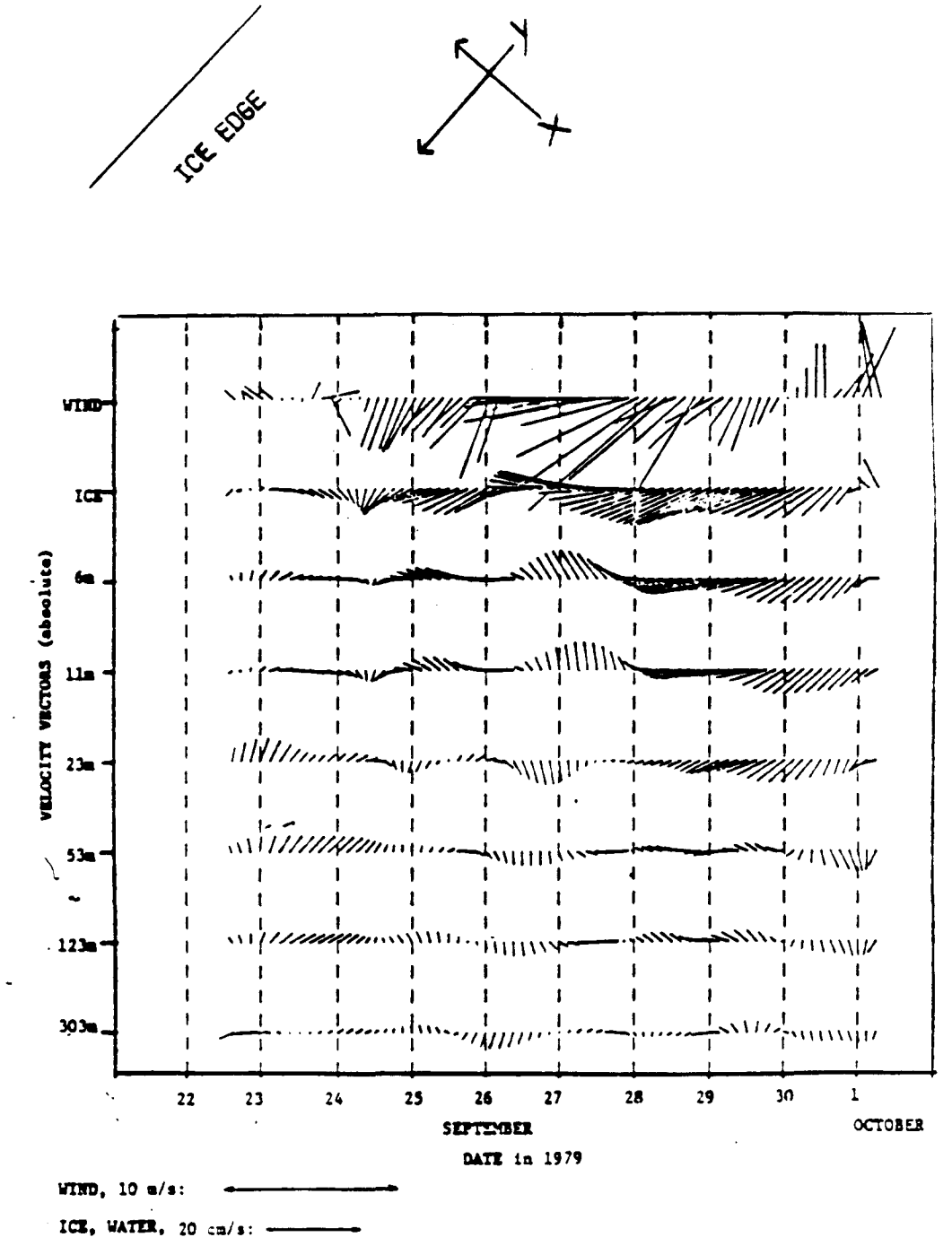

FIGURE 38: TIME SERIES OF WIND, ICE AND WATER VELOCITIES AT SVALBARD IN 1979, FROM JOHANNESSEN ET AL. (1983)

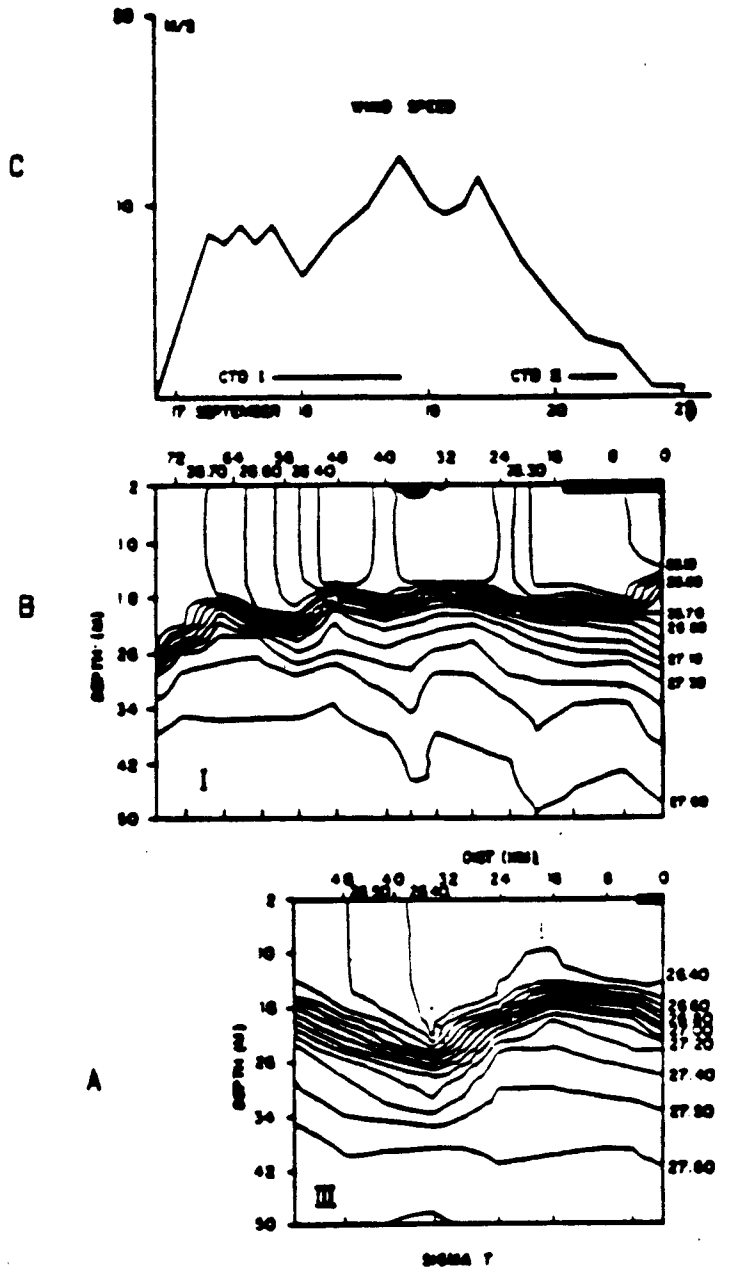

FIGURE 39: DATA TAKEN BY JOHANNESSEN ET AL. (1983) AT SVALBARD IN 1979, A) SIGMA-T SEPT.18, B) SIGMA-T SEPT. 20, C) WIND SPEED

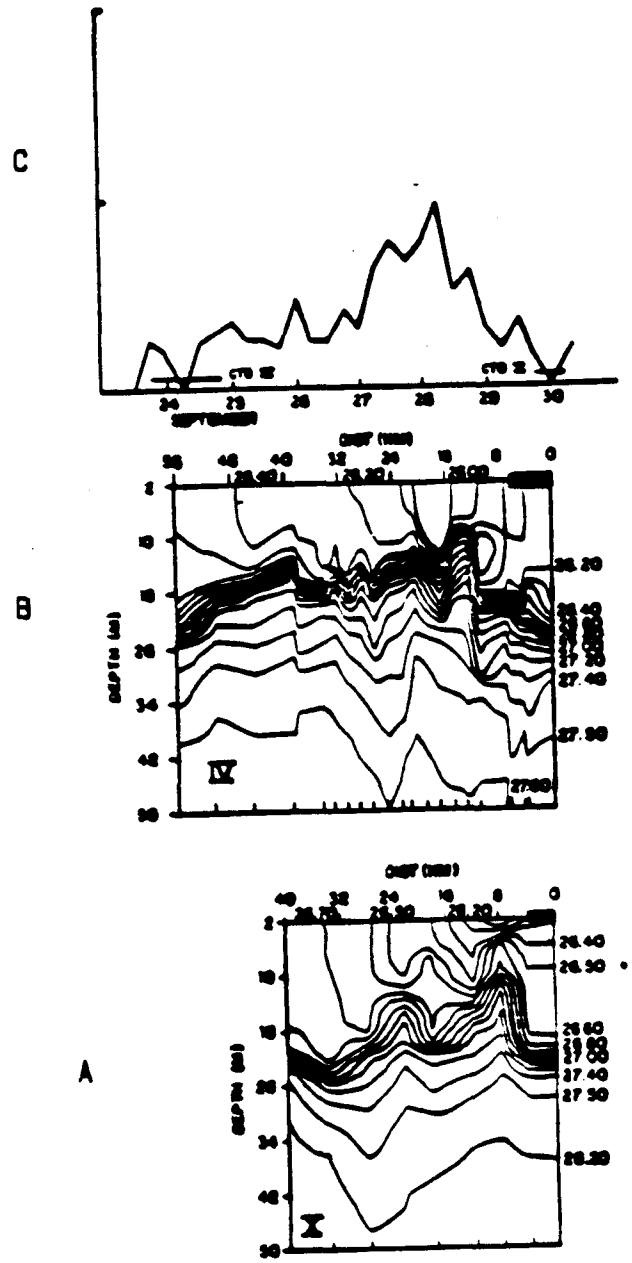

FIGURE 40: DATA TAKEN BY JOHANNESSEN ET AL. (1983) AT SVALBARD IN 1979, A) SIGMA-T SEPT.24, B) SIGMA-T SEPT. 30, C) WIND SPEED

9b and 9c) moves at about 210° to the right of the ice. The along-ice (y) water velocities are 5 cm/sec and the across-ice (x) water velocities are 1 cm/sec.

Later on Sept. 23 Johannessen et al. (1983) observed that the wind rotated quickly to right with time (figure 38). A few hours after it started it was almost off-ice with a magnitude of about 5 m/sec. For example see the last vector of the day on Sept. 23 (figure 38). Then it calmed on the morning of Sept. 24 and we can observe that the ice velocities after the wind stopped, continued to rotate to the right. In our model we see similar rotation of the vectors (figure 13a). Our wind was stopped at 18 hours and the ice and surface water at subsequent times rotate with some similarity to their data. Unfortunately, in their situation, the wind started again (figure 38, about 10.00 Sept 24) making it difficult to compare our model data with their real data. After a calm period on the 24 of Sept. the wind vectors vary from approximately along-ice with ice to right (pos. y) to not quite on-ice (pos. x). The ice moves from 20° to 60° to the right of the wind and converges. This may be seen in the model in our case IIIa1. Here with an along-ice wind with ice to right (pos. y) we get ice convergence.

In the vertical our model predicts upwelling for the same wind as the models by Roed and O´Brien (1983) and Markham (1983), on-ice (pos. x) or along-ice with the ice to the right (pos. y). Johannessen et al. (1983) from collected data interpret the upward displacement of the isopycnals (figure 39a at 18 km) as evidence of ice edge upwelling. The wind at the time their data were taken was blowing in approximinely the same direction as it does for our model to produce upwelling. They record an easterly wind with an northeast-southwest ice edge (figure 39c). The position of the ice a day after the wind started to blow (September 17) is approximately at 15 km (figure 39b). The upward bend in the isopycnals on September 20 (figure 39a) is near the position of the ice edge when the wind started to blow (ie. ~16 km in figures 39a and 39b). In our model the upward displacement of the isopycnals (figure 30a at about 42 km) for this wind is also near the position of the ice edge before the wind was turned on (figure 27).

The easterly component of the wind became small and went to zero on September 21 (figure 39c) not appearing again until about mid-day on September 23 (third panel figure 40). The CTD section taken on the 23-24 of Sep-

tember (second panel figure 40) shows upwelling in approximately the same position as it was before the easterly wind component decreased on September 21 (compare second panels figures 40 and 39). The ice at this time is located at about the 8 km position having advanced about 4 km since the easterly wind stopped. After six days (figure 40a, September 30) the upbent isopycnals are at the 8 km position. Once again this is near where the ice was before it began to retreat. In our case IIIa the wind direction is about the same as that observed by these investigators, along-ice with ice to the right (pos. y). Here we find upward motion of the isopycnals at about the same position with respect to where the ice edge was located before the wind was applied as that found in the real data (figures 30a and 31a at about 40-44 km).

Downward displacement of the isopycnals at about 30 km away from the ice edge is also evident (figure 39a), but the authors give no explaination for this. This was not present when the easterly wind event commenced (figure 39b). In our model we note a small downwelling behind the following edge of the ice (figure 14c) at the 68-74 km position which is about 6-8 km away from the ice and in case IIIa (figure 29c) at 32-40 km. Re-

gions of downwelling such as these could possibly cause downward motion of the isopycnals. In the data this motion is also evident directly behind the upwelling on September 30 (figure 40a at about 12 km). This is only approximately 6-8 km behind the ice, about the exact position that the model predicts downwelling behind a following ice edge (figure 14c, 70 km). We suggest that the observations of the downward displaced isopycnals might have been formed when the ice was closer to that position by the mechanism our model suggests, downwelling somewhat behind the following ice edge, and since that time the ice has advected out of the region.

With an along-ice wind with the ice to the left (neg. y) or an off-ice (neg. x) wind, we have downwelling conditions at the leading edge (figure 14c and 9c). However, return flows (upwelling) are noted in adjacent regions. This result is opposite to those of the previous models, where definite vertical velocities in one direction or the other were obtained. Markham (1983) did get a mixed profile of vertical velocities but only when melting was included. This upwelling-downwelling may be very important to the biological dynamics of the system and will be discussed later. In our model, with wind from the opposite directions up-

welling is predominant but once again the return flows are noted (see figure 14b, case Ib).

Melting and ice banding

Markham (1983) and Niebauer (1982) include melting in their models simulated by a constant buoyancy flux around the ice edge. Both studies show that melting produces a low density layer near the surface. In our study melting is modelled as a function of ice compactness and becomes a driving mechanism that generates horizontal baroclinic geostrophic velocity fields (see case IIa1, figures 20b and 20c) the effects of which will be discussed in the following sections.

Defining the position of the ice edge at sea is difficult because in many instances it is a series of zones or ice bands of varying ice compactness from 0% to 100% (personal observations on the ice edge cruise 1983). Wadhams (1983) with the use of a model suggests a possible ice banding mechanism through the wind and wind generated waves. He claims that the wind moves the outermost flows faster than the innermost opening up random polynyas. This is followed by wind generated waves which produce pressure on the flows located on

the downwind side of the polynya increasing their velocity even further. Martin et al. (1983) suggest that the cause of the increases in speed of the ice bands is due to wind wave stress on the upward side of the band. Our model suggests an additional mechanism.

Johannessen et al. (1983) observed that the ice goes into a divergence mode when the wind is not blowing. They attribute this to the "lack of packing" (internal ice stress), and eddies and meanders. In our model baroclinic water velocities are established by the differential input of fresh water due to the compactness dependent melting scheme (equation 11). If wind is eliminated as a driving force, the ice velocities are functions of only surface water velocity. Spatially varying ice velocities lead to regions of ice convergence and divergence (e. g. figure 34c). In regions of convergence, ice compactness increases causing the melt rate to decrease (figure 34a). In regions of divergence, ice compactness decreases, increasing the melt rate. The variations in melt rate cause variations in the baroclinic velocities which result in ice banding. Here we see a positive feedback mechanism. In regions of high ice coverage, as the ice melts, baroclinic water velocities advect the

ice out of that region. This causes increased water velocities because of the faster melt rate which causes the ice to advect out even faster. If a wind is blowing these effects might be small enough to be overwhelmed. Since this mechanism for ice banding occurs only during periods of melting, it is probably only significant during the late spring, summer and early fall.

Ice edge blooms are localized phenomenon that occur at the ice edge. However, if ice banding is prevalent in the Bering sea as suggested by some authors (Martin et al., 1983; Muench et al., 1983), the potential for a more widespread ice primary production due to many more ice edges exists.

Stratification and blooms

The stratification in the spring which leads to a phytoplankton bloom eventually becomes the causative factor which ends the bloom by nutrient depletion due to the inhibition of mixing (Parsons, Takahashi and Hargrave, 1979). Sambrotto et al. (1984) state that spring blooms occur in the Bering sea when the mixed layer depth shoals to 1/3 the critical depth. On the

shelf in the Bering sea during early spring the water temperatures are typically 0 to -1 degree Celcius. Assuming a 5 m mixed layer, a solar input of 500 cal/cm ^{2} will raise the temperature of the mixed layer from 0 to 1 ^{o}C. Assuming a constant salinity of 32 ppt the mixed layer sigma-t decreases from 25.71 (0 ^{o}, 32 ppt s) to 25.66 (1 ^{o}C, 32 ppt s) by this change in temperature. This same 500 calories of heat could melt approximately 12.5 g of ice, assuming a latent heat of fusion of 39 cal/g, for sea ice of 10 ppt (Neumann and Pierson, 1966). Such melting would lower the salinity of the mixed layer (5 m) to 31.49 ppt, assuming an ice salt concentration the same as that assumed in the model of 10 ppt. This salinity decrease, assuming temperature is constant, would reduce sigma-t from 25.71 (0 ^{o}C, 32 ppt s) to 25.27 (0^{o}C, 31.49 ppt s). This means that the addition of heat to the system in the spring in regions with ice cover results in almost an order of magnitude greater stratification than in cold regions without ice. Perhaps this suggests that in the regions of the world where ice edges are a yearly occurrence the stratified water column conditions necessary for most phytoplankton blooms can occur with less solar input, therefore earlier in the season than in regions

without ice present.

A comparison of case IIIa1 with case IIIc illustrates the importance of melt water from the ice. In IIIa1 ice is melted and the low salinity water is added to the surface layers. In IIIc the same wind is applied but ice is not allowed to melt. The sigma-t, chlorophyll and inorganic nitrogen cross-sections for each of the subcases look very different (figures 30a, 30d and 30e case IIIa1; 35a, 35b and 35c, case IIIc). Without melt water, water column stability never develops (case IIIc). For this model it means the vertical eddy diffusivities remain high (K_z~55 cm^2/sec). The plants grow but the concentrations never increase much over 10 mg/m^3 because they are being mixed downward. Additionally, the surface nutrient concentrations remain high for the same reason.

Sambrotto et al. (1984) conclude that light at the surface in the Bering sea is not a limiting factor for primary production after late March. If ice is present, stratification and therefore the shallowing of the mixed layer will occur earlier. These conditions are conducive to bloom events and may be sporadic or may not even occur each year in very early spring. But in some years between storms (storm paths vary year to

year, see Overland, 1981) a few days of calm, warm weather may lead to a bloom. Our model suggests that in 5 days, chlorophyll concentrations in excess of 20 mg/m^3 are possible. In addition because ice melt stratifies the water column more rapidly than water warming, the possiblity of two spring blooms exist. The sequence of events would be as follows:

1- Thermal input melts ice and stratifies the water column, solar input is high enough so that the phytoplankton are not limited by light and a bloom occurs.

2- A storm follows which mixes the water column.

3- This is followed by calm, warm weather which drives a temperature density stratification and a second bloom.

In 1983 during the spring ice edge cruise some of the stations showed chlorophyll concentrations of 4-5 mg/m^3 mixed quasi-homogeneously through the water column (cruise reports, HX43). If we integrate all the chlorophyll and place it in the surface 5 m the resultant concentration would be over 30 mg/m^3 at many stations. One mechanism for this significant amount of

chlorophyll is that primary production is occurring even while the cells are being mixed out of the euphotic zone as in case IIIc (figure 35c). Another possibility is a single or a series of miniblooms. Very little heat is needed to stratify the water column if ice is present. Just a day or two of calm weather could lead to a minibloom. A mixing event now will result in the chlorophyll that was produced during this minibloom to be mixed throughout the entire water column. If this sequence of events happens a number of times before the main bloom a substantial amount of chlorophyll might be present at the start of the bloom cycle.

The role of the ice algae

Though our experiments suggest that the ice flora are not significant in stimulating the beginning of the bloom, this is probably not the case in the real world. The model bloom occurs with or without input of algae from the ice (case IIc, figures 27d and 27e). However in experiment IIc1 we started with 5 mg Chl/m^3 in the water column. If the initial amount of chlorophyll had been as low as 1 mg/m^3 in the water column perhaps the

algae input from the ice would have been more important.

Assuming a two and a half day doubling time and no input of algae from from the ice, it would take five days for the concentrations to reach over 5 mg Chl/m^3 in the surface water (our initial condition). If algae are input from the ice at our initial condition (35 mg Chl/m^3 of ice) in a region of 50% ice cover, 1.68 mg/m^3 of chlorophyll will be put into the upper 2.5 m of the water column in one day. Therefore the amount of chlorophyll from just melting, not including growth, would increase from 1 to 2.68 mg/m^3 or 268%. At the initial conditions used in the experiments, 5 mg Chl/m^3 in the water, the increase would only be from 5 to 6.28 or about a 30% increase in the chlorophyll concentration. Therefore in a situation of low chlorophyll concentrations in the water column the plants input from the ice may become significant by accelerating the bloom. This may be important because if mixing events are frequent the possibility exists that the bloom may never have enough time to establish itself. The added input from the ice could speed up the ice edge the blooming process. As future work with this model, this hypothesis should be tested by varying the initial con-

ditions of the water column chlorophyll concentrations.

The ice edge upwelling

Muller-Karger (1984) found primary production at the Bering sea ice edge to exceed the initial available inorganic nitrogen after the water column stratification occurs. A source for this nutrient must exist and three possibilities are:

1- upwelling from depth,
2- vertical eddy diffusivity and
3- regeneration of phytoplankton nitrogen to inorganic nutrient nitrogen.

The second could probably be ruled out because of the strength of the stratification. The Richardson number is calculated to be over 1000 and therefore the vertical eddy diffusivity (equation, 5a) would be less than 1. The third possibility regeneration, could account for the additional primary production but this hypothesis is not testable by the model in its present form. Perhaps ice edge upwelling which has been shown to probably exist (Johannessen, et al, 1983; Alexander and Niebauer, 1981) and has been inferred in this model

as well as others (Roed and O'Brien, 1983; Markham, 1983; Niebauer, 1982) pumps nutrients to the surface layers. Our experiments show that upwelling maintains the nutrient concentration, though they remain low because of phytoplankton uptake. This might enable the phytoplankton to remain "healthier" so they sink slower (Parsons, et al., 1979). In the early spring when ice is present. its movement which is driven by the wind, causes upwelling. The ice is also melting, if thermal input is high enough, creating a buoyancy flux from the surface. The upwelling process supplies nutrients to the euphotic zone and the melting maintains the stability. This can be seen in figures 30a and 30e of experiement IIIa1.

Unlike the coastal situation, spatial as well as temporal variability are prominent features of ice edge upwelling. This is because it is dependent on the location of the ice edge. When a bloom occurs at a location then dies out due to a lack of nutrients, if the ice passes over the region at this time the possiblity for replenishment of the nutrients is greatly enhanced because of the additional vertical velocity generated. This may happen over and over again because of the variability in wind direction. On the other

hand because of this variability not too much upwelling may occur at any particular position at a particular time. Therefore ice edge upwelling may not be very important.

If we assume upwelling is important, then because regeneration transforms some of the phytoplankton nitrogen to inorganic nitrogen it appears as though the bloom may be maintained longer because the nutrient concentrations below the mixed layer always remain high. This water with high nitrogen concentration is then advected by upwelling into the surface layers.

The importance of the ice edge upwelling in the model is illustrated in case IV. In regions of upwelling (figure 36) phytoplankton growth is maintained for longer periods than in regions with no upwelling. The magnitude of the slope of the 15 mg Chl/m^3 isopleth is smaller where upward velocities are evident. Nitrogen is being advected into the surface layers in areas of upwelling (figure 36) while in regions of no upward vertical velocities (figure 37) the only mechanism for the input of nitrogen from below is eddy diffusion.

Ice edge upwelling and its relationship to primary production at the Bering sea ice edge is discussed by

Alexander and Niebauer (1981). They suggest that frontal structure as indicated by the isopleths of sigma-t (figure 41a) is due to a combination of ice edge upwelling and melting. This surfacing of the isopleths looks very similar to many of our experiments (figures 34a and 30a, for examples). The upward displacement of the isopleths of chlorophyll right at the ice edge (figure 41b) also looks strikingly like the results of case IIIb (figure 29d) but the values are different, 20 as opposed to 30 mg Chl/m^3. Here we attribute this curvature to upwelling. Alexander and Niebauer (1981) show nitrate values less than 3 mg atoms/m^3 (42 mg/m^3) at depths from 0 to 15 m (figure 41c) but chlorophyll values higher than 30 mg/m^3 (figure 41b) at depths shallower than 5 m.

From the model results it appears that both horizontal and vertical velocities generated by wind stress are greater in regions of ice than regions without ice. In addition the efficiency of heat induced water column stratification is also greater in areas where the heat is used to melt ice as opposed to heating water. The above two factors appear to be the main components which determine the amount of primary production that occurs. Therefore it seems as though

the conditions for high primary production exist near ice edges at certain times of the year.

The bloom and wind direction

The data collected by Niebauer and Alexander (1984) during an off-ice wind event (neg. x) (figures 30f, 30g and 30h) are in qualitative agreement with those produced by the model (for example, case IIIa1, figures 34a, 34d and 34e). The model, after 120 hours, produces a lens of low density water. Associated with this stratified region are high chlorophyll and low nutrient values. The lenses in the data are about the same size and in about the same position as in the simulation. This type of water column structure is shown to develop with any of the winds we applied to the model as long as the ice was allowed to melt. In case IIIc we ran a similar experiment but did not allow the ice to melt. The water column never stratifies (figure 35a) and the bloom is never established. Chlorophyll values of about 10 mg/m^3 are reached but nutrient depletion does not occur because of the high K_z values (figure 35c). We consider this one of the major findings of the study. In the model, without

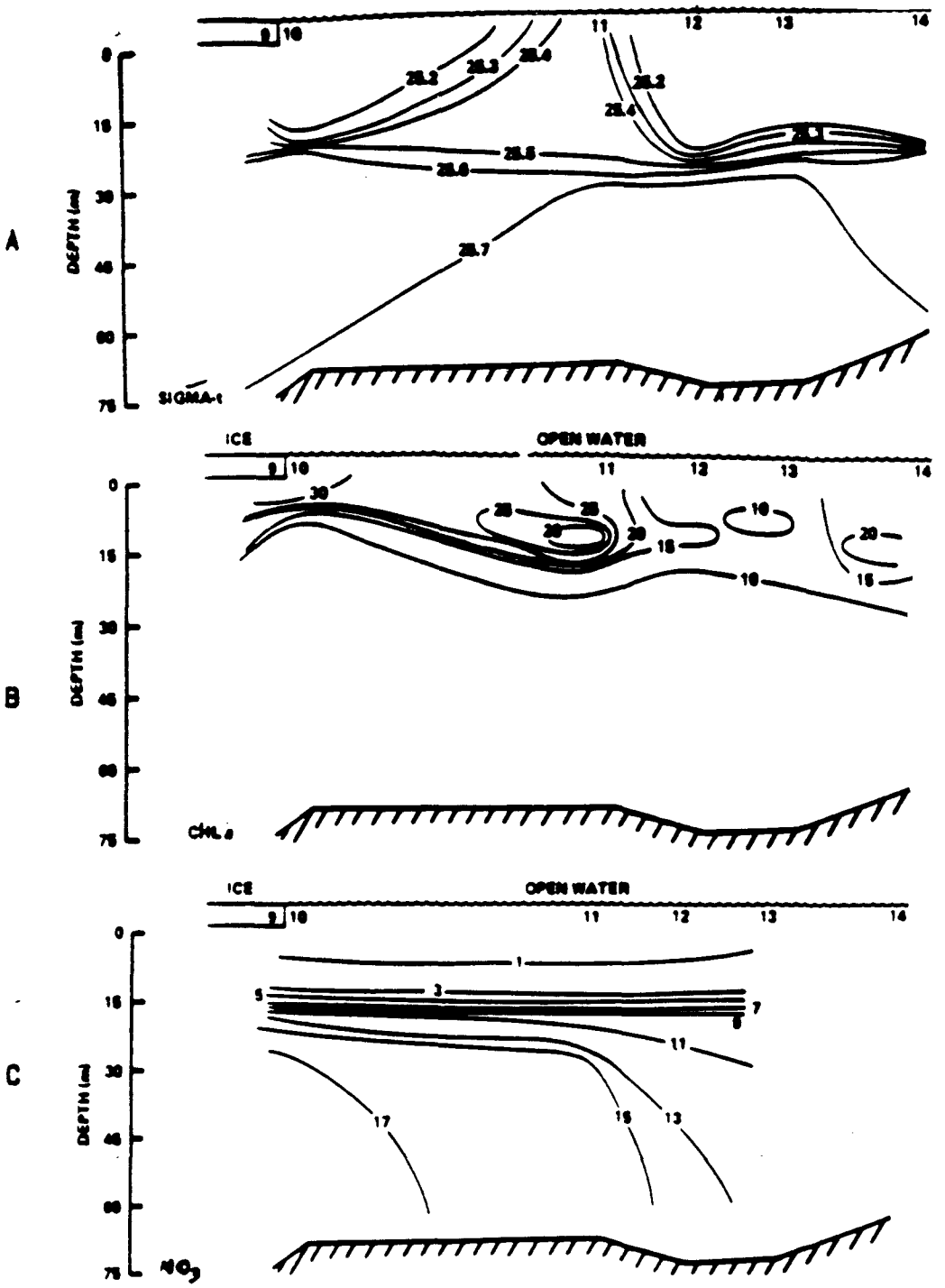

FIGURE 41: CROSS-SECTIONS OF SIGMA-T (A), CHLROPHYLL (B) AND NITRATE (C) AT THE 1975 ICE EDGE IN THE BERING SEA, AFTER ALEXANDER AND NIEBAUER (1981)

meltwater input the bloom conditions do not occur.

During an along-ice with ice to left (neg. y) wind, the bloom occurs (figure 31b and 31c) but the structure is different than that in the off-ice (neg. x) case IIIb. The ice advects out from the pack slower in the neg. y case so that the percent coverage in the areas that it has just entered is larger. This leads to slower melting which in turn leads to an deccelerated temporal change in density, 25.2 vs. 25.15 (figure 31a), and a decreased rate of input of ice algae into the water column (figure 31c). These two factors cause a phytoplankton bloom where chlorophyll concentrations are lower and the spatial extent smaller. In addition it develops a bit slower than case IIIb.

Problems and improvements

In this section we will discuss the problems and possible improvements to the model. Four general areas are emphasized:

1- light attenuation through the ice

2- tidal velocities

3- the melting scheme

4- ice/atmosphere coupling

One of the hypotheses that was not tested in this model is that the ice absorbs light before it penetrates into the water column. The bloom occurs when enough ice melts so that the light levels in the water column are no longer limiting (D. Schell, personal communication). Here we simply assume that light transmission is the same through ice or water. This is justified by measurements of light taken during the ice edge cruises of 1982 and 1983. This data does not appear to be correlated with compactness. However many researchers claim to have established such a correlation and say that light transmission through ice is a function of snow cover, ice density, age and thickness (D. schell, personal communication). It would be informative to include this type of light transmission scheme to observe its interaction with the stratification formation in the blooming process.

Tidal velocities in the Bering sea are up to 50 cm/sec (Pearson et al., 1981). Niebauer and Alexander (1984) suggest that around the 50 m isobath on the Bering sea shelf, upwelling is produced by this tidal velocity shear at the bottom. This upwelling may in

part be responsible for the raised nutrient levels they observed (figure 30h at ~60 km). In addition this velocity shear results in small Richardson numbers because the vertical gradient in velocity becomes large at the bottom (equation 6). This results in large eddy diffusivities in the same region which further results in more vertical mixing. If nutrient values are high near the bottom they now will be mixed upward into the photic zone more efficiently. This shear also produces turbulence at the bottom which may mix some nutrients upward from the sediments. Because the thrust of this study was to investigate the relationship between ice and phytoplankton blooms, this type of velocity is not included. However, to fully examine the Bering sea spring blooming process, tidal cycles should be taken into account.

The melting of sea ice is a very complicated process including heat input from the water, heat input from the atmosphere and ice compactness. Langleben (1972) claims that melting of sea ice is a very strong function of the ice compactness. Because the thermodynamics of this process was beyond the scope of this study we simplified the melting scheme by assuming that melting is a linear function of compactness (equation

11) and that the thermal input for the duration of the experiments is a constant. While this appears to work reasonably well, the inclusion of the thermodynamics might add additional insight into the physical and biological processes. An additional problem due to the melting scheme is the piling up of ice. Because, in nature, this phenomenon would require large wind velocities and/or waves, it would probably be more realistic not to allow the ice percent coverages to go beyond 100% in the model.

Finally, in this model, for simplicity, we assume that the ice/atmosphere coupling coefficient is a constant at two times the atmosphere/ocean coupling constant. A few investigators have suggested that the ice/atmosphere coupling is a function of ice compactness (Wadhams, 1983; Johannessen et al., 1983). They claim that in regions of small ice flows, like around the edges, greater vertical surface area of ice is exposed for the wind to act upon than in regions of larger flows. This results in a greater acceleration of the ice in these regions which may be a mechanism for ice banding (Wadhams, 1983). We suggest that future ice edge models incorporate this feature because the more rapid outward advection of ice may lead to

more rapid melting and even faster stratification than our model has shown.

References

Alexander, V. and T. Chapman, 1981. The role of epontic algal communities in Bering Sea ice. In: The Eastern Bering Sea Shelf: Oceanography and Resources vol. 2:773-780.

Alexander, V. and T. Cooney, 1979. A quantitative study of the phytoplankton from the eastern Bering Sea. In: Environmental assessment of the Alaska continental shelf, NOAA/OCSEAP, ann. rep.

Alexander, V. and H. J. Niebauer, 1981. Oceanography of the eastern Bering Sea ice-edge in spring. Limnol. Oceanogr. , 26:1111-1125.

Bennett, J. R., 1973. On the dynamics of wind driven lake currents. Ph.D. thesis, University of Wisconsin, Madison, 85 pp.

Buckley, J. R., T. Gammelsrod, J. A. Johannessen, O. M. Johannessen and L. P. Roed, 1979. Upwelling: Oceanic structure at the edge of the artic ice pack in winter. Science , 203:165-167.

Clarke, A. J., 1978. On wind driven quasi-geostrophic water movements near fast ice edges. Deep-Sea research , 25:41-51.

Cooney, R. T. and K. Coyle, 1982. Tropic implications of cross-shelf copepod distributions in the southeastern Bering Sea. Mar. Biol. , 9:187-196.

Cox, R. A., M. J. McCartney and F. Culkin, 1970. The specific gravity/salinity/temperature relationship in natural sea water. Deep-Sea Research , 17:679-689.

Cushing, D. H., 1969. Upwelling and fish production. F. A. O. Fisheries Biology Technical Papers , 84:40 pp

El Sayed, S. Z. and Taguchi, 1981. Primary production and standing crop of phytoplankton along the ice edge in the Weddell Sea. Deep-Sea Research , 28A:1017-1032.

Eppley, R. W., R. W. Holmes and J. D. Strickland, 1967. Sinking rates of marine phytoplankton measured with a fluorometer. J. exp. mar. Biol. Ecol., Vol I:191-208.

Feldman, U., P. J. Howarth, and J. A. Davies, 1981. Estimating surface wind direction over drifting open pack ice. J. Geophys. Res. , 86:8117-8120.

Gammelsrod, T., M. Mork and L. P. Roed, 1975. Upwelling possiblity at the ice edge, homogeneous model. Marine Science Communications , 1:115-145.

Goering, J. J. and R. L. Iverson, 1981. Phytoplankton Distribution on the Southeastern Bering Sea Shelf. In: The Eastern Bering Sea Shelf: Oceanography and Resources , volume 2, Hood, D. W. and J. A. Calder editors, University of Washington Press, Seattle.

Hamilton, P. and M. Rattray, Jr., 1978. A numerical model of the depth-dependent, wind-driven upwelling circulation on a continental shelf. J. Phys. Ocn., 8:437-457.

Hibler, W. D., III, 1979. A dynamic thermodynamic sea ice model. J. Phys. Ocn. , 9:815-846.

Hood, D. W., 1981. introduction to The Eastern Bering Sea Shelf: Oceanography and Resources , volume 1, Hood, D. W. and J. A. Calder editors, University of Washington Press, Seattle.

Ivanov, A. I., 1964. Characteristics of the phytoplankton in Antartic waters at the whaling grounds of the flottilla Slava in 1957-1958. Sov. Antarct. Exped. Inform. Bull. , 1:394-396.

Johannessen, O. M., J. A. Johannessen, J. Morison, B. A. Forrelly and E. A. S. Sundsen, 1983. NORSEX III: The Mesoscale Oceanographic Conditions in the Marginal Ice Zone North of Svalbard in the early Fall 1979. J. Geophys. Res. , 88:2755-2769.

Langleben, M. P., 1972. Decay of an annual cover of sea ice. J. of Glaciology vol. 11 no. 63:337-344.

Markham, G. M., 1983. Ocean mixing and circulation response in the Marginal Ice Zone. Masters thesis, Naval Postgraduate School, Monterey, California.

Marshall, P. T., 1957. Primary production in the Artic. J. Conseil. , 23:173-177.

Martin, S., P. Kauffman and Clare Parkinson, 1983. The movement and decay of ice edge bands in the winter Bering Sea. J. Geophys. Res. , 88:2803-2812.

McPhee, M., 1979. An analysis of pack ice drift in summer. in Sea Ice Processes and models , edited by R. S. Pritchard, Ed., University of Washington, Seattle.

Muench, R., P. H. LeBlonde and L. E. Hachmeister, 1983. On some possible interactions between internal waves and sea ice in the marginal ice zone. J. Geophys. Res. , 88:2819-2826.

Muller-Karger, F., 1984. Lower trophic level studies in the marginal sea-ice zone. Master thesis, University of Alaska.

Nansen, F., 1902. The oceanography of the north polar basin. In: The Norwegian North Polar Expedition, 1893-1896. Scientific Results, volume 3 no. 9.

Neori, A. and O. Holm-Hansen, 1982. Effect of temperature on rate of photosynthesis in Antartic phytoplankton. Polar Biology 1:33-38.

Neumann, G. and W. J. Pierson, 1966. Principles of Physical Oceanography. Prentice-Hall inc., Engelwood Cliffs, N. J.

Niebauer, H. J., 1980a. Sea ice and temperature fluctuations in the eastern Bering Sea and the relationship to meteorogical fluctuations. J. Geophys. Res. , 85:7505-7515.

Niebauer, H. J., 1980b. A numerical model of circulation in a continental shelf-silled fjord coupled system. Estuarine and Coastal Marine Science, 10:507-521.

Niebauer, H. J., 1982. Wind and melt driven circulation in a marginal sea ice edge frontal system: A numerical model. Continental Shelf Research , 1:49-98.

Niebauer, H. J., V. Alexander and R. T. Cooney, 1981. Primary production at the Bering Sea ice edge: The physical and biological regimes. in: The Eastern Bering Sea Shelf: Oceanography and Resources , volume 2, Hood,D. W. and J. A. Calder, editors, University of Washinton Press, Seattle.

Niebauer, H. J. and V. Alexander, 1984. On the influence of the physical oceanographic processes on biological production in the marginal ice edge zone. submitted to Continental Shelf Research.

Overland, J. E., 1981. Marine climatology of the Bering Sea. The Eastern Bering Sea Shelf: Oceanography and Resources , volume 1, Hood, D. W. and J. A. Calder, editors, University of Washington Press, Seattle.

Overland, J. E. and C. H. Pease, 1982. Cyclone climatology of the Bering Sea and its relation to sea ice extent. Mon. Wea. Rev. , 110:5-13.

Parsons, T. R., M. Takahashi and B. Hargrave, 1979. Biological Oceanographic Processes , second edition. Pergamon Press, New York, N. Y..

Pond, S. and G. L. Pickard, 1978. Introductory Dynamic Oceanography , Pergamon Press, New York, N.Y.

Pearson, C. A., H. O. Mofjeld and R. B. Tripp, 1981. Tides of the eastern Bering Sea. In: The Eastern Bering Sea: Oceanography and Resources volume 1, Hood, D. W. and J. A. Calder, editors, University of Washington Press, Seattle.

Reeburgh, W. S. and M. Springer-Young, 1983. New measurements of sulfate and chlorinity in natural sea ice. J. Geophys. Res. 88, no.c5:2959-2966.

Riley. G. A., 1956. Oceanography of Long Island Sound, 1952-1954, II, Physical Oceanography. Bull. Bingham. Oceangr. Coll. , 15:324-343.

Roed, L. P. and J. J. O'Brien, 1983. A coupled ice-ocean model of upwelling in the marginal ice zone. J. Geophys. Res. , 88:2863-2872.

Ryther, J. H., 1969. Photosynthesis and fish production in the sea. Science, 166:72-76.

Sambrotto, R., 1983. Nitrogen utilization during spring phytoplankton bloom development in the Southeast Bering Sea. Ph. D. thesis, Institute of Marine Science, University of Alaska, Fairbanks.

Sambrotto, R. N., H. J. Niebauer, J. J. Goering and R. L. Iverson, 1984. Relationships among vertical mixing, nitrate uptake, and growth during the spring bloom in the southeast Bering Sea middle shelf. (submitted to Continental Shelf Research).

Steele, J. H., 1962. Environmental control of photosynthesis in the sea. Limnol. Oceanogr. 7, 137-150.

Wadhams. P., 1983. A mechanism for the formation of ice edge bands. J. Geophys. Res. , 88:2813-2818.

Walsh, J. J., 1975a. A biological interface for numerical models and the real world-An elegy for E. J. Ferguson Wood. In: Numerical Models of Ocean Circulation , National Academy of Sciences, Washington, D.C.

Walsh, J. J., 1975b. A spatial simulation model of the Peru upwelling ecosystem. Deep-Sea Research , 22:201-236.

Winter, D. F., K. Banse and G. C. Anderson, 1975. The dynamics of phytoplankton blooms in Puget Sound, fjord in the northwestern United States. Mar. Bio. , 29:139-176.

Wroblewski, J. S., 1977. A model of phytoplankton plume formation during variable Oregon upwelling. Mar. Res. , 35,2:357-394.